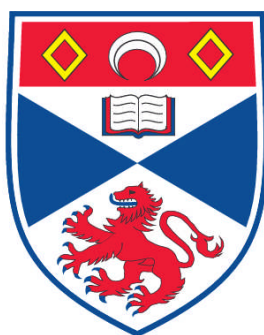# CATHODE DEVELOPMENT FOR SOLID OXIDE ELECTROLYSIS CELLS FOR HIGH TEMPERATURE HYDROGEN PRODUCTION

Xuedi Yang

A Thesis Submitted for the Degree of PhD
at the
University of St. Andrews

2010

**Full metadata for this item is available in the St Andrews
Digital Research Repository
at:
https://research-repository.st-andrews.ac.uk/**

**Please use this identifier to cite or link to this item:
http://hdl.handle.net/10023/979**

Cathode Development for Solid Oxide Electrolysis Cells for High Temperature Hydrogen Production

A thesis presented for the degree of Doctor of Philosophy

Xuedi Yang
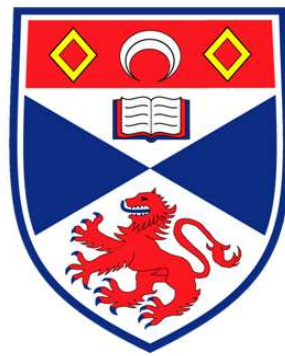
University of St Andrews

Supervised by Prof. John. T. S. Irvine

Submitted September 2009

Declaration

I, Xuedi Yang, hereby certify that this thesis, which is approximately 30,000 words in length, has been written by me, that it is the record of work carried out by me and that it has not been submitted in any previous application for a higher degree.

I was admitted as a research student in September 2006 and as a candidate for the degree of Doctor Philosophy in September 2007; the higher study for which this is a record was carried out in the University of St Andrews between 2006 and 2009.

Date   signature of candidate

I hereby certify that the candidate has fulfilled the conditions of the Resolution and Regulations appropriate for the degree of Doctor of Philosophy in the University of St Andrews and that the candidate is qualified to submit this thesis in application for that degree.

Date   signature of candidate

In submitting this thesis to the University of St Andrews we understand that we are giving permission for it to be made available for use in accordance with the regulations of the University Library for the time being in force, subject to any copyright vested in the work not being affected thereby.   We also understand that the title and the abstract will be published, and that a copy of the work may be made and supplied to any bona fide library or research worker, that my thesis will be electronically accessible for personal or research use unless exempt by award of an embargo as requested below, and that the library has the right to migrate my thesis into new electronic forms as required to ensure continued access to the thesis. We have obtained any third-party copyright permissions that may be required in order to allow such access and migration, or have requested the appropriate embargo below.

Date   signature of candidate   signature of supervisor

Acknowledgements

ABSTRACT

This study has been mainly focused on high temperature solid oxide electrolysis cells (HT-SOECs) for steam electrolysis. The compositions, microstructures and metal catalysts for SOEC cathodes based on $(La_{0.75}Sr_{0.25})_{0.95}Mn_{0.5}Cr_{0.5}O_3$ (LSCM) have been investigated. Hydrogen production amounts from SOECs with LSCM cathodes have been detected and current-to-hydrogen efficiencies have been calculated. The effect of humidity on electrochemical performances from SOECs with cathodes based on LSCM has also been studied.

LSCM has been applied as the main composite in HT-SOEC cathodes in this study. Cells were measured at temperatures up to 920^oC with 3%steam/Ar/4%H_2 or 3%steam/Ar supplied to the steam/hydrogen electrode. SOECs with LSCM cathodes presented better stability and electrochemical performances in both atmospheres compared to cells with traditional Ni cermet cathodes. By mixing materials with higher ionic conductivity such as YSZ(Y_2O_3-stabilized ZrO_2) and CGO($Ce_{0.9}Gd_{0.1}O_{1.95}$) into LSCM cathodes, the cell performances have been improved due to the enlarged triple phase boundary (TPB).

Metal catalysts such as Pd, Fe, Rh, Ni have been impregnated to LSCM/CGO cathodes in order to improve cell performances. Cells were measured at 900^oC using 3%steam/Ar/4%H_2 or 3%steam/Ar and AC impedance data and I-V curves were collected. The addition of metal catalysts has successfully improved electrochemical performances from cells with LSCM/CGO cathodes.

Improving SOEC microstructures is an alternative to improve cell performances. Cells with thinner electrolytes and/or better electrode microstructures were fabricated using technics such as cutting, polishing, tape casting, impregnation, co-pressing and screen printing. Thinner electrolytes gave reduced ohmic resistances, while better

electrode microstructures were observed to facilitate electrode processes.

Hydrogen production amounts under external potentials from SOECs with LSCM/CGO cathodes were detected by gas chromatograph and current-to-hydrogen efficiencies were calculated according to the law of conservation of charge. Current-to-hydrogen efficiencies from these cells at $900^{o}C$ were up to 80% in 3%steam/Ar and were close to 100% in 3%steam/Ar/4%H_2.

The effect of humidity on SOEC performances with LSCM/CGO cathodes has been studied by testing the cell in cathode atmospheres with different steam contents (3%, 10%, 20% and 50% steam). There was no large influence on cell performances when steam content was increased, indicating that steam diffusion to cathode was not the main limiting process.

Table of Contents

Chapter 3 Initial Studies on (La$_{0.75}$Sr$_{0.25}$)$_{0.95}$Mn$_{0.5}$Cr$_{0.5}$O$_3$ Cathodes for Solid Oxide Electrolysis Cells

Chapter 4 Studies on Catalyst Addition

Chapter 5 Improvements on cell microstructures

Chapter 6 Hydrogen production from SOECs with cathodes based on LSCM

Chapter 1 Introduction

1.1 Hydrogen economy

Hydrogen is the most abundant element on earth and is considered as a leading fuel candidate in the future[1]. However, elemental hydrogen is not in significant amounts on earth and hydrogen has to be extracted from fossil fuels or renewable energy[2,3].

Hydrogen is a flexible energy carrier that can be produced from a variety of energy resources and used in many sectors of the economy. An energy system based on hydrogen from renewable resources, if accomplished on a large scale, could improve energy security, air quality, and greenhouse gas management. Such a system will require development across a series of technologies for hydrogen production, transportation, storage, and use[4].

1.1.1 Energy history

The trend of energy use is to use fuel with lower carbon to hydrogen ratio (see Figure 1.1). Initially, mankind burnt wood for heating and lighting. In 1780s, coal replaced wood to be the prime energy source. In the late 19th century, oil was introduced and replaced coal for many applications. In the middle of 20th century, natural gas was found in large volume and became a prime fuel[3].
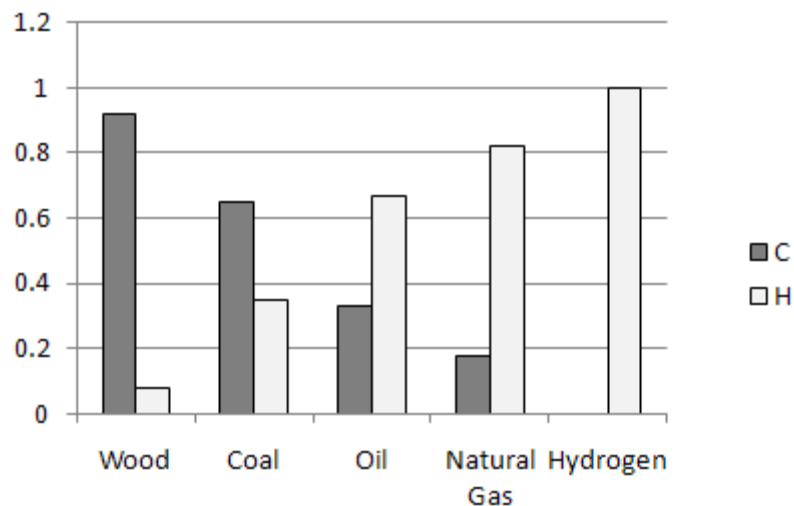
Figure 1.1 Trend in energy use[3].

As the combustion of fossil fuels is attributed to be the main cause of the global climate change and correlated environmental problems, we need a fuel that is clean which would not cause global warming or people's health problems[5]. Hydrogen is such a kind of energy as it is clean, especially when it is produced from non-fossil energy.

Apart from causing damages to our environment, using fossil fuels has the problem of increasing price of crude oil due to the decreasing oil reserves[6]. Hydrogen has the potential to be produced from renewable sources which are clean and sustainable.

1.1.2 The Hydrogen economy

Hydrogen is already widely used as a chemical in industry. Apart from as a chemical, hydrogen could also be employed as a fuel and a fuel carrier especially if fuel cells are to be successful. The global market of hydrogen is already greater than $40 billion per year[7].

The basis of hydrogen energy is that hydrogen reacts with oxygen to produce energy and water (see Equation. 1)[8]:

$H_2 + 1/2O_2 \rightarrow H_2O \quad \Delta H^o = -286$ kJ/mol   at 25 ^{o}C;   Equation. 1

$\Delta G^o = -237.2$ kJ/mol   at 25 ^{o}C.
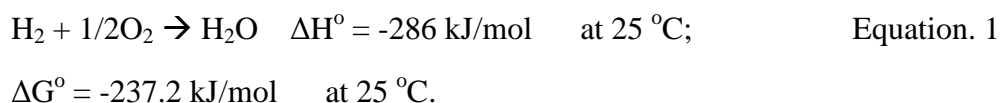
Hydrogen has a high gravimetric energy density of 122 kJ/g (kilojoule per gram), which is 2.75 times greater than hydrocarbon fuels[9].

Figure 1.2 is a schematic diagram of hydrogen energy system. It is regarded as an ideal system which could be the solution to the depletion of conventional fuels and global environmental problems.
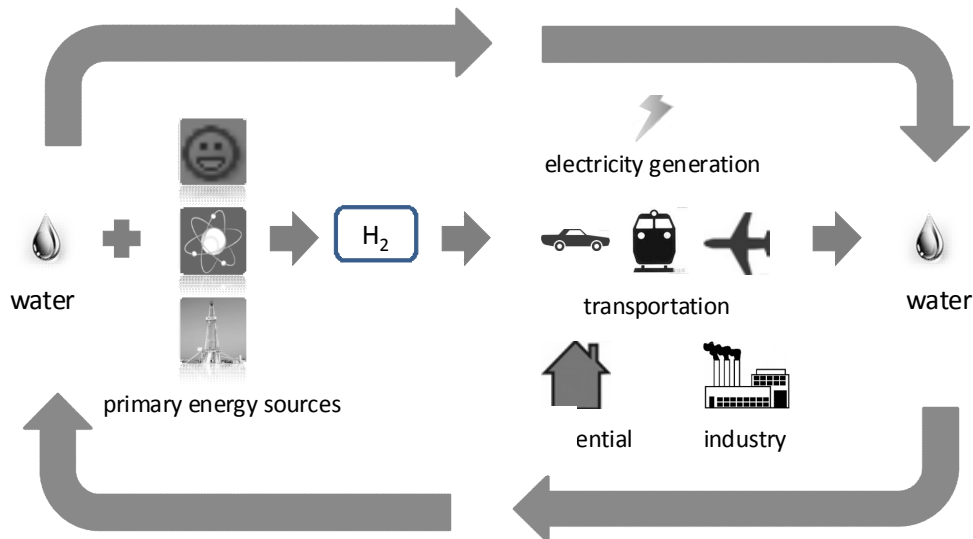
Figure 1.2 A sustainable Hydrogen Economy[10].

Utilizing renewable resources, such as solar, wind, tidal, wave and geothermal sources, is the trend of future energy, which faces the problem of time mismatch of energy supply and demand in that the electricity production from these sources depends on variable weather conditions[11]. Hydrogen produced from excess electricity can be easily stored and transported, and it could be consumed by fuel cells to supply electricity later and elsewhere. Hydrogen produced from renewable sources is regarded to be an environmentally friendly energy and could be a substitute of oil to feed the increasing demand of energy while we are in the exhaustion situation of oil.

1.1.3 Hydrogen storage and transportation

One of the key issues of hydrogen economy is efficient and affordable store/distribution of hydrogen produced in large-size central plants or in small-scale local plants.

1.1.3.1 Gaseous hydrogen

There are three major ways to storage/transport gaseous hydrogen[2,12]:

Pipeline. Via pipeline is the most obvious way to convey hydrogen to market.

Hydrogen can be transmitted through pipelines similar to those for natural gas. Hydrogen is compatible with low-carbon steels, polymers, aluminum and brass; new pipelines or modified natural-gas pipelines can be employed in delivering hydrogen.

Large scale storage. To store hydrogen in bulk is based on the experiences of natural gas. Depleted gas and oil fields or aquifers could be used for holding natural gas in huge scale. It depends on the nature of the rock strata.

Gas cylinder. Smaller scaled hydrogen could be stored and transported in substantial cylinders or tanks at high pressure, which require special compressors. Industrial users of hydrogen often use cylinders at pressures ranging from 20 MPa to 80 MPa.

1.1.3.2 Liquid hydrogen

Liquid hydrogen (LH$_2$) has a low density of 70.8 kg$^.$m^{-3} and boils at a very low temperature (20.6 K)[3]. The problem of storage is bulk and low temperature. Gaseous hydrogen is liquefied and held in a cryostat. As hydrogen liquefaction and cryostat are both costly, liquid hydrogen is mostly used for aircraft rather than road vehicles.

1.1.3.3 Metal hydrides

Some metal alloys absorb hydrogen reversibly to form metal hydrides, which serves as an alternative way to store hydrogen.

1.1.4 Hydrogen future

Hydrogen serves as a chemical and as a fuel. As a new energy, the introduction of hydrogen energy will be based on an adequate platform of science, engineering and economics concerning hydrogen production, purification, storage, distribution and utilization.

1.2 Hydrogen production

All primary energy sources can be used in the hydrogen producing process[13]. There are many ways to produce hydrogen such as from fossil fuels, from biomass, and by electrochemical means.

Among the several methods of producing hydrogen, reforming fossil fuels, such as natural gas and oil, is currently the major way of hydrogen production. However, carbon dioxide is a byproduct from hydrocarbon reforming, and is considered to be the main cause of the 'greenhouse effect'. Considering the global environment and people's health, the world needs to turn gradually to renewable energy resources. Hydrogen production without carbon emissions, that is from renewable energy sources, will be needed in the future.

1.2.1 Hydrogen from fossil fuels

Much of current hydrogen production relies on fossil fuels which occupy above 90% percent of hydrogen production (see Figure 1.3). And most of the hydrogen produced is obtained from natural gas, which is mainly made up of methane.
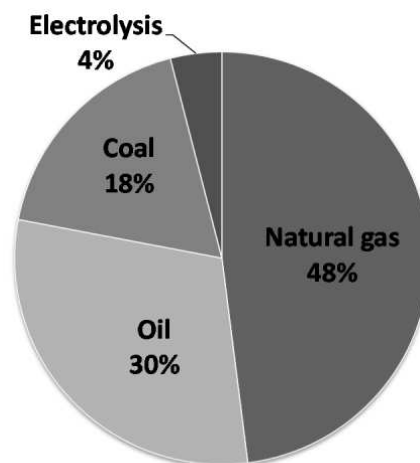
Figure 1.3 Global hydrogen production share by source[14].

There are three major ways of producing hydrogen from hydrocarbon fuels: steam reforming, partial oxidation (POX), and autothermal reforming (ATR)[14,15].

The reactions can be generalized as follows:

Steam reforming .

$C_nH_m + nH_2O \rightarrow nCO + (n+m/2)H_2$

$CO + H_2O \rightarrow CO_2 + H_2$

Partial oxidation (POX).

$2C_mH_n + mO_2 \rightarrow 2mCO + nH_2$

Autothermal reforming.

$4C_mH_n + 2mH_2O + mO_2 \rightarrow 4mCO + 2(m+n)H_2$
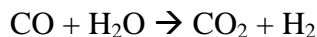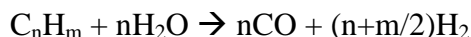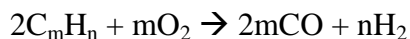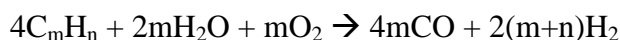
All three methods have large amount of carbon monoxide produced and usually have one or more water-gas-shift (WGS) reactors in the processes to convert CO to low level.

Through producing hydrogen from fossil fuel is currently preferred method, pollutants (CO, CO_2, C_nH_m, SO_x, NO_x, radioactivity, heavy metals, ashes[16]) emitted by fossil energy systems are much more than the emissions that might be produced by renewable hydrogen system.

1.2.2 Hydrogen from biomass

Biomass is a carbon-containing fuel but is a renewable fuel of energy. It derives from the carbon dioxide in atmosphere by photo-synthesis. It is available from a wide range of sources such as agriculture waste, animal waste, municipal waste, and many more[17]. There are currently several technologies for hydrogen production from biomass:

Biological hydrogen production from biomass. Biological hydrogen production works through dark fermentation or photofermentation. Dark fermentation of biomass is a microbial processes under anaerobic conditions. Some substrates are oxidized and some others are reduced. Protons are reduced to molecular hydrogen by electrons produced in this process. The low yield and the remaining substrates from dark fermentation were used in a bacterial photosynthetic hydrogen production process.

Biomass conversion in biorefineries. A biorefinery is a facilitaty that combines

biomass conversion with production of fuels, powder and chemicals. Hydrogen and methane could be produced in two steps. By producing multiple products, a biorefinery could take advantage of biomass with different components and maximize the value from the biomass feedstock.

Chemical conversion of biomass to hydrogen. Hydrogen could also be produced from biomass in chemical ways, which are similar to coal gasification or steam reforming. In principle, one molecule of glucose could be steam reformed to produce 12 molecules of hydrogen in the presence of proper catalysts.

1.2.3 Hydrogen from water

Water is a clean and abundant source of hydrogen. Splitting water to produce hydrogen and oxygen for commercial use dates back to the 1890s[15]. Breaking water molecule to hydrogen and oxygen molecules requires energy input as water is very stable compared to hydrogen and oxygen. There are three major ways to produce hydrogen from water: electrolysis, thermolysis and photoelectrolysis[3,15].

1.2.3.1 Electrolysis

Though water electrolysis is not currently mainstream for hydrogen production, from a long-term perspective, producing hydrogen by electrolytic water splitting is viable in that it is simple, reliable, carbon-free and produces high purity hydrogen. It is historically important and plants have been built in several countries.

Three major methods currently under consideration for electrolytic hydrogen production are alkaline electrolysis, proton exchange membrane (PEM) electrolysis and ceramic oxide electrolysis.

Alkaline electrolysis.

An alkaline electrolysis cell usually contains two electrodes, an aqueous alkaline electrolyte and a microporous ion-conduction separator. The OH^- produced at cathode are transported to anode side and the H^+ remaining at cathode combine with electrons

to form hydrogen gas. The cathode is typically a metal coated with catalysts and the anode is usually a metal with a layer of oxide coating. For aqueous electrolyte, a ~30 wt% KOH or NaOH solution are commonly employed. The microporous ion-conducting separator allows the transit of OH⁻ and prevents the mixing of produced hydrogen and oxygen. Efficiencies of alkaline water electrolysis could reach 70%[13].

The electrolysis process is driven by the application of an external potential. During the process, a reduction reaction takes place at the negative electrode (cathode) and an oxidation reaction occurs at the positive electrode (anode) (see Figure 1.4).
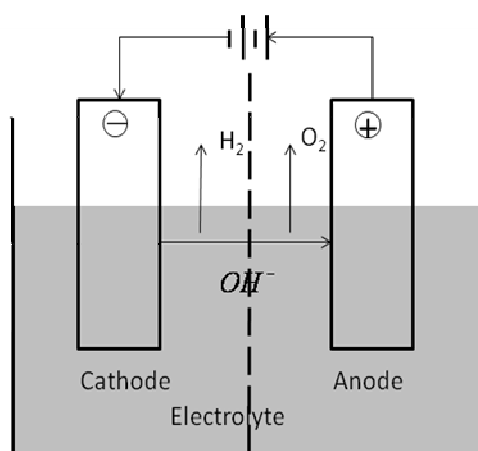
Figure 1.4 Alkaline electrolysis process[2,3].

The electrode reactions of alkaline electrolysis are as follows[2,15]:

At anode: $4H_2O + 4e^- \rightarrow 2H_2 + 4OH^-$

At cathode: $4OH^- \rightarrow 2H_2O + 4e^- + O_2$

Overall reaction: $H_2O \rightarrow H_2 + 1/2O_2$ $\Delta H = -288 \text{ kJ·mol}^{-1}$
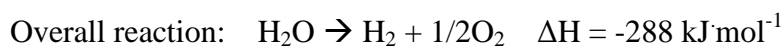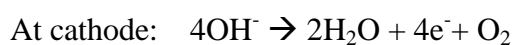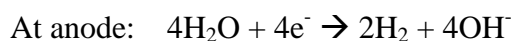
Proton exchange membrane (PEM) electrolyzer.[15,18,19].

A PEM electrolyzer typically involves a Nafion membrane which is proton-conducting and could separate hydrogen and oxygen at two electrodes. Water is split into protons and oxygen at the anode and the protons produced are transported to the cathode side via the Nafion membrane. The protons at cathode combine with electrons to form hydrogen gas. PEM electrolyzers could achieve efficiencies of

55–70%[15]. Reactions are as follows:

At anode: $2H_2O \rightarrow O_2 + 4H^+$

At cathode: $4H^+ + 4e^- \rightarrow 2H_2$

Overall reaction: $2H_2O \rightarrow O_2 + 2H_2$

Solid oxide electrolysis cells.

Solid oxide electrolysis cells (SOECs) are expected to provide the highest efficiency of electrolytic hydrogen production[20]. What is more, high temperature SOECs have a potential to be combined with high-temperature nuclear reactors to utilize the nuclear heat generated. The solid oxide cells operate at temperatures ranging from 750-1000°C[21].

The process of solid-oxide high temperature electrolysis of steam is the reverse reaction of the solid oxide fuel cell. Because the device is all solid state, it has a longer lifetime by avoiding the corrosion and evaporation caused by liquid electrolyte. And as the cell works at high temperature(800°C-1000°C), it needs lower ΔG and is not necessary to use expensive noble metals as its electrodes. In addition, the heat discharged by a system could also be utilized. The electrical efficiencies of solid oxide electrolyzers can be 85–90%[15].

The details of solid oxide electrolysis cells will be explained in detail in section 1.3.

1.2.3.2 Thermochemical hydrogen production

Water will decompose at 2500°C, but heat sources and stable materials at this temperature are not easily feasible[15]. Therefore, some methods to lower the temperatures have been developed. However, most of the proposals that reduced the temperature significantly require higher pressures and aggressive chemical systems. There are some main processes[15]:

Ispra Mark-10

$2H_2O + SO_2 + I_2 + 4NH_3 \rightarrow 2NH_4I + (NH_4)_2SO_4$ $T = 50^oC$

$2NH_4 + 2NH_3 \rightarrow H_2 + I_2$ $\qquad\qquad\qquad\qquad$ T = 630°C

Sulfuric acid decomposition:

$SO_2 + H_2O \rightarrow H_2O + SO_2 + 1/2O_2$

$2H_2O + Br_2 + SO_2 \rightarrow H_2SO_4 + 2HBr$

$2HBr \rightarrow Br_2 + H_2$

$2H_2O + I_2 + SO_2 \rightarrow I_2 + H_2$

ZnO/Zn:

$ZnO \rightarrow Zn + 1/2O_2$ $\qquad$ T = 1800°C

$Zn + H_2O \rightarrow ZnO(s) + H_2$ $\qquad$ T = 475°C
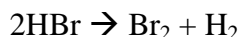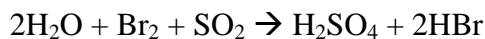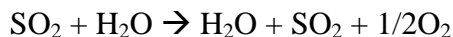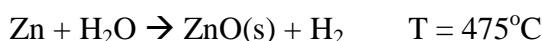
The overall efficiencies could reach 50% for these thermochemical processes[22]. But they are still not competitive compared to other hydrogen production technologies.

1.2.3.3 Water splitting with solar energy

There are three types of water splitting with solar energy: solar cell driving electrolysis, semiconductor photoelectrode and photoelectrolysis. Photoelectrolysis uses solar energy to directly split water to hydrogen and oxygen. The device converts solar energy to electricity via photovoltaic(PV) cells. Semiconductor materials are employed as photoanode and photocathode (commonly a p-n junction). The two photoelectrodes immersed in an aqueous electrolyte absorb solar energy and dissociate water. The target solar energy to hydrogen efficiency is >16%[3,15].

1.2.3.4 Conclusion

Electrolytic hydrogen is a very clean fuel, which is free from carbon and sulfur impurities. The high purity is an important necessity for proton-exchange membrane fuel cells. In the short term, it is costly compared to producing hydrogen from fossil

fuels. But from a long-term perspective, producing hydrogen by water splitting is viable in that it is simple, reliable, carbon-free and produces high purity hydrogen.

1.3 High Temperature Solid Oxide Steam Electrolysis cells

1.3.1 Theory background

1.3.1.1 Solid oxide steam electrolysis principles

The principle of a solid oxide oxide electrolysis cell is illustrated in Figure 1.5.

Solid oxide electrolysis reactions are reverse reactions of SOFC. When the SOFC runs backwards it works as a SOEC.
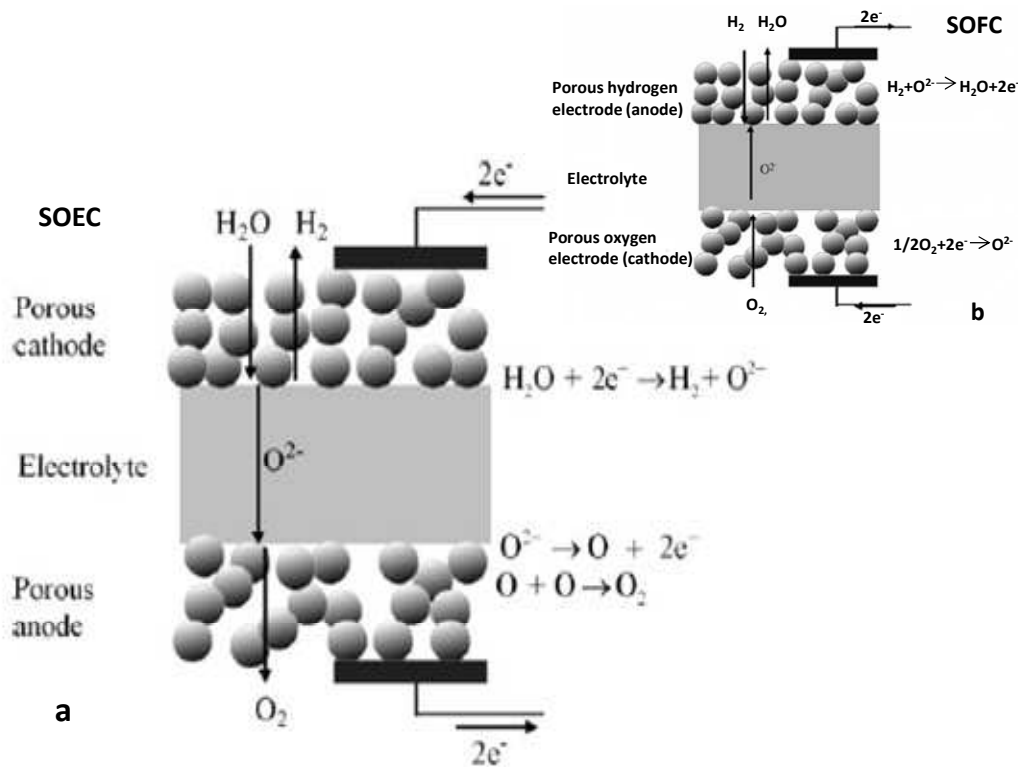
Figure 1.5 a. Process of Hydrogen production by a Solid Oxide Steam Electrolysis (SOSE) [23]; b. Process of a solid oxide fuel cell.

The chemical reactions in an solid oxide electrolysis cell are:

Cathode $H_2O\,(g) + 2e^- \rightarrow H_2\,(g) + O^{2-}$

Anode $O^{2-} \rightarrow 1/2O_2\,(g) + 2e^-$

Overall H_2O (gas, cathode) → H_2 (gas, cathode) + $1/2O_2$ (gas, anode)
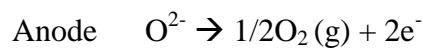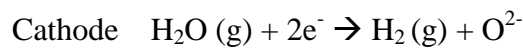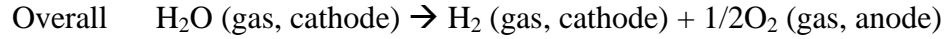
Using external electricity, the H_2O molecule splits to H^+ and O^{2-}, and H^+ combines with e^- to form H_2. The oxygen ions produced are transported through the electrolyte, which is an oxygen ionic conductor. At the anode, the O^{2-} transfers its charge to the anode, and combines with another O^{2-} to form O_2.

1.3.1.2 Energy Equation

The reaction can be expressed by:

$$H_2O(g) → H_2(g) + 1/2O_2(g)$$
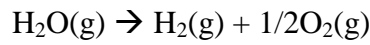
The equation of energy change is:

$$\Delta H = \Delta G + T\Delta S$$

Where T is absolute temperature; ΔH is enthalpy change; ΔS is entropy change; and ΔG is the Gibb's Free Energy, the maximum work for formation of water, or specifically the minimum work to split water. This energy equation can be seen in Figure 1.6.
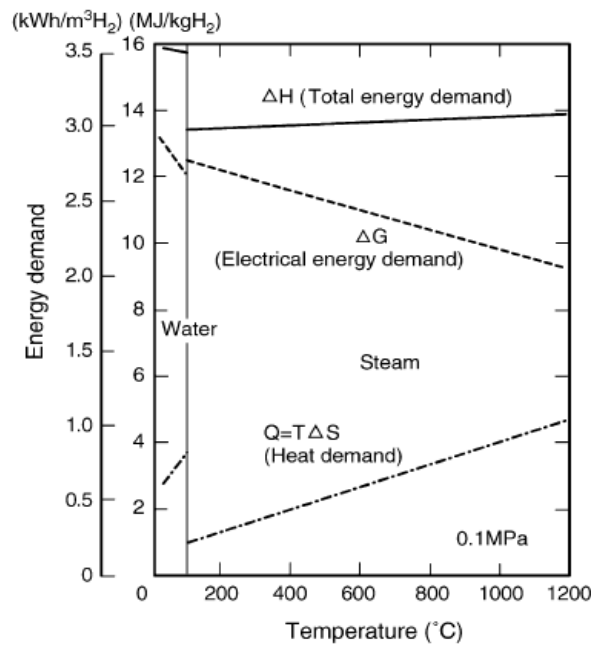
Figure 1.6 Energy demand for water and steam electrolysis[24].

The minimum demand for electrical energy, ΔG, decreases with increasing

temperature. In the gas phase, with temperature increasing, thermal energy (TΔS) provides a larger portion of the total energy demand (ΔH) and the electrical energy demand (ΔG) decreases. The decrease of electrical energy demand leads to higher electrical efficiency. High operating temperature also generally improves electrode reaction kinetics[25,26].

The total energy required for splitting water is given by[13]:

$H_2O \rightarrow H_2 + 1/2O_2$
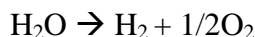
$\Delta H^o = 285.8$ kJ/mol at 25^oC;

The Gibbs free energy may also be impressed by

$\Delta G = -zEF = -2EF$.

z is the number of electrons involved in reaction; E is the reversible voltage of the cell (at equilibrium when the current is zero; also known as 'open circuit voltage'); F is the Faraday constant (charge on one mole electrons, F=96485 coulombs).

1.3.1.3 Nernst Equations and OCV

From the energy equation,

for

$H_2O(g) \rightarrow H_2(g) + 1/2O_2(g)$,
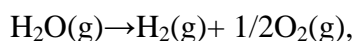
there is

$\Delta G = -zEF = -2EF$,

which can also be expressed by

$$E = \frac{\Delta G}{2F} = \frac{\Delta G^o}{2F} - \frac{RT}{2F} \ln \frac{(P_{H_2O}/P^o)}{(P_{H_2}/P^o)(P_{O_2}/P^o)^{\frac{1}{2}}} = E^o + \frac{RT}{4F} \ln \frac{(P_{H_2}/P^o)^2(P_{O_2}/P^o)}{(P_{H_2O}/P^o)^2}$$

Such equations, which give a potential in terms of product and reactant activity or partial pressure are known as Nernst Equations. The Nernst potential E, which is also known as the open circuit potential (OCV), is the voltage difference between the anode and the cathode under open circuit conditions. P_{O2} is the oxygen partial

pressure in the cathode gas. P_{H2} and P_{H2O} are respectively the partial pressures of hydrogen and steam in the anode gas. R is the gas constant, which equals 8.314 J K^{-1} mol^{-1} if pressure is in kiloPascals(kPa), volume is in litres(L), temperature is in Kelvin(K). T is the absolute temperature.

Over the temperature range between 500°C to 1500°C, E° for this reaction can be written as[27]:

$$E° = \frac{\Delta G°}{2F} = 1.29 - 0.000292(T - 273)$$

1.3.1.4 Polarisation

From the Nernst Equations we know that if the partial pressures of different species P_{H2}, P_{O2}, P_{H2O} are fixed regardless of the local current density, the Nernst potential, E, is not a function of current density. This assumption is only valid when the flow rate of each species is high enough that the gas components at anode and cathode are actually fixed. If it is not the case, E is a function of current density.
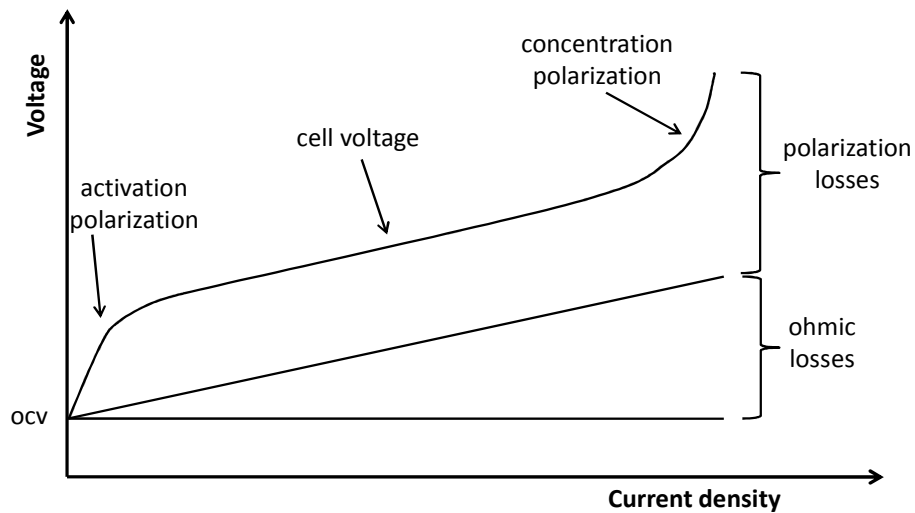
Figure 1.7 Schematic plot of voltage versus current density showing different types of polarizations.

With no potential load, the cell is reversible and works at OCV. With an applied potential the system becomes irreversible and there is a voltage loss known as

polarization or overpotential. The different polarization are termed: ohmic polarization, concentration polarization and activation polarization.

$$\eta = \eta_{ohm} + \eta_{conc} + \eta_{act}$$

Where η is the total cell polarization, η_{ohm} are the ohmic polarization, η_{conc} is the concentration polarization, η_{act} is the activation polarization (see Figure 1.7).

Activation polarisation is usually dominant at low current densities, while concentration polarization is usually dominant at high current densities when the transport of reactive species to the electrolyte/electrode interface becomes a limiting factor for the cell reaction.

(1) η_{ohm}

All materials (except superconductors) have a resistance to the movement of electrical charge. The linear relationship between voltage drop and current density is a material property which can be described by resistivity. The ohmic losses, also called resistance polarization, are electrical resistance of the electrical contacts, interconnections, lead wires, and electrodes, as well as the ionic resistance of the electrolyte. The ohmic polarization at a given current density can be expressed by:

$$\eta_{ohm} = (\rho_e l_e + \rho_a l_a + \rho_c l_c + R_{contact})\, i$$

Where η_{ohm} is the ohmic polarization, ρ_e, ρ_a and ρ_c are the resistivities of electrolyte, anode and cathode, l_e, l_a and l_c are the thicknesses of electrolyte, anode and cathode. $R_{contact}$ refers to any contact resistance. i is the current density.

The ohmic polarization shows a linear response and expressed by:

$$\eta_{ohm} = ir$$

Where i is the cell current density; r is the area resistance of the cell[21,28].

The ohmic resistance of electrolyte corresponds to the transportation of oxide ions through YSZ electrolyte; ohmic resistances of electrodes are correlated with the transportation of electrons through electrodes. Other components generally have much higher conductivity than the electrolyte. Therefore, the ohmic losses can be roughly equal to the electrical resistance of electrolyte.

(2) η_{conc}

The reactants and products are all gaseous. As the reactions occur at a three-phase boundary (TPB), the reaction species need to be transported from the surfaces of electrodes to the electrode/electrolyte surfaces and the products need to leave. Cathode processess involve diffusion, adsorption, chemical reaction, surface diffusion, and desorption. One possible scheme is that steam is dissociated to O^{2-} and H^+ at cathode/electrolyte interface where the produced O^{2-} could be transported through YSZ electrolyte to the anode side to form oxygen gas. It is also possible that some intermediates are produced at gas/cathode boundary during water splitting and diffuse to the cathode/electrolyte surface for further reactions. H^+ remaining at cathode combines with electrons to form hydrogen. The produced hydrogen and oxygen gases must be transported away from the cathode/electrolyte and anode/electrolyte interfaces respectively. The concentration polarization is caused by the resistance to the transport of reactant and product species. The concentration polarization is affected by the diffusivities of gases, the porous electrode microstructure, the partial pressures of species.

η_{conc} = f (Diffusivity, Microstructure, Partial Pressures, Current Density)

The concentration polarizations can be generally expressed by:

$$\eta_{conc} = \frac{RT}{zF}\ln(1-\frac{i}{i_l})$$

Where i_l is the limiting current density at which the steam is used up at a rate equal to its maximum supply speed and is a function of the diffusivity of the gas and the partial pressure. It is non-linear to current[21,28,29].

(3) η_{act}

The activation polarization is related to the electrode kinetics at the reaction site. It represents the overpotential due to the activation necessary for charge transfer[28]. It is highly dependent on the charge transfer mechanism and electrocatalysis at the three phase boundaries.

In general, the activation polarization is in function of material properties,

microstructure, temperature, atmosphere and current density.

η_{act} = f (material properties, microstructure, temperature, atmosphere, current density)

A relation between activation polarization and current density is given by Butler-Volmer equation. When the current density is high, the Butler-Volmer equation can be written as:

$$\eta_{act}^c \approx \frac{RT}{\beta zF}\ln i_o^c - \frac{RT}{\beta zF}\ln i \approx a + b\ln i$$

This equation is also known as Tafel equation. where i_o is the exchange current density, which can be affected by several factors：

i_o = f (TPB, partial pressure of oxygen in the atmosphere, oxygen vacancy concentration in the electrolyte, oxygen vacancy mobility in the electrolyte, electron concentration in the electrocatalyst, and temperature)[29].

1.3.1.5 SOEC Advantages and disadvantages

Comparing with other methods of producing hydrogen in section 1.2, the high temperature solid oxide electrolysis has advantages:

- High efficiency
- Carbon free
- Produce high purity hydrogen
- Small-scale and responsive
- Potential to utilize solar concentrator and geothermal heat and nuclear heat generated by nuclear reactors
- All solid state device, long lifetime

However, it has some drawbacks that need to be overcome:

- High operating temperature
- Fragile ceramic components[30]
- High electrode polarization

1.3.2 SOEC components

1.3.2.1 Electrolyte

The electrolyte of an SOEC serves as an ionic transporter between two electrodes. As the electrolyte is solid state, the cell may be cast into different shapes such as tubular and planar. The electrolyte material for high temperature SOECs must be stable in both oxidizing and reducing environments at high temperatures. It also required to possess high ionic conductivity and low electronic conductivity at operating temperatures. Moreover, it needs to be able to be made into thin but strong and nonporous films. Nowadays, Y_2O_3-stabilized ZrO_2, with a fluorite structure, is the most favoured material for SOEC electrolyte as it exhibits good thermal and chemical stability, high oxide-ionic conductivity, and mechanical strength at high temperature[29,30,33].

The fluorite structure is a face centered cubic arrangement of cations with a cubic arrangement of anions in the center[31] (see Figure 1.8). At high temperatures, the zirconia (ZrO_2) has a cubic fluorite structure which could be stabilized to lower temperatures by substitute Zr^{4+} with divalent or trivalent larger cations such as Ca or Y. Doping lower valence cations could also introduce defects. When Zr^{4+} are substituted by lower valence cations, the concentration of oxygen ions would decrease to maintain electroneutrality. Thus, oxygen vacancies and therefore oxide-ionic conductivity are introduced. Sufficient dopants are required for stabilizing the cubic structure. About 8~9 mol% Y_2O_3 is needed for zirconia cubic structure stabilization[29].
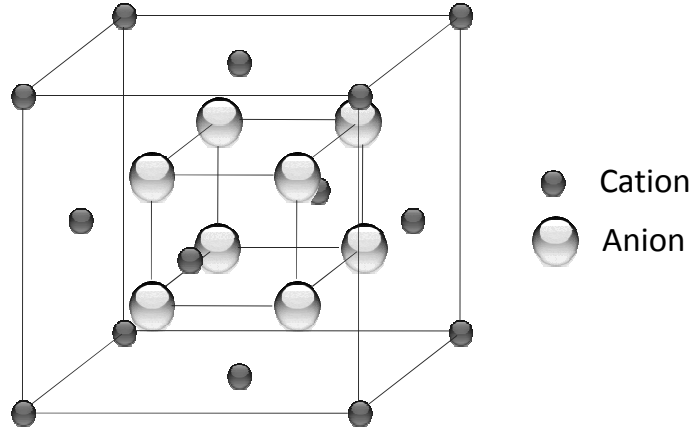
Figure 1. 8 The cubic fluorite structure[31].

The dissolution of yttria into the fluorite phase of ZrO_2 can be expressed by:

$$Y_2O_3(ZrO_2) \rightarrow 2Y'zr + 3O_o^x + V_o^{\cdot\cdot}$$
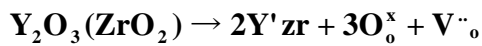
Each Y_2O_3 creates one oxygen vacancy.

1.3.2.2 Anode

Reaction at anode:

$O^{2-} \rightarrow 1/2O_2\,(g) + 2e^-$.
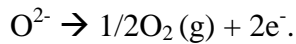
The most important properties that high temperature SOEC anode needs to possess are: electronic conductivity, catalytic activity for anodic reaction, and compatibility with electrolyte material. Noble metals such as platinum could be used as the anode material but is not practical in cost-effective commercial cells due to its high cost. Some metal oxides have the required properties for SOEC anode but are much less expensive.

Strontium-doped lanthanum manganite (LSM), which shows a good performance in SOFC as a cathode when YSZ is used as an electrolyte[32,34], is a commonly favorable material for SOEC anodes. Pure $LaMnO_3$ shows orthorhombic structure or rhombohedral structure[29]. When La^{3+} is substituted by lower valence cations such as

Sr^{2+} and Ca^{2+}, the amount of Mn^{4+} increases and therefore the oxygen content increases. And the transformation temperature is eventually reduced. Sr doped $LaMnO_3$ (($La_{1-x}Sr_x$)MnO_3) shows cubic perovskite structure at high temperatures.

The $LaMnO_3$ based perovskites have electrical conductivity of above 10 S·cm^{-1} at 700^oC[29]. The electrical conductivity originates from the valence change of Mn. Mn^{4+} content is increased when the $LaMnO_3$ is doped with lower valence cations such as Sr^{2+}, thus the electrical conductivity is enhanced.

$$(La_{1-x}Sr_x)MnO_3 \sim La_{1-x}^{3+} + Sr_x^{2+} + Mn_{1-x}^{3+} + Mn_x^{4+} + O_3$$
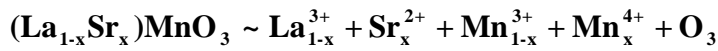
Another interesting property of $LaMnO_3$ based perovskite structure is its nonstoichiometry of oxygen and therefore the oxygen vacancies[29,35]. Figure 1.9 shows the oxygen defect and excess regions of $LaMnO_3$. Oxygen-excess shows up at high oxygen partial pressure, and oxygen-defect (which would supply oxygen vacancies) is exhibited when oxygen partial pressure is low.
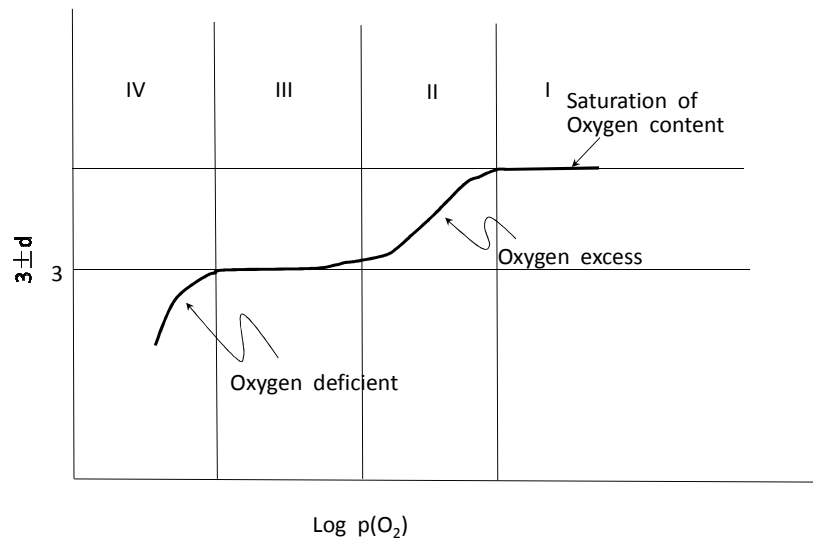
Figure 1.9 . Schematic representation of oxygen nonstoichiometry of LaMnO$_{3\pm d}$ as a function of oxygen partial pressure[29].

1.3.2.3 Cathode

Reaction at cathode:

H_2O (g) + 2e$^-$ → H_2 (g) + O^{2-}
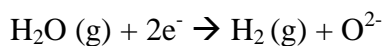
For cathode of high temperature SOECs, the material should have catalytic activity for water splitting which is necessary for the kinetics of the reaction. Besides, the cathode is required to have ionic conductivity which allows the transportation of oxygen ions to the anode/electrolyte border. In addition, the cathode material has to be electrical conductivity in order to convey the electrons produced at cathode to the outside circuit.

One of the possible reaction schemes at cathode could be:

1. Adsorption of H_2O molecule to the surface of cathode, which is also the electrocatalyst.

   $H_2O(gas) \rightarrow H_2O(cathode)$

2. Surface diffusion of adsorbed H_2O to the three phase boundary (TPB)

   $H_2O(cathode) \rightarrow H_2O(TPB)$

3. Electrochemical reaction at TPB

$$\mathbf{H_2O(TPB) + 2e^- (cathode) + V_O^{\cdot\cdot}(electrolyte) \rightarrow H_2(TPB) + O_o^x(elextrolyte)}$$
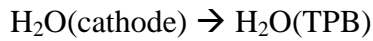
Reactions take place at the three phase boundary (TPB) where the electrolyte, electrocatalyst and gas reactants meet. Water is fed into porous cathode side and dissociated into H^+ and O^{2-} at the three phase boundary where electrocatalyst is available. Oxygen ions produced are transported across YSZ electrolyte to anode side via the oxygen vacancies in electrolyte. Hydrogen ions remaining at cathode side combine with electrons supplied by electronic conducting cathode to form hydrogen gas and diffuses out of the electrode (see Figure 1.10).
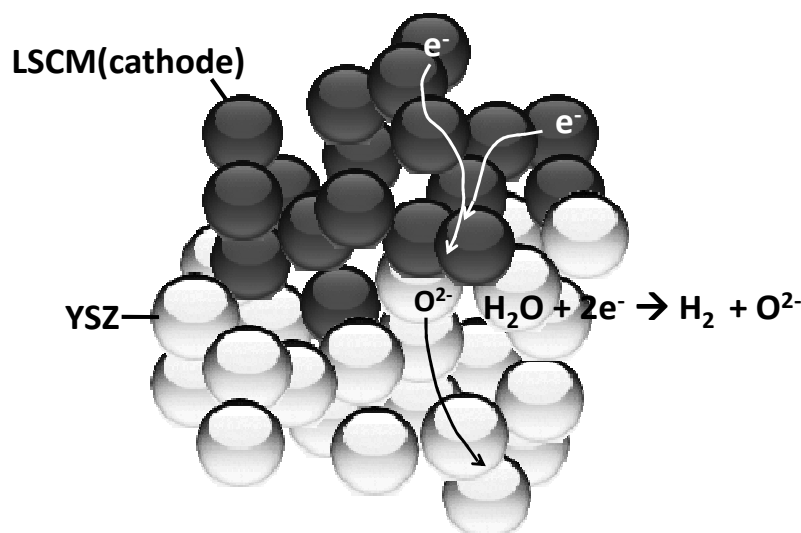
Figure 1.10 Schematic cathode reactions at three phase boundary in a SOEC with YSZ electrolyte and LSCM cahtode. The reactive sites are the contact zones of the two conducting phases which are accessible to gases through the pores.

Reactions in SOECs are the reverse reactions in SOFCs. If a SOFC runs backwards, it works as a SOEC. In high temperature SOFCs, several materials have attracted attention as anode materials. Platinum, as some other noble metals, which is stable at high temperatures and has high catalytic activity on electrode processes as well as electronic conductivity[36], is expensive and may bond with the electrolyte[29]. Nickel metal is high in catalytic activity and low in cost, but it has evidently thermal mismatch to Stabilized Zirconia[37]. A cermet which has the nickel catalytic activity and proper thermal match with the ceramic, is produced by mixing nickel metal with a ceramic support. Nickel cermet, a porous composite of Ni and YSZ, is the currently favoured cathode material for SOEC cathode. The perovskite $(La_{0.75}Sr_{0.25})_{0.95}Mn_{0.5}Cr_{0.5}O_3$ (LSCM) is an active and redox-stable material and has attracted a lot of attention in the high temperature solid oxide fuel cell field[38-41].

And the anode materials of SOFCs could be the candidates for cathode materials for SOECs. Platinum is not a cost-effective SOEC cathode material due to its high price. Ni/YSZ cermet is currently preferred cathode material for high temperature solid oxide electrolysis system due to its excellent catalytic properties and good current collection. But Ni cermets do display some disadvantages, such as low

tolerance to oxidizing condition and reduction of TPB due to agglomeration after long operation and poor redox cycling causing volume instability[41]. It requires a significant concentration of H_2 flowing over it, if it is not to be oxidized to NiO. Lack of reducing atmosphere would not only cause a loss of electronic conductivity but is also likely to lead to mechanical failure of the electrode[42]. LSCM has attracted much attention as an SOFC anode material or as anode/cathode material for a symmetrical SOFCs[43,44,45]. Nevertheless, LSCM has not been reported as a possible cathode for high temperature solid oxide steam electrolysis cells, which work with high temperature steam and under external potential load.

LSCM.

Perovskite-related material, $(La_{0.75}Sr_{0.25})_{0.95}Mn_{0.5}Cr_{0.5}O_3$ (LSCM), has been reported for its remarkable stability with reduction or oxidation occurring at high temperature, say 900^oC[44]. The A-site deficiency in $(La_{0.75}Sr_{0.25})_{0.95}Mn_{0.5}Cr_{0.5}O_3$ has been questioned[65]. It also shows chemical compatibility with yttria-stabilized zirconia to at least $1300°C$[41]. It has been reported to be able to work effectively for both cathode and anode operation in a symmetrical reversible SOFC[44]. This character enables LSCM to work as a cathode material in an high temperature solid oxide steam electrolysis cell.

Introduction of alkaline earth and first series transition metal elements into $LaCrO_3$ has been shown to improve promote the catalytic properties for methane reforming[46]. The electrochemical properties and electrochemical performance of LSCM catalyst in SOFC have been reported[41,47]. Some other substitutions such as Fe at B-site are more commonly used for steam reforming.

In general, a minimum electronic conductivity of 1 S/cm is required to minimize the ohmic loss. The transitions of Mn^{3+} to Mn^{4+} and Cr^{3+} to Cr^{4+} provides high conductivity.

$$\frac{1}{2}O_2 + V_O^{\cdot\cdot} + 2Mn_{Mn}^X = 2Mn_{Mn}^{\cdot} + O_O^X$$
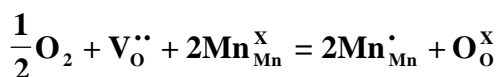
$Mn_{Mn}^{\cdot}$, the charge carrier for p-type conduction, would be reduced at low oxygen

partial pressure, and therefore the conductivity. Figure 1.11 shows the conductivity of LSCM versus oxygen partial pressure. When P_{O2} is in the range of $10^{-8} \sim 10^{-16}$ atm, conductivity of LSCM increases with oxygen partial pressure increase. When $P_{O2} > 10^{-8}$, the conductivity changes little. In reducing atmosphere, LSCM conductivity will be lowered. At 900°C, its total conductivities are about 38.6 S/cm in air and 1.49 S/cm in 5% H_2 ($p_{O2} \sim 10^{-21}$ atm)[41].
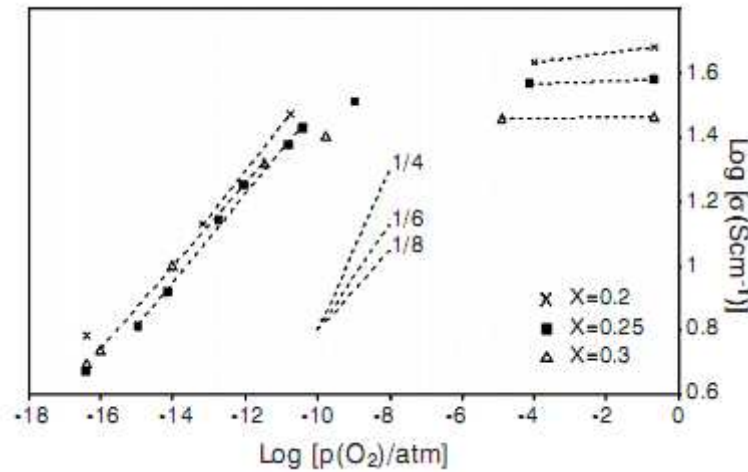
Figure 1.11 Log(σ) vs. log(p_{O2}) for La$_{1-x}$Sr$_x$Cr$_{0.5}$Mn$_{0.5}$O$_{3\pm\delta}$[64].

1.3.2.4 SOEC designs

Research on high temperature solid oxide electrolysis for hydrogen production has been carried on in several groups in the world. For most of the work, cells were made with LSM anode, YSZ electrolyte and Ni/YSZ cermet cathode[48-50]. Proton conducting ceramic has been used as an electrolyte at lower temperatures in some groups[51,52]. Stacks have been developed in a number of groups such as the Idaho National Laboratory in the US and the Risø DTU in Denmark. Some of the water electrolysis were carried out by coelectrolysis of steam and carbon dioxide to produce syngas (H_2 + CO)[53-55]. And some are the electrolysis only of water[42,56-58].

Anode	electrolyte	cathode	SOEC design	Electrolysis mode

LSM	Ionic conductor (YSZ)	Ni/YSZ	Planar	Coelectrolysis
LSF	Proton conductor	Noble metal	Tubular	Steam electrolysis
		LSCM	Stake	

1.4 Catalysis

1.4.1 Principle of Catalysis

Catalyst is a chemical substance by which the rate of the reaction is increased or decreased. Catalyst may participate in multiple chemical processes but is not consumed by the reaction itself. Positive catalyst works by providing a different transition state with lower activation energy (see Figure 1.12). The overall thermodynamics and the final results are not changed by catalysts.
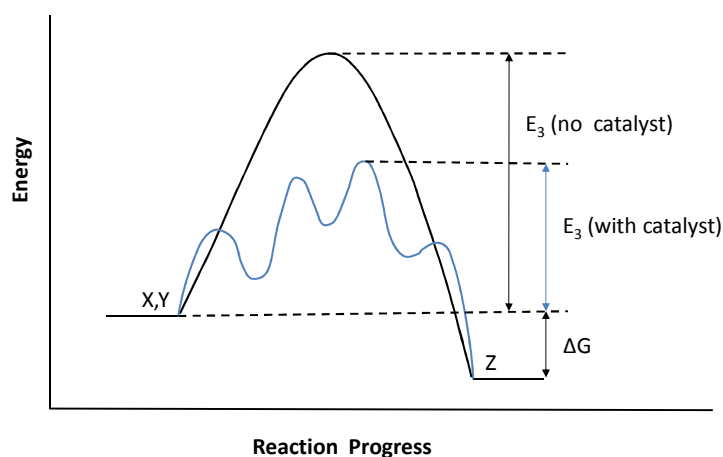
Figure 1.12 Principle energy diagram of catalysis.

Reagents are adsorbed on the surface of solid catalyst before catalysis process takes place. Reactions happen on the exterior surface of the solid catalyst. The diffusion and adsorption of reactants onto the surface is a necessity for the chemical reactions on the surface which are followed by the desorption and diffusion of products from the surface. The process of a reaction with catalyst can be illustrated in Figure 1.12.
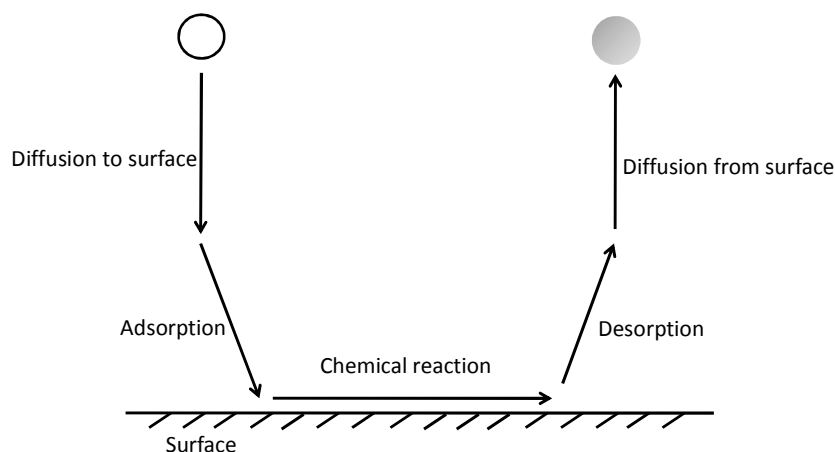
Figure 1.12 Schematic steps of a catalysis process on surface[59,63].

1.4.2 Perovskite Catalysts

Oxides play an important role in catalysis. In SOEC, they can work as active components themselves and as supports for active materials[60]. It has been reported that materials with mixed electronic and ionic conductivity could accelerate the methane oxidation[46].
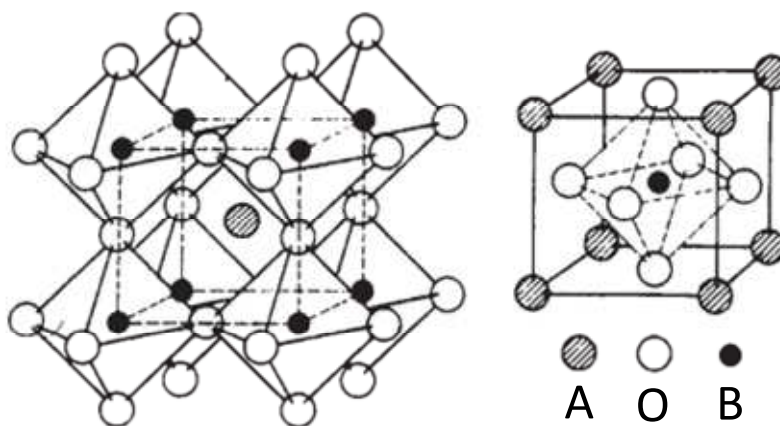
Figure 1.13 ABO$_3$ perovskite structure[61].

Perovskites (ABO$_3$), containing A^{m+} and B^{n+} cations, is a structure has potential to be partially substituted with a wide range of ions at both A and B sites[60]. The substitution of ABO$_3$ with alkali earth elements on the A sites and transition metal elements on the B sites allows modification of electronic and catalytic behaviors[62]. Perovskites with mixed electronic and ionic conductivities are considered to promote

oxidation reactions[62].

1.4.3 Metal catalysts

Metals have been widely used in catalysis. Ni, Pt, Pd and Rh are the most frequently used in heterogeneous catalysis[60]. Metal catalysts such as iron and ruthenium are used for synthesis of ammonia, palladium for hydrogenation and hydrogenolysis, platinum for hydrocracking of oil, and nickel for partial saturation of oils[59].

Catalytic reactions happen at catalyst surfaces. Electronic structures of metal atoms on surfaces affect the interaction between catalyst and reactants. The unsaturated coordination of metal atoms on catalyst surfaces allows available d orbits to accept electrons. Metal catalysts are usually transition metals rather than alkali earth metals or alkali metals.

References

1. V. Utgikar, and T. Thiesen, *Int. J. Hydrogen Energy,* 2006, 31, 939.

2. R. M. Dell, D. A. J. Rand, *Clean energy*, Cambridge : Royal Society of Chemistry, 2004.

3. R. M. Dell, D. A. J. Rand, *Hydrogen energy : challenges and prospects*, Cambridge : Royal Society of Chemistry, 2008.

4. The National Academies, *The Hydrogen Economy Opportunities, Costs, Barriers and R & D Needs*, The National Academies Press, Washington, D.C., 2004.

5. D. J. Wuebbles and K. J. Atul, *Fuel Process. Technol.*, 2001, 71, 99.

6. B. Wang, W. Wan, and J. Wang, *Bioresour. Technol.*, 2009, 100, 1211.

7. *GE Global Research's Hydrogen Electrolyzer Receives Popular Mechanics 2006 Breakthrough Award*, 5 Oct 2006.

8. Hydrogen, from Wikipedia, *http://en.wikipedia.org/wiki/Hydrogen*, 2009.

9. I. K. Kapdan, F. Kargi, *Enzyme Microb. Technol.*, 2006, 38, 569.

10. M. Momirlan, T.N. Veziroglu, *Renew. Sustain. Energy. Rev.*, 2002, 6, 141.

11. M. Ni, M. K. H. Leung and D. Y. C. Leung, *Int. J. Hydrogen Energy*, 2008, 33, 2337.

12. Hydrogen Storage, from Wikipedia, *http://en.wikipedia.org/wiki/Hydrogen_storage*, 2009.

13. M. Balat, *Int. J. Hydrogen Energy*, 2008, 33, 4013.

14. R. Kothari et al., *Renew. Sustain. Energy. Rev.*, 2008, 12, 553.

15. J.D. Holladay et al., *Catal. Today*, 2009, 139, 244.

16. M. Momirlan, T. N. Veziroglu, *Renew. Sustain. Energy. Rev.*, 1999, 3, 219.

17. P. Westermann et al., *Int. J. Hydrogen Energy*, 2007, 32, 4135.

18. National Academy of Science, *The Hydrogen Economy: Opportunities, Costs, Barriers, and R&D Needs*, National Academies Press, Washington, DC, 2004.

19. J.D. Holladay, J. Hu, D.L. King, Y. Wang, *Catal. Today*, 2009, 139, 244.

20. H. Uchida, N. Osada, and M. Watanabe, *Electrochem. Solid-State Lett.*, 2004, 7, A500.

21. K. L. Eccleston, *PhD thesis,* St Andrews, 2006.

22. J.E. Funk, *Int. J. Hydrogen Energy*, 2001, 26, 185.

23. M. Ni, M. K. H. Leung, and D. Y. C. Leung, *Chem. Eng. Technol.*, 2006, 5, 29.

24. R. Hino, K. Haga, H. Aita, and K. Sekita, *Nucl. Eng. Des.*, 2004, 233, 363.

25. A. Momma, T. Kato, Y. Kaga, and S. Nagata, *J. Ceram. Soc. Jpn.*, 1997, 105, 398.

26. K. Eguchi, T. Hatagishi, and H. Arai, *Solid State Ionics*, 1996, 86-88: 1245.

27. M. V. Perfiliev, *Int. J. Hydrogen Energy*, 1994, 19, 227.

28. J. R. Ferguson, J. M. Fiard, R. Herbin, *J. Power Sources*, 1996, 58, 109.

29. S. C. Singhal and K. Kendall, *High Temperature Solid Oxide Fuel Cells (Fundamentals, Design and Applications)*, Elsevier Ltd, 2003.

30. U.S. Department of Energy, *Fuel Cell Handbook(Seventh Edition)*, by EG&G Technical Services, Inc., 2004.

31. J. B. Goodenough, *Annu. Rev. Mater. Res.*, 2003, 33, 91.

32. M. Juhl, S. Primdahl, C. Manon, and M. Mogensen, *J. Power Sources*, 1996, 61, 173.

33. S. Srinivasan, *Fuel Cells - From Fundamentals to Applications*, Springer Science & Business Media, LLC, 2006.

34. S. P. Jiang, *J. Mater. Sci.,* 2008, 43, 6799.

35. F. W. Poulsen, *Solid State Ionics*, 2000, 129, 145.

36. H. H. Mobius, *J. Solid State Electrochem.*, 1997, 1, 2.

37.   S. Primdahl, B. F. Sørensen, and M. Mogensen, *J. Am. Ceram. Soc.*, 2000, 83, 489.

38. *Electrochemical Measuring Method (in Chinese)*. Beijing, Peking U. Press, 1995.

39. A.G. King,*Ceramic Technology and Processing*. New York: William Andrews Publishing, 2002.

40. *Print Process Descriptions*: Printing Industry Overview: Screen Printing, http://www.pneac.org/printprocesses/screen/, 2009.

41. S. W. Tao and T. S. I. John, *J. Electrochem. Soc.,* 2004, 151, A252.

42. X. D. Yang and J. T. S. Irvine, *J. Mater. Chem.,* 2008, 18, 2349.

43. S. W. Tao and J. T. S. Irvine, *Nat. Mater.*, 2003, 2, 320.

44. D. M. Bastidas, S. W. Tao, and J. T. S. Irvine, *J. Mater. Chem.*, 2006, 16, 1603.

45. S. P. Jiang, X. J. Chen, S. H. Chan, J. T. Kwok, K. A. Khor, *Solid State Ionics*, 2006, 177, 149.

46. J. Sfeir, R. Vasquez, J. V. Herle and K. R. Thampi, *J. Catal.*, 2001, 202, 229.

47.   S. W. Tao, J. T. S. Irvine, and J. A. Kilner, *Adv. Mater.*, 2005, 17, 1734.

48. A. Hauch, S. D. Ebbesen, S. H. Jensen and M. Mogensen, *J. Mater. Chem.*, 2008, 18, 2331.

49. C. M. Stoots, J. E. O'Brien, J. S. Herring, K. G. Condie, and J. J. Hartvigsen, *Proceedings of the 4th International Topical Meeting on High Temperature Reactor Technology*, Washington, DC USA, September 28-October 1, 2003.

50. J. S. Herring, J. E. O'Briena, C. M. Stootsa, G. L. Hawkesa, J. J. Hartvigsen, and M. Shahnam, *Int. J. Hydrogen Energy,* 2007, 32, 440.

51. H. Matsumoto, M. Okubo, S. Hamajima, K. Katahira and H. Iwahara, *Solid State Ionics,* 2002, 152-153, 715.

52. T. Sakai, S. Matsushita, H. Matsumoto, S. Okada, S. Hashimoto, T. Ishihara, *Int. J. Hydrogen Energy*, 2009, 34, 56.

53. S. H. Jensen, P. H. Larsen, and M. Mogensen, *Int. J. Hydrogen Energy*, 2007, 32, 3253.

54. Z. Zhan, W. Kobsiriphat, J. R. Wilson, M. Pallai, I. Kim, and S. A. Barnett, *Energ. Fuel.*, 2009, 23, 3089.

55.   J. B. Goodenough, *Rep. Prog. Phys.*, 2004, 67, 1915.

56. A. Brisse, J. Schefold, and M. Zahid, *Int. J. Hydrogen Energy*, 2008, 33, 5375.

57. A. Hauch, S. H. Jensen, S. Ramousse, and M. Mogensena, *J. Electrochem. Soc.*, 2006, 153, A1741.

58. S. Herring et al.., 2005 DOE Hydrogen, *Fuel Cells & Infrastructure Technologies Program Review*, 2005.

59. J. M. Thomas and W. J. Thomas, *Principles and practice of Heterogeneous Catalysis*, Wiley-VCH, 1997.

60. G. Ertl, H. Knozinger, F. Schuth, and J. Weitkamp, *Handbook of Heterogeneous Catalysis*, Wiley-VCH, 2008.

61. J. B. Goodenough, *Rep. Prog. Phys.,* 2004, 67, 1915.

62. E. S. Raj, J. A. Kilner, and J. T.S. Irvine, *Solid State Ionics,* 2006, 177, 1747.

63. Hermenegildo de A.L.Viana, *PhD thesis,* St Andrews, 2007.

64. S. M. Plint, P. A. Connor, S. Tao, and J. T.S. Irvine, *Solid State Ionics*, 2006, 177, 2005.

65. S. Tao and J. T. S. Irvine, *Chem. Mater.*, 2006, 18, 5453.

Chapter 2 Experimental

2.1 Fabrication of electrolysis cells

Electrolysis cells with different cathodes were fabricated in different ways. Typical solid oxide electrolysis cells (SOECs) with 2mm thick YSZ electrolyte were fabricated for initial tests. Thereafter, several ways have been tried to decrease electrolyte thicknesses and to improve electrode microstructure to enhance cell performances.

2.1.1 Cells with 2mm YSZ electrolytes
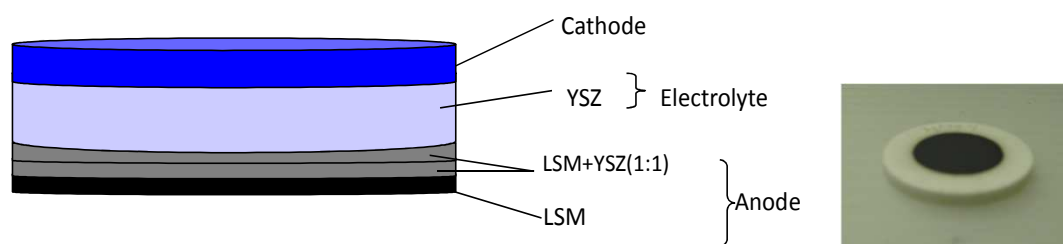
Figure 2.1. a. Structure of a SOEC with 2mm YSZ electrolyte; b. photo of a SOEC with 2mm pressed YSZ electrolyte.

2.1.1.1 Electrolyte preparation

Approximately 3.7g 8% commercial YSZ (P$_1$-kem) powder was uniaxially pressed at a pressure of approximately 1.5 tons/cm^2, using 2.5mm discs in stainless steel pellet dies to form pellets. The mass of powder was weighed on an electronic balance. The powder was then grounded using a pestle and put in the die. A small depression in the centre of the powder was formed using a stainless steel column before pressing in order to avoid uneven compaction due to the friction between the powder and the die walls. Uneven compaction can lead to cracks and inner fracture in the sintered pellet. The pellets pressed were placed on an alumina plate and then sintered at 1500°C for 10 hours, with a raising rate of 1°C per minute[1].

2.1.1.2 Electrode preparation

The electrode is made by firing electrode ink which is applied on YSZ electrolyte. Commercial LSM and CGO powders from Praxair company and LSCM powder from EMPA company were used in electrodes.

Ink preparation.

Ball milling is a method that can be used to grind chemicals to a finer consistency. It is often useful to grind chemicals in order to increase their surface area and make mixtures more homogenous[2].

An exact mass of electrode materials was weighed out (total mass of materials was 10 grams) with 0.2 gram of polyester/polyamide copolymer KD-I dispersant, which helps to enhance the consistency of the ink. The mixed powder was put in a plastic bottle with fixed number of ceramic balls. Acetone was then added to the bottle until just covering the balls. The bottle was put on a roller ball milling machine for a fixed period of time at 28 volt to mill the powder.

The mixture was then poured into a 250ml beaker with 5.4g medium (Johnson Matthey Direct Screen Medium Batch P05AP24). Acetone was added to about 1/3 volume of the beaker and then the mixture was stirred on a electromagnetic plate for about 3 days to evaporate acetone to form ink.

Screen printing.

Screen printing consists of three elements: the screen which is the image carrier, the blade, and ink. The screen printing process uses a porous mesh stretched tightly over a frame made of metal. Proper pressure is essential for accurate ink registration. The mesh is made of porous fabric. A stencil is produced on the screen, defining the image to be printed[3].

Electrode ink was applied to the substrate by placing the screen over the pellet. Ink with a paint-like consistency was placed onto the top of the screen. The ink was then forced through the fine mesh openings using a blade that was drawn across the screen, applying tension to force the ink through the open areas of the screen. Ink will pass through only in areas where no stencil was applied, thus forming an image on the

pellet. The diameter of the threads and the thread count of the mesh will determine how much ink was deposited onto the substrates (see figure 2.2).

The screen printing process was repeated several times on each electrode for enough electrode thicknesses. The printed electrodes were dried in 90°C for about 20 minutes before next printing. The samples should be kept away from dust during the whole process. For LSM anode, two layers of LSM/YSZ (50% LSM by weight) ink were printed next to the YSZ pellet, and one layer of pure LSM ink was then printed. For cathode, generally three layers of ink were screen printed.
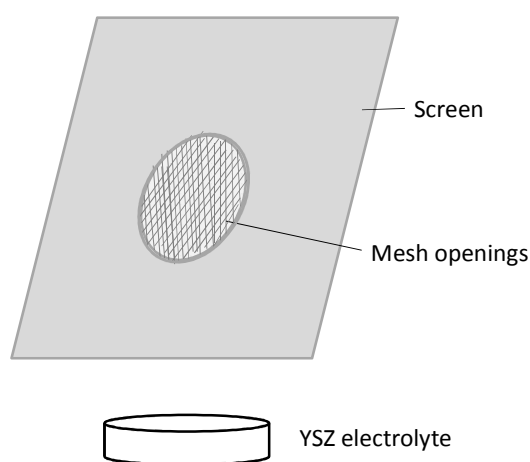
Figure 2.2. Schematic of screen printing.

Sintering electrodes.

The screen printed electrodes are sintered in order to combine together and to adhere to electrolyte. The electrode with higher sintering temperature was calcined first. In the electrode sintering process, the increasing rate was 2°C per minute for temperatures from 50°C to 500°C and was 3°C per minute for temperatures above 500°C. Sintering temperatures for different materials are:

Electrode Material	Sintering Temperature
LSM, LSM/YSZ (Anode)	1250°C for 3h
NiO/YSZ	1300°C for 5h
LSCM	1200°C for 2h

LSCM/YSZ	1200°C for 2h
LSCM/NiO	1300°C for 3h
LSCM/CGO	1300°C for 1h

Table 2.1   Sintering temperatures for electrode materials.

2.1.2 Cells with ~250 micron YSZ electrolytes

Cells with thinner YSZ electrolyte disks (~250 micron thickness) were also made. These were prepared similarly to the thick ones except by cutting and polishing the pressed and sintered YSZ pellet with a diamond blade to ~250 micron thickness electrolytes.

First, YSZ thick pellets were prepared in the same way as preparing 2mm YSZ discs. The thick die was then fixed to a cutting machine with diamond blade. The distance between the blade and the sample edge was adjusted to the thickness required. Cooling fluid was added till the blade was dipped in the liquid. The die was cut at a lower speed on the edge and higher speed later. The cut thin YSZ pellet was polished by sand paper to get an appropriate thickness and smooth surface.

2.1.3 Tape-cast and impregnated cells

Cells with LSCM cathode and LSF anode were also prepared by tape casting and impregnation methods. The first step of preparing this cell was to make a YSZ backbone, by casting three YSZ tapes, two with and one without graphite pore formers, and then laminating them together[4, 5].

Tape casting is an easy and low cost way to fabricate thin and flat ceramic sheets and multilayer structures mainly for the electronic industry[6]. Tape casting process basically involves preparing a suspension consisting of the ceramic powder in a solvent, with addition of dispersants, binders and plasticizers. This suspension is then cast to a tape moving at a fixed speed. The tape with solvents is then dried in air and could be cut to an appropriate shape[7, 8]. The dispersant controls the stability of the slips, and the binder and plasticizer are responsible for proper strength and flexibility

to the tape, respectively[9] (see figure 2.3).The detailed process is: 30 g YSZ powder with acetone was milled by 'planetary micro milling' machine for 2 hours at the speed of 2.5. The milled YSZ was dried for 20 minutes in air and room temperature to evaporate acetone and then transferred to a plastic bottle with 36 balls. 14g solvent (3AEK:2LETH) and 0.195g dispersant (Phosphate ester) were added into the YSZ which was then ball milled for 18 hours under 28V. After that, 2.19g DBP, 2.43g PEG, 3.36g PVB and 0.5g solvent were added to the mixture for another 4 hour ball milling under 18 volts. Then the slurry was ready to be cast. The height of the blade was set to be 0.125mm which can produce 0.100mm YSZ tape after sintering (~25% shrinkage). The suspension was cast through the blade to a moving plastic tape at a speed of 50. This tape was dried overnight and then cut to a round shape (R= 1.5cm), and sintered at 1350°C for 5 hours.
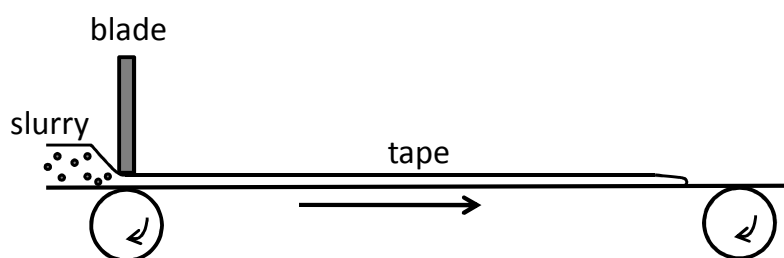
Figure 2.3. Schematic process of tape casting.

An aqueous solution containing $La(NO_3)_3 \cdot 6H_2O$, $Sr(NO_3)_2$, $Cr(NO_3)_3 \cdot 9H_2O$ and $Mn(CH_3COO)_2 \cdot 4H_2O$ was impregnated to the porous YSZ cathode support to reach a 50 wt% LSCM content. An aqueous solution containing $La(NO_3)_3 \cdot 6H_2O$, $Sr(NO_3)_2$ and $Fe(NO_3)_3 \cdot 9H_2O$ was impregnated to the porous YSZ anode support to reach 40 wt%[10-13] (see figure 2.4). The impregnated solutions were calcined at relevant temperatures.

	P - YSZ
	d - YSZ
	P - YSZ
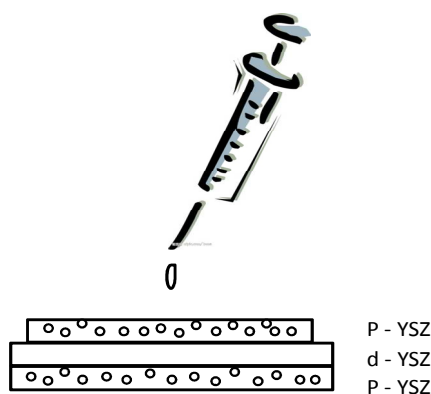
Figure 2.4 . Schematic process of impregnation.

The cell made by tape casting and impregnation method has a 50 micron thick dense YSZ electrolyte, a 110 micron thick porous YSZ cathode support with about 50% weight impregnated LSCM load and a 120 micron thick porous YSZ anode support with about 40% weight impregnated LSF load.

2.1.4 Cells with tape-casted electrolytes and printed electrodes

SOECs with thin YSZ electrolyte were also made by applying electrode inks on sintered single layer dense YSZ tape. As the electrode is thin, the inks are painted onto the surfaces of YSZ disk by soft brush rather than by screen printing. In this way, a cell with 50 micron thick electrolyte and 20~30 micron thick electrodes was made. These cells do not have high mechanical strength and thus need careful handling with. These cells have the same thin YSZ electrolyte with cells made by tape casting and impregnation methods..

2.1.5 Other methods

Some other ways were tried to produce cells with thinner YSZ electrolytes but failed.

2.1.5.1 Cells with thin YSZ by co-pressing method
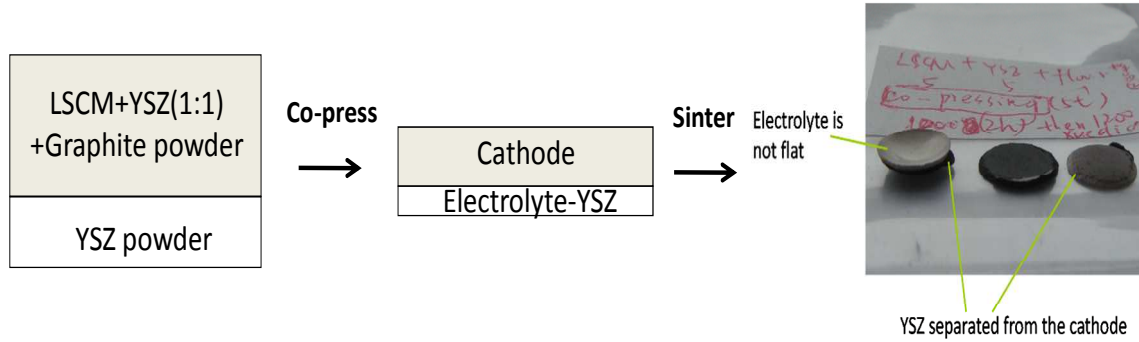
Figure 2.5. fabricating process and picture of a co-pressed cell with YSZ electrolyte and LSCM/YSZ cathode.

The cell was planned to be made by applying anode ink on co-pressed YSZ-LSCM/YSZ pellet. LSCM/YSZ (50% LSCM by weight) powder was poured into the pressing die and pressed lightly by hand to make surface flat. YSZ powder was then poured on top of cathode powder. The two layers of powders were co-pressed to form a disk which is fired to high temperature subsequently.

I failed to make a good cell by co-pressing in my work. Thermal expansion coefficients of the electrolyte and cathode did not match well. It might be improved by adjusting components of the powders. Photo in figure 2.5 shows the separation of the two parts after sintering.

2.1.5.2 Cells with screen printed thin YSZ electrolyte

Figure 2.6. A cell with screen printed YSZ electrolyte.

LSCM/YSZ powder was pressed to a column and calcined to form a cathode support. An interlayer and a layer of YSZ ink were applied on one side of the cathode pellet and then sintered. Figure 2.6 is the photo and SEM picture of the pellet after been si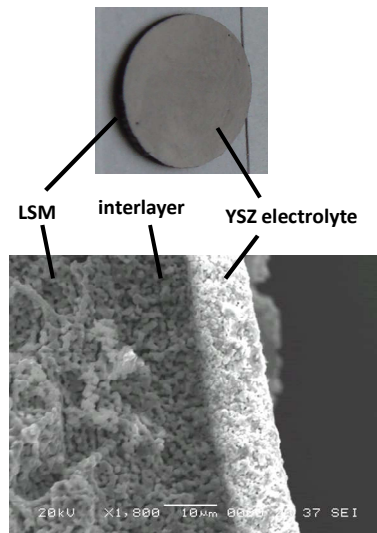ntered. It does exhibit any problem of separation between electrolyte and electrode however the YSZ electrolyte was not as dense as was required. The density might be improved by changing the formula of YSZ ink.

2.1.5.3 Electrodes with pore formers

Glassy carbon and/or flour were added to cathode powders and ball milled for 18 hours to get homogeneous distribution of pore formers. The mixed powders were made into cathode inks and applied on surface of YSZ electrolyte by screen printing. SEM pictures of sintered cathodes were obtained.

2.2 Characterization

2.2.1 Scanning Electron Microscopy (SEM)

Scanning Electron Microscopy (SEM) can tell us the microstructures and the local compositions[14]. When the sample is hit by the electron beam, a series of signals are generated by the interaction of the beam electrons and the atoms of the sample (see Figure 2.7). These beams can include secondary electrons (electrons from the sample itself), backscattered electrons (beam electrons from the filament that bounce off nuclei of atoms in the sample), X-rays, light, heat, and even transmitted electrons (beam electrons that pass through the sample), depending on samples[15].
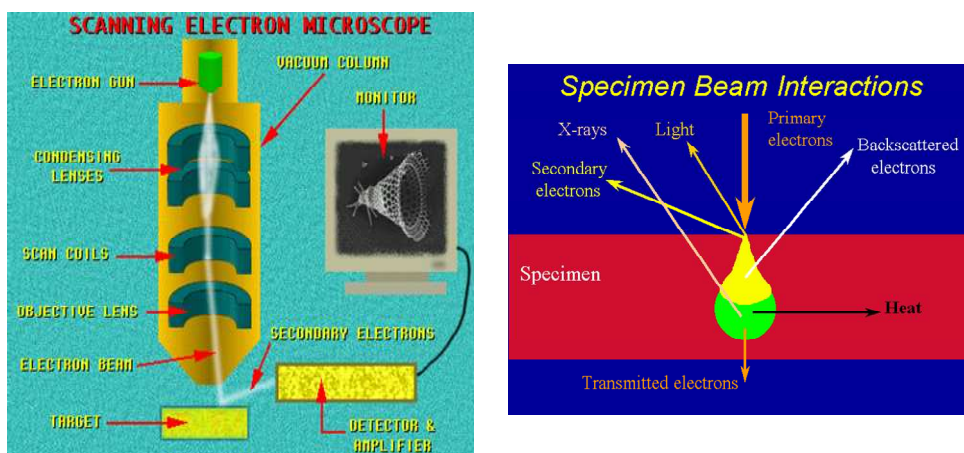
Figure 2.7.   Structure and principle of SEM[15].

Scanning electron microscopy (SEM) was performed using JEOL JSM-5600 to characterize the morphology of the cross sections of the electrolysis cells before and after electrochemical tests.

2.2.2 Energy Dispersive System (EDS)
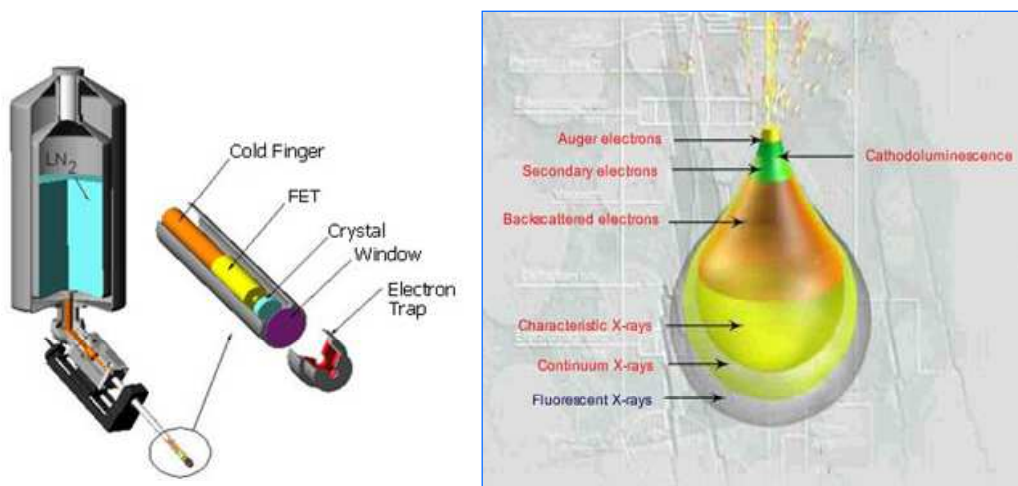
Figure 2.8.   Structure and principle of EDS[16].

EDS system is often works integrated with SEM to analyze the x-ray emitted from a sample. The detector is at the end of a long arm with is cooled by liquid nitrogen. The most common detector is made of sensitive Si(Li) crystals to absorb x-rays and produce free electrons. Thus the x-ray energy is converted into electrical voltages

which could be amplified and analyzed. The energies correspond to diverse atoms and therefore the local chemical compositions could be analyzed.

2.2.3 X-Ray Diffraction (XRD)

X-ray diffraction is a versatile and nondestructive method to analyze chemical composition and crystallographic structure of materials.

A crystal lattice is a three dimensional arrangement of atoms. These atoms are arranged in a series of parallel planes separated by a distance *d*. For a crystal, planes exist in a number of directions - each with its own interplanar spacing *d*.
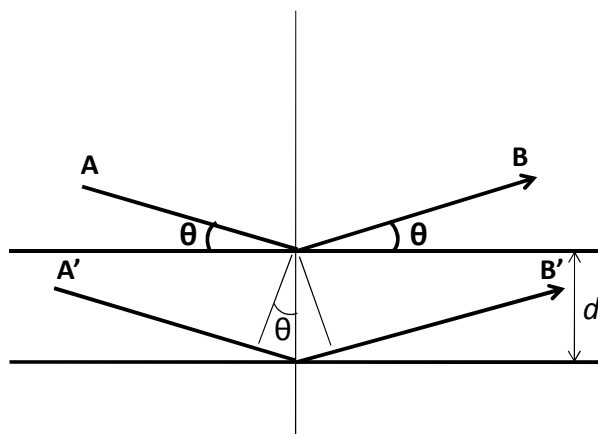
Figure 2.9. Bragg diffraction.

The two parallel incident rays have an angle with these planes (θ). The most intense reflection beam will occur when the two waves are in phase. That is, reflection beam with maximum intensity occurs when the difference of path length between A-B and A'-B' is an integral number of wave length.

$$2dSin\theta = n\lambda$$

The compositions of the cathode before and after electrolysis tests were characterized by X-ray diffraction (XRD). XRD was carried out using a Stoe STADI/P powder diffractometer over the range of 10 to 90°, step width 2θ. Incident radiation was generated using a CuKα1 source (λ = 1.54056 Å).

2.3 Electrochemical tests

2.3.1 Current collector

Gold paste and Au mesh were applied on electrode surfaces as current collector. For cathode with Ni, Ni pieces were used (but proven to be oxidized when using steam without H_2) rather than Au as current collector in order to avoid unwanted reaction between Ni and Au. The specimens with gold paste were fired at 900^oC for 2 hours.

2.3.2   Electrochemical tests

Two-probe and four-probe tests were done for whole-cell impedance and I-V measurements.

2.3.2.1 Two-probe tests

Initial thick cells were measured by two-probe tests. The jig for the two-probe electrolysis measurement is illustrated in figure 2.10. It can provide the cell with controlled atmosphere at both electrode surfaces at temperatures up to 950^oC. The jig is a custom-made alumina cylinder with holes for gas flow and electrode access. The counter electrode was made from single-bore alumina tube with a Pt-wire electrical contact. The working electrode was a two-bore alumina tube with Pt wire electrical contact and Pt/Rh thermocouple wire which measures the real temperature inside the jig. The prepared pellets were then sealed in the jig with gold rings and with pressures on top to help sealing. Gas inlet for the anode was O_2, and for the cathode was 3%steam/Ar/4%H_2 or 3%steam/Ar. Steam was produced by sending pure Ar/5% H_2 or pure Ar though a steam generator. The steam generator was a gas bubbler in water surrounded by a heating mantle set at temperature for required amount of steam. The electrodes were connected to a Solartron SI 1255 Frequency Response Analyzer for impedance measurements.
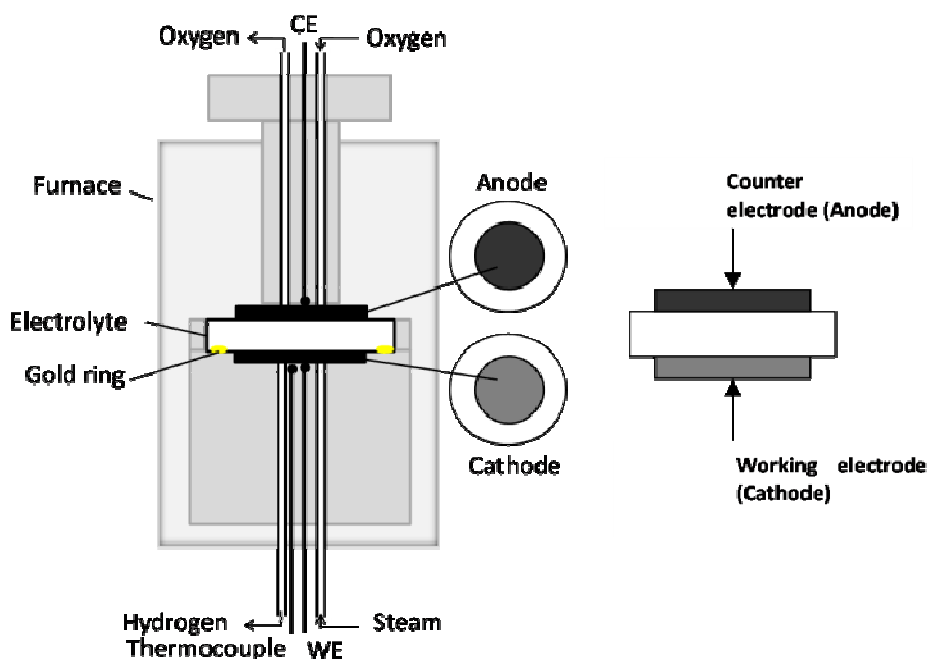
Figure 2.10. a. Two-probe test setup for polarizations measurements; b. Schematic drawing of the four probe test.

SOECs with 2mm YSZ electrolyte and six different cathode structures were tested: NiO/YSZ (35% YSZ by weight), LSCM, LSCM/CGO (50% LSCM by weight), LSCM/YSZ (75% LSCM by weight), LSCM/YSZ (50% LSCM by weight), and LSCM/NiO(50% LSCM by weight). Cathodes with NiO were pre-reduced to Ni by checking OCV stabilization before test.

2.3.2.2 Four-probe tests

The four-probe test is a test that could eliminate the stray resistance from the system, eg from thin leads. An SOEC was fixed in an electrolysis measurement jig by attaching the pellet to the alumina tube in the jig using Ceramabond 552-VFG (Aremco Products, INC.), which could prevent leakage and separate two atmospheres for the two electrodes. The method for sealing cells with Ceramabond, which avoids compressive stresses, could also prevent cracking of thin cells that do not have high mechanical strength. Cells were tested by two-electrode four-wire measurement. Two wires on the same side should be insulated to each other. The cells worked with

controlled flowing mixture gas (either 3%steam/Ar/4%H$_2$ or 3%steam/Ar) for the cathode surface and with the anode side open to air. Steam in the mixture gas for cathode side was generated by a gas bubbler in water sitting in a heating mantle which provides different water temperatures for required amounts of steam compositions.
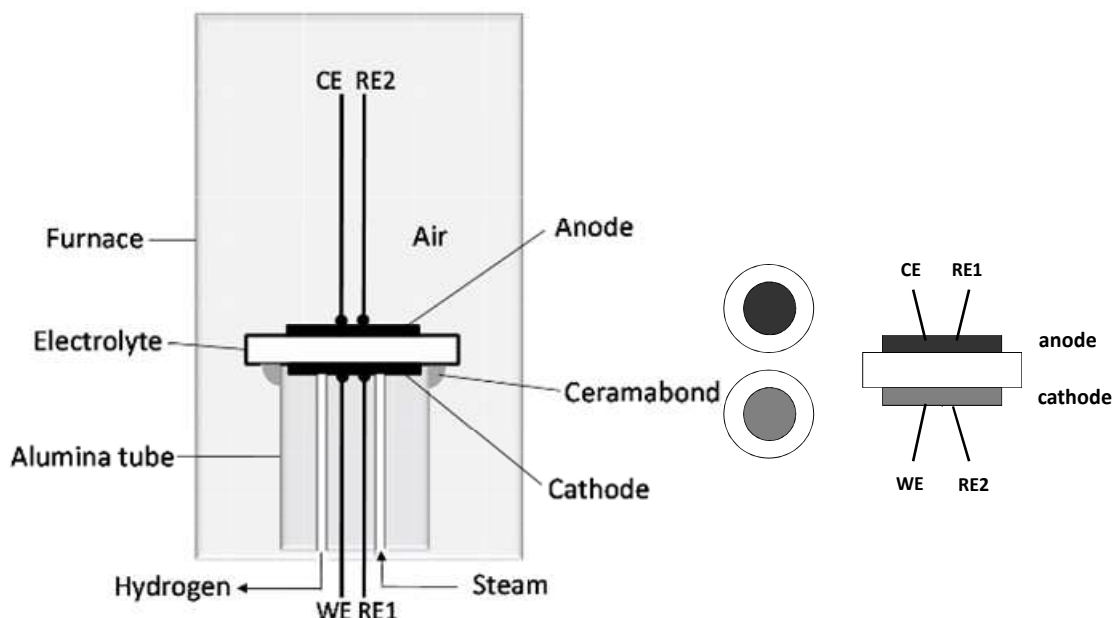
Figure 2.11. a. Four-probe, 2-electrode test setup for polarization measurements; b. Schematic drawing of the four probe test.

Measurements of impedance, current-voltage curve and potential step were done by a Solartron SI 1255 Frequency Response Analyzer at different temperatures and in two different cathode atmospheres (3%steam/Ar/4%H$_2$ or 3%steam/Ar). The potential step was set to sweep the potential between -1.0V and -1.5V / -2.0V across cell in three discrete potential steps and to keep each step for 960 seconds. Each step was long enough for cell stabilization. Gas chromatography was applied to analyze the composition of outlet gas from testing jig while constant voltage was applied.

2.3.2.3 AC Impedance

AC impedance is a powerful method for characterization of many electrochemical properties of materials and the interfaces between electrolyte and electrodes.

AC impedance.

A monochromatic signal $V(t) = V_m \sin(wt)$, involving the single frequency f= $w/2\pi$, is applied to a cell and the resulting steady state current $i(t) = I_m \sin(wt + \theta)$ measured. The complex resistance can be illustrated by Figure 2.12.
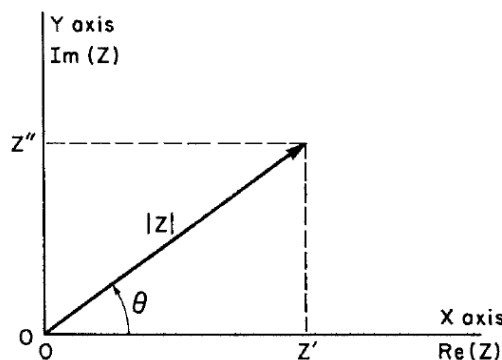

Figure 2.12. The impedance *Z* plotted as a planar vector using rectangular and polar coordinates[17]

The total impedance, which is termed as Z, can be expressed by:

$$Z = |Z| \cos(\theta) + |Z| \sin(\theta)$$

$$Re(Z) \equiv Z' = |Z| \cos(\theta)$$

$$Im(Z) \equiv Z'' = |Z| \sin(\theta)$$

Where Re(Z) and Im(Z) are the real impedance and imaginary impedance. θ is the phase difference between the voltage and the current; it is zero for purely resistive behavior[14]

Equivalent circuits.

The real circuit may be very complicated and we can approximate the real system to an equivalent circuit to determine the different contributions.

The impedance of a typical electrochemical system could consist of the resistance of electrolyte (R_Ω), the capacitance of the interface (C_d), and Faraday Impedance (Z_f) which is caused by the charge move and species transfer during the oxidation and reduction. When it works under alternating current (AC), Warburg Impedance (Z_w), which is due to the resistance and capacitance caused by periodical change of species concentrations in the interfaces, should also be considered. The

equivalent circuit can be shown by Figure 2.13.

Figure 2.13. Equivalent circuit. Where R_Ω is the resistance of electrolyte, C_d is the capacitance of the interface, Z_f is the Faraday Impedance, R_s is the resistance in Z_f; C_d is the capacitance in Z_f, Z_w is the Warburg Impedance, R_{CT} is the resistance of charge transfer[18].

Suppose that the electrochemical reaction is only under control of charge movement and species transfer, the total impedance can be illustrated in the following (Figure 2.14):

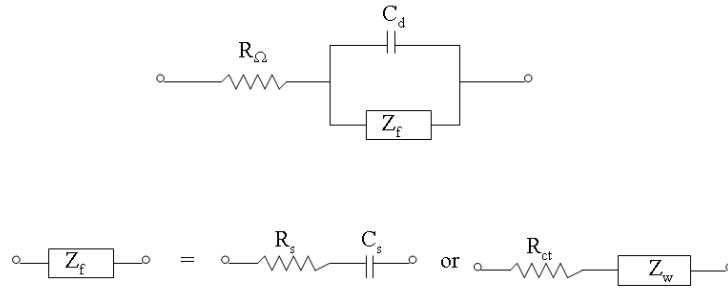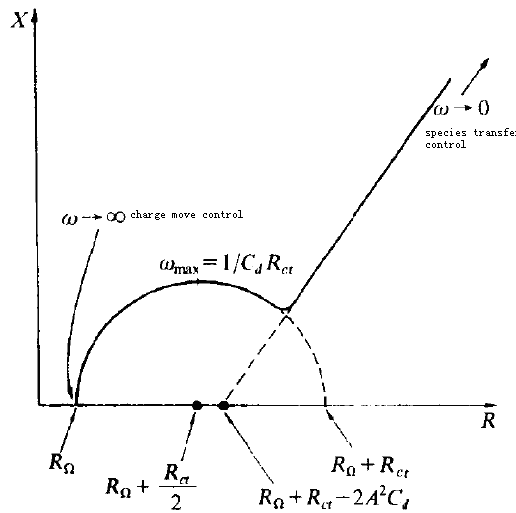**Figure 2.14. Complex impedance spectroscopy picture. Where R_Ω is the resistance of electrolyte, C_d is the capacitance of the interface, Z_f is the Faraday Impedance, R_s is the resistance in Z_f; C_d is the capacitance in Z_f, Z_w is the**

Warburg Impedance, R_Ω is the resistance of charge transfer[18].

2.4 Gas Components by Gas Chromatography (GC)

Gas chromatography is a gas separation technology. The sample mixture is injected and vaporized, if a liquid, at the beginning of the column. The sample mixture is carried through the column by a carrier gas.

Adsorption and partitioning occur according to the characteristic concentration ratio when the sample is introduced to the two phases (stationary phase and a mobile phase). Gas components are separated through continuous repetition of concentration equilibration. Different levels of adsorption or partition for each component results in differences in the moving rate for each component in the column[19, 20]. The schematic diagram and principle of a gas chromatograph is shown in figure 2.15.
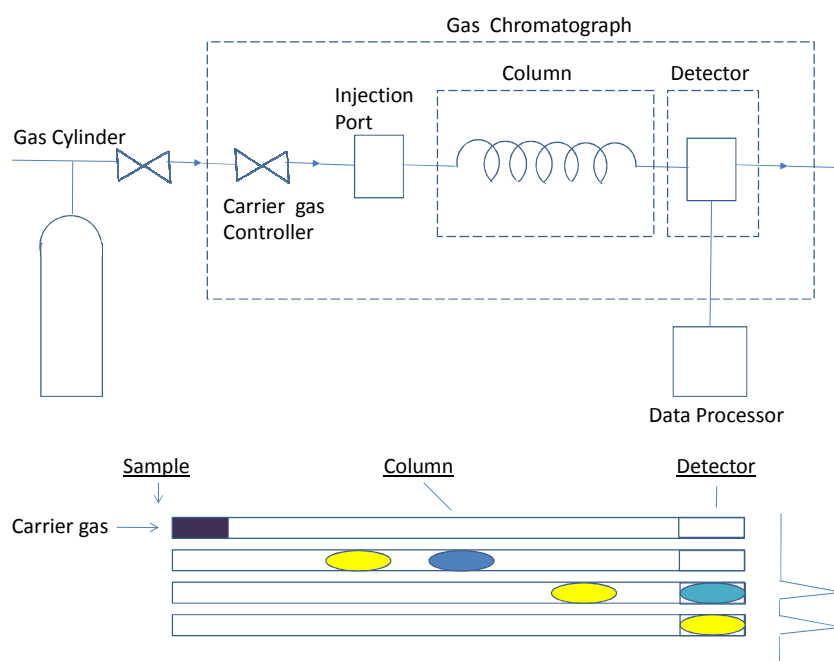

Figure 2.15. a. schematic diagram of a gas chromatograph; b. Principles of Gas Chromatography.

An Agilent 3000 Micro gas chromatograph, equipped with an injector, was connected with the testing jig to check hydrogen production while external potential

load was applied to the SOEC. The Agilent 3000 Micro GC has a thermal conductivity detector (TCD) which is more sensitive than conventional TCDs and a performance enhancement that allows the CG to analyze trace-level in the low ppm range[22]. Hydrogen was detected by the chromatograph according to the relative retention time. And the volume percentage of hydrogen was given by GC analysis on the mixture gas going out from the jig. A cooling setting was applied to the outlet gas in order to get rid of water before the sample entering the gas chromatograph. Six gas samples were collected at each potential step and hydrogen production level kept constant under constant potential load.

2.5 Calculation of Efficiency

The current-to-hydrogen production efficiency from HTSE is the ratio of the amount of hydrogen actually produced to the theoretical amount of hydrogen production. The theoretical amount of hydrogen production was calculated from cell current obeying the law of conservation of charge. The real amount of hydrogen production was calculated by the gas flow rate and the volume percentage of hydrogen which was given by gas chromatograph[21].

2.6 Generation of Steam

Steam was generated by a water bubbler sitting in a heating mantle which can provide different required temperatures for generating steam (see figure 2.16).
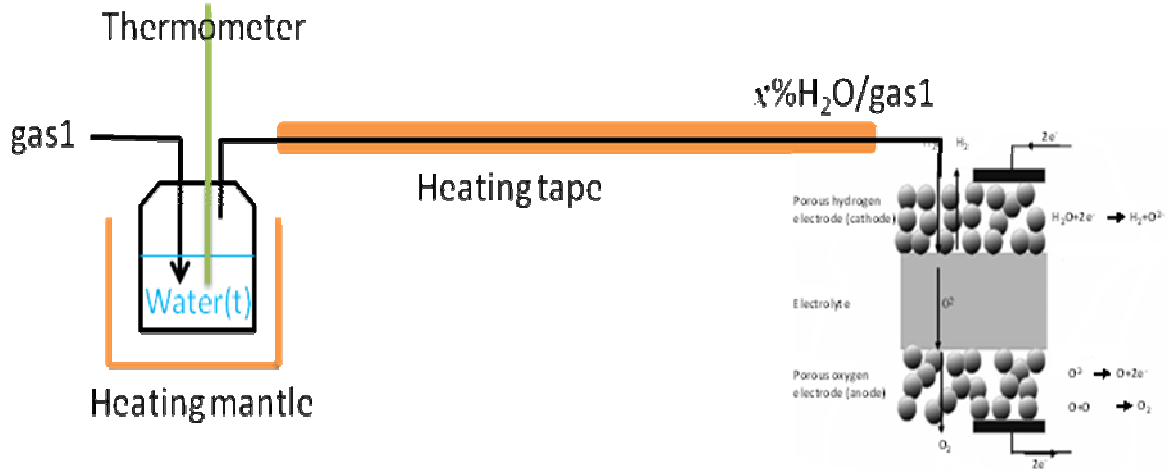
Figure 2.16. Schematic process of generating different amounts of steam.

Gas going through the bubbler with water at a given temperature would come out with a fixed steam content. The relationship between water temperature and percentage of steam could be calculated according to the 'Saturated water vapor pressures at different temperatures'.

For example,

3% Steam=0.03atm=0.03*101.3*10^3Pa =3.039*10^3Pa

According to 'Saturated water vapor pressures at different temperatures', 3.039*10^3Pa corresponds to the temperature of 24°C. Water temperatures for required water content in my work are shown in table 2.

x%H_2O	3%H_2O	10%H_2O	30%H_2O	50%H_2O
Water (t)	24°C	46°C	69°C	81°C

Table 2 . Temperatures required for given steam percentages.

The generated steam then passed a gas line which is heated by a heating tape to keep the mixture of gas at a high temperature all the way between water bubbler and testing jig. This could help preventing steam liquefaction during the path (see figure 2.16).

References

1. A. G. King, *Ceramic Technology and Processing*, New York: William Andrews Publishing, 2002.

2. Ball mill, *From Wikipedi*, http://en.wikipedia.org/wiki/Ball_mill, 2009.

3. *Print Process Descriptions*, Printing Industry Overview: Screen Printing, http://www.pneac.org/printprocesses/screen/, 2009.

4. R. J. Gorte, S. Park, J. M. Vohs, and C. Wang, *Adv. Mater.*, 2000, 12, 1645.

5. S. Park, R. J. Gorte, J. M. Vohs, *J. Electrochem. Soc.*, 2001, 148 ,A443.

6. N. Q. Minh, *J. Am. Ceram. Soc.*, 1993, 76, 563.

7. M. P. Albano, L. B. Garrido, *Mater. Sci. Eng.*, 2006, A 420, 171.

8. C. Pagnoux, T. Chartier, M. de F. Granja, F. Doreau, J. M. Ferreira, J. F. Baumard, *J. Eur. Ceram. Soc.*, 1998, 18, 241.

9. J. H. Feng, F. Dogan, *Mater. Sci. Eng.*, 2000, A 283, 56.

10. W. Wang, M. D. Gross, J. M. Vohs, R. J. Gorte, *J. Electrochem. Soc.*, 2007, 154, B439.

11. Y. Huang, K. Ahn, J. M. Vohs, R. J. Gorte, *J. Electrochem. Soc.*, 2004, 151, A1592.

12. Y. Huang, J. M. Vohs,R. J. Gorte, *J. Electrochem. Soc.*, 2006, 153, A951.

13. G. Kim, G. Corre, J. T. S. Irvine, J. M. Vohs, and R. J. Gorte, *Electrochem. Solid-State Lett.,* 2008. 11, B16.

14. W. Zhou, *Introduction to electron microscopy (lectures)*, 2007.

15. *Principle of SEM Imaging*, http://academic.udayton.edu/ShirleyWright/SEM/Principle/2_Imaging.htm, 2008.

16. *EDS operation*, http://www.advancedanalysistech.com/eds.html, 2009.

17. E. Barsoukov, J. R. Macdonald, *Impedance Spectroscopy Theory, experiment, and Applications(Second Edition)*, John Wiley & Sons, Inc., Publication, 2005.

18. *Electrochemical Measuring Method* (in Chinese), Beijing, Peking U. Press, 1995, 351.

19. *Gas chromatography* , http://teaching.shu.ac.uk/hwb/chemistry/tutorials/chrom/gaschrm.htm, 2009.

20. *Gas-liquid chromatography, From Wikipedi*,

http://en.wikipedia.org/wiki/Gas_chromatography, 2009.

21. F. S. Roberto; C. P. Janine; S. G. Reinaldo; O. S. Michele; R. B. Jo¨elle, *J. Power Sources,* 2007, *164*, 792.

66. *3000 Micro GC,*

http://www.chem.agilent.com/en-us/products/instruments/gc/3000microgc/pages/default.aspx, 2009.

Chapter 3 Initial Studies on $(La_{0.75}Sr_{0.25})_{0.95}Mn_{0.5}Cr_{0.5}O_3$ Cathodes for Solid Oxide Electrolysis Cells

3.1 Introduction

The cathode material is an important factor in determining the overall performance of the solid oxide electrolysis cell (SOEC). Cathode materials for high temperature SOECs should have catalytic activity for water splitting which is necessary to enhance the kinetics of the reaction. Furthermore, the cathode is required to have ionic conductivity which allows the transport of oxygen ions to the anode/electrolyte interface. The cathode material has also to be electrical conductive in order to convey the electrons produced at cathode to the outside circuit. Several materials have attracted attention as possible SOEC cathode materials.

Platinum, is stable at high temperatures and has high catalytic activity as well as electronic conductivity[1], but is expensive and may bond with the electrolyte[2].

Ni cermet, the currently preferred cathode material for high temperature solid oxide electrolysis systems, requires a significant concentration of H_2 flowing over it, if it is not to be oxidized to NiO. Not only would this cause a loss of electronic conductivity but is also likely to lead mechanical failure of the electrode. Most reported work has been done with an inlet gas containing a considerable amount of hydrogen, typically with pre-reduction of the cathode[3, 4].

Here we are seeking an electrode that can start with low content of H_2 or even without H_2 and work with high efficiency. The perovskite $(La_{0.75}Sr_{0.25})_{0.95}Mn_{0.5}Cr_{0.5}O_3$ (LSCM), which satisfies many of the requirements for SOEC cathode, is an active and redox-stable material and has attracted a lot of attention in the high temperature solid oxide fuel cell field[5-8]. Nevertheless, LSCM has not been reported as a possible cathode for high temperature electrolysis cells, which work with high temperature steam and under external potential load. In this study, materials based on LSCM were applied in SOEC cathode and measured with controlled atmospheres at temperatures

up 920°C. Small amount of hydrogen (3%H_2O/Ar/4%H_2) or no hydrogen (3%H_2O/Ar) were supplied for cathode atmosphere. AC impedance data and current-voltage curves were obtained using a Solartron SI 1255 Frequency Response Analyzer. Scanning electron microscopy (SEM) was performed using a JEOL JSM 5600 to characterize the morphology and local compositions of the cross sections of the electrolysis cells.

3.2 Ni/YSZ

SOECs (solid oxide electrolysis cells) with 2 mm thick YSZ electrolyte and different cathodes were made and tested (2-terminal test) at 920°C using 3%steam/Ar/4%H_2 and 3%steam/Ar for cathode and oxygen for anode. Rs from these cells has been subtracted from the data. The value of Rs, at 3.5 $\Omega \cdot cm^2$, corresponds to the sum of the ionic resistance of the electrolyte and the electrical resistance of the Pt leads.

Figure 3.1 shows the morphology of Ni/YSZ cathode before electrochemical test. The screen printed Ni/YSZ cathode, with a thickness of around 20 microns, shows a microstructure with good porosity.

Figure 3.2 shows the performance of the cell with Ni/YSZ (65% NiO by weight) cathode and LSM anode with 3%steam/Ar/4%H_2 at 920°C. As shown in the impedance data and polarization property, the performances from Ni/YSZ cell in low content of hydrogen (4% hydrogen) is acceptable although it is not as good as state of the art[19].

On changing from reducing to inert atmospheres(3%steam/Ar) at open circuit, after a short period of operation the impedance of the cell increased dramatically, to several thousand ohms. Althrough the cell has smaller resistances when higher voltages were applied, data shown in figure 3.3 from the electrolysis cell with Ni/YSZ (65% NiO by weight) cathode and LSM anode in 3%steam/Ar at 927°C reveal that with a fairly bad performance, Ni/YSZ cathode is not practicable for high temperature steam electrolysis in atmospheres without hydrogen or other reductant. The current-voltage curve, with a very large slope, also illustrates an

extremely high resistance. The poor performance is thought to result from Ni oxidation in the cathode during the test. Figure 3.3 c, the photo of Ni/YSZ cathode after test using gas with no hydrogen content at 927^oC for about two hours, shows clearly that a considerable amount of Ni metal (which is black) turned to NiO (which is green) after test. It is obvious that Ni has been seriously oxidized during the electrolysis in wet Ar without hydrogen. As NiO does not have very good electronic conductivity, Ni oxidation suppressed the performance of Ni/YSZ in electrolysis. Therefore, the traditional Ni/YSZ cathode is not suitable for the operation in feed-in gas with no hydrogen.
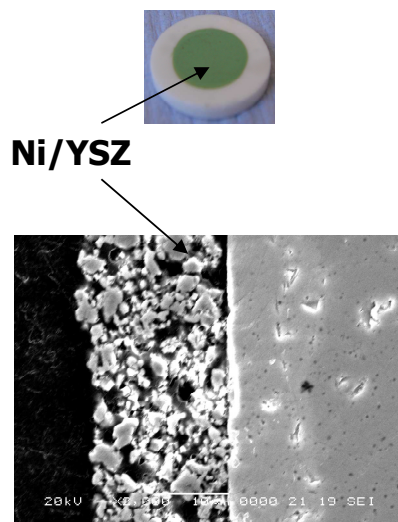

Figure 3.1. SEM picture of the cross-section of Ni/YSZ cathode .

Figure 3.2. Performance from an SOEC with Ni/YSZ cathode, 2mm thick YSZ electrolyte and LSM anode at 917°C with 3%steam/Ar/4%H₂. a. AC impedance data measured at OCV, 1.0 V, 1.5 V; b. Current-voltage curve.

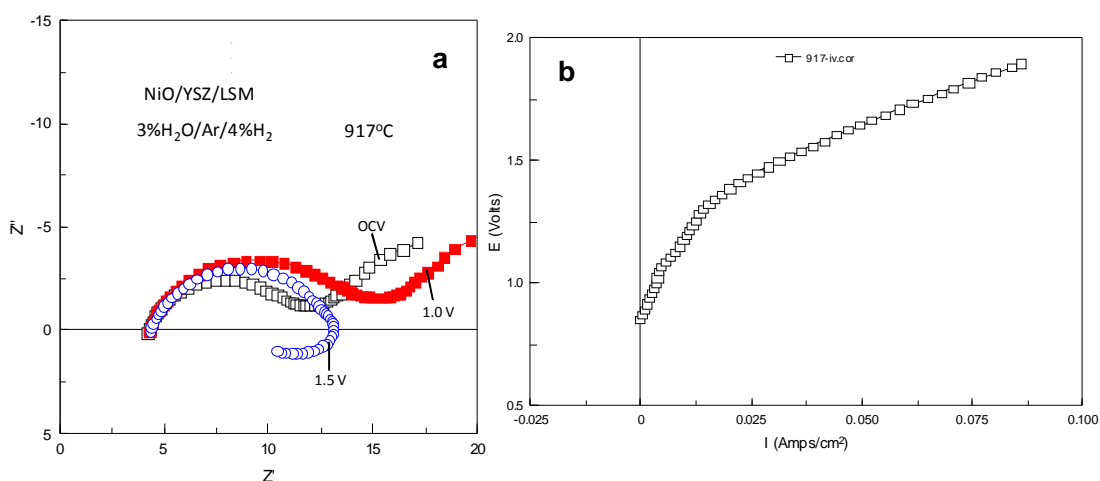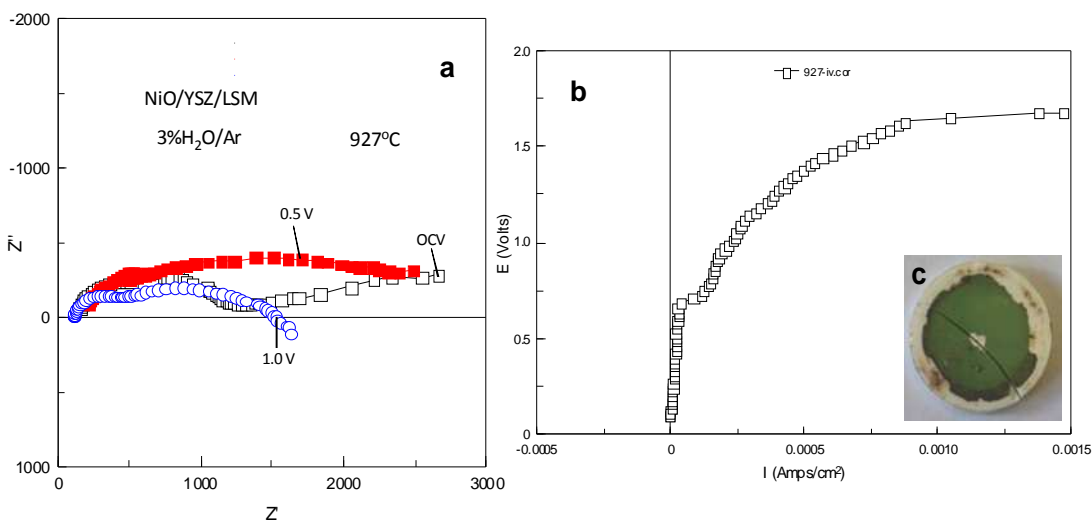**Figure 3.3. Performance from an SOEC with Ni/YSZ cathode, 2mm YSZ electrolyte and LSM anode at 927°C with 3%steam/Ar. a. AC impedance data measured at OCV, 0.5 V, 1.0 V; b. Current-voltage curve.**

54

3.3 LSCM/CGO

3.3.1 LSCM/CGO and LSCM

$(La_{0.75}Sr_{0.25})_{0.95}Mn_{0.5}Cr_{0.5}O_3$ (LSCM), has been reported for its remarkable stability with respect to reduction or oxidation occurring at high temperature, eg 900^oC[9]. It has also been reported to show chemical compatibility with YSZ to at least $1300°C$[10] and to work efficiently as an anode for a SOFC[9]. In my work, cells with LSCM cathode were initially tested and were found to have promising performance, meriting further study. Whilst not as good as best state of the art materials in hydrogen containing gas streams the data obtained were better than cells made by similar methodology with a Ni/YSZ cathode (see figure 3.4).

$Ce_{0.9}Gd_{0.1}O_{1.95}$ (CGO) has been reported as a promising electrolyte material due to its high oxygen ion vacancy conductivity[11, 12]. And it has been reported that a CGO interlayer between LSCM and YSZ could improve the SOFC performance[13]. Cathode ionic conductivity could be increased by mixing LSCM with CGO, and therefore extend the three phase boundary zones in cathode/electrolyte interface region. Figure 3.4 shows that the performances are improved by adding CGO to pure LSCM cathode. The series resistance (Rs), at about $3.5\Omega^.cm^2$, has been subtracted from the data in figure 3.4. LSCM/CGO has smaller polarization resistances than LSCM either under open circuit voltage or under -1.5 V potential applied. This might be due to the increased cathode ionic conductivity and improved three phase boundary. Water splitting which takes place at the three phase boundary could be facilitated by TPB increasing and the oxygen ions produced at cathode by water splitting could be transported faster to the electrolyte. AC impedance arcs from two cells have different shapes. The cell with CGO has fairly small high frequency arcs under open circuit or at -1.5 V. By comparison, the cell with pure LSCM has obvious high frequency arcs. These high frequency arcs might stem from charge transfer limitations. Pure LSCM has comparatively lower ionic conductivity than cathode with CGO and therefore

poorer charge transfer processes. The low frequency arc from LSCM/CGO is slightly smaller than that from pure LSCM under open circuit, which might relate to the enlarged three phase boundary (TPB). Under -1.5 V, the low frequency arc from pure LSCM is much larger than that from LSCM/CGO. This might be due to the large activation polarization (electrode activation/LSCM reduction) at this potential. Different cathode composites based on LSCM will be discussed later in this chapter.
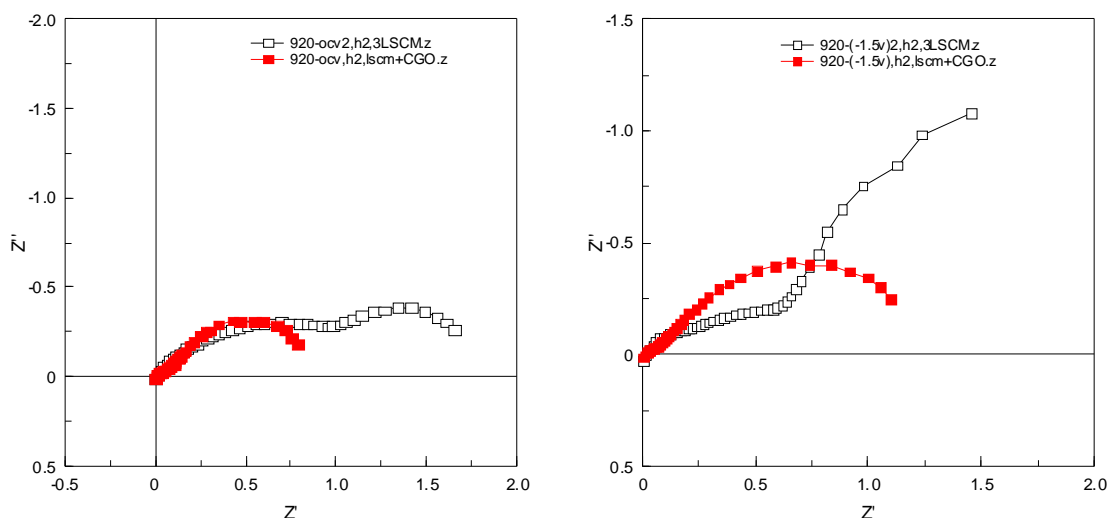

Figure 3.4. Impedance data from cells with LSCM cathode and LSCM/CGO (50% CGO by weight) cathode at 920°C in 3%steam/Ar/4%H$_2$.

3.3.2 LSCM/CGO in 3%steam/Ar/4%H$_2$

Figure 3.5 shows the SEM pictures of the cross-section of LSCM/CGO cell. The cell has a 2mm thick dense YSZ electrolyte and a porous cathode of ~30 micron thick. The morphology of the LSCM/CGO composite cathode shows a good porosity.
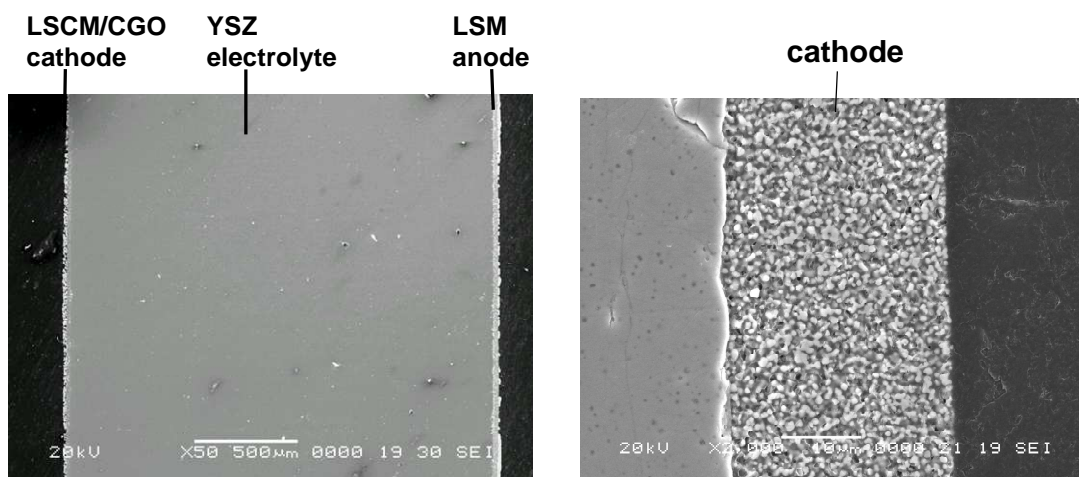
Figure 3.5. SEM picture of the cross-section of LSCM/CGO cell.

Figure 3.6 shows the performance of the electrolysis cells with LSCM/CGO (50% CGO by weight) cathode running with 3%steam/Ar/4%H_2 at 920°C. The impedance data and current-voltage curve reveal a good performance of cathode composed of materials based on $(La_{0.75}Sr_{0.25})_{0.95}Mn_{0.5}C_{r0.5}O_3$ (LSCM) in gas with a low content of hydrogen (4% H_2). Compared to the Rp value of more than 10 Ω·cm^2 from the cell with Ni/YSZ cathode operated in 3%steam/Ar/4%H_2 at 917°C, the cell with LSCM/CGO cathode shows a better Rp of around only 1 Ω·cm^2. The overall area resistance of LSCM/CGO cell in 3%steam/Ar/4%H_2 is 6.77 Ω·cm^2 (ohmic resistance from the jig is estimated to be around 2.8 Ω) (see figure 3.6b).
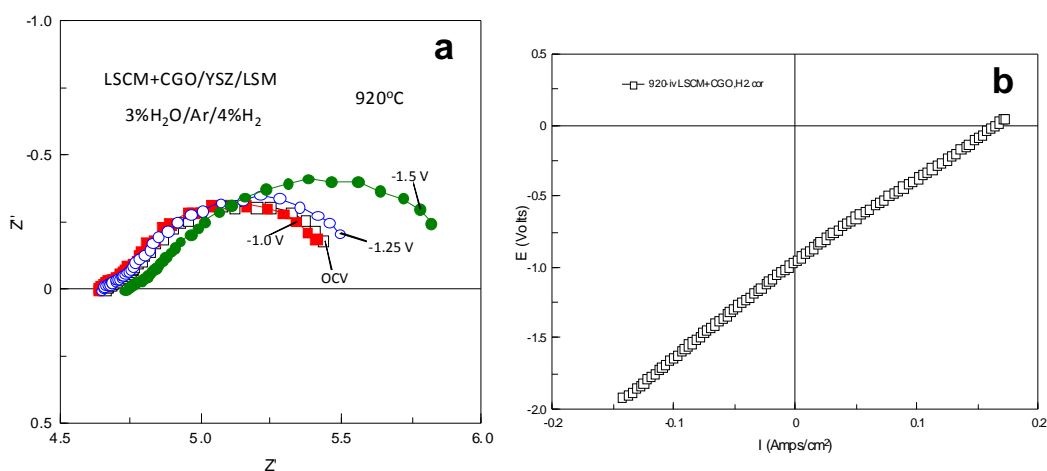
Figure 3.6. Performance from an SOEC with LSCM/CGO cathode, 2mm thick YSZ electrolyte and LSM anode at 920°C with 3%steam/Ar/4%H$_2$. a. AC impedance data measured at OCV, 1.0 V, 1.25 V, 1.5 V; b. Current-voltage curve.

Water splitting at the SOEC cathode might involve gas diffusion, desorption/adsorption of H_2O, surface diffusion of H_2O to the three phase boundary (TPB), water splitting and charge transfer at TPB, and transportation of oxygen ions produced at TPB through the electrolyte[14, 15]. Several steps could be the rate limiting processes.

Figure 3.7 shows Bode plots (real and imaginary parts of impedance vs. frequency) of the LSCM/CGO electrolysis cell at three different applied potentials at 920°C with 3%steam/Ar/4%H$_2$. Impedance arcs below 10 kHz are related to the electrode processes[16]. For this cell, two limiting process affected the impedance and the low frequency one is dominating. The summit frequency of the low frequency arc drops in the range of 0.35~0.50Hz. The low frequency process is the dominating rate limiting process which may be caused by gas diffusion limitation at one of the electrodes[16, 17]. The summit frequency of the low frequency arc shifts from 0.50 Hz to 0.32 Hz with increasing potential from ocv to -1.5 V. The summit frequency of the high frequency arc is around 316 Hz. The high frequency peaks, which are below 0.03 $\Omega\cdot cm^2$ in magnitude, are not obvious. The f$_{max}$ of the high frequency arc is independent of the applied potential. The low frequency process increases in magnitude as the potential is increased, and the high frequency arc is independent of potential. The phenomena shown in figure 3.6 indicate that the cause for Rp increasing as potential is increased could be ascribed to the low frequency process.
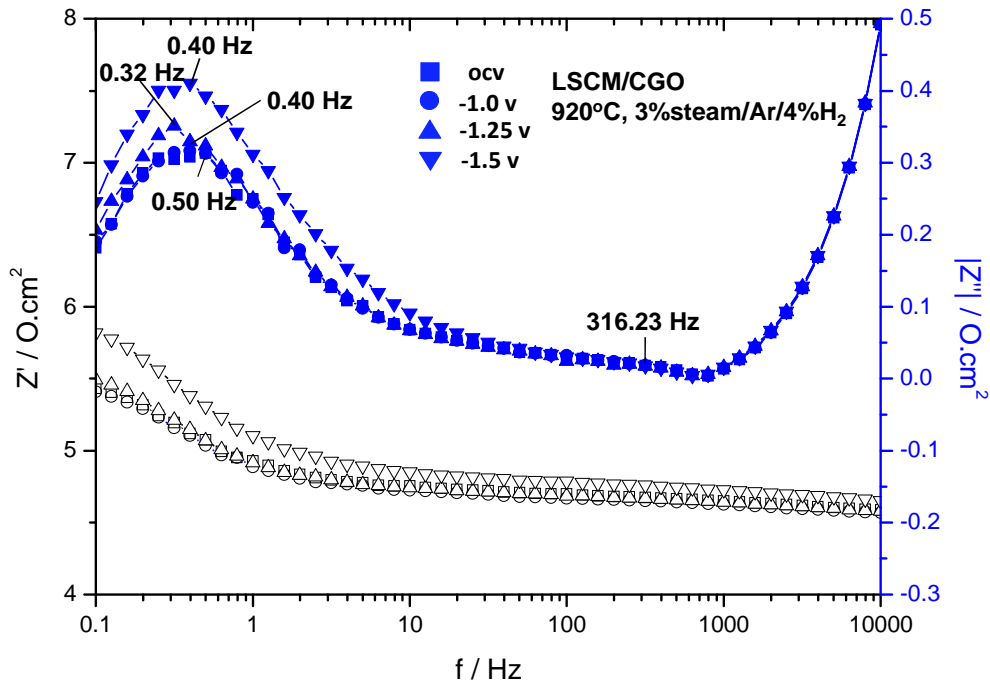
Figure 3.7. Bode plot obtained at different potentials from LSCM/CGO cell at 920°C in atmosphere of 3%steam/Ar/4%H$_2$.

Polarization data from this LSCM/CGO cell in 3%steam/Ar/4%H$_2$ at three different temperatures are shown in figure 3.8. The current-voltage curves are close to linear and the slope of current-voltage curve decreases with temperature increase. And the slope increases faster from 750°C to 840°C than from 840°C to 920°C due to significant ohmic resistance.
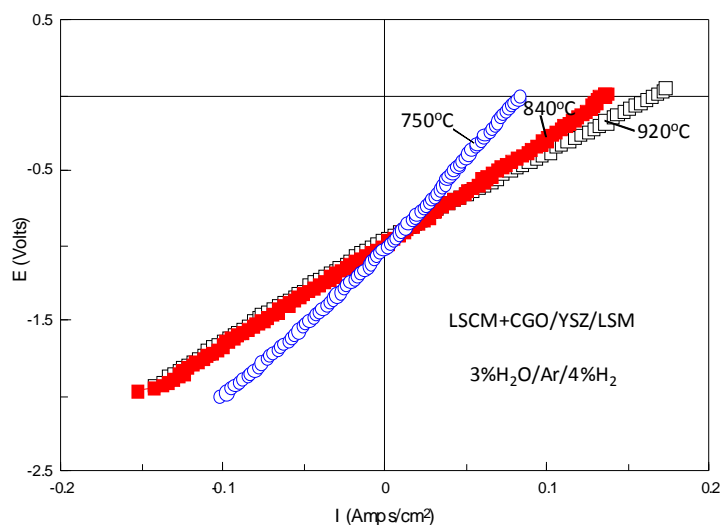
Figure 3.8. polarization properties at different temperatures from a cell with LSCM/CGO anode in 3%steam/Ar/4%H$_2$.

Figure 3.9 shows a comparison of typical EIS results, from the cell with the LSCM/CGO cathode running with 3%steam/Ar/4%H$_2$ under open circuit at different temperatures. The cell exhibits less total impedance ($R_s + R_p$) at higher temperature in humidified hydrogen, which is in good agreement with the results shown in figure 3.8. Figure 3.9 also shows that Rp is higher at higher potential for 920°C and 840°C; however it is higher at open circuit voltage for 750°C.
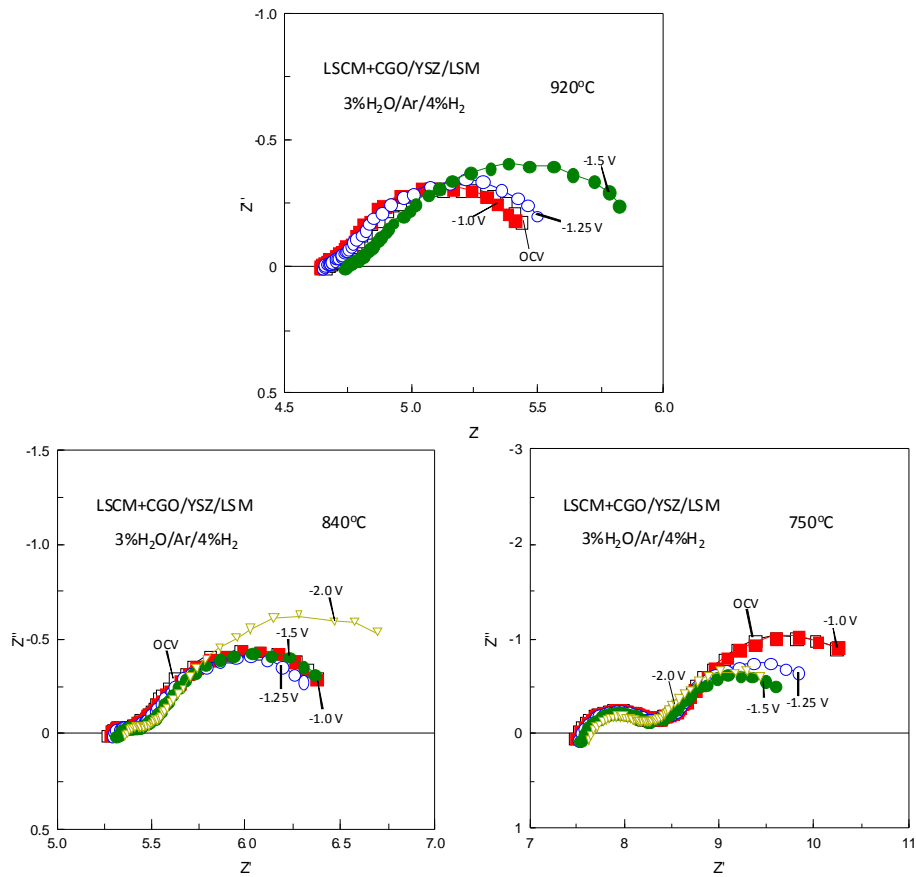
Figure 3.9. Impedance data under open circuit from LSCM/CGO cell at different temperatures in3%steam/Ar/4%H₂.

The slope of current-voltage curve corresponds to the cell resistances and is referred to as the area specific resistance (ASR). ASR data to be presented are taken from the linear fit of the current-voltage curves. Figure 3.10 shows the overall ASR, series resistance and polarization resistance at three temperatures which are determined from the current-voltage curves in figure 3.8 and impedance spectra (under open circuit) in figure 3.9. For this cell (with 2 mm YSZ electrolyte), Rs is the main contributor for overall ASR. ASR decreases with temperature increase. As temperature is increased, the ionic conductivity of YSZ electrolyte is reduced and therefore the Rs decreases. Higher temperature could also facilitate the electrochemical reaction as well as species transfer, and as a result, Rp is reduced. Rp is decreased by 74% when temperature increases from 750°C to 920°C, and Rs is
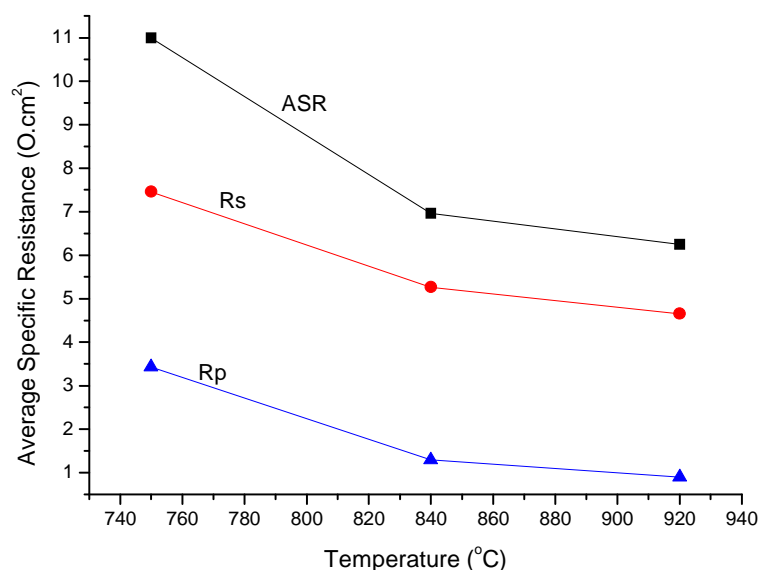
reduced by 37%.

Figure 3.10. Overall area specific resistance, series resistance (under open circuit) and polarization resistance (under open circuit) at three temperatures from LSCM/CGO cell in 3%steam/Ar/4%H₂.

Series resistance (Rs) and polarization resistance (Rp) of the LSCM/CGO cell at different potentials at 750°C, 840°C and 920°C with 3%steam/Ar/4%H₂ are plotted in figure 3.11. Rs shifts very slightly as the potential changes for all temperatures and Rp has different trends with potential for different temperatures. Rp increases a bit with potential at 920°C and almost maintains the same at 850°C, while it has a small decrease with potential at 750°C. This result also means that the current-voltage curves shown in figure 3.8 are not strictly linear; in other words, the area specific resistance values are slightly in dependence with current/voltage.
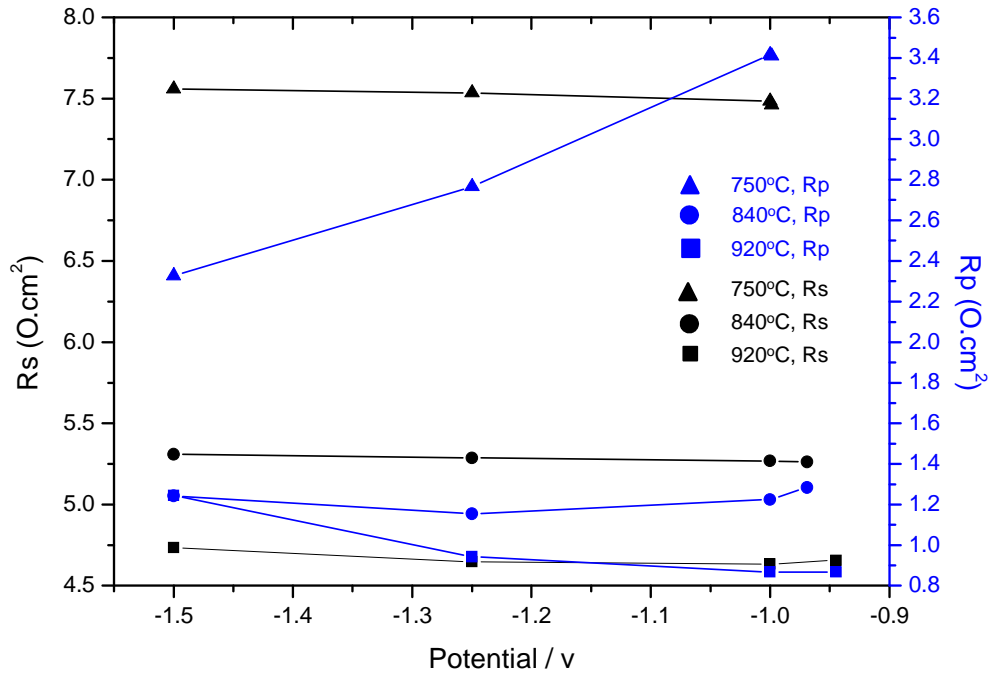
Figure 3.11. Series resistance (Rs) (ohmic resistance from the jig is estimated to be around 2.8 Ω) and polarization resistance (Rp) under different potentials at three temperatures from LSCM/CGO cell running with 3%steam/Ar/4%H₂.

Figure 3.12 shows Bode plots at open circuit voltage at three different temperatures with 3%steam/Ar/4%H₂ which are given by impedance data in figure 3.9.

At all three temperatures, there are two rate limiting processes affecting the impedance. From figure 3.12, it is assumed that the low and high frequency arcs for different temperatures represent the same low and high frequency processes respectively. The low frequency process with characteristic frequency of 0.2 Hz ~ 0.5 Hz might stem from gas diffusion and/or adsorption/desorption limitations. The low frequency process is much higher in magnitude than the high frequency process for all temperatures and is regarded to be the dominating limiting process. The characteristic frequency for low frequency arc shifts from 0.5 Hz to 0.2 Hz with decreasing temperature from 920°C to 750°C. And the low frequency process decreases by 70% in magnitude as temperature climbs from 750°C to 920°C.

The summit frequency of the high frequency arc drops in the range of 350 Hz ~ 550 Hz and shows an increase from 390 Hz to 510 Hz as temperature decreases. The high

frequency process, which might be charge transfer process, decreases in magnitude with increasing temperature; it almost disappears at 920°C and is easy to identify as temperature decreases to 750°C.
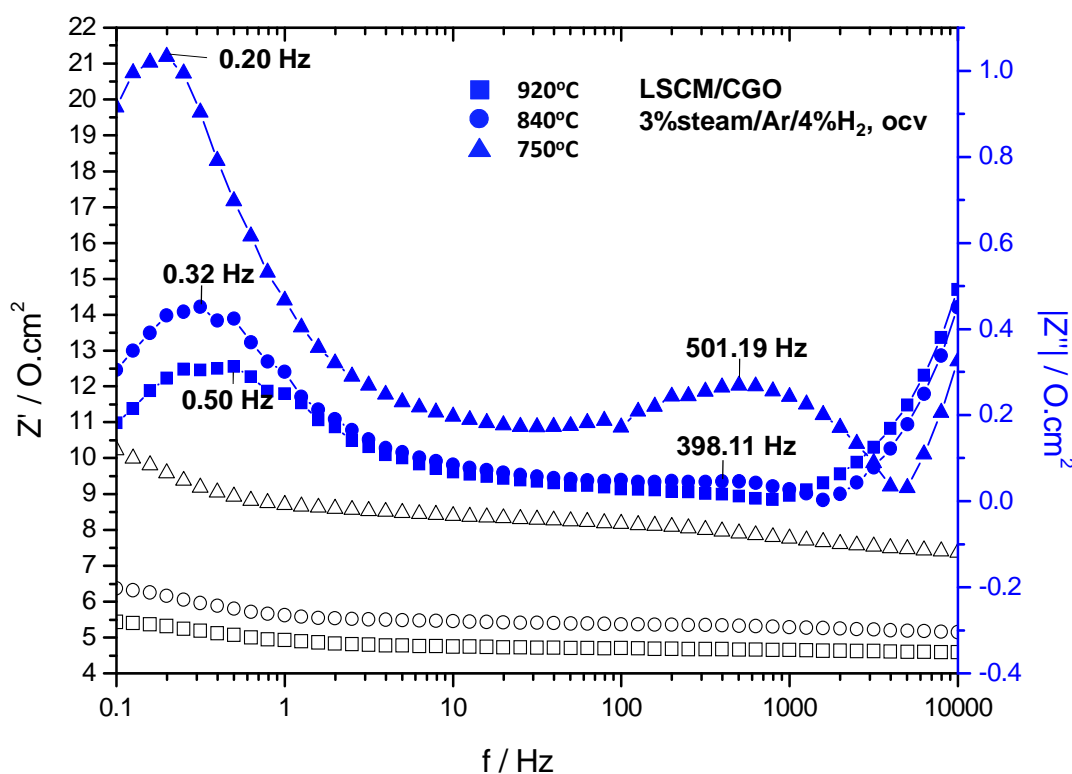

Figure 3.12. Bode plot obtained under open circuit at different temperatures from LSCM/CGO cell in atmosphere of 3%steam/Ar/4%H$_2$.

3.3.3 LSCM/CGO in 3%steam/Ar

The main purpose for this study is that SOECs with cathodes based on LSCM material might be promising candidates in high temperature steam electrolysis when there is no hydrogen content in the feed-in gas. Cells with LSCM/CGO (50% CGO by weight) cathode performed a lot better than that with traditional Ni cermet cathode in 3%steam/Ar at 920°C. Its performances are displayed in figure 3.13. The LSCM/CGO cell has a fairly small Rp when the external potential load is comparatively low, say, below -0.5 V, which is close to the open circuit voltage (The OCV is -0.14 V in

3%steam/Ar at 920°C). However, it seems that something happened to the cell under higher loading voltages during the electrolysis. From the impedance data, the cell with LSCM/CGO cathode shows larger Rp when the potentials are higher compared to the Rp values under lower voltages. And the current-voltage curve also show an abrupt increase in gradient when the voltages are higher. Figure 3.14 shows dE/dI data from IV curve (see figure 3.13) at OCV (-0.14 V), -0.25 V and -0.75 V. dE/dI value is around 5.8 $\Omega \cdot$cm^2 at -0.25 V and goes up to 48 $\Omega \cdot$cm^2 at -0.75 V. Rs at voltages is also shown in figure 3.14. Rs takes a majority of the overall dE/dI at comparatively low potentials and shows a slightly drop as potential is increased to -0.75 V. The value of dE/dI minus Rs, which is roughly the value of Rp, shows a similar increase with potential and is a dominating contributor to the overall dE/dI at -0.75 V.

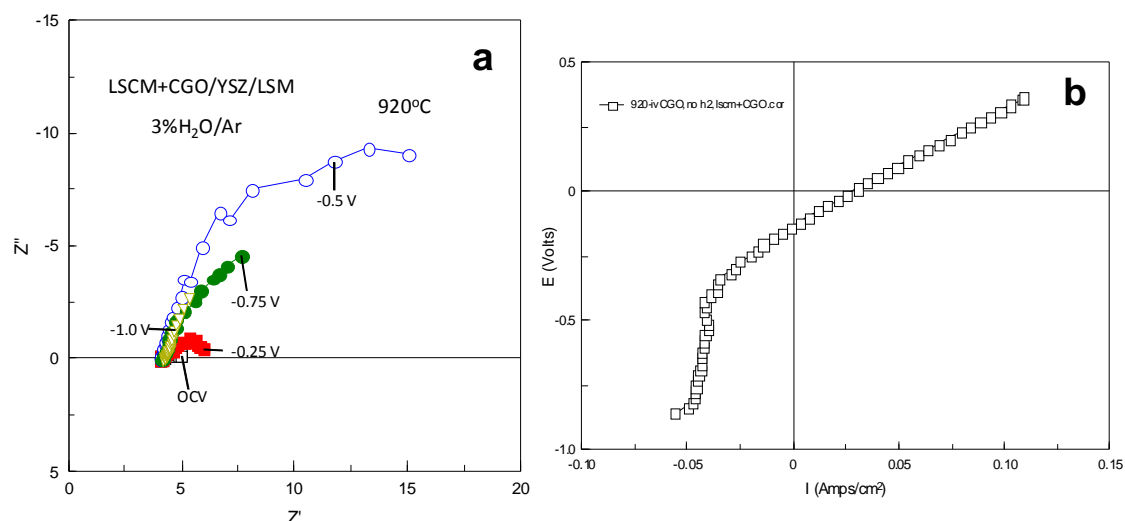**Figure 3.13. Performance from an SOEC with LSCM/CGO cathode, 2mm thick YSZ electrolyte and LSM anode at 920°C with 3%steam/Ar. a. AC impedance data measured at ocv, 0.25 V, 0.5 V, 0.75 V, 1.0 V; b. Current-voltage curve.**
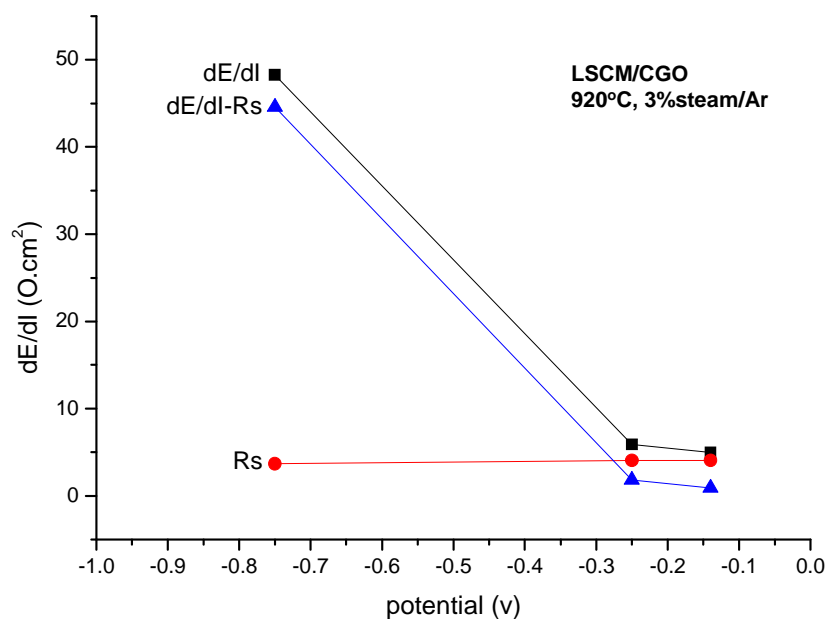
Figure 3.14. dE/dI, polarization resistance and series resistance from LSCM/CGO cell at 920°C with 3%steam/Ar.

Polarization data at three temperatures are shown in figure 3.15. Current-voltage curves for three temperatures give essentially the same response, with a bit higher slope for lower temperature. There is a turning point for every curve where slope increases sharply when potential is increased to around -0.5 V. The higher potential curve has much bigger slope than the lower potential curve. The IV curve at 920°C has the biggest increase as potential turns to high value. However, the turning of curve becomes smoother as temperature is decreased. At 920°C the cell has the highest slope of segment B-C in IV curve which might relate to LSCM redox and electrode activation.
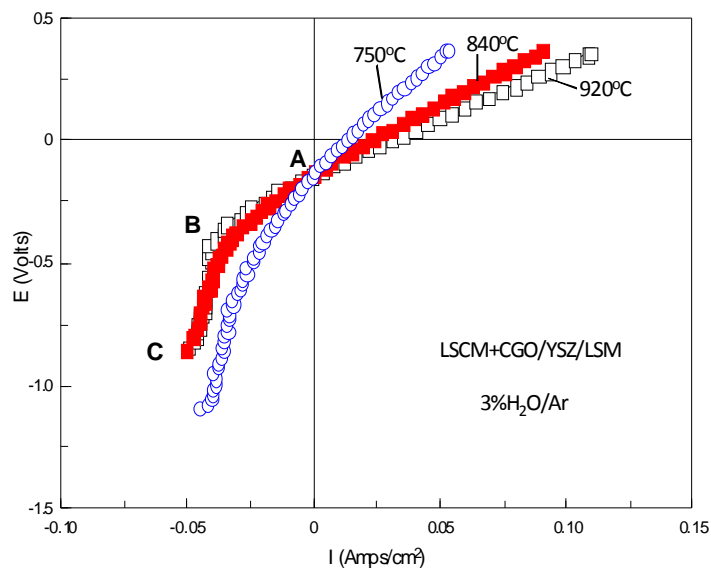
Figure 3.15 . Polarization properties at three temperatures from LSCM/CGO cell with 3%steam/Ar.

Polarization properties in 3%steam/Ar and 3%steam/Ar/4%H_2 from LSCM/CGO cell at 920°C are compared in figure 3.16. The cell has an open circuit voltage of -0.95 V in 3%steam/Ar/4%H_2 and -0.14 V in 3%steam/Ar at 920°C. The current-voltage curve is close to linear for test in 3%steam/Ar/4%H_2 however in 3%steam/Ar atmosphere it has a sudden change at around -0.4 V. The segment A-B in I-V curve with 3%steam has a slope of 5.5$\Omega \cdot cm^2$, which is close to the slope of I-V curve in 3%steam/Ar/4%H_2 (6.25$\Omega \cdot cm^2$).
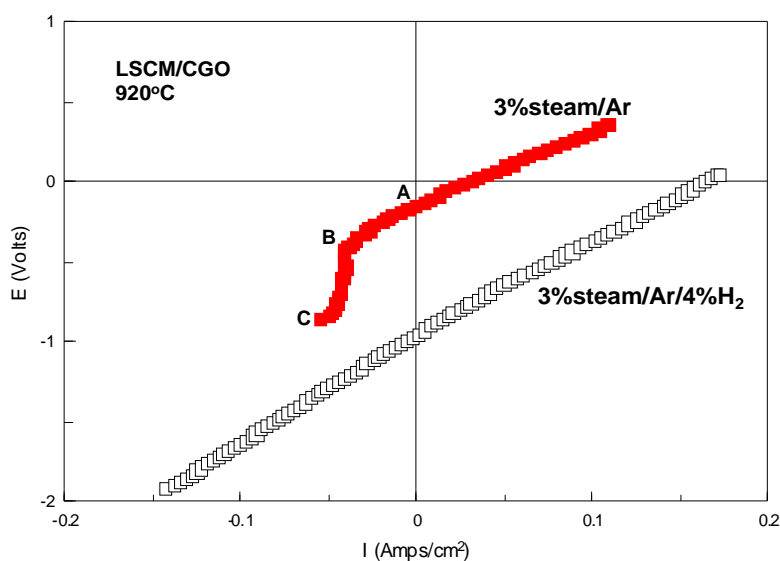
Figure 3.16. Polarization properties in 3%steam/Ar and 3%steam/Ar/4%H$_2$ from LSCM/CGO cell at 920°C.

Figure 3.17 shows the impedance data from the cell at 750°C, 840°C and 920°C with 3%steam/Ar. Impedance measurements were taken in the frequency range of 10^5 Hz~0.1 Hz. The spectrum has two semicircles at 750°C, while the high frequency semicircles become smaller at 840°C and 920°C. This indicates that the high frequency process becomes less influencial as temperature increases which could also be illustrated by Bode plots in figure 3.19. The low frequency process shows roughly a shape of semicircle at OCV and -0.25 V. And the low frequency semicircle becomes bigger as voltage gets higher and is almost linear at -1.0 V in frequency range of 10^5 Hz~0.1 Hz. Polarization resistance becomes very high when high voltage is applied.
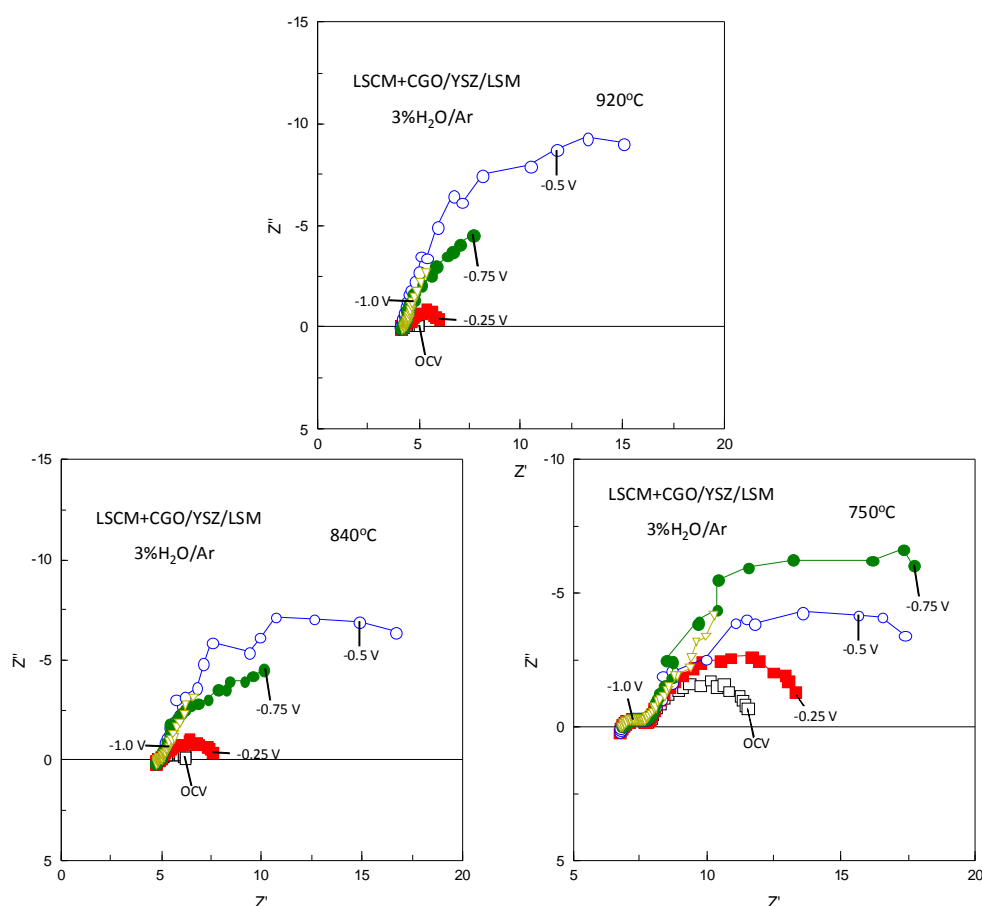

Figure 3.17. Impedance data at different temperatures from LSCM/CGO cell running with3%steam/Ar.

Impedance data from measurements in 3%steam/Ar/4%H$_2$ and 3%steam/Ar/4%H$_2$ are compared in figure 3.18. Impedance in 3%steam/Ar has a slightly smaller series resistance (Rs) than impedance in 3%steam/Ar/4%H$_2$. Impedance data are roughly in shape of semicircle except for those in 3%steam/Ar with high potentials applied. Impedance data in 3%steam/Ar at high potentials have similar Rs but much larger Rp than impedance at low potentials. The polarization resistance is the main contributor for the high slope in I-V curve at high potentials (see figure 3.16).
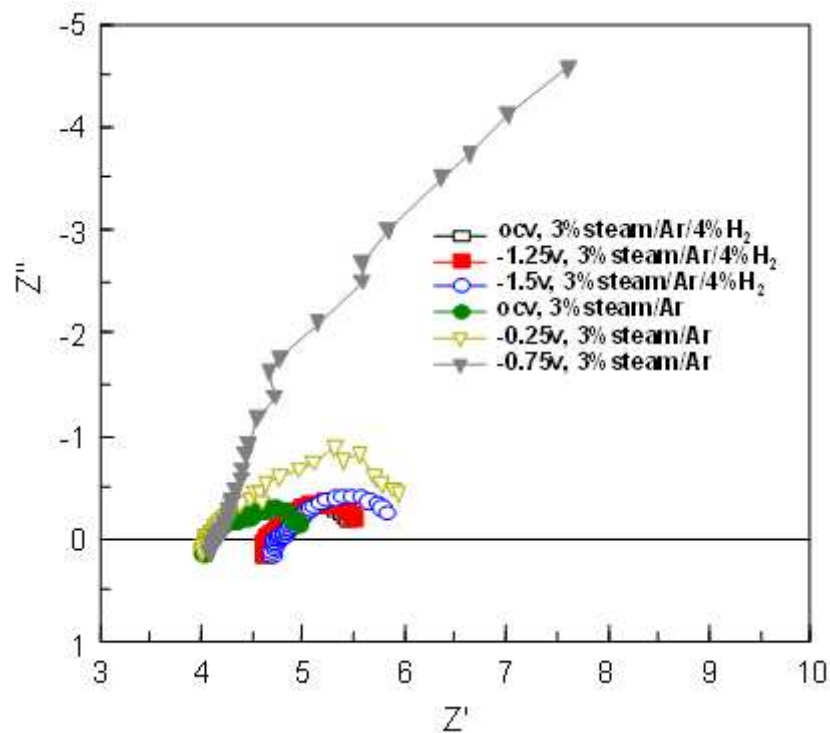
Figure 3.18. Impedance data in 3%steam/Ar and 3%steam/Ar/4%H$_2$ from LSCM/CGO cell at 920°C.

Bode plots which drives from impedance data under open circuit (see figure 3.17) at three temperatures in 3%steam/Ar are shown in figure 3.19. At 750°C, there are two limiting processes for atmosphere of 3%steam/Ar, with the summit frequencies of 0.50 Hz and 501.19 Hz for low and high frequency processes respectively. Neglecting the noisy points, there are similar characteristic frequency of around 1 Hz for low frequency arcs at 840°C and 920°C. However, the high frequency process is not evident at 840°C and 920°C. It indicates that the low frequency process is the

69

dominating rate limiting process in 3%steam/Ar, which is similar to results in 3%steam/Ar/4%H_2. The comparison of Bode plots in 3%steam/Ar and 3%steam/Ar/4%H_2 as illustrated in figure 3.20.
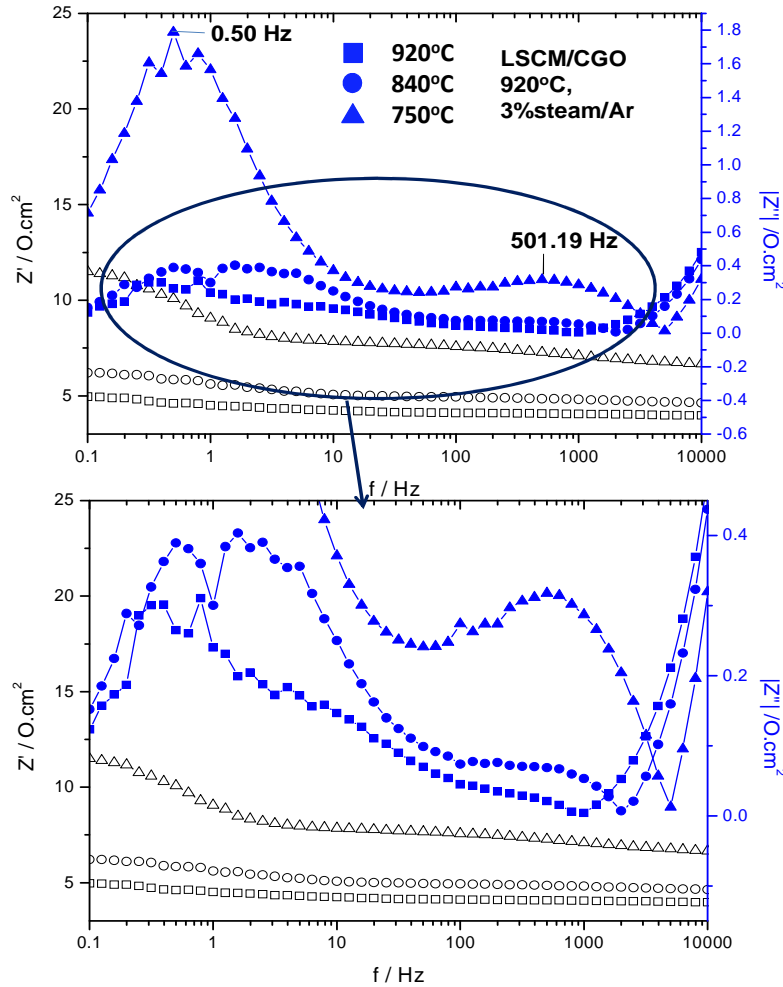
Figure 3.19. Bode plots at different temperatures from LSCM/CGO cell running with 3%steam/Ar.

Bode plots in 3%steam/Ar and 3%steam/Ar/4%H_2 at three temperatures are shown in figure 3.20. With similar characteristic frequencies, it is assumed that there are similare rate limiting processes for both atmospheres. Summit frequencies of low and high frequency processes are in the range of 0.2~1 Hz and 300~500 Hz respectively. The dominating rate limiting process for both atmospheres are the low frequency process.

Low frequency process might be gas diffusion in a stagnant gas layer above the

electrode structure, or surface adsorption process at electrodes. Maximum frequency of low frequency arc is slightly lower in 3%steam/Ar/4%H$_2$ than in 3%steam/Ar. Low frequency process in 3%steam/Ar is almost twice in magnitude of that in 3%steam/Ar/4%H$_2$ at 750°C; the difference between two atmospheres is minimized as temperature increasing.

The high frequency processes for both atmospheres are diminished in magnitude as temperature is increased. Maximum frequencies of the high frequency arcs for two atmospheres are close to each other at one temperature, and both decrease slightly with temperature. It has been reported that the surface adsorption of chemical species could decrease with temperature increase, however, the reported adsorption process occurs at a low frequency of around 0.1 Hz[18].
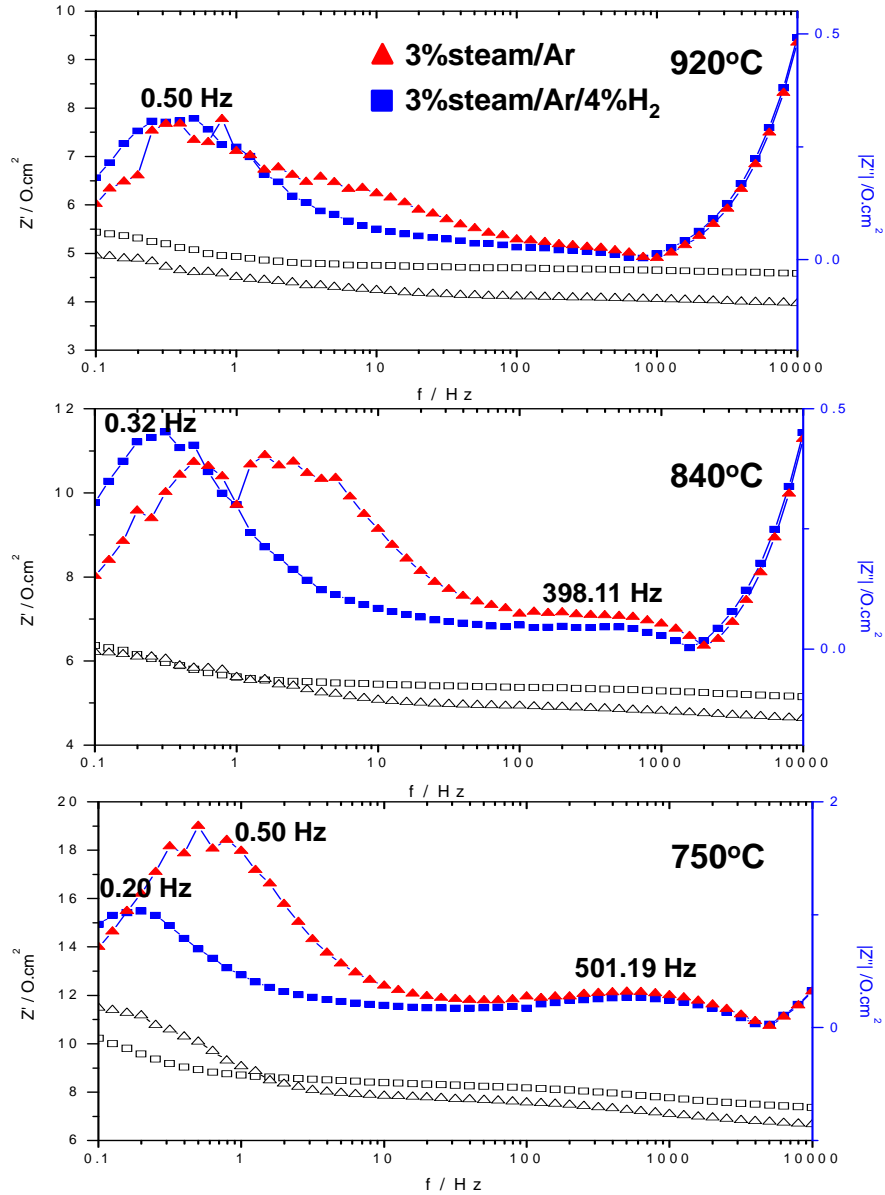
Figure 3.20. Bode plots in 3%steam/Ar and 3%steam/Ar/4%H$_2$ from LSCM/CGO cell at three temperatures.

3.2 Other cathode composites based on LSCM

Performances from cells with 2 mm YSZ electrolytes, LSM anodes and cathodes with different composites based on LSCM have been studied. Cathode composites studied were LSCM, LSCM/CGO (50% CGO by weight), LSCM/YSZ (50% YSZ by weight), and LSCM/YSZ (25% YSZ by weight). Cathode ionic conductivity and three phase boundary were considered to be improved by adding CGO to the cathode.

Thermal expansion matching and adherence between cathode and electrolyte were expected to be improved by adding YSZ into LSCM cathode. The high ionic conductivity of YSZ could also facilitate the electrochemical reaction at cathode.

Figure 3.21 displays impedance data under open circuit from cells with different cathodes with 3%steam/Ar/4%H_2 at 920°C. The value of Rs, at about 3.5 $\Omega^.cm^2$, has been deducted from the data. The four cells have similar polarization resistances. The cell with LSCM/CGO cathode shows an Rp value of 0.87 $\Omega^.cm^2$ at open circuit. LSCM/YSZ (50% YSZ by weight) cell also has a small Rp value of below 1.0 $\Omega^.cm^2$.
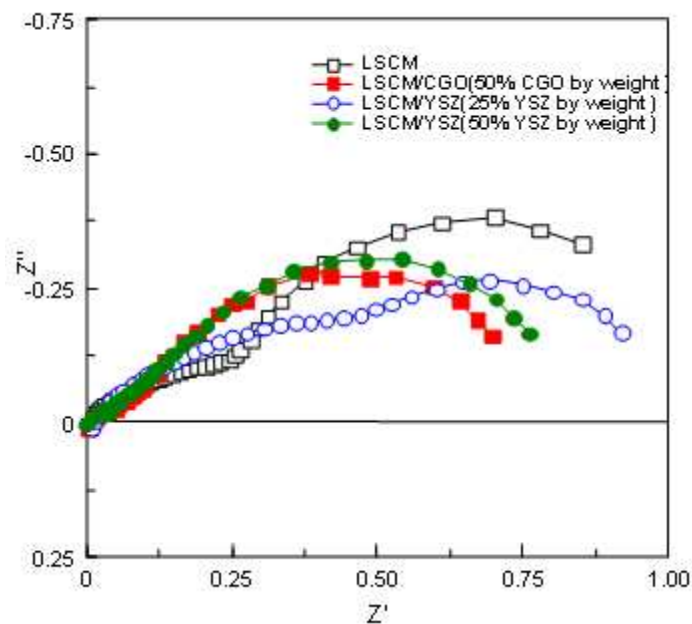
Figure 3.21. Impedance data under open circuit from cells with different cathodes at 920°C in 3%steam/Ar/4%H_2.

Figure 3.22 shows impedance data under -1.5 V from cells with different cathodes with 3%steam/Ar/4%H_2 at 920°C. The Rs value has been deducted from the data. Under -1.5 V potential applied, the LSCM/CGO cell also shows the smallest polarization resistance (of ~1.2 $\Omega^.cm^2$) among all the cells. The cell with LSCM cathode shows the largest Rp value at -1.5 V.
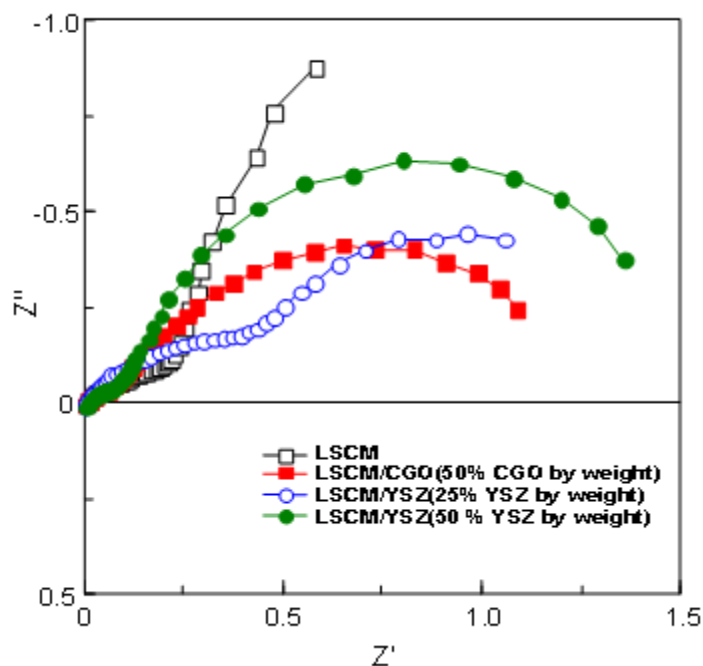
Figure 3.22. Impedance data under -1.5 V from cells with different cathodes at 920°C in 3%steam/Ar/4%H$_2$.

Bode plots derived from impedance data (under open circuit) of four cells at 920°C in 3%steam/Ar/4%H$_2$ are shown in figure 3.23. All four cells have a low frequency limiting process which might be gas diffusion and/or adsorption/desorption processes. The characteristic frequency of low frequency process increased when YSZ or CGO was added to pure LSCM. The summit frequency of low frequency arc from the cell with LSCM cathode is 0.15 Hz; while the maximum frequencies from the other three cells are at 0.40 Hz. The low frequency process of cell with pure LSCM cathode is the largest in magnitude. This means the cell with LSCM cathode has a more difficult low frequency process. This might relate to the comparatively smaller three phase boundary (TPB) zones (where the gas, electrolyte and electrocatalyst meet) from pure LSCM cathode compared to cathodes with ionic conductors.

Comparing to cells with 50 weight% YSZ (or CGO), the cell with 25 weight% YSZ has an extra limiting process at around 4 Hz. This process may also relate to the gas diffusion and/or adsorption/desorption limitations. With comparatively lower amount of ionic conductor, the cathode may have decreased TPB zones.

The LSCM/CGO cell has the smallest high and low frequency process among the four cells.
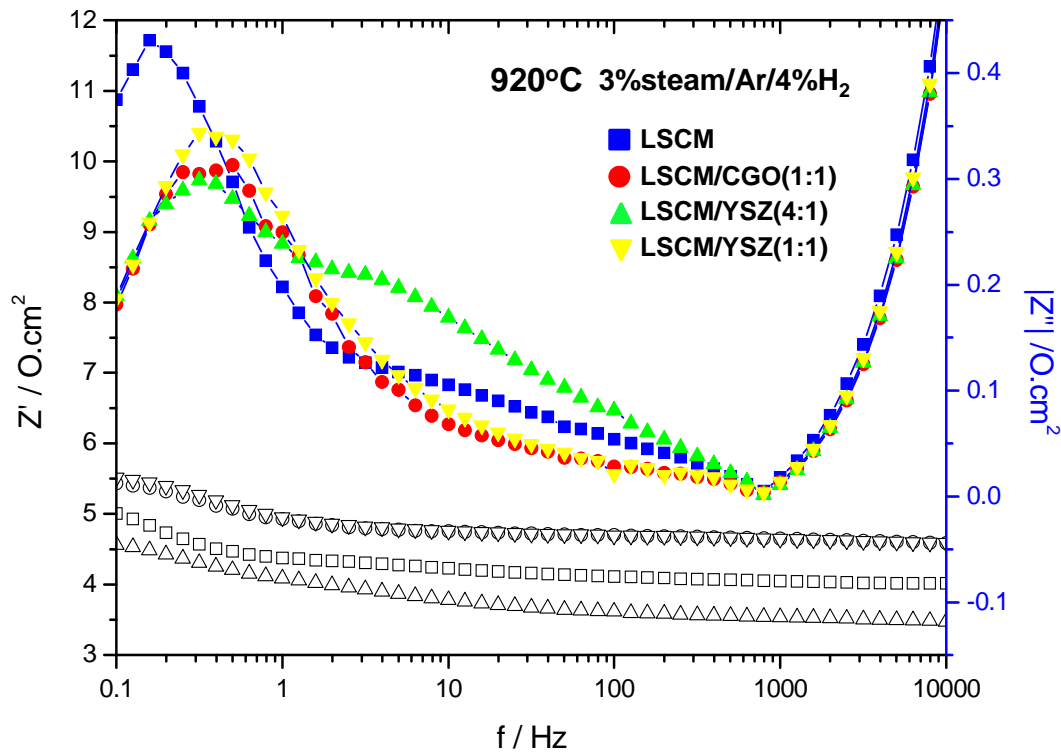

Figure 3.23. Bode plots (under open circuit) from cells with different cathodes at 920°C in 3%steam/Ar/4%H₂.

3.3 Conclusions

The conventional cathodes for YSZ-based SOECs are Ni/YSZ cermets, which exhibit good catalytic properties and current collection; however, they suffer from such problems as poor redox cycling and low tolerance to non-reducing environment. The nickel metal in the cermet may also have problems of agglomeration in prolonged operation, resulting in reduced three phase boundary. In order to overcome the drawbacks of Ni/YSZ cermet anode, alternative cathodes based on $(La_{0.75}Sr_{0.25})_{0.95}Mn_{0.5}Cr_{0.5}O_3$ (LSCM) were investigated for SOECs. LSCM, with remarkable stability with reduction or oxidation occurring at high temperature, gives good performances when working as cathodes for SOECs in atmosphere of 3%steam/Ar/4%H₂ and 3%steam/Ar.

By mixing $Ce_{0.9}Gd_{0.1}O_{1.95}$ (CGO) to LSCM cathode, cell performances could be improved further. Compared to the Rp value of more than 10 $\Omega \cdot cm^2$ from the cell with Ni/YSZ cathode operated in 3%steam/Ar/4%H_2 at 917°C, the cell with LSCM/CGO cathode shows a better Rp of around only 1 $\Omega \cdot cm^2$. Running with 3%steam/Ar, LSCM/CGO cell has a fairly small Rp when the external potential load is comparatively low, say, below -0.5 V. However, the resistance increased sharply when applying higher potentials. It seems that something unknown happened to the cell under higher loading voltages during the electrolysis.

There are two rate limiting processes for LSCM/CGO cell with both atmospheres (3%steam/Ar/4%H_2 and 3%steam/Ar). The summit frequencies of low frequency arcs locate in the range of 0.2 Hz~1 Hz. The low frequency process, which is much larger in magnitude than high frequency process, is the dominating rate limiting process which might stem from gas diffusion limitation in a stagnant gas layer above the electrode structure or a surface adsorption limitation. The high frequency process has a characteristic frequency of 300 Hz~500 Hz, which might relate to charge transfer processes, is quite small in magnitude and almost close to zero as temperature is increased to 920°C.

References

1. H. H. Mobius, *J. Solid State Electrochem.*, 1997, 1, 2.

2. S. C. Singhal and K. Kendall, *High Temperature Solid Oxide Fuel Cells (Fundamentals, Design and Applications)*, Elsevier Ltd, 2003.

3. J. S. Herring, J. E. O'Brien, C. M. Stoots, G. L. Hawkes, J. J. Hartvigsen and M. Shahnam, *Int. J. Hydrogen Energy*, 2007, 32, 440.

4. K. Eguchi, T. Hatagishi and H. Arai, *Solid State Ionics*, 1996, 86, 1245.

5. S. W. Tao and J. T. S. Irvine, *J. Electrochem. Soc.*, 2004, 151, A252.

6. S. W. Tao, J. T. S. Irvine and J. A. Kilner, *Adv. Mater.*, 2005, 17, 1734.

7. D. M. Bastidas, S. W. Tao and J. T. S. Irvine, *J. Mater. Chem.*, 2006, 16, 1603.

8. S. W. Tao, J. T. S. Irvine and S. M. Plint, *J. Phys. Chem. B*, 2006, 110, 21771.

9. D. M. Bastidas, S. W. Tao, and J. T. S. Irvine, *J. Mater. Chem.*, **2006, 16, 1603.**

10. S. W. Tao and T. S. I. John, *J. Electrochem. Soc.*, **2004, 151, A252.**

11. S. J. A. Livermore, J. W. Cotton, and R. M. Ormerod, *J. Power Sources,* **2000, 86, 411.**

12. J. D. Nicholas, and L. C. D. Jonghe, *Mater. Res. Soc. Symp. Proc.*, **2007, 1023.**

13. C. Lee, S. W. Baek, and J. Bea, *Solid state Ionics*, **2008, 179, 1465.**

14. X. J. Chen, Q. L. Liu, K. A. Khor, and S. H. Chan, *J. Power Sources*, **2007, 165, 34.**

15. J. M. Thomas and W. J. Thomas, *Principles and practice of Heterogeneous Catalysis*, **Wiley-VCH, 1997.**

16. A. Brisse, J. Schefold, and M. Zahid, *Int. J. Hydrogen Energy*, **2008, 33, 5375.**

17. S. Primdahl and M. Mogensen, *J. Electrochem. Soc.*, **1999, 146, 2827.**

18. X. J. Chen, Q. L. Liu, K. A. Khor, and S. H. Chan, *J. Power Sources*, **2007, 165, 34.**

19. S. H. Jensen, P. H. Larsen and M. Mogensen, *Int. J Hydrogen Energy*, **2007, 32, 3253.**

Chapter 4 Studies on Catalyst Addition

4.1 Introduction

The solid oxide electrolysis cell (SOEC), which converts electricity to chemical energy of fuels through electrochemical processes, is considered as an efficient clean method for hydrogen production. Although the commonly used Ni/YSZ(Y_2O_3-stabilized ZrO_2) cathodes perform well in hydrogen based steam, Ni cermets do display some disadvantages such as low tolerance to oxidizing condition and reduction of TPB due to agglomeration after long operation and poor redox cycling causing volume instability[1]. It requires a significant concentration of H_2 flowing over it, if it is not to be oxidized to NiO. Lack of reducing atmosphere would not only cause a loss of electronic conductivity but is also likely to lead to mechanical failure of the electrode[2].

Development of Ni-free materials as alternative cathodes has attracted attention recently. In chapter 3, cathodes based on $(La_{0.75}Sr_{0.25})_{0.95}Mn_{0.5}Cr_{0.5}O_3$ (LSCM) have been discussed and reasonable performance has been acquired in gas with small amount of hydrogen or without hydrogen. The addition of precious metals porous electrodes is known to improve the electrocatalytic activity and performance. Pd, Ce, Rh and Fe have been reported to promote electrode performance significantly in SOFCs[3, 4, 5]. Ni is well known as an efficient catalyst for SOEC cathodic reactions and SOFC anodic reactions. In order to investigate the effect of precious metals on the performance of high temperature SOECs, a small amount of metals (Pd, Fe, Rh, and Ni) were impregnated into LSCM/CGO($Ce_{0.9}Gd_{0.1}O_{1.95}$) (50% CGO by weight) cathodes. A Solartron SI 1255 Frequency Response Analyzer was applied to characterize the electrochemical properties from these cells with various catalysts and without catalyst. In this study, the obvious implication is that adding catalysts (especially Pd) could enhance performance from SOECs with LSCM/CGO cathode running at high temperature in steam with low content of hydrogen ($3\%H_2O/Ar/4\%H_2$) or without hydrogen ($3\%H_2O/Ar$). Among the four metal catalysts, the LSCM/CGO

cathode impregnated with palladium particles shows the best performance. Cells with LSM anodes, ~1.93 mm YSZ electrolytes and LSCM/CGO cathodes were made and loaded with various catalysts in LSCM/CGO cathode. Cells with diverse catalysts were tested in $3\%H_2O/Ar/4\%H_2$ and $3\%H_2O/Ar$ at 900^oC. Their electrochemical performances are discussed in this chapter.

4.2 Cells with various catalysts running with $3\%H_2O/Ar/4\%H_2$

Five SOECs were fabricated in an approach similar to that described in chapter 3. The cells have LSCM/CGO cathodes, ~1.93 mm thick YSZ electrolytes and LSM anodes. Four of these cells were loaded with Pd, Fe, Rh, Ni catalysts respectively at LSCM/CGO cathodes.

As five cells were made in the same batch and the conditions for fabricating the cells are quite similar to each other, it is feasible to compare the performances from different cells and discuss the effect of catalysts on cell performances. Thicknesses of electrolytes for different cells are: 1.93 mm for cell with Pd, 1.88 mm for cell with Fe, 1.94 mm for cell with Rh, 1.93 mm for cell with Ni and 1.92 mm for cell without catalyst. Electrolyte thicknesses of cells are 1.93 ± 0.01 mm except the cell with Fe (1.88 mm), however the thickness difference would result in an YSZ resistance difference of less than 0.01 $\Omega^.cm^2$ at 900^oC theoretically[6]. Electrode inks are painted and sintered to form electrodes.

All cells were tested at 900^oC with $3\%H_2O/Ar/4\%H_2$. Figure 4.1 shows the polarization properties of the cells. Open circuit voltages are -0.935 ± 0.005 volt for the cells at 900^oC with $3\%H_2O/Ar/4\%H_2$ at the cathode and air at the anode, as expected from the Nernst equation

Polarization curves from all cells are close to linear in fuel cell mode. In electrolysis mode, as potential is increased, current-voltage curves from all cells show a slightly slope increase starting from around -1.5 V and then a decrease at the final voltage (around -2.0 V). The higher slope at -1.5 V, which might be due to the heated

cell when thermoneutral point is exceeded, is in good accordance with AC impedance data in figure 4.2. The small slope at the final point (~ -2.0 V) might be not reliable as it is not consistent with the high impedance data at -2.0 V in figure 4.2. Cell currents are around 40 mA as highest potential is applied.

It can be seen in figure 4.1 that the addition of catalysts increased cell performance in $3\%H_2O/Ar/4\%H_2$. Neglecting the slightly differences in electrolyte thickness, the cells show a sequence of their performances: Pd > Fe > Rh > Ni > no catalyst. According to their polarization performances, cells with Pd and Fe work well and cells with Rh and Ni catalysts have only slightly improvements in cell performances. Current at the highest potential (OCV+(-1.0 V)) from cell with Pd catalyst is 45 mA (at -1.92 V), compared to 35 mA (at -1.93 V) from the cell without catalyst. Polarization performance from the cell with Fe catalyst is almost as good as that from cell with Pd. As all other cells have electrolyte thicknesses of 1.93 ± 0.01 mm except cell with Fe (1.88 mm), the performance improvement from the cell with Fe catalyst could partially be due to the thinner electrolyte and therefore smaller ohmic resistance. However, as the difference in YSZ thickness (0.06 mm) between the cell with Fe and other cells results in ohmic resistance of less than 0.01 $\Omega \cdot cm^2$ at 900^oC theoretically, the thickness influence is negligible compared to the cell resistances of several ohms. Therefore, comparisons of results from the cell with Fe and other cells are reasonable. It is shown that the cheap material, Fe, performs well as a catalyst for cell with LSCM/CGO cathode at 900^oC with $3\%H_2O/Ar/4\%H_2$.
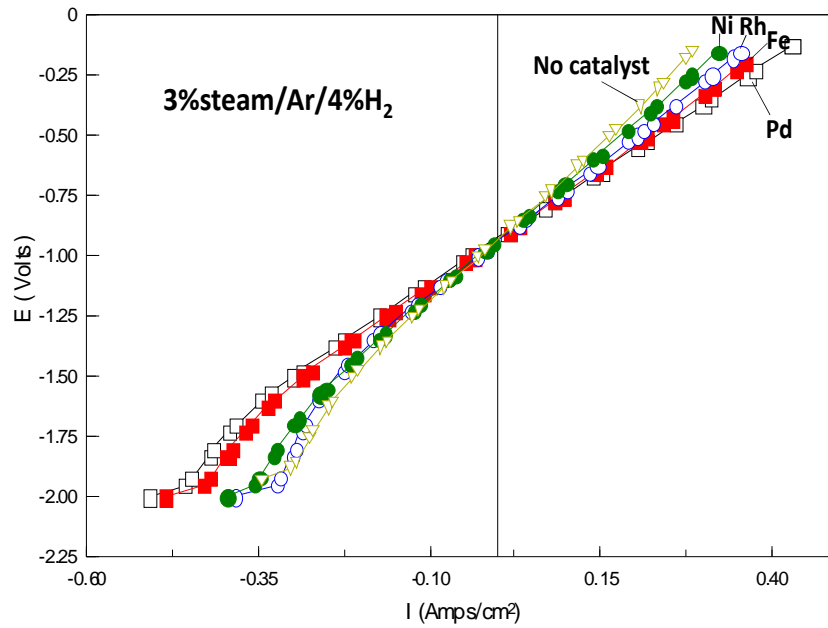
Figure 4.1. Polarization properties from cells having various catalysts in LSCM/CGO cathodes at 900°C with 3%H$_2$O/Ar/4%H$_2$.

Figure 4.2 displays the AC impedance data from a cell with Pd catalyst in LSCM/CGO cathode at 900°C with 3%H$_2$O/Ar/4%H$_2$. It has a series resistance of 1.52 Ωcm^2 and a small polarization resistance of 0.32 Ωcm^2 under open circuit. Impedance data from the cell with Pd at -1.0 V are quite similar to that under open circuit. The total resistance under open circuit for the cell with Pd catalyst is 1.85 Ωcm^2. When potential increases to -1.5 V, the low frequency semicircle gets bigger and Rp value increases to 0.67 Ωcm^2. This is in good accordance with the I-V curve displayed in figure 4.1. At -2.0 V, impedance is getting even bigger which conflicts with the small slope at -2.0 V from I-V curve in figure 4.1. The series resistance value decreases slightly when increasing potential. This might relate to improved conductivity in the electrode structure as potential is increased.
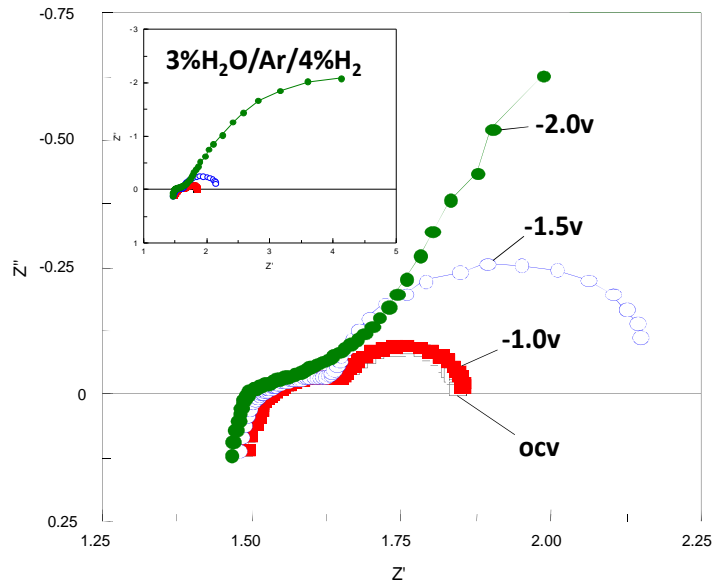
Figure 4.2. AC impedance data from a cell with Pd in LSCM/CGO cathode at 900°C with 3%H₂O/Ar/4%H₂.

dE/dI values taken from I-V curve (see figure 4.1) from the cell with Pd catalyst at 900°C with 3%H$_2$O/Ar/4%H$_2$ are displayed in figure 4.3. When potential changes from fuel cell side to -1.5 V (electrolysis mode), the dE/dI value has a decrease and then an increase but always keeps at around a small value of -1.85 $\Omega \cdot cm^2$. However, the dE/dI value increases a lot as potential increases to above -1.5 V. The highest value is around 3.8 $\Omega \cdot cm^2$ and occurs at -1.8 V. The dE/dI value decreases from -1.8 V and has a smallest value of 1.0 $\Omega \cdot cm^2$ at -2.0 V, which conflicts with impedance data. The low resistance values at around -2.0 V is probably unreliable in that the resistance of YSZ electrolyte (ohmic resistance) is 1.5 $\Omega \cdot cm^2$ at 900°C and it is unreasonable to have a resistance of 1.0 $\Omega \cdot cm^2$ for the whole cell. That is, impedance gets larger when potential is higher than -1.5 V.
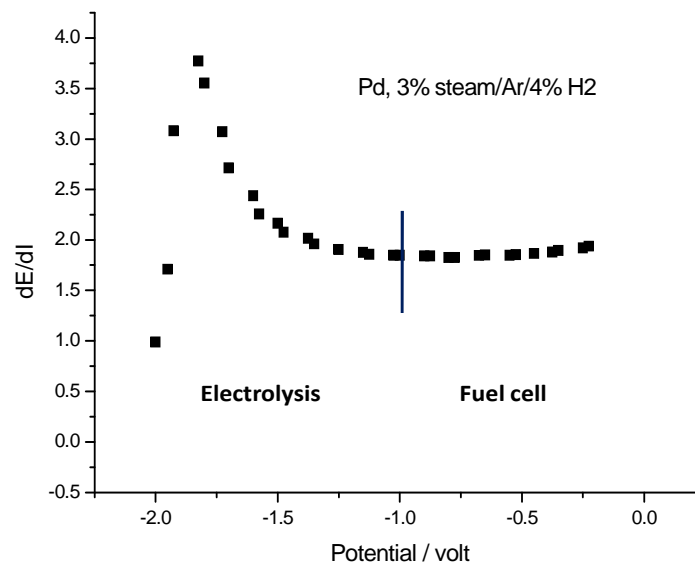
Figure 4.3. dE/dI value taken from I-V curve from a cell with Pd catalyst at 900°C with 3%H$_2$O/Ar/4%H$_2$.

Comparisons of impedance data under open circuit from cells with different catalysts and without catalyst at 900°C with 3%H$_2$O/Ar/4%H$_2$ are shown in figure 4.4. Neglecting the small difference in ohmic resistance caused by thickness of electrolyte, the series resistances are compared as follows. Ohmic resistances are 1.5 Ω·cm^2 to 1.9 Ω·cm^2 for these cells. There are not complete semicircles for low frequency process for these cells except the cell with Pd catalyst. The cell with Pd catalyst, with a complete low frequency semicircle, has the smallest Rp value (see figure 4.5). Interactions between Pd and Ce have been reported to have an enhancement in catalytic activity[7, 8]. It was reported that Pd/Ce catalyst does not work by interact with LSCM[10]. And Pd/CeO$_2$ has been reported to have a good catalytic activity for fuel cell with LSCM anode, although it is unclear how the catalysts play its role[9]. As there is CGO in cathode material, Pd in LSCM/CGO cathode might works in a similar way.

Impedance from the cell with Rh catalyst shows three distinct semicircles/processes within the measurement limit of 100 KHz ~ 0.1 Hz. Other cells only have two evident processes in the measurement frequency range. One possibility is that there are only

two processes for other cells; or the two high frequency processes overlap with each other and become undistinguishable. The processes will be analyzed by bode presentations in figure 4.6.
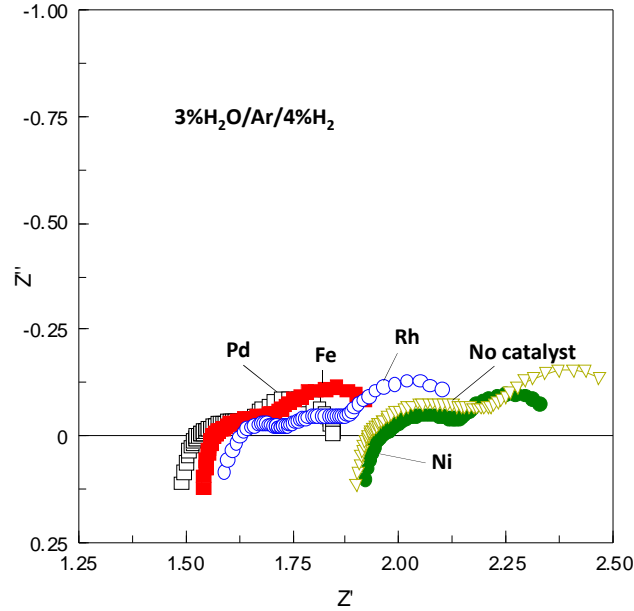

Figure 4.4. AC Impedance data under open circuit from cells having various catalysts in LSCM/CGO cathodes at 900°C with 3%H$_2$O/Ar/4%H$_2$.

Polarization resistances under open circuit from different cells are displayed in figure 4.5. Rp values are decreased by adding catalysts, especially by the addition of Pd. The cell with Pd catalyst has a small Rp value of 0.32 Ω·cm^2, compared to the Rp value of 0.65 Ω·cm^2 from cell without catalyst. Polarization resistance from the cell with Pd is smaller than other cells, indicating Pd has the best enhancement for cathode processes.

Fe is also a good catalyst for SOEC cathode reactions but is much cheaper than Pd. It results in a polarization resistance of 0.41 Ω·cm^2 at 900°C with 3%H$_2$O/Ar/4%H$_2$, which is the second smallest value among the cells. The cell with Ni has an Rp value of 0.43 Ω·cm^2, which is only a bit higher than the cell with Fe. Ni reduced the polarization resistance much more than Rh did. This suggests Ni might have a better catalytic activity than Rh for electrode process in 3%H$_2$O/Ar/4%H$_2$.

Cell with Rh catalyst gives an polarization value of 0.56 Ω·cm^2. Although it is the

highest Rp among cells with catalysts, it reduced the Rp value by 0.1 $\Omega \cdot cm^2$ from the cell without catalyst.

All catalysts have improved electrode performances in SOECs with LSCM/CGO cathodes. Pd did best in reducing the polarization resistance. Fe and Ni, which are much cheaper than Pd, also work well in improving electrode processes.
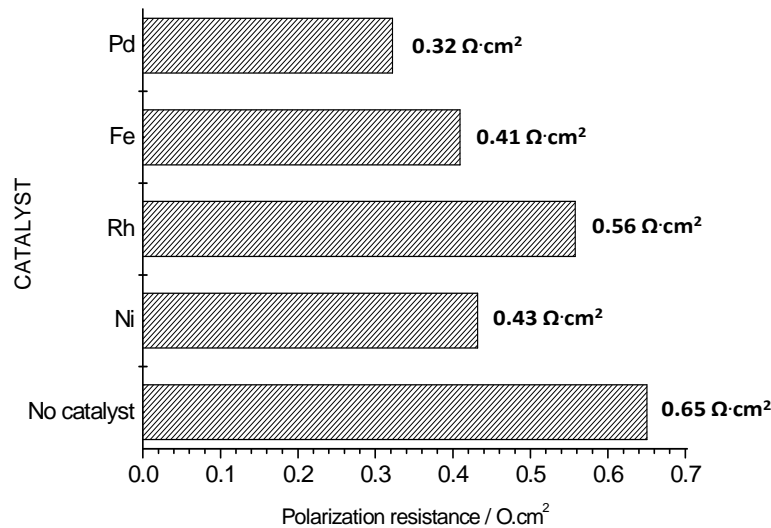

Figure 4.5. Polarization resistances under open circuit from cells having various catalysts in LSCM/CGO cathodes at 900°C with 3%H$_2$O/Ar/4%H$_2$.

Figure 4.6 shows Bode presentations under open circuit from cells with various catalysts in LSCM/CGO cathodes at 900°C with 3%H$_2$O/Ar/4%H$_2$.

The cell without catalyst has two rate limiting processes with characteristic frequencies of 0.2 Hz and 63 Hz respectively. And the low frequency process is the major process. By adding catalysts, the low frequency process is reduced in magnitude but the summit frequency of the low frequency arc does not change. The magnitude sequence of the low frequency processes from cells with different catalysts is: Pd < Ni < Fe < Rh < no catalyst. The low frequency process might originate from gas diffusion limitation or surface adsorption/desorption limitation. Gas diffusion processes are commonly affected by the microstructure of electrode. It is less easy to change cathode microstructure by loading catalyst. As the low frequency process is affected much by catalysts, it is more likely to be an adsorption/desorption processes

85

rather than a gas diffusion process. The adsorption/desorption processes occurring at a cathode might include: adsorption of water, desorption of hydrogen, desorption of oxygen intermediates and oxygen ions. Adsorption/desorption of species on different metals are distinct. This could result in various magnitude of the process.

Cells with different catalysts and without catalyst have different characteristic frequencies for the high frequency processes, which might relate to charge transfer processes. Cells with smaller characteristic frequencies have more reduced high frequency processes in magnitude. There might be a third process with highest frequency and it overlaps with the high frequency process (13~63 Hz). When the third process (at highest frequency) decreases in magnitude, the overlapped peak would shift to lower frequencies. In figure 4.6, there is the trend that Bode plots with smaller magnitude at around 1000 Hz have lower characteristic frequencies for high frequency process (13~63 Hz). The third process (at around 1000 Hz) stem from charge transfer limitation. The magnitude of high frequency processes from cells are in sequence of Pd < Fe < Rh < Ni < no catalyst. The high frequency process has the same sequence as the low frequency process except for cells with Ni and Fe. The cell with Ni has a larger high frequency process and a smaller low frequency process compared to the cell with Fe. This results in similar polarization resistances for these two cells (see figure 4.5).

The cell with Pd catalyst has the smallest magnitude for both low and high frequency processes. It confirms Pd as a best catalyst for cathode process with $3\%H_2O/Ar/4\%H_2$.
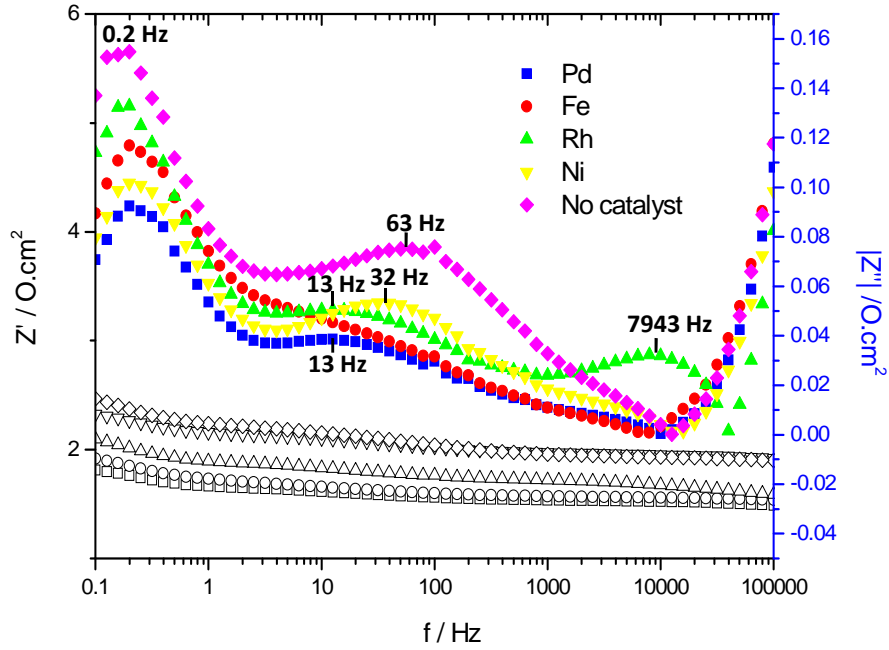
Figure 4.6. Bode plots under open circuit from cells having various catalysts in LSCM/CGO cathodes at 900°C with 3%H$_2$O/Ar/4%H$_2$.

When an external potential is applied, the cell with Pd shows a more obviously better performance than other cells. Figure 4.7 displays AC impedance data under -1.5 V from cells with various catalysts at 900°C with 3%H$_2$O/Ar/4%H$_2$. Impedance from the cell with Pd has a complete low frequency semicircle and has a small polarization resistance of 0.68 Ω·cm^2. Cells without catalyst and with other catalysts do not have complete semicircles within the measurement limit of 0.1 Hz.

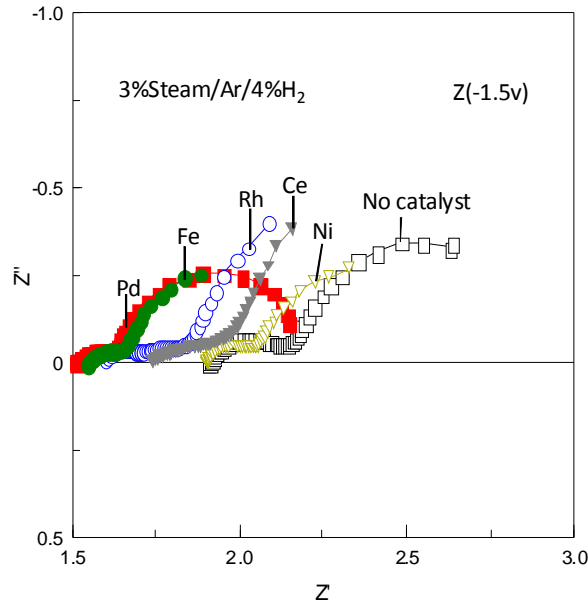**Figure 4.7. AC Impedance data at -1.5 V from cells having various catalysts in LSCM/CGO cathodes at 900°C with 3%H$_2$O/Ar/4%H$_2$.**

4.3 Cells with various catalysts running with 3%H$_2$O/Ar

Polarization properties from cells with different catalysts at 900°C with 3%H$_2$O/Ar, figure 4.8, have slight differences between each other. In fuel cell side, catalysts has the same impact on cell performance in 3%H$_2$O/Ar/4%H$_2$ with that in 3%H$_2$O/Ar. In electrolysis mode, the differences from cells running with 3%H$_2$O/Ar are less than running with 3%H$_2$O/Ar/4%H$_2$ (see figure 4.1).

Current-voltage curves from all these cells have segments with high slopes when cells are running with 3%H$_2$O/Ar. The high slope occurs when applying -0.3 ~ -0.75 V potentials. This is the same phenomena with the results discussed in section 3.3.3. For segment C-D (see figure 4.8), the addition of catalysts promoted cell performance and have a same trend with 3%H$_2$O/Ar/4%H$_2$ for different catalysts. Cell with Pd catalyst has the smallest slope in segment C-D, followed by Fe, Rh and Ni.

However, something unusual happed to the cell at voltages of -0.3 to -0.75 V and there is a strange phenomena that the catalysts seems to have a negative effects on cell performances for segment B-C. In segment B-C, with voltages of -0.3 to -0.75 V, cell

with no catalyst has a comparatively small slope of segment B-C. In addition, cell with no catalyst has the highest current when the same voltage is applied. By contrast, cell with Pd catalyst has the largest slop as well as lower currents when the same voltage is applied. There is similar strange phenomena in section 3.3.3 (figure 3.15), polarization curve from LSCM/CGO cell running with $3\%H_2O/Ar$ has a bit higher slope at higher temperature, while it is supposed to have better performances at higher temperatures. In segment B-C, it seems that cell has poorer performance in better conditions.
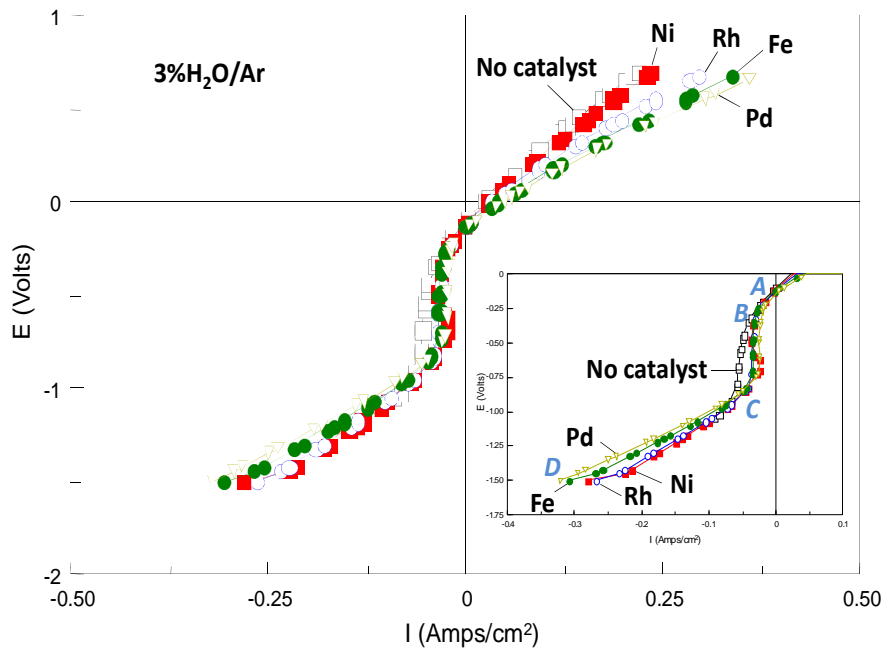

Figure 4.8. Polarization properties from cells having various catalysts in LSCM/CGO cathodes at 900^oC with $3\%H_2O/Ar$.

It could be seen from figure 4.8 that the cell with Pd catalyst performs slightly better than other cells except in segment B-C (-0.3 to -0.75 V) at 900^oC with $3\%H_2O/Ar$. AC impedance data at different voltages from the cell with Pd are shown in figure 4.9. It has bigger resistance under open circuit than at high voltages (-1.0 V, -1.25 V and -1.5 V). Low frequency process has a complete semicircle at open circuit. Impedance at high voltages (-1.0 V, -1.25 V and -1.5 V) do not have complete semicircles within the measurement limit of 0.1 Hz but have smaller resistances than

89

under open circuit. This could be confirmed by dE/dI value (see table 4.1) derived from the I-V curve of cell with Pd catalyst.

dE/dI values are derived from the linear fit of current-voltage curve (see figure 4.8) from the cell with Pd catalyst at $900^{\circ}C$ with $3\%H_2O/Ar$. They could be roughly regarded as total resistances of the cell. Rs values are taken from AC impedance data in figure 4.9. When Rs values are deducted from dE/dI values, the values could be considered as the Rp values. Table 4.1 shows the dE/dI, Rs and dE/dI-Rs values from the cell with Pd catalyst running at $900^{\circ}C$ with $3\%H_2O/Ar$. It has higher series resistance at open circuit than at high voltages, which is similar to the phenomena with $3\%H_2O/Ar/H_2$. Polarization resistance (roughly equal to dE/dI-Rs value) under open circuit is much larger than at high voltages (-1.0 V, -1.25 V and -1.5 V). This is a different phenomena to that in $3\%H_2O/Ar/H_2$ (see figure 4.2)
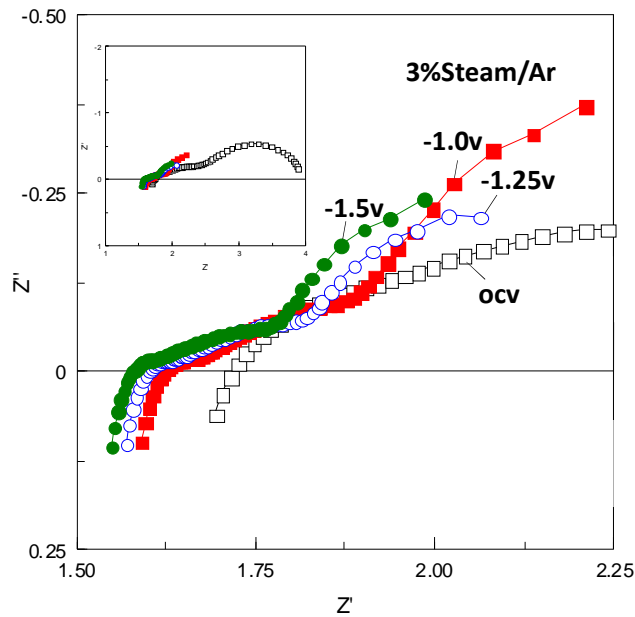

Figure 4.9. AC impedance data from a cell with Pd in LSCM/CGO cathode at $900^{\circ}C$ with $3\%H_2O/Ar$.

Potential (v)	ocv (-0.14 V)	-1.0	-1.25	1.5
dE/dI ($\Omega\cdot cm^2$)	4.10	2.48	2.23	2.20
Rs ($\Omega\cdot cm^2$)	1.72	1.62	1.60	1.58

dE/dI–Rs ($\Omega \cdot cm^2$)	2.38	0.86	0.63	0.62

Table 4.1 dE/dI, Rs and dE/dI-Rs values from a cell with Pd in LSCM/CGO cathode at 900^oC with $3\%H_2O/Ar$.

Figure 4.10 shows the comparison of AC impedance data at -1.0 V from the cell with Pd in $3\%H_2O/Ar/4\%H_2$ and $3\%H_2O/Ar$. Rs value is a bit higher in more oxidizing atmosphere than in 4% H_2. Polarization resistance at -1.0 V in $3\%H_2O/Ar$ is much higher than in $3\%H_2O/Ar/4\%H_2$.

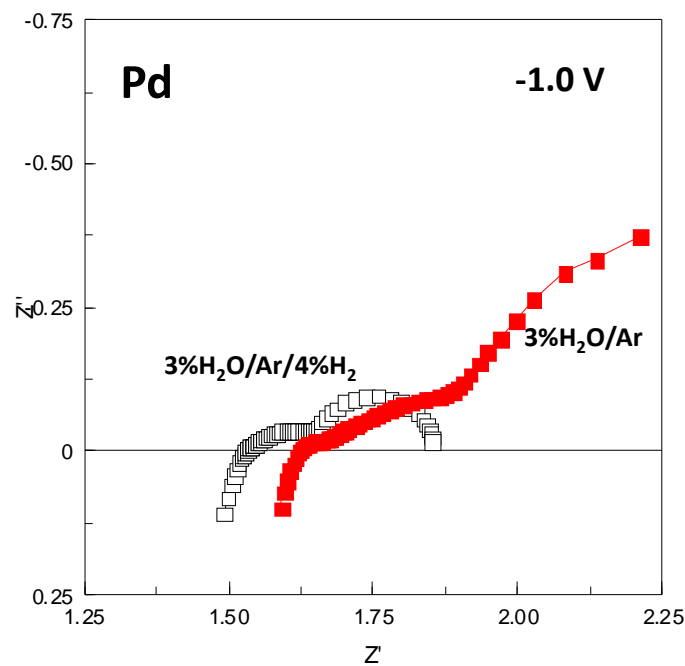**Figure 4.10 AC impedance data at -1.0 V from a cell with Pd in LSCM/CGO cathode at 900^oC with $3\%H_2O/Ar/4\%H_2$ and $3\%H_2O/Ar$.**

Bode presentations in figure 4.11 show the difference in rate limiting processes under different potentials from the cell with Pd at 900^oC with $3\%H_2O/Ar$. The low frequency process shifts to lower frequencies when high potential is applied. On the other side, the magnitude of high frequency process almost decreased to zero at high potential than at OCV. The main process might stem from LSCM reduction under open circuit and may relate to steam dissociation at potentials. The decrease of high

frequency process might be the reason of the low total resistance at high potential. As higher potential could result in better charge transfer process, there is a chance that the high frequency characteristic frequency of 100 Hz might be charge transfer process.
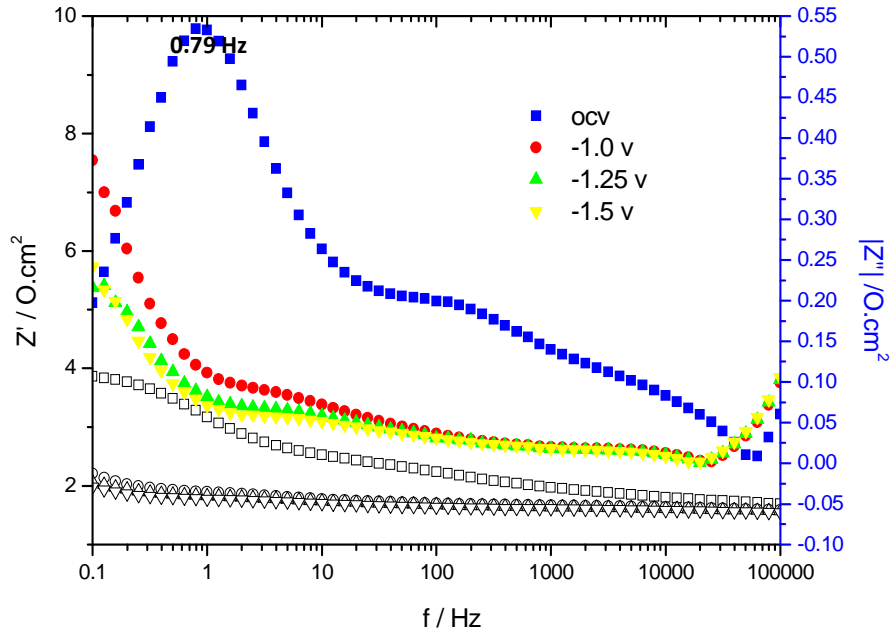

Figure 4.11. Bode plots under open circuit from a cell with Pd in LSCM/CGO cathode at 900^oC with $3\%H_2O/Ar$.

AC impedance data under open circuit from cells with various catalysts are compared in figure 4.12. Series resistances are between 1.7 $\Omega^.cm^2$ and 2.4 $\Omega^.cm^2$ for these cells which are in agreement with the expected ohmic resistance of a 2 mm YSZ electrolyte, 1.8 $\Omega^.cm^2$. Total resistances are 3.5~4.8 $\Omega^.cm^2$ for these cells. Running with $3\%H_2O/Ar$, cell with Ni has a slightly larger total resistance than cell without catalyst. The cell with Fe catalyst has the smallest resistance instead of cell with Pd.

Polarization resistances taken from impedance data are shown in figure 4.13. The cell with Fe has the smallest Rp value of 1.79 $\Omega^.cm^2$, followed by the cell without catalyst. Cells with other catalysts have slightly larger polarization resistances than the cell without catalyst. Electrode processes of cells under open circuit at 900^oC with $3\%H_2O/Ar$ are discussed in figure 4.14.
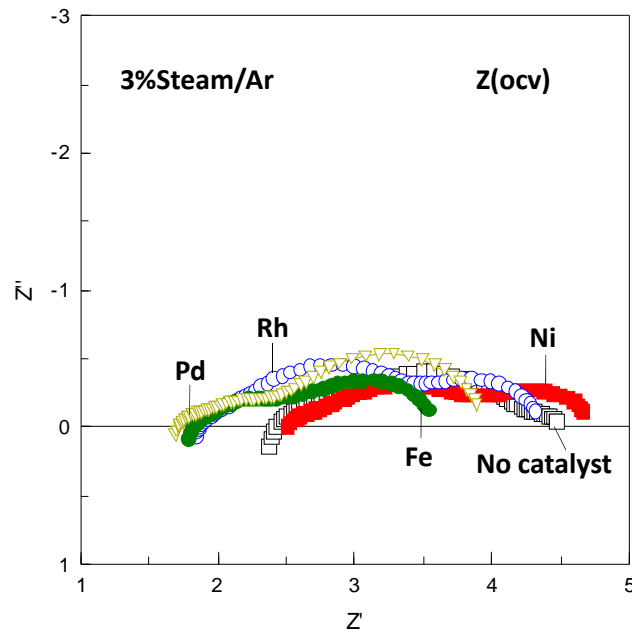
Figure 4.12. AC Impedance data under open circuit from cells having various catalysts in LSCM/CGO cathodes at 900°C with 3%H$_2$O/Ar.
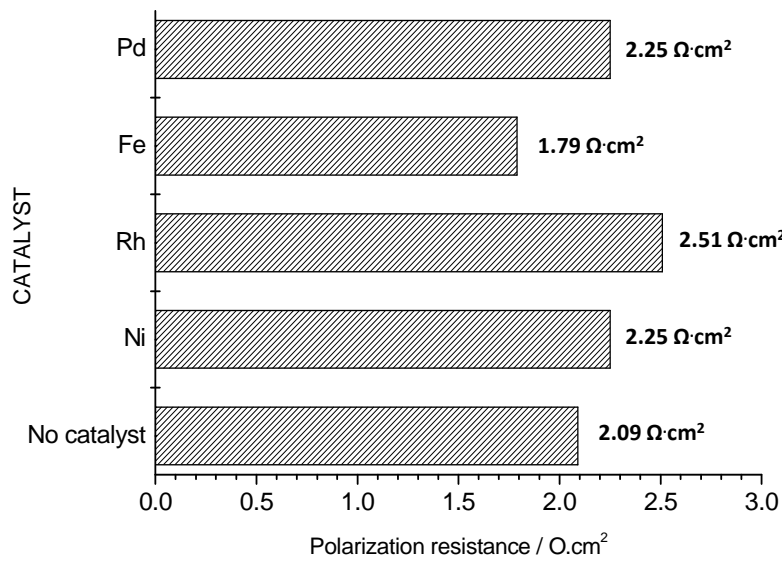

Figure 4.13. Polarization resistances under open circuit from cells with various catalysts in LSCM/CGO cathodes at 900°C with 3%H$_2$O/Ar.

Figure 4.14 is the Bode presentations from cells with various catalysts under open circuit at 900°C with 3% H$_2$O/Ar. There are two major rate limiting processes for all cells in this atmosphere.

Cells with different catalysts differ a lot in their electrode impedance processes. Cell without catalyst has the smallest low frequency process however this gives largest high frequency process. In contrast, cell with Pd catalyst has the highest low frequency process but smallest high frequency process. Cell with Fe has the smallest high frequency process and comparatively small low frequency process. Fe has the best effect on electrode process which is in agreement with the Rp value.

The low frequency process for all cells have a summit frequency of 0.79 Hz, and the magnitude of low frequency process from these cells in $3\%H_2O/Ar$ are quite different from each other. The low frequency process might be a gas diffusion process or an adsorption/desorption process. It has been discussed in section 4.2 that with quite distinct magnitude for different cells, the low frequency process is more probable to be surface adsorption/desorption processes rather than gas diffusion process. The adsorption of species on the surface of a catalyst might affect the adsorption/desorption process. As different metals have diverse binding energies of species, it could result in different magnitude in different adsorption/desorption processes. Supposing the low frequency process stem from adsorption/desorption process, adsorption of hydrogen molecule on metal surface would affect adsorption/desorption of water molecule in atmosphere with hydrogen. And this might result in the lower characteristic frequency of low frequency process with $3\%H_2O/Ar/4\%H_2$.

The characteristic frequency of low frequency process in $3\%H_2O/Ar$ is higher than the frequency in $3\%H_2O/Ar/4\%H_2$. If suppose the low frequency processes in two atmospheres both stem from adsorption/desorption process, this indicates that these cells could have better low frequency processes in $3\%H_2O/Ar$ than in $3\%H_2O/Ar/4\%H_2$. Adsorption/desorption processes occurring at cathode might include: adsorption of water, desorption of hydrogen, desorption of oxygen intermediates and oxygen ions. Hydrogen has been reported to have a small adsorption energy on pure metal surface[11]. The adsorption of hydrogen might compete with the adsorption of water on the surface of catalyst. For cathode reactions, better adsorption/desorption process means better water adsorption and/or better hydrogen

desorption. The presence of hydrogen in cathode might depress the adsorption/desorption process in cathode. If the low frequency processes for two atmospheres are both surface adsorption/desorption processes, it is reasonable to have a slightly better low frequency process in $3\%H_2O/Ar/4\%H_2$. And the similar phenomena from another cell shown in figure 3.20 (section 3.3.3) could be explained as well.

Cells with different catalysts are also quite different in magnitude of high frequency process. The high frequency process has a summit frequency of 126 Hz except the cell with Rh (63 Hz). The high frequency processes might be the transport of oxygen intermediates/oxide ions[12]. Cells with Pd and Fe have the lowest high frequency processes while cells with Rh and without catalyst have larger high frequency processes. High frequency process decreases to almost zero in magnitude for the cell with Pd catalyst when high potential is applied (see figure 4.10). This indicates potentials could affect the high frequency process. And it is reasonable to have better charge transfer at higher voltages.
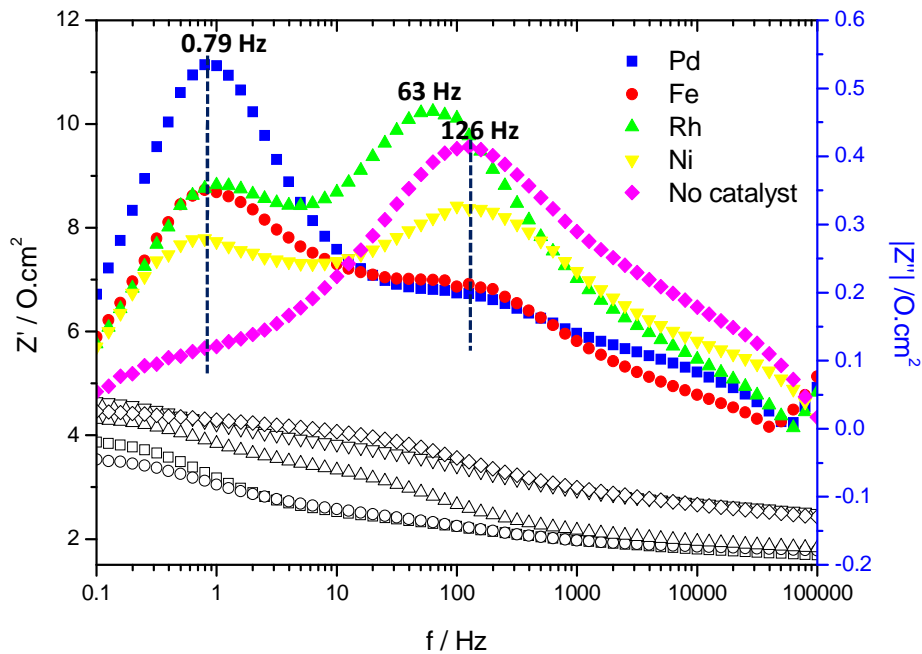

Figure 4.14. Bode plots under open circuit from cells having various catalysts in LSCM/CGO cathodes at 900°C with 3%H$_2$O/Ar.

Cells have diverse performances when external potential is applied. Figure 4.15 shows AC impedance data at -1.25 V from cells with various catalysts at 900^oC with $3\%H_2O/Ar$. Total resistances at -1.25 V are smaller than under open circuit for all these cells. AC impedance data do not have complete semicircles for low frequency process. Cell with Pd has the smallest polarization resistance under -1.25 V among the cells. Cells without catalyst and with Rh catalyst have bigger Rp_1 values (from the first semicircle of impedance data) than other cells.
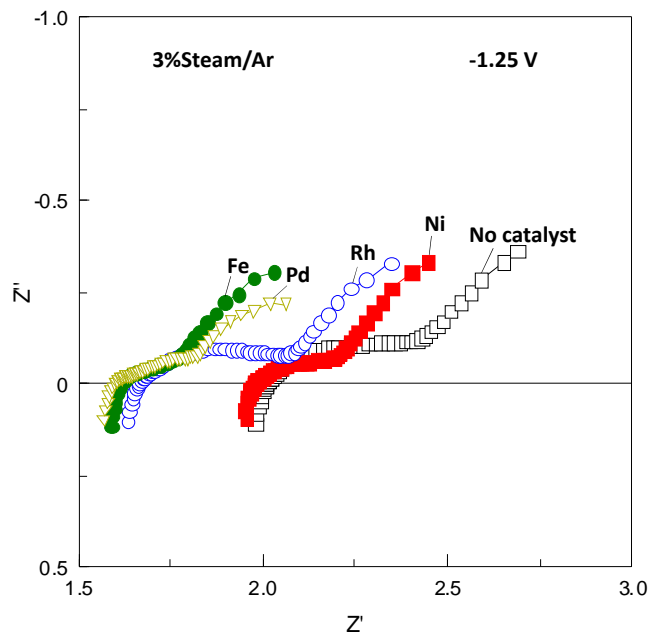

Figure 4.15. AC Impedance data at -1.25 V from cells having various catalysts in LSCM/CGO cathodes at 900^oC with $3\%H_2O/Ar$.

Bode presentations (derived from impedance data in figure 4.15) under -1.25 V from cells at 900^oC with $3\%H_2O/Ar$ are shown in figure 4.16. The high frequency process decreases a lot in magnitude for all cells compared to that under open circuit. This confirms that applied potential would decrease the high frequency process in magnitude for all these cells. All the cells (except cell with Rh) have smaller characteristic frequency for high frequency process at -1.25 V than under open circuit. The low frequency processes shift to lower frequency as potential is applied. Pd has the smallest low frequency process as well as high frequency process, which is in

good accordance with the smallest polarization resistance of cell with Pd shown in figure 4.15.
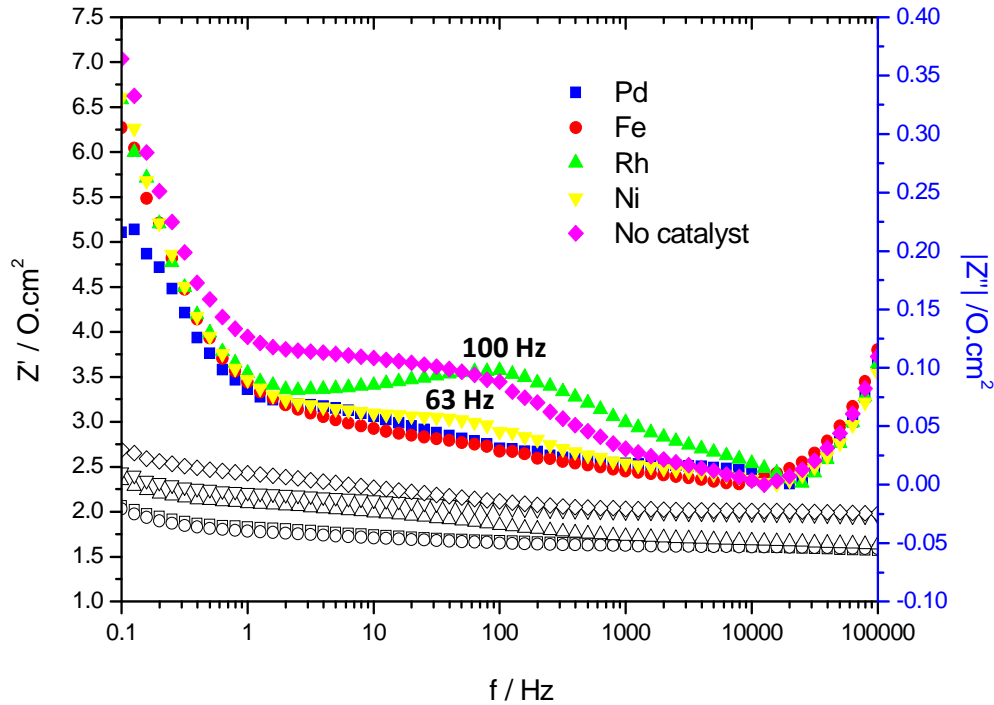

Figure 4.16. Bode plots under -1.25 V from cells having various catalysts in LSCM/CGO cathodes at 900°C with 3%H$_2$O/Ar.

4.4 Conclusions

The additions of catalysts in SOEC cathodes are shown to have enhancements on electrode performances.

The In 3%H$_2$O/Ar/4%H$_2$, Pd is able to catalyze the highest cathode performance. With presence of hydrogen, the cell with Pd has the smallest Rp value and lowest magnitude in rate limiting processes. Fe, which is much cheaper than Pd, also catalyzes a high cathode performance in 3%H$_2$O/Ar/4%H$_2$.

In 3%H$_2$O/Ar, the cell with Fe has the smallest polarization resistance under open circuit. At -1.25 V, the cell with Pd has the smallest Rp value. The cell with Pd has a good performance except when potentials are -0.3~-0.75 V. There is a strange phenomena that, between -0.3 and -0.75 V, I-V curve from the cell without catalyst

has lowest slope but from the cell with Pd has the highest slope in $3\%H_2O/Ar$.

There are two obvious rate limiting processes for $3\%H_2O/Ar/4\%H_2$ and $3\%H_2O/Ar$. The low frequency processes are the major process for both atmospheres. Different catalysts result in diverse magnitude of low frequency process in each atmosphere. The characteristic frequency of low frequency process in $3\%H_2O/Ar$ is smaller than that in $3\%H_2O/Ar/4\%H_2$. It could be supposed that the low frequency process might stem from surface adsorption/desorption limitations.

Future work could examine the measurement of the effect of concentration and distribution of added catalysts on the electrode performance.

References

1. S. W. Tao and J. T. S. Irvine, *J. Electrochem. Soc.,* **2004, 151, A252.**

2. X. D. Yang and J. T. S. Irvine, *J. Mater. Chem.,* **2008, 18, 2349**

3. S. McIntosh, J.M. Vohs, R.J. Gorte, *Electrochem. Solid-State Lett.*, **2003, 6, A240.**

4. H. Uchida, H. Suzuki, M.Watanabe, *J. Electrochem. Soc.*, **1998, 145, 615.**

5. G. Kim, G. Corre, J. T. S. Irvine, J. M. Vohs, and R. J. Gorte, *Electrochem. Solid-State Lett.*, **2008, 11, B16.**

6. F. T. Ciacchi, K. M. Crane, and S. P. S. Badwal, *Solid State Ionics*, **1994, 73, 49.**

7. S. Sharma, S. Hilaire, J. M. Vohs, R. J. Gorte, and H.-W. Jen, *J. Catal.,* **190, 199 2000.**

8. X. Wang and R. J. Gorte, *Catal. Lett.*, **2001, 73, 15.**

9. G, Kim, S. Lee, J. Y. Shin, G. Corre, J. T. S. Irvine, J. M. Vohs, and R. J. Gorte, *Electrochem. Solid-State Lett.*, **2009, 12, B48.**

10. S. Lee, G. Kim, J. M. Vohs, and R. J. Gorte, *J. Electrochem. Soc.*, **155, B1179.**

11. J. Rossmeisl and W. G. Bessler, *Solid State Ionics*, **2008, 178, 1694.**

12. M. J. Jorgensen and M. Mogenson, *J. Electrochem. Soc.*, **2001, 148, A433.**

Chapter 5   Improvements on cell microstructures

5.1 Introduction

SOEC performance could be promoted by improving cell microstructures. Among various cell configurations, planar and tubular cells are the most common designs in recent years[1]. In this study, measurements were done with planar cells.

Total cell resistance consists of ohmic resistance and polarization resistance. Ohmic resistance is mostly composed of electrical resistance of YSZ electrolyte, and polarization resistance mainly stems from species transfer and charge transfer limitations in electrodes.

The electrical resistance R of a conductor of uniform cross section can be computed as

$$R = l \cdot \rho / A.$$

l is the length of the conductor, A is the cross-sectional area, ρ is the electrical resistivity. The electrical resistance of a conductor could be reduced by decreasing length l or increasing area A. As ohmic resistance of the cell mainly origins from YSZ electrolyte, decreasing YSZ electrolyte thickness is an alternative to decrease the ohmic loss in order to improve cell performance. Solid oxide electrolytes for SOFCs have to present sufficient mechanical strength, no pores or cracks, which is difficult for a thin membrane. Several methods have been studied and reported in making cells with thin electrolytes. Tape casting has been reported to be a promising method to fabricate thin electrolyte[2, 3, 4]. It has also been reported to prepare electrode supported cells with thin electrolytes using co-pressing technique[5, 6].

Improving electrode microstructures is important in decreasing cell polarization resistance. Sufficient porosity in electrodes could facilitate gas diffusion processes. Gorte *et al.* fabricated cells with thin electrolyte and impregnated electrodes which present good electrochemical performances[7, 8].

In this study, several improvements on cell configurations have been attempted to

promote cell performances, such as tape casting and co-pressing ways to fabricate thin electrolytes and impregnation method to obtain better microstructure in electrodes.

5.2 Cell performance from cells with 250 micron thick YSZ electrolytes

Cells with 250 micron thick YSZ electrolytes (by cutting YSZ column) were made to improve the performances and were tested (4-terminal test) in 3%steam/Ar/4%H_2 and 3%steam/Ar at 920°C. SEM pictures of LSCM/CGO cathode and cell cross-section are shown in figure5.1, which show that the LSCM/CGO cathode has a porous structure and the thickness of the electrolyte is about 250 microns.
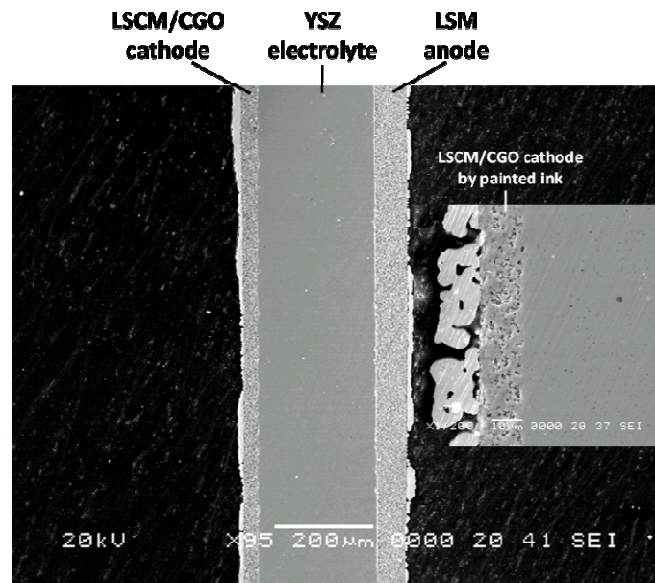

Figure 5.1. SEM pictures of cross-section from a cell with LSCM/CGO cathode, 250 micron thick YSZ electrolyte and LSM anode.

The cell performance at 920°C with 3%steam/Ar/4%H_2 is presented in figure 5.2. The ionic resistances are about 0.4 $\Omega\cdot$cm^2, under open circuit or under different external potential load. The cell has the highest polarization resistance under -1.5 volt and the Rp has smaller values under lower and higher voltages. This is in good

agreement with the nonlinear current voltage curve in figure 5.2. In chapter 3, it is shown that there is no obvious slope change in I-V curves when the thick cell is running with 3% steam/Ar/4%H_2. But diverse Rp values under different potentials indicate that the I-V curve with 3%steam/Ar/4%H_2 is not strictly linear and the impedance for these thick cells shows the highest polarization resistance under -1.5 volt (see section 3.3.2). Results in figure 5.2 show that a SOEC with LSCM/CGO cathode has a nonlinear relationship in its I-V curve with 3%steam/Ar/4%H_2-with regions of high slope between -0.07 and -0.6V and between -1.2 and -1.6 V.
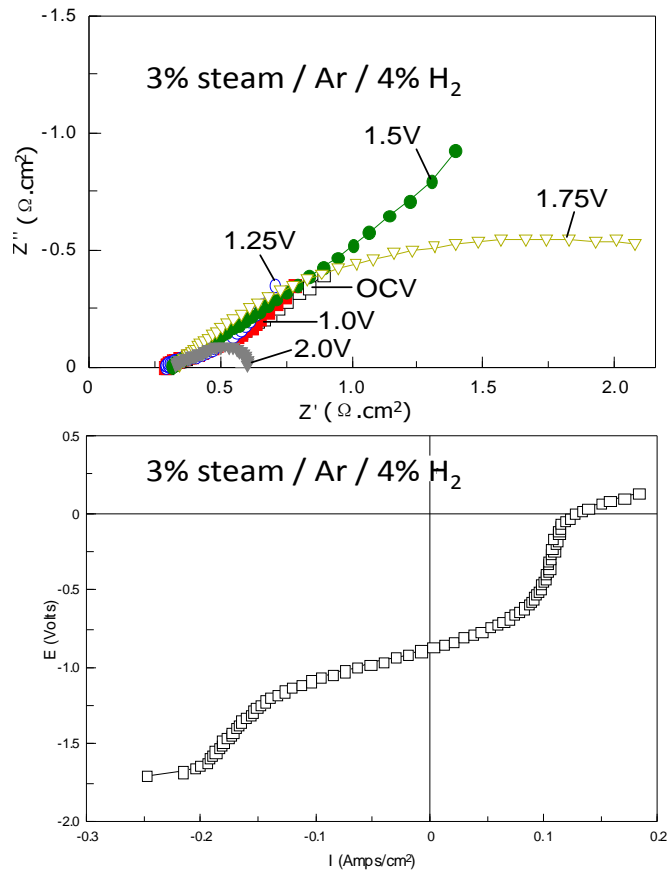

Figure 5.2. Performance from an SOEC with LSCM/CGO cathode, 250 micron thick YSZ electrolyte and LSM anode at 920°C with 3%steam/Ar/4%H_2. a. AC impedance data measured at OCV, 1.0 V, 1.25 V, 1.5 V, 1.75 V, 2.0 V; b. Current-voltage curve.

Figure 5.3 shows the cell performance in 3%steam/Ar at 920°C. The ionic

resistances in hydrogen-free gas under different potential loads are also very small which are about 0.4 $\Omega \cdot cm^2$, while the Rp have the same problem with those of the thick cells under higher potentials and the current-voltage curve also shows a steep slope at voltages between 0.2 and 0.9V.
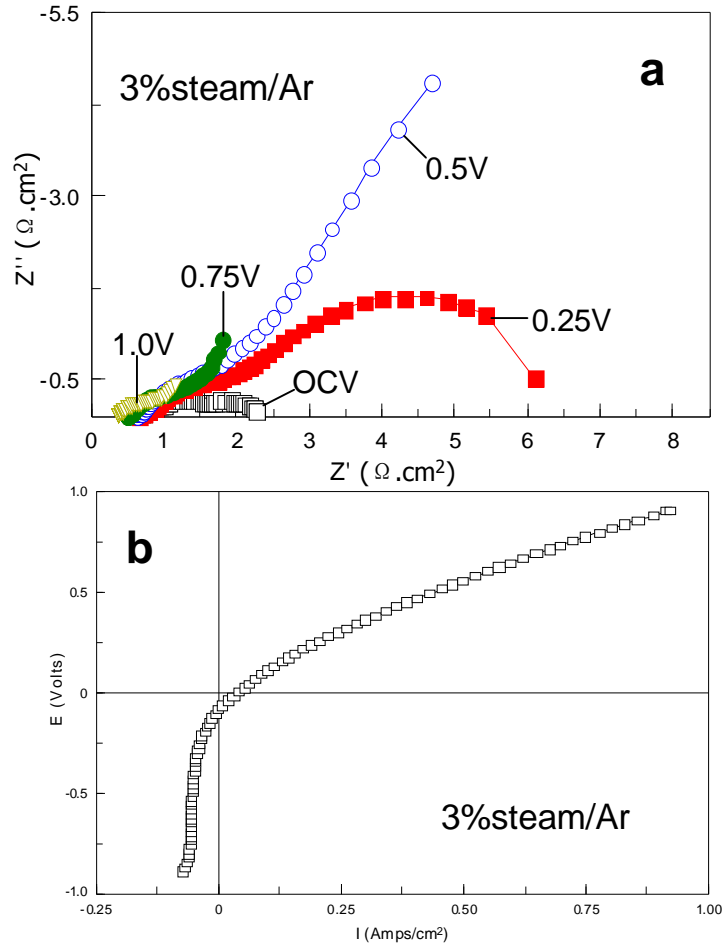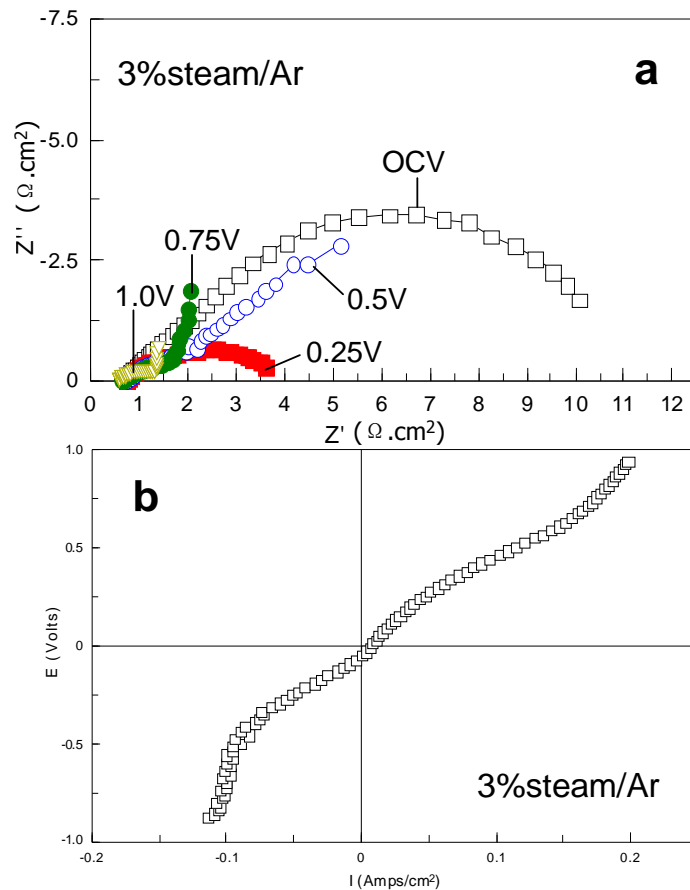

Figure 5.3. Performance from an SOEC with LSCM/CGO cathode, 250 micron thick YSZ electrolyte and LSM anode at 920°C with 3%steam/Ar. a. AC impedance data measured at OCV, 0.25 V, 0.5 V, 0.75 V, 1.0 V; b. Current-voltage curve.

In order to find out the possible reason for the abrupt slope in the current-voltage curve under higher voltages from the cells with LSCM cathodes in gas with no hydrogen supplied, a cell with 250 micron thick YSZ electrolyte, LSCM/CGO cathode and Au anode was made and tested in 3%steam/Ar at 920°C. The cell

performance is displayed in Figure 5.4. The current-voltage curve shows a strange large slope (almost vertical) under higher voltages, which is similar to that of the cell with 250 micron thick YSZ electrolyte, LSCM/CGO cathode and LSM anode. The impedance data also shows that large Rp when the external potential load is comparatively high. Figure 5.4 c shows comparison of I-V curves from cells with Au anode and LSM anode. In fuel cell side, the polarizaion has been dramatically reduced by replacing Au anode with LSM anode, which indicates LSM is better fuel cell cathode than Au. In electrolysis mode, there is only small differences between two cells and both I-V curves have increased slopes at higher potentials (-0.3 to -0.8 V). As in this cell, LSM anode was taken place by Au, it is confirmed that this behaviour is related to the LSCM cathode that results in the sharp slope in polarization curve.
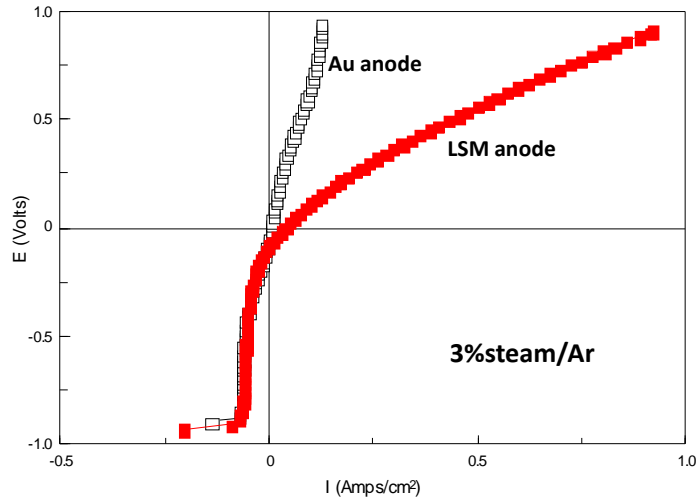
Figure 5.4. Performance from an SOEC with LSCM/CGO cathode, 250 micron thick YSZ electrolyte and Au anode at 920°C with 3%steam/Ar. a. AC impedance data measured at OCV, 0.25 V, 0.5 V, 0.75 V, 1.0 V; b. Current-voltage curve; c. Comparison of I-V curves from cells with Au anode and LSCM anode.

5.3 Cell performance from cells with 50 micron thick YSZ electrolytes made by tape casting and wet impregnation

A cell with LSCM cathodes with improved microstructure was made by tape casting and wet impregnation methods. The cell has a 50 micron thick dense YSZ electrolyte, a 110 micron thick porous YSZ cathode support with about 50% weight impregnated LSCM load and a 120 micron thick porous YSZ anode support with about 40% weight impregnated LSF load. Cell cross-section and cathode morphology are shown in figure 5.5. The electrodes have good adherence with electrolyte and have a good microstructure of big pores in the YSZ support together with small pores in the YSZ/LSCM structure.
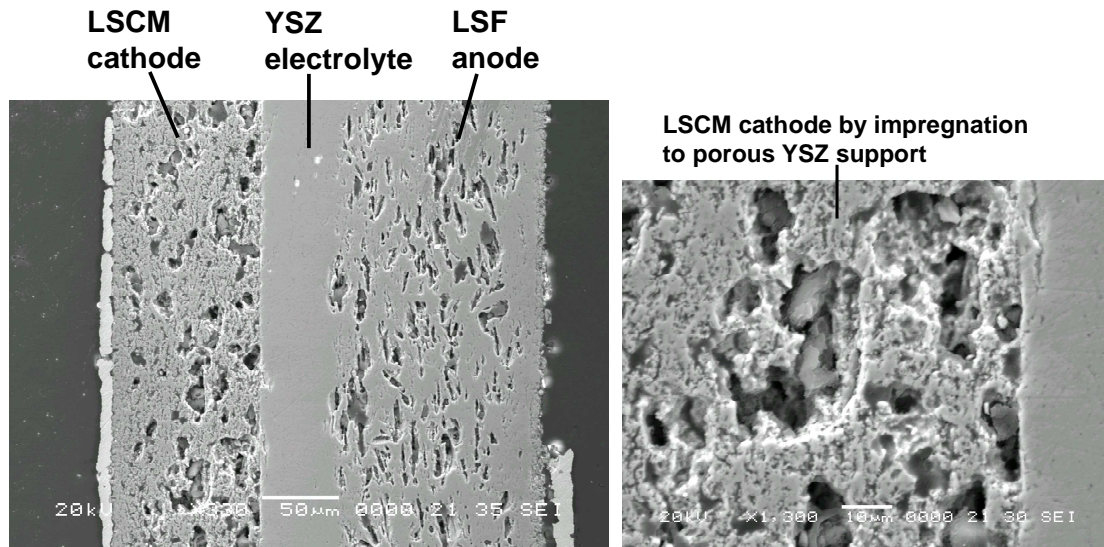
Figure 5.5. SEM pictures of the cell with 50 micron thick YSZ electrolyte made by tape casting and wet impregnation.

This tape cast electrolysis cell was tested by (4-terminal test) 700°C, 750°C, 800°C, 850°C. Figure 5.6 shows its performances in 3%steam/Ar at different temperatures. The ionic resistances at 850°C is 0.17 $\Omega^{.}$cm^{2}, which is much smaller compared to the Rs of 3.5 $\Omega^{.}$cm^{2} from cell with 2 mm YSZ electrolyte. However, the polarization resistance has high values under higher voltages, which is the same phenomena with those cells mentioned before (see section 3.3.3 and section 5.2). However the largest Rp does not come with the highest voltage (-1.0 V); the largest polarization resistance occurs when -0.75 V is applied.
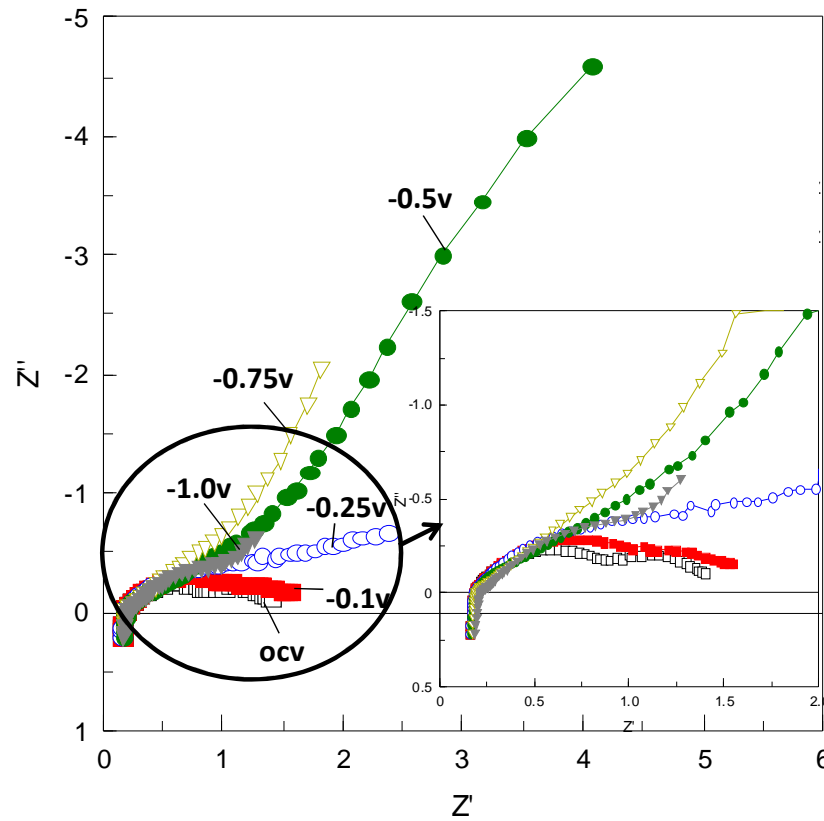
Figure 5.6 AC impedance data from cells with 50 micron thick YSZ electrolytes made by tape casting and wet impregnation measured at OCV, 0.1 V, 0.25 V, 0.5 V, 0.75 V, 1.0 V at 850°C with 3%steam/Ar.

Polarization curve from this cell at 850°C with 3%steam/Ar is shown in figure 5.7 a, which also has a sharp slope at higher voltages.

The high slope in I-V curve at higher voltages from the cell made by tape casting and impregnation methode is similar to the high slope in I-V curve from the cells discussed before (see section 3.3.3 and 4.3). The sharp slopes strat at around -0.3 V and ends at around -0.8 V. Current increase is quite small when potential increases within this range. Current starts to increase faster as potential is increasd to above -0.8 V and slopes of I-V curves start to decrease from around -0.8 V. This is in good accordance with AC impedance results in figure 5.6.
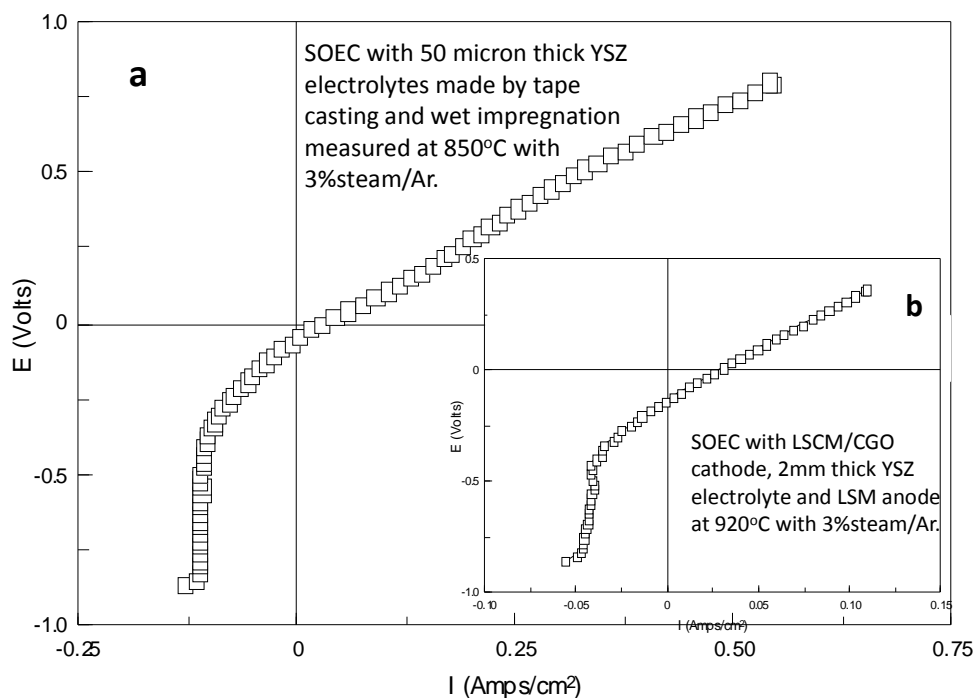
Figure 5.7. a. Current-voltage curve from an SOEC with 50 micron thick YSZ electrolytes made by tape casting and wet impregnation measured at 850°C with 3%steam/Ar; b. Current-voltage curve from an SOEC with LSCM/CGO cathode, 2mm thick YSZ electrolyte and LSM anode at 920°C with 3%steam/Ar.

Figure 5.8 shows Bode plots obtained at different potentials from the cell with 50 micron thick YSZ electrolytes made by tape casting and wet impregnation measured at 850°C with 3%steam/Ar. At open circuit and -0.1 V, there are two limiting processes with characteristic frequencies of around 1 Hz and 30 Hz for low and high frequency arcs respectively. The low frequency process (1 Hz) might stem from gas diffusion limitation in a stagnant gas layer on the electrode surface or surface adsorption/desorption process of species[9, 10]. High frequency process (30 Hz) may be the one-dimensional diffusion in a gas layer of finite thickness[11] or transportation of oxygen ions. At higher potentials, however, the summit frequencies do not show up within the low frequency measurement limit of 0.1 Hz. The summit frequencies at higher potentials drop at frequencies below -0.1 V, which indicates a considerable time constant that might ascribe to a very poor gas diffusion process or segregates at

TPB and/or poor surface adsorption/desorption. It seems that impedance under different potentials do not have the same limiting processes. Processes at high voltages are much larger in magnitude than processes at low potentials (open circuit and -0.1 V). However, when potential increases to -1.0 V, impedance is decreased and is smaller than that at -0.75 V and -0.5 V.
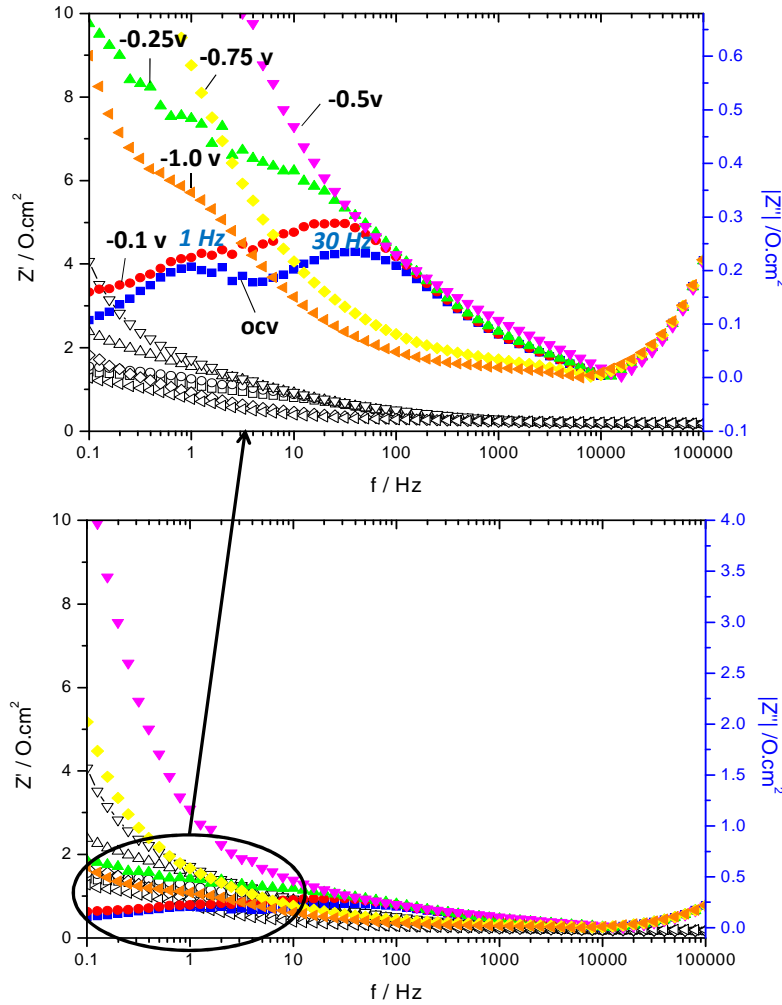

Figure 5.8. Bode presentations obtained at different potentials from an SOEC with 50 micron thick YSZ electrolytes made by tape casting and wet impregnation measured at 850°C with 3%steam/Ar.

Figure 5.9 is the comparison of bode presentations from the cell with 50 micron thick YSZ electrolytes made by tape casting and impregnation measured at 850°C and a cell with 2 mm thick YSZ electrolyte measured at 840°C with 3%steam/Ar. The two cells with different thicknesses of electrolytes both have two limiting processes. Thin

cell has the same low frequency process (with same summit frequency of 1 Hz) as the thick cell, however its low frequency process is less evident than the thick cell (see figure 5.9). This indicates that thin cell made by tape casting and impregnation is probably better in low frequency process. On the other side, the thin cell has lower characteristic frequency (of 40 Hz) of high frequency arc than the thick cell (500 Hz) and its high frequency process is much larger in magnitude than the high frequency process of thick cell. The dominating processes are high frequency process for thin cell and low frequency process for thick cell respectively. The low frequency process might stem from gas diffusion process in a stagnant gas layer above the electrode structure and/or adsorption/desorption process. The high frequency process (with characteristic frequency of 40 Hz) of thin cell might be the one-dimensional diffusion in a gas layer of finite thickness[11]. As the thin cell has a thick electrodes (110 micron thick cathode and 110 micron thick anode, see figure 4.5) and a good porous microstructure in electrodes, it is possible for the thin cell to have comparatively bigger one-dimensional diffusion limitation in a gas layer of finite thickness and smaller gas diffusion limitation in a stagnant gas layer above the electrode structure. The thick cell with thinner electrodes (of ~30 micron thick) and comparatively poorer porosity in electrodes, could have a dominating limiting process of gas diffusion in a stagnant gas layer above the electrode structure rather than one-dimensional diffusion limitation in a gas layer.
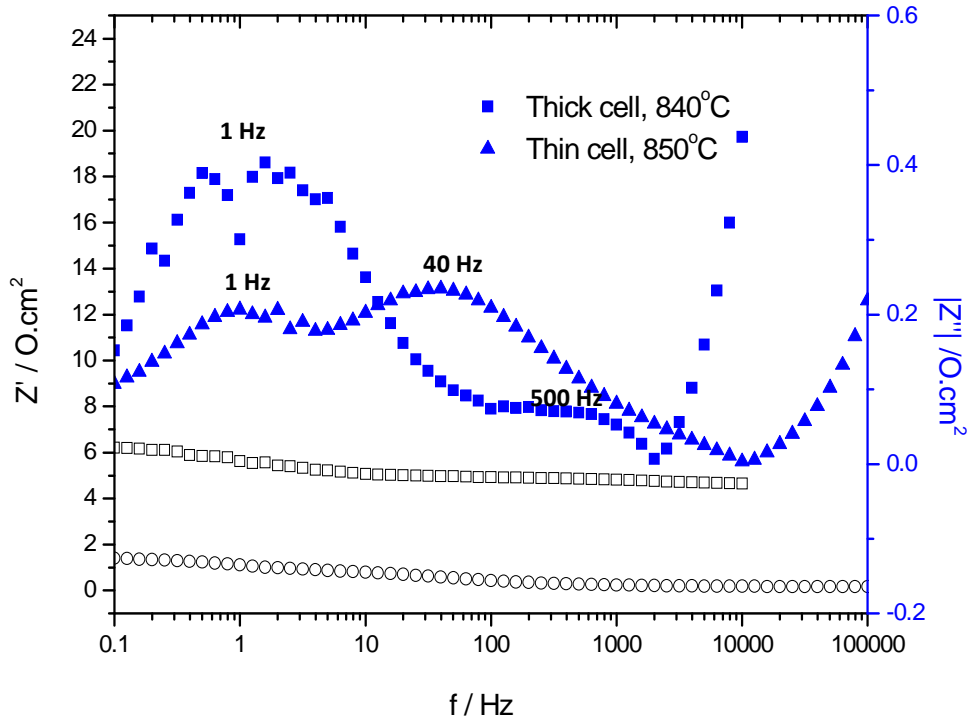
Figure 5.9. Bode plots obtained at open circuit from an SOEC with 50 micron thick YSZ electrolytes made by tape casting and wet impregnation measured at 850°C with 3%steam/Ar and an SOEC with LSCM/CGO cathode, 2mm thick YSZ electrolyte and LSM anode measured at 840°C with 3%steam/Ar.

The ionic resistances at 700°C, 750°C, 800°C, 850°C are 0.43 Ω·cm², 0.29 Ω·cm², 0.21 Ω·cm², and 0.17 Ω·cm² (see figure 5.10). And there are larger polarization resistances at higher potentials at all temperatures. Figure 5.11, the current-voltage curves at 700°C, 750°C, 800°C, 850°C, with strange higher slopes, confirms this phenomena. Current-voltage curve has the biggest slope change at 850°C, with almost vertical segment B-C. And the strange slope under higher potentials becomes smaller as temperature is decreased. At open curcuit, the I-V curves at four temperatures starts with curves of distinct slopes, however terminate at points with similar current values (45.2 mA at 0.847 V for 850°C, 43.2 mA at 0.846 V for 800°C, 40.9 mA at 0.846 V for 750°C, 39.4 mA at 0.845 V for 700°C). Comparasions of AC impedance data at different temperatures under open circuit and -0.75 V (see figure 5.12) are in good accordance with this phenomena. Similar

phenomena could also be seen in thick SOEC with 3%steam/Ar (see section 3.3.3). Within this potential range, it seems like the current was restricted to be not higher than a value regardless of temperature increase/potential increase.
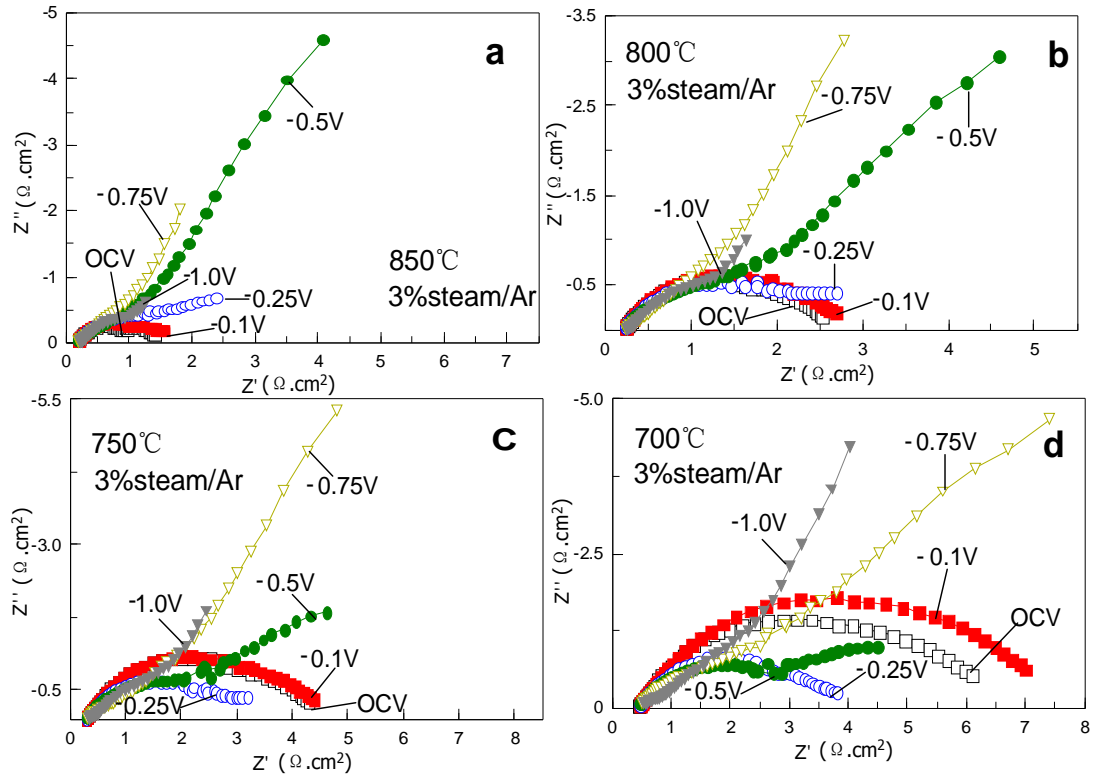

Figure 5.10.   AC impedance data from cells with 50 micron thick YSZ electrolytes made by tape casting and wet impregnation measured at OCV, 0.1 V, 0.25 V, 0.5 V, 0.75 V, 1.0 V at different temperatures with 3%steam/Ar.a. 850ᵒC; b. 800ᵒC; c. 750ᵒC; d. 700ᵒC.
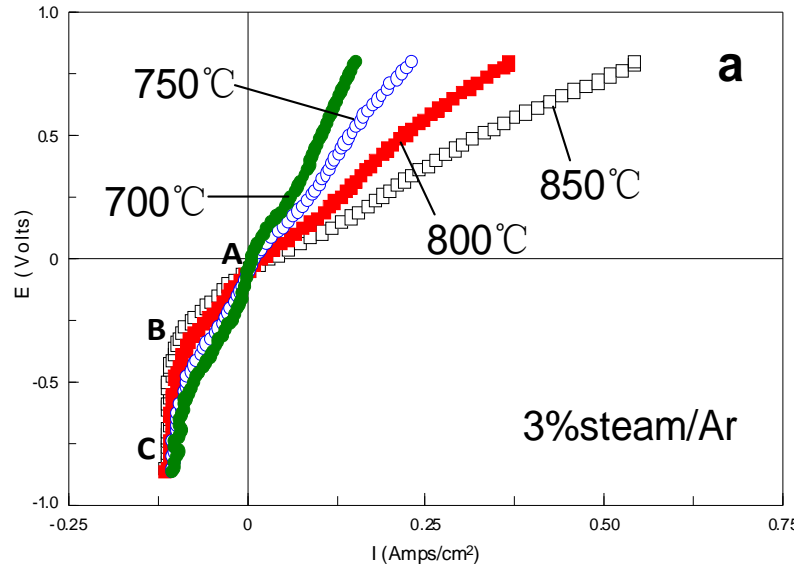
Figure 5.11. Current-voltage curve from cells with 50 micron thick YSZ electrolytes made by tape casting and wet impregnation measured at 850°C, 800°C, 750°C, 700°C with 3%steam/Ar.
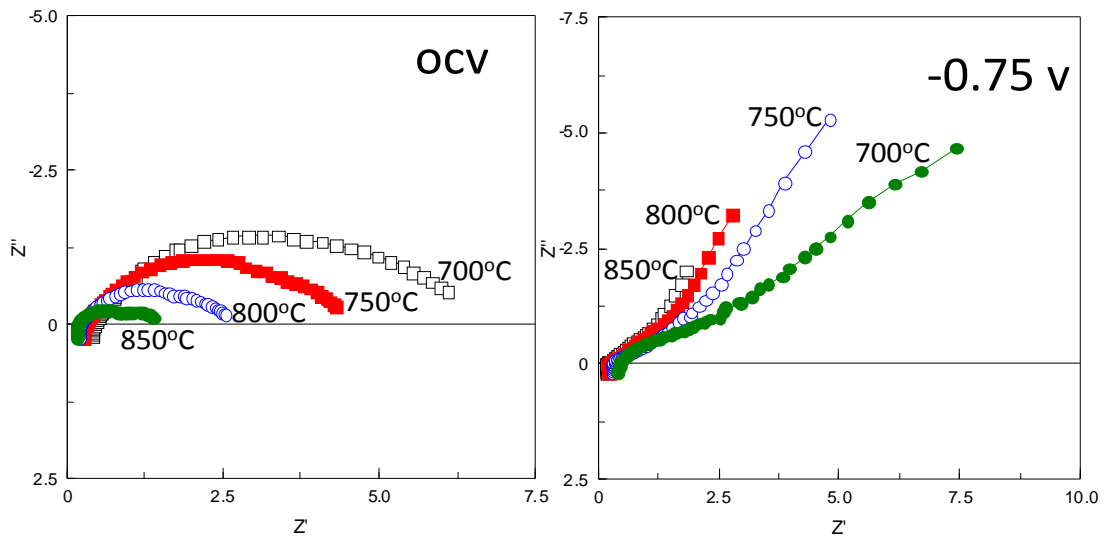

Figure 5.12. AC impedance data under open circuit and -0.75 v from cells with 50 micron thick YSZ electrolytes made by tape casting and wet impregnation measured at 850°C, 800°C, 750°C, 700°C with 3%steam/Ar.

Figure 5.13 shows comparisons of bode plots under open circuit from cells with 50 micron thick YSZ electrolytes made by tape casting and wet impregnation measured

at 850°C, 800°C, 750°C, 700°C with 3%steam/Ar. There are two rate limiting processes under open circuit however the two processes overlap with each other at lower temperatures. The high frequency process has smaller characteristic frequency as temperature is decreased (from 39.8 Hz at 850°C to 3.2 Hz at 700°C) which indicates higher time constant as decreasing temperature for high frequency process. If supposing the high frequency process is the one-dimensional gas diffusion, it is reasonable to have poorer gas diffusion as temperature decreases. The low frequency process increases in magnitude as temperature is decreased however it has close summit frequencies at different temperatures.
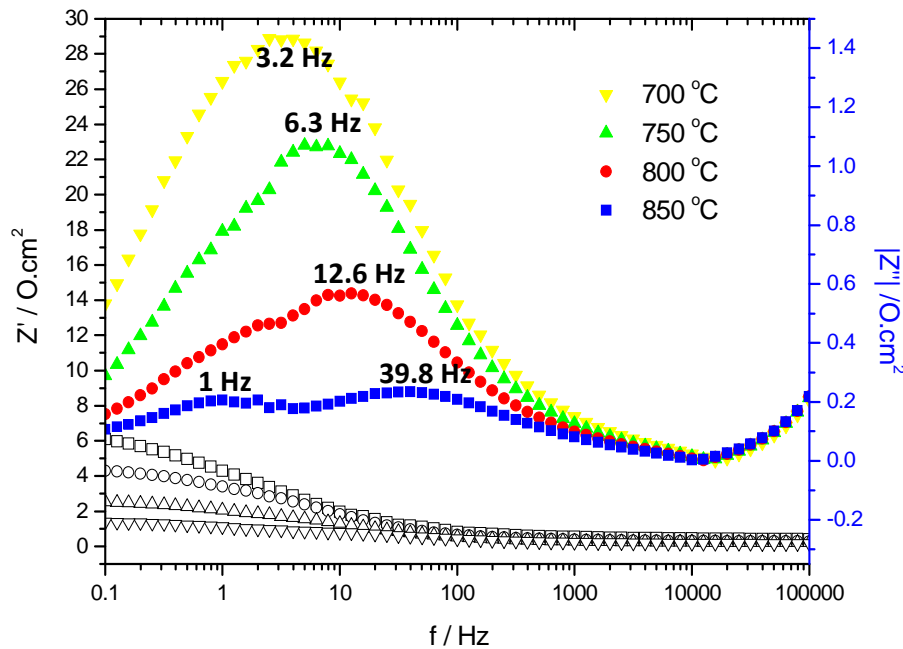

Figure 5.13. Bode plots under open circuit from cells with 50 micron thick YSZ electrolytes made by tape casting and wet impregnation measured at 850°C, 800°C, 750°C, 700°C with 3%steam/Ar.

Figure 5.14 is the comparison of bode presentations at -0.25 V from cells with 50 micron thick YSZ electrolytes made by tape casting and wet impregnation measured at 850°C, 800°C, 750°C, 700°C with 3%steam/Ar. When -0.25 V is applied, the high frequency process has an increase in characteristic frequency as decreasing temperature, which is opposite phenomena to that under open circuit. It still needs
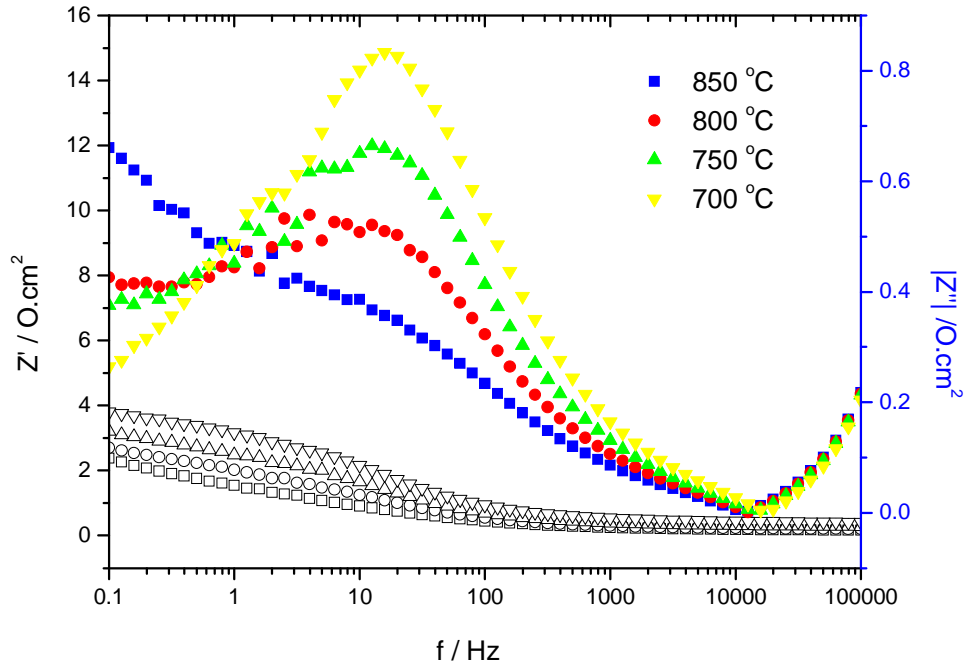
further explanation.

Figure 5.14. Bode plots under -0.25 V from cells with 50 micron thick YSZ electrolytes made by tape casting and wet impregnation measured at 850°C, 800°C, 750°C, 700°C with 3%steam/Ar.

Figure 5.15 is the XRD of cathode materials before and after electrolysis at 850°C in 3% H_2O/Ar. Though there is no obvious change of XRD results, from the current-voltage curves with 3% H_2O/Ar, there probably may be some chemical or microstructure change in the electrode in electrolysis process which needs more attention in future work.
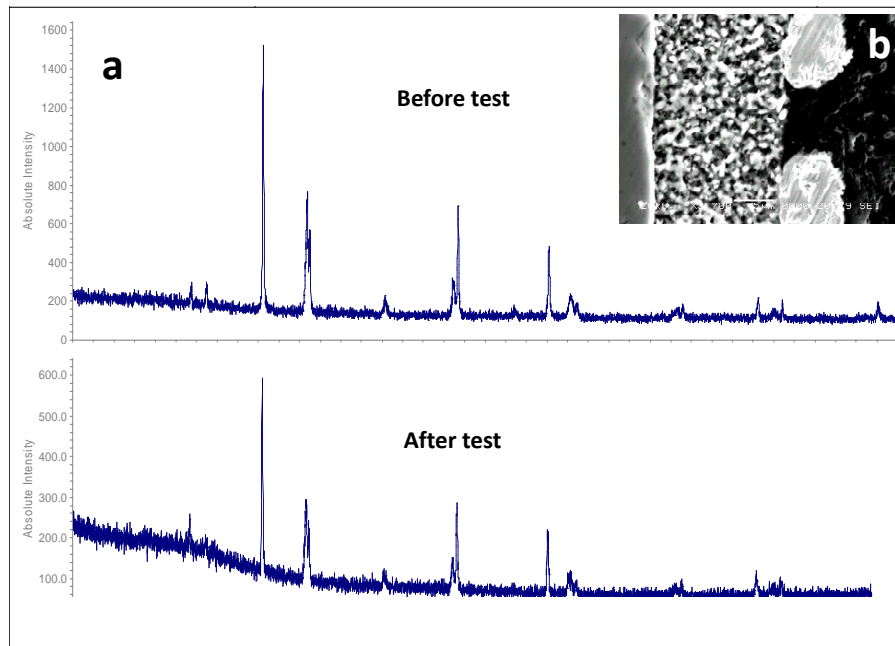
Figure 5.15. a. XRD of cathode before and after electrolysis with 3% H$_2$O/Ar; b. SEM picture of the cross section of the LSCM/CGO cathode.

5.4 Cell with thin YSZ electrolyte by co-pressing

Figure 5.16 are photos of cells made by co-pressing LSCM/YSZ cathode and YSZ electrolyte. Thermal expansion coefficients of the electrolyte and cathode do not match well under the experimental conditions. It might could be improved by adjusting components of the powders. Photo in figure 5.16 shows the separation of the two parts after sintering.

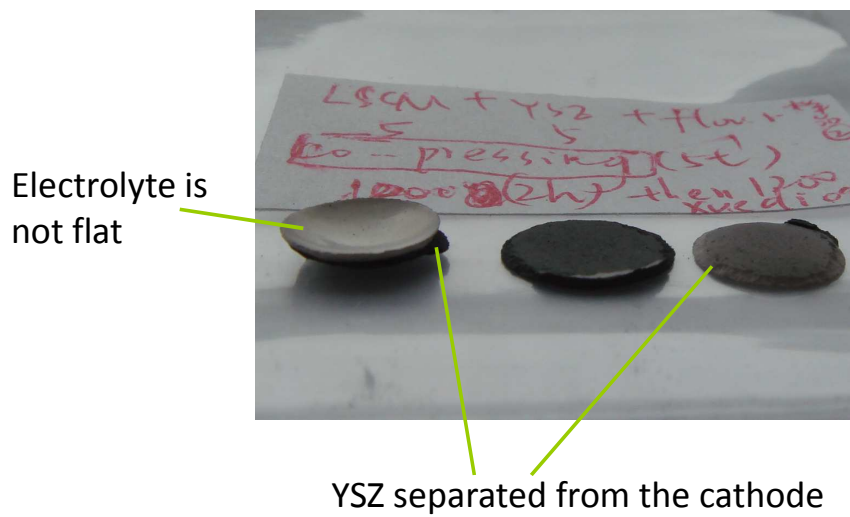Electrolyte is not flat

YSZ separated from the cathode

Figure 5.16. Picture of of co-pressed cells with YSZ electrolyte and LSCM/YSZ cathode.

5.5 Cell with thin electrolyte by screen printing YSZ ink

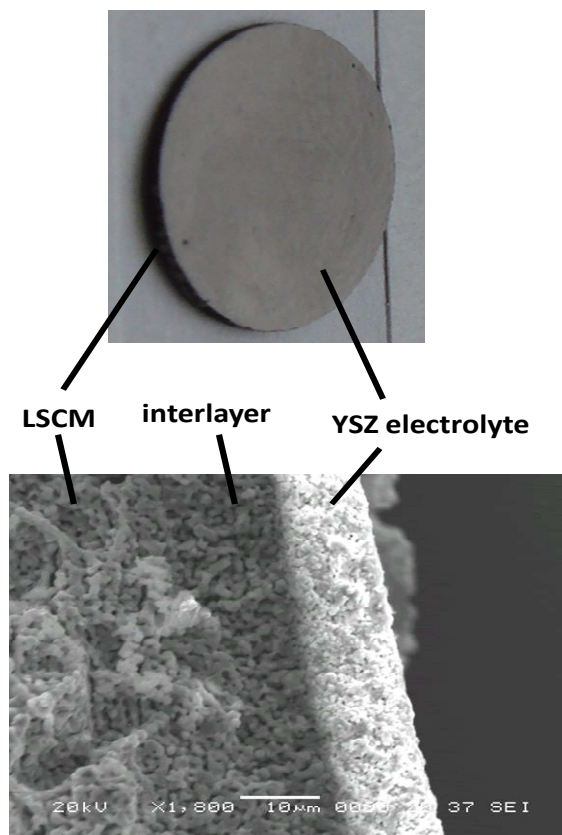LSCM   interlayer   YSZ electrolyte

Figure 5.17. A cell with screen printed YSZ electrolyte.

Figure 5.17 is the photo and SEM picture of a cell with screen printed YSZ electrolyte. It does not have the problem of segregation between electrolyte and electrode. However, the YSZ electrolyte is not as dense as it is required. The density of YSZ electrolyte might be improved by changing the formula of YSZ ink.

5.6 Increase porosity of cathode by adding pore formers

5.6.1 LSCM + Glassy Carbon

Figure 5.18 shows SEM picture of cathode from a cell with glassy carbon as pore formers in LSCM cathode. Pores produced from burning off glassy carbon are in round shape and with an average pore size of ~12 μm. In general, the distribution of the pores in the cathode material is homogeneous. However, the big pores are unconnected with each other and therefore could not efficiently facilitate gas diffusion through the material.
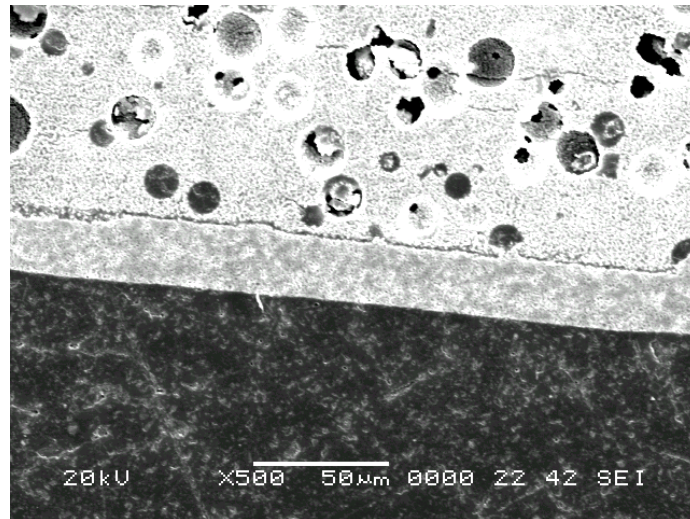

Figure 5.18. Micrograph of cathode from a cell with glassy carbon as pore former in LSCM cathode.

5.6.2   LSCM + flour and Glassy Carbon

In order to increase porosity, flour was added to LSCM cathode as a kind of pore

former. However, pores produced from sintering flour powders are in big size (around 100 μm) and unconnected. What is worse, there are some cracks in cathode which might origin from burning off big size flour powders (see figure 5.19).
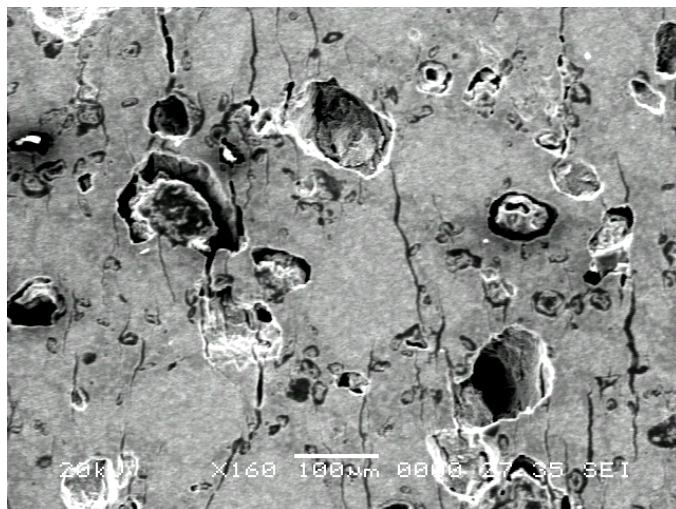

Figure 5.19. Micrograph of cathode from a cell with flour and glassy carbon as pore former in LSCM cathode.

5.7 Conclusions

Several methods have been tried to improve performances of SOECs with LSCM cathodes.

By cutting and polishing dense YSZ column, thin YSZ electrolyte could be made. In this way, the electrolyte is strong but its thickness is limited and could not be thin enough. A cell with 50 micron thick YSZ electrolyte made by tape casting and wet impregnation has good electrochemical performances. It has much smaller ionic resistance than the cell with 2 mm thick YSZ electrolyte. It has a low frequency limiting process at around 1 Hz at 850°C with 3%steam/Ar, which is similar to the cell with screen printed LSCM/CGO cathode and 2 mm thick YSZ electrolyte. And with improved microstructure, the impregnated cell might have a better gas diffusion at low frequency.

However, electrode microstructures of the cells made by tape casting and impregnation are not stable enough at temperatures higher than 850°C. A cell with 50

micron thick YSZ electrolyte (made by tape casting) and painted LSCM/CGO cathode has stable electrode microstructure and performs well at high temperatures. It has a high current density of 140 mA at -1.5 V and 126 mA at -1.25 V at 900°C with 3%steam/Ar.

Some other methods to improve cell microstructures have been tried but failed. Co-pressing LSCM/YSZ cathode and YSZ electrolyte did not succeed because of the mismatch of thermal expansion coefficients. Fabricating thin electrolyte by printing YSZ ink on LSCM/YSZ cathode failed because the sintered YSZ ink is not dense enough. By adding glassy carbon as pore former, the pores are homogeneously distributed in cathode but unconnected with each other. Adding flour does produce good porosity but leads to mechanical failure of the cathode.

References

1. T. Jardiel, B. Levenfeld , R. Jimenez, and A. Varez, *Ceram. Int.*, 2009, 35, 2329.

2. S. McIntosh, J. M. Vohs, and R. J. Gorte, *J. Electroanal. Chem.*, 2003, 150, A1305.

3. J. H. Song, S. I. Park, J. H. Lee, and H. S. Kim, *J. Mater. Process. Technol.*, 2008, 198, 414.

4. X. G. Capdevila, J. Folch, A. Calleja, J. Llorens, M. Segarra, F. Espiell, and J. R. Morante, *Ceram. Int.*, 2009, 35, 1219.

5. Y. Yin, S. Li, C. Xia, and G. Meng, *J. Power Sources.*, 2007, 167, 90.

6. D. Prakash, T. Delahaye, O. Joubert, M. T. Caldes, and Y. Piffard, *J. Power Sources.*, 2007, 167, 111.

7. G. Kim, S. Lee, J. Y. Shin, G. Corre, J. T. S. Irvine, J. M. Vohs, and R. J. Gorte, *Electrochem. Solid-State Lett.*, 2009, 12, B48.

8. Y. Huang, K. Ahn, J. M. Vohs, and R. J. Gorte, *J. Electrochem. Soc.*, 2004, 151, A1592.

9. M. J. Jorgensen and M. Mogensen, *J. Electrochem. Soc.*, 2001, 148, A433.

10. X. J. Chen, Q. L. Liu, K. A. Khor, and S. H. Chan, *J. Power Sources.*, 2007, 165, 34.

11. S. Primdahl and M. Mogensen, *J. Electrochem. Soc.*, 1999, 146, 2827.

Chapter 6   Hydrogen production from SOECs with cathodes based on LSCM

6.1 Introduction

In order to decompose steam into hydrogen and oxygen in SOECs, thermal energy and electrical energy are supplied. The total energy demand for steam electrolysis without any losses can be calculated as

$\Delta H = \Delta G + T\Delta S$ (Eq. 6.1)

ΔH is the enthalpy change. ΔG, the Gibbs free energy change, is supplied with electrical energy input. $T\Delta S$ is the thermal energy input.

In real systems, losses are inevitable. Efficiencies are important performance parameters for solid oxide steam electrolyzer plant. The most commonly discussed efficiency is the overall energy efficiency [1, 2, 3].

The efficiency discussed in this chapter is referred to the current-to-hydrogen production efficiency from HT-SOECs. It is the electrical efficiency, which is the ratio of the amount of hydrogen actually produced to the theoretical amount of hydrogen production. The theoretical amount of hydrogen production was calculated from cell current obeying the law of conservation of charge. The actual amount of hydrogen production was calculated by the gas flow rate and the volume percentage of hydrogen which was given by gas chromatograph[4].

To demonstrate the capability of hydrogen production by HT-SOECs with LSCM cathodes, cells with LSCM/CGO (50% CGO by weight) cathodes (some were loaded with catalysts), YSZ electrolytes and LSM anodes were tested. An Agilent 3000 micro gas chromatograph, equipped with an injector, was connected to the testing jig to determine hydrogen production while external potential load was applied to the SOEC. Hydrogen was detected by chromatograph according to the relative retention time, with the volume percentage of hydrogen given by GC peak analysis on the mixture gas going out from the jig. The gas was cooled to get rid of water before the sample entering the gas chromatograph. Test condition was atmosphere pressure, $900^{\circ}C$ in operation temperature. $3\%H_2O/Ar$ or $3\%H_2O/Ar/4\%H_2$ was supplied to

cathode and anode was open to air.

6.2 Hydrogen production from cells with LSCM/CGO cathode, 2 mm thick YSZ electrolyte and LSM anode

6.2.1. 3%H$_2$O/Ar

Electrochemical performances from an SOEC with LSCM/CGO cathode, 2 mm YSZ electrolyte and LSM anode in 3% H$_2$O/Ar at 900°C are shown in figure 6.1. OCV in 3%H$_2$O/Ar at 900°C for this cell is -0.093±-0.001V. The frequency range used in the impedance measurement is from 100 kHz to 0.1 Hz. The impedance data includes an ohmic resistance mainly originating from the electrolyte and a polarization resistance which is due to several electrode processes. Ohmic resistance decreases with temperature increase. Series resistances from this cell at 900°C are between 2.05 Ω·cm^2 and 2.9 Ω·cm^2 under different potentials, which are reasonable compared with the expected ohmic resistance of a 2 mm YSZ electrolyte, 1.8 Ω·cm^2. At 900°C, ohmic resistance of the cell in 3% H$_2$O/Ar decreases with potential, which is similar to the phenomena described before (see section 3.3.3). This may relate to improved conductivity in the electrode structure, either to a more reducing condition for the LSCM cathode, although conductivity would be expected to decrease under reduction or possibly to more oxidizing conditions for the LSM anode. Impedances at higher potentials (-1.0 V, -1.25 V, -1.5 V) have the more difficult electrode process at low frequency (around 0.1 Hz).

The I-V curves were measured from electrolysis side (-1.5 V) to fuel cell side (around 1.0 V) (see arrow in figure 6.1). They have higher slopes at -0.35to -0.8 V and -1.25 to -1.5 V. At potentials approaching -1.5 V, the current increases sharply and the slope of I-V curve at -1.5 V is even smaller than the ohmic resistance of the cell. It is suspected that the very initial data points at high potentials might be unreliable. The real slope may be higher than that shown in the I-V curve. The strange high slope near -1.5 V might relate to the high starting current at the beginning of the measurement.
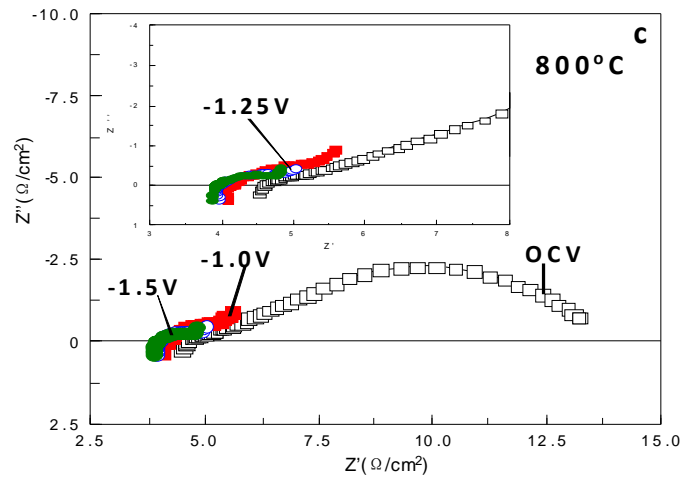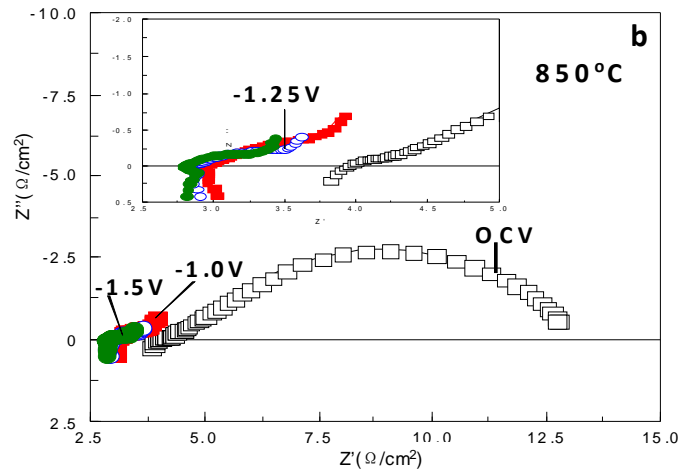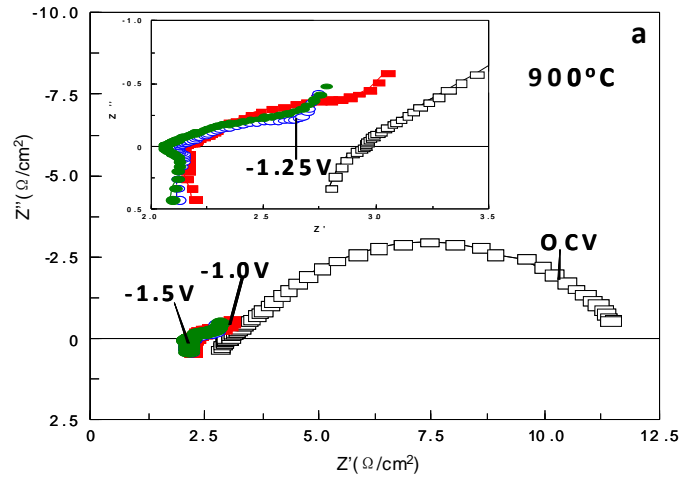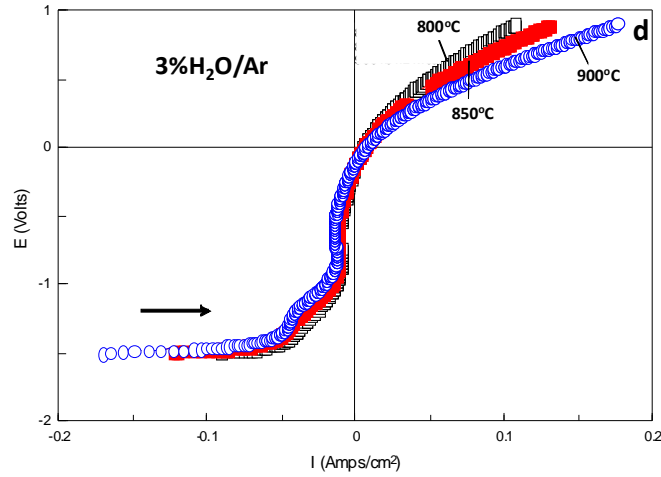
Figure 6.1. a, b, c. Performance from an SOEC with LSCM/CGO cathode, 2 mm thick YSZ electrolyte and LSM anode measured at 800°C, 850°C and 900°C with 3% H₂O/Ar. a, b, c. Impedance data (OCV(-0.093±-0.001 V), -1.0 V, -1.25 V, -1.5 V); d. Current-voltage curves.

The cell was applied various constant potentials to produce hydrogen. Six gas samples were collected at each potential step and hydrogen production level kept constant under constant potential load. Hydrogen produced was monitored by a micro gas chromatograph and efficiencies were calculated according to the volume percentage of hydrogen and gas flow rate. Cell current, hydrogen production and current-to-hydrogen efficiency are plotted versus potential in figure 6.2-6.4.

Figure 6.2 displays the current as a function of potential load at 800°C, 850°C and 900°C with 3% H₂O/Ar in cathode atmosphere. Current increase is smaller when voltage changes from -1.25 to 1.5 V than from -1.0 to -1.25 V, which is in good accordance with the I-V curve in figure 6.1-d. Current rises very slightly (from 56 mA/ cm^2 to 60 mA/ cm^2) from -1.25 to -1.5 V at 900 °C (see figure 6.2), which suggests that the high current at -1.5 V shown in the I-V curve in figure 6.1 is only stable in the short-term.

The increase of current as potential is depressed at higher temperatures. It is a similar phenomena described in section 3.3.3. The current-voltage curve at 800°C is more linear comparing to those at higher temperatures. At -1.5 V, current at 900°C is

not higher than at 850°C. Cell current seems to be restricted at high potential and high temperature which are supposed to give the highest performance. As gas at the cathode only contains 3% steam, steam concentration might be not high enough for steady state reactions when high potential and/or high temperature are applied. And gas diffusion could be a possible reason for the limited performance at high potential. The impedance data in figure 6.1 also shows some evidence for gas diffusion limitation appearing at low frequencies when high voltages are applied.
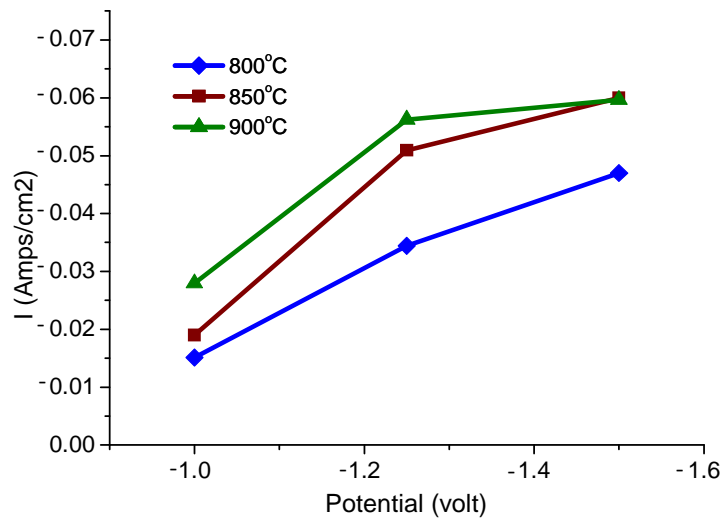

Figure 6.2. Currents at -1.0 V, -1.25 V and -1.5 V from an SOEC with LSCM/CGO cathode, 2 mm thick YSZ electrolyte and LSM anode measured at 800 °C , 850 °C and 900 °C using 3% H$_2$O/Ar.

Figure 6.3 shows hydrogen production amount at different potentials in 3% H$_2$O/Ar . It is shown that starting with fed-in gas containing no hydrogen, SOEC with LSCM/CGO cathode could produce hydrogen when external potential is applied.

The hydrogen production amount shows similar trends with the current. The line at 800°C is almost linear. At each potential, the yield of hydrogen at 850°C is about twice of that at 800°C and is close to the yield at 900°C. By increasing voltage from -1.0 to -1.25 V, hydrogen production increases a lot. However, hydrogen production only rises a little when potential is improved from -1.25 to -1.5 V and the increase is more evident at lower temperature. Steam conversion was up to 67% when no
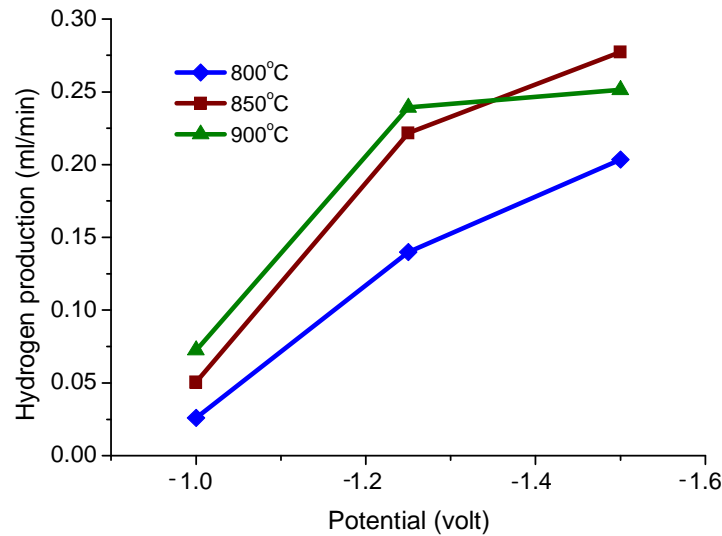
124

hydrogen was supplied.

Figure 6.3. Amounts of hydrogen production (ml/min) at -1.0 V, -1.25 V and -1.5 V from an SOEC with LSCM/CGO cathode, 2 mm thick YSZ electrolyte and LSM anode measured at 800 ^{o}C , 850 ^{o}C and 900 ^{o}C using 3% H$_2$O/Ar.

Measurements on other SOECs with the same components show that hydrogen could be produced by SOECs with LSCM/CGO cathodes at lower voltages. Figure 6.4 is hydrogen production (by volume percentage) from another SOEC (thin YSZ electrolyte) at potentials from -0.25 to -2.0 V. It is illustrated that hydrogen could be produced at potentials lower than -1.0 V. The hydrogen production amount at low potentials could not be easily detected. At lower potential, current was mainly used in reducing electrode material and activating electrode. When current is higher, steam starts to decompose obviously. And as the system has slight leakage, a small amount of air could be detected at cathode and the hydrogen initially produced is consumed by oxygen. When the oxygen is all consumed, it is more easy to detect hydrogen. This might be the reason for the big increase of hydrogen at -1.0 V.
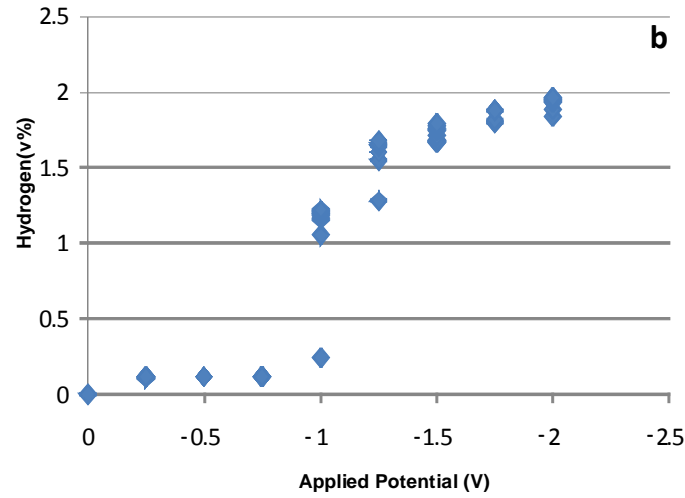
Figure 6.4. Hydrogen production rate (volum percentage) at voltages from another SOEC with LSCM/CGO cathode and thin YSZ electrolyte.

The current-to-hydrogen efficiencies were calculated as the ratio between the amount of hydrogen produced and the amount of hydrogen theoretically produced, which was calculated from the charge consumed during the experiment obeying the law of conservation of charge. Results are shown in figure 6.5. From this figure, the current-to-hydrogen production efficiency is up to 80%. Hydrogen production at -1.5 V is considered to be close to the amount of theoretical value calculated from applied current.

Though the performance seems limited at high potential and high temperature, these results show that starting with no content of hydrogen, the current-to-hydrogen efficiency from SOECs with LSCM/CGO cathodes could reach up to 80% under -1.5 V at 850°C.
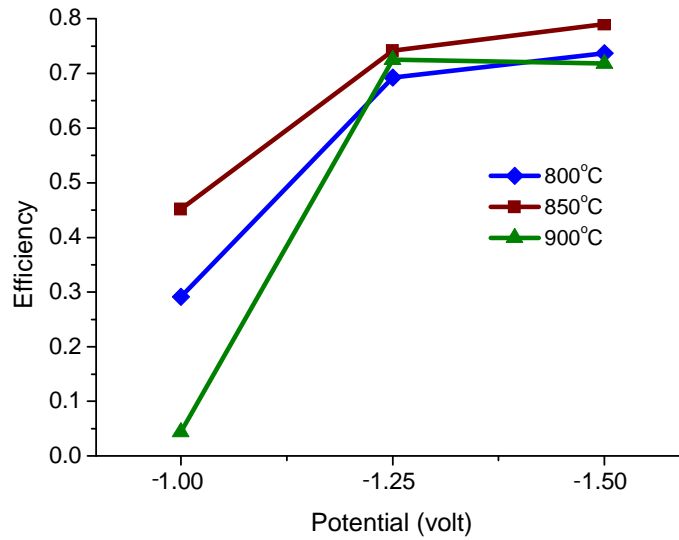
Figure 6.5. Current-to-hydrogen production efficiencies at -1.0v, -1.25v and -1.5v from an SOEC with LSCM/CGO cathode, 2 mm thick YSZ electrolyte and LSM anode measured at 800 ^{o}C , 850 ^{o}C and 900 ^{o}C using 3% H$_2$O/Ar.

Hydrogen production amount versus current at different temperatures in 3% H$_2$O/Ar are plotted in figure 6.6. The dashed line shows the theoretical hydrogen production amount calculated by cell current obeying the law of conservation of charge. Lines at three temperatures are a bit below the theoretical line. The errors may stem from leakage, flowmeter and GC. When current becomes higher, the distance between hydrogen actually produced and hydrogen theoretically produced becomes a smaller portion compared to the total hydrogen production amount and therefore the efficiency increases with current.

Lines are almost linear and roughly parallel to the theoretical line. This indicates hydrogen production increases with current at a constant rate which equals to the theoretical rate for all temperatures. Lines at 800°C and 850°C overlap with each other, which means hydrogen production at 800°C and 850°C are the same when the cell has the same current. The line at 900°C is slightly lower.

The three dots in each line are at -1.0 V, -1.25 V and -1.5 V respectively. It could be seen that although the cell has similar hydrogen-current lines at three temperatures,

127

the current and hydrogen amount at the same potential are higher when the cell is running at higher temperatures.
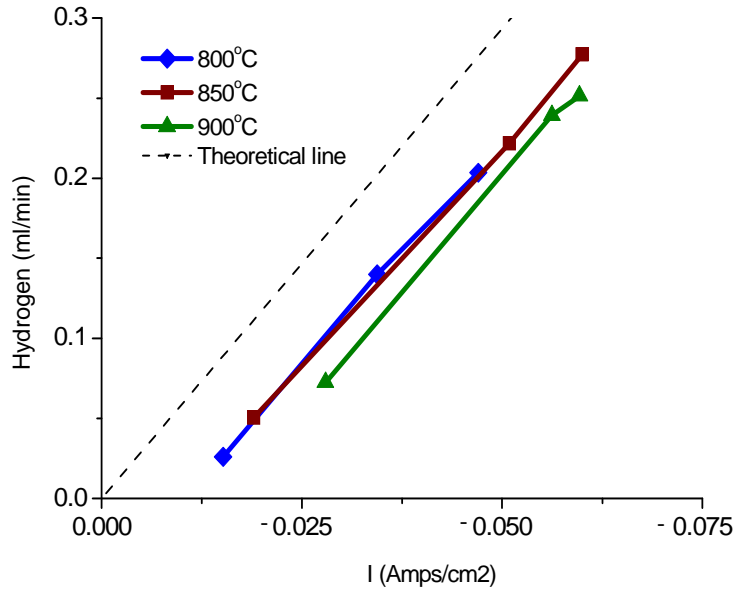

Figure 6.6. Hydrogen production with current density from an SOEC with LSCM/CGO cathode, 2 mm thick YSZ electrolyte and LSM anode measured at 800 ^{o}C , 850 ^{o}C and 900 ^{o}C using 3% H$_2$O/Ar.

Figure 6.7 shows current-to-hydrogen efficiency versus hydrogen production. This figure indicates that hydrogen production efficiency increases in accordance with the rise of hydrogen production but becomes almost constant after hydrogen reaches a high value.
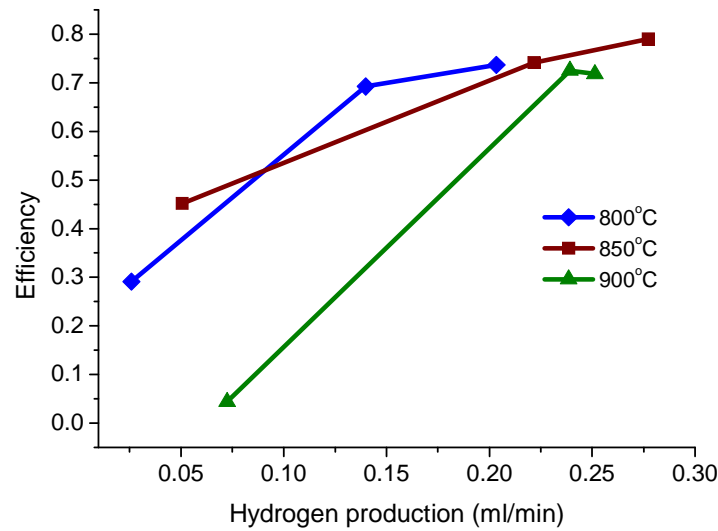
Figure 6.7. Efficiency with current density from an SOEC with LSCM/CGO cathode, 2 mm thick YSZ electrolyte and LSM anode measured at 800 ^{o}C , 850 ^{o}C and 900 ^{o}C using 3% H$_2$O/Ar.

6.2.2 3%H$_2$O/Ar/4%H$_2$

The cell with LSCM/CGO cathode, 2 mm YSZ electrolyte and LSM anode were then tested in 3%H$_2$O/Ar/4%H$_2$. Figure 6.8 displays the performance at 800°C, 850°C and 900°C with 3% H$_2$O/Ar/4% H$_2$. OCV in 3% H$_2$O/Ar/4% H$_2$ is -0.92±-0.01 V. The frequency range used in impedance measurement is from 100 kHz to 0.1 Hz. I-V curves were measured from -2.0 to 1.0 V (see arrow in figure 6.8-d).

With slightly bigger Rs but smaller Rp, performances in 3% H$_2$O/Ar/4% H$_2$ are better than those in 3% H$_2$O/Ar. Comparing with Z(ocv) in 3% H$_2$O/Ar, Z(ocv) in 3%H$_2$O/Ar/4%H$_2$ has no intercept with real axis at low frequency (around 0.1 Hz). Ohmic resistance drops slightly when potential is applied, which is the same phenomena with many other results discussed before. The impedance data at low frequency range indicates a slow species transfer process. As a similar cell described in other chapters has no such problem in 3%H$_2$O/Ar/4%H$_2$ (see section 3.3.2), the poor low frequency process might relate to long operation time in hydrogen production measurements.

From figure 6.8-d, it can be seen that I-V curves from this cell in $3\%H_2O/Ar/4\%H_2$ are not linear. It has a more obvious slope increase at high potential than that from other cells described in previous chapters. This might be due to comparatively low gas flow rate in this test (13~15ml/min).

Slope at -2.0 V is very small which is similar to that in 3% H_2O/Ar (see figure 6.1). However, from impedance data, Z(-2.0 V) is no better than Z(-1.0 V). It shows an inconsistency with the I-V curve. The initial data points at around -2.0 V in I-V curve may be unreliable (see figure 6.8).

Figure 6.9 shows two I-V curves with different sweep directions (from -2.0 to 0.8 V and from 0.8 to -2.0 V, see arrows in figure 6.9) from another cell in $3\%H_2O/Ar/4\%H_2$. It could be seen that the two curves overlap with each other except at the very high voltage when potential sweeps from -2.0 V. It is suspected that the initial data points with very small slope are unreliable because of the high current when potential starts to be applied.
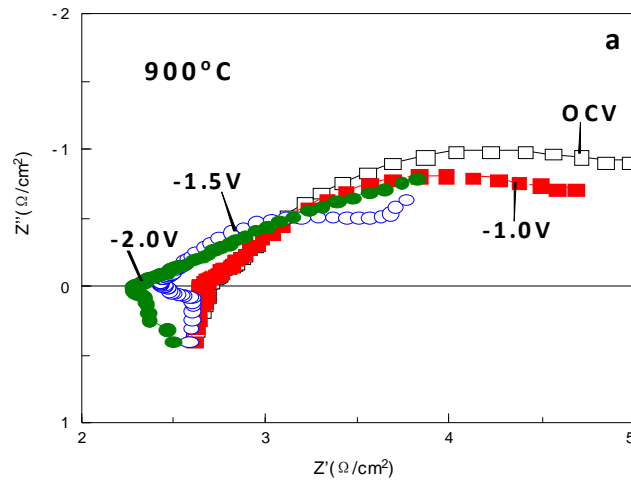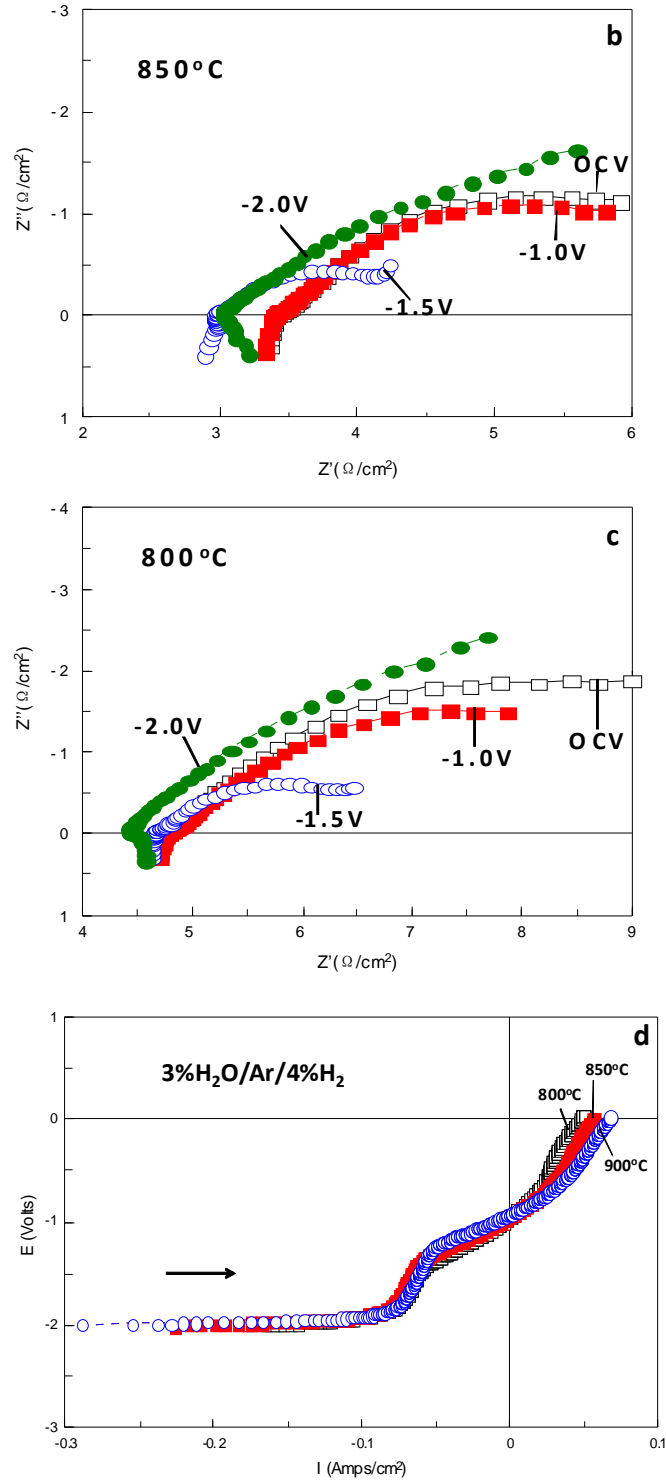
Figure 6.8. a, b, c. Performance from an SOEC with LSCM/CGO cathode, 2 mm thick YSZ electrolyte and LSM anode measured at 800ºC, 850ºC and 900ºC with 3% H₂O/Ar. a, b, c. Impedance data (OCV(-0.92±-0.01V), -1.0 V, -1.5 V, -2.0 V); d. Current-voltage curves.
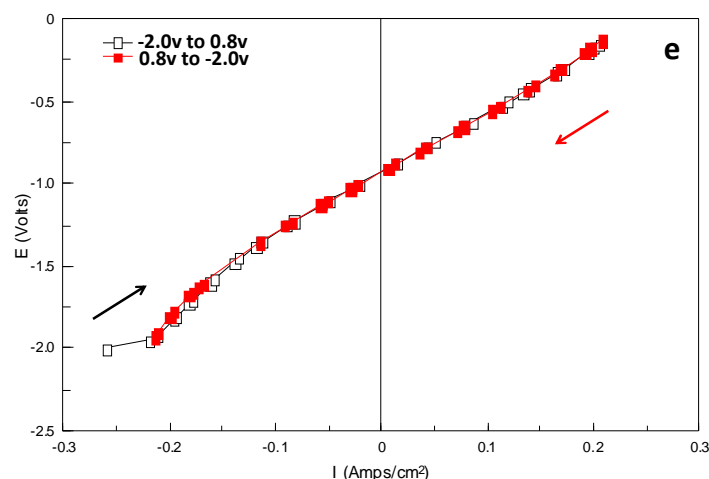
Figure 6.9. I-V curves with different sweep directions (from -2.0 to 0.8 V and from 0.8 to -2.0 V) from a cell with LSCM/CGO cathode, 2 mm thick YSZ electrolyte and LSM anode in 3%H$_2$O/Ar/4%H$_2$.

The cell was investigated at various constant potentials (-1.0 V, -1.5 V and -2.0 V) with 3%H$_2$O/Ar/4%H$_2$ to produce hydrogen. Six gas samples were collected at each potential and hydrogen production level kept constant under constant potential load. Hydrogen produced was detected by a micro gas chromatograph and efficiencies were calculated according to the volume percentage of hydrogen and gas flow rate. Cell current, hydrogen production rate and current-to-hydrogen efficiency versus potential are shown in figure 6.10-6.12.

Figure 6.10 is cell current versus voltage at different temperatures. Current increases significantly as potential increases from -1.0 to -1.5 V but only rises a bit when potential is from -1.5 to -2.0 V. It is in agreement with the I-V curves (see figure 6.8-d) and is similar to the phenomena in 3%H$_2$O/Ar. Cell current increases with temperature but has no big difference at different temperatures. Correspondingly, the amount of hydrogen production has similar trends (see figure 6.11).
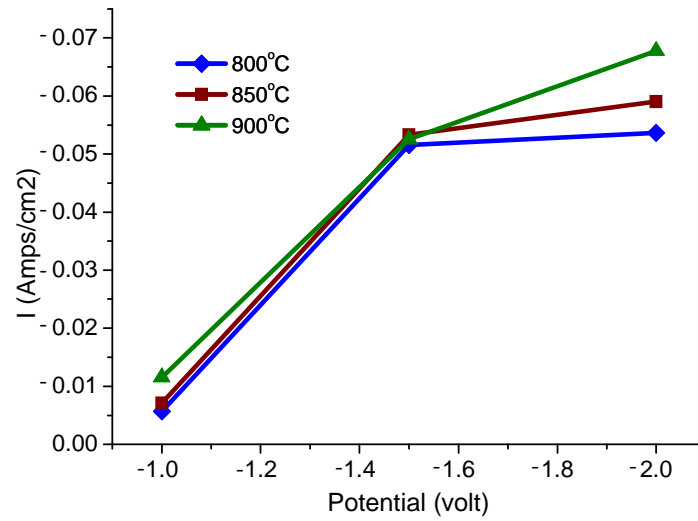
Figure 6.10. Currents at -1.0 V, -1.5 V and -2.0 V from an SOEC with LSCM/CGO cathode, 2 mm thick YSZ electrolyte and LSM anode measured at 800 °C , 850 °C and 900 °C using 3% H₂O/Ar/4% H₂.

The amounts of hydrogen production at different voltages and different temperatures are displayed in figure 6.11. As hydrogen production relates to cell current, hydrogen production is in accordance with current. Three curves at different temperatures only differ slightly from each other. The yield of hydrogen increases quicker at lower potentials than at higher potentials.

Hydrogen production reaches a maximum amount of around 0.35 ml/min at -1.5 V, and keeps consistent as potential increases to -2.0 V. The flow rate for cathode gas is 13~15 ml/min, which gives a flow rate of 0.39~0.45 ml/min for steam. According to the equation of $H_2O \rightarrow H_2 + 1/2O_2$, it is supposed to yield 0.39~0.45 ml/min hydrogen with 0.39~0.45 ml/min steam theoretically. There is 0.35 ml/min hydrogen actually produced at -1.5 V, and is close to the maximum amount of hydrogen production from 0.39~0.45 ml/min steam. And I-V curves in figure 6.8-d indicates current increases slowly when the operating voltage is over -1.5 V. This might stem from higher H_2O conversion ratio as shown in figure 6.11. It is assumed that high steam decomposition ratio restricted cell current because of steam starvation. According to literature survey, steam starvation has been reported to cause cathode concentration overpotential [5, 6].

And it has been reported by Kobayashi *et al.* that current efficiency of steam electrolysis from a cell with proton conductive electrolyte depends on the partial pressure of water vapor[7].
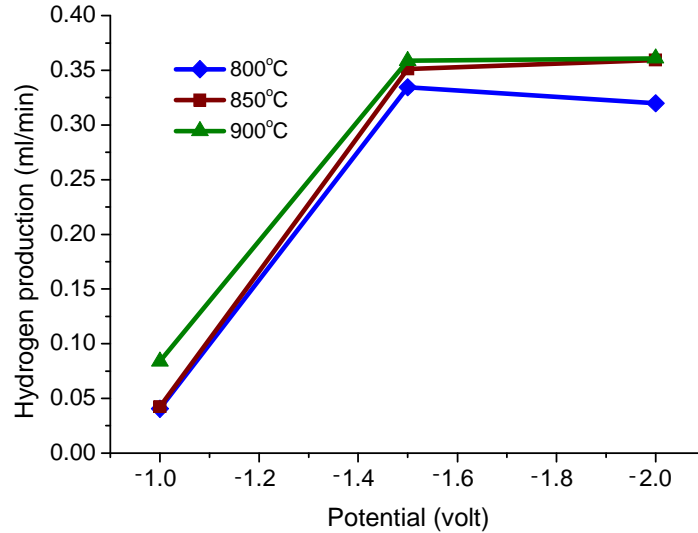

Figure 6.11. Amounts of hydrogen production (ml/min) at -1.0 V, -1.5 V and -2.0 V from an SOEC with LSCM/CGO cathode, 2 mm thick YSZ electrolyte and LSM anode measured at 800 ^{o}C , 850 ^{o}C and 900 ^{o}C using 3% H$_2$O/Ar/4% H$_2$.

Figure 6.12 shows the efficiencies under -1.0 V, -1.5 V and -2.0 V at 800 ^{o}C , 850 ^{o}C and 900 ^{o}C. With a small content of hydrogen (4% H$_2$), the current-to-hydrogen efficiencies reaches around 100% which are higher than efficiencies in 3% H$_2$O/Ar. Efficiencies at different potentials and different temperatures do not show much difference. As hydrogen production rate is high at high potentials, hydrogen production might be limited by the amount of fed-in steam (only 3% steam in inlet gas for cathode). Some efficiencies are slightly higher than 100%. This might be due to the precision of gas chromatograph and gas flow meter.
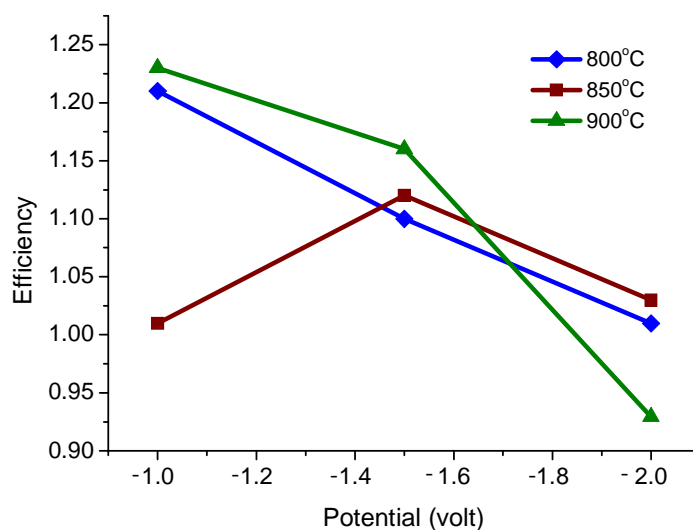
Figure 6.12. Current-to-hydrogen production efficiencies at -1.0 V, -1.5 V and -2.0 V from an SOEC with LSCM/CGO cathode, 2 mm thick YSZ electrolyte and LSM anode measured at 800 ^{o}C , 850 ^{o}C and 900 ^{o}C using 3% H$_2$O/Ar/4% H$_2$.

Hydrogen production amount versus cell current at different temperatures are plotted in figure 6.13. Lines are roughly parallel with the theoretical line except at high currents. Hydrogen production amounts at low currents are almost equal to theoretical amounts. The amount increases slightly as current is increased until hydrogen amount reaches 0.35 ml/min. Compared to results in 3%H$_2$O/Ar (see figure 6.6), actual hydrogen production in 3%H$_2$O/Ar/4%H$_2$ is higher and is more close to the theoretical line. Although some hydrogen production amounts are slightly higher than theoretical amount due to precision, it is assumed the cell has a satisfactory current-to-hydrogen efficiency from this SOEC in 3%H$_2$O/Ar/4%H$_2$.

The three dots in each line represent data at -1.0 V, -1.5 V and -2.0 V. At -2.0 V, cell has a higher current but the same hydrogen amount at 900°C compared to those at lower temperature. It results in the low efficiency at this point (see figure 6.12).
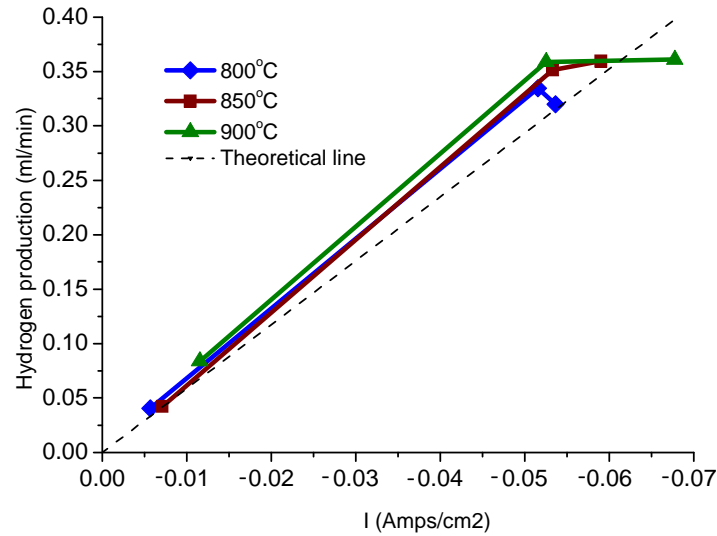
135

Figure 6.13. Hydrogen production with current density from an SOEC with LSCM/CGO cathode, 2 mm thick YSZ electrolyte and LSM anode measured at 800°C , 850°C and 900°C using 3%H$_2$O/Ar/4%H$_2$.

Comparing hydrogen production for cells with LSCM/CGO cathode, 2 mm YSZ electrolyte and LSM anode running at 800°C in 3%H$_2$O/Ar and in 3%H$_2$O/Ar/4%H$_2$, it could be seen that higher current-to-hydrogen efficiency could be gained in gas with 4%H$_2$ (see figure 6.14 and figure 6.15).

It is shown in figure 6.14 that hydrogen production is in accordance with cell current in both atmospheres except when hydrogen produced is close to theoretical amount. Hydrogen production has a similar increasing rate with current in both atmospheres. A cell could produce more hydrogen in 3%H$_2$O/Ar/4%H$_2$ than in 3%H$_2$O/Ar at the same current.

Figure 6.15 shows efficiency versus current in 3%H$_2$O/Ar and in 3%H$_2$O/Ar/4%H$_2$. Efficiency in 3%H$_2$O/Ar is up to 80% and increases with cell current, while efficiency in 3%H$_2$O/Ar/4%H$_2$ varies around 100% and decreases when current is increased. The decrease of efficiency with current in 3%H$_2$O/Ar/4%H$_2$ might be due to the steam starvation when steam decomposition ratio is high.

As gas chromatograph has a low tolerance limitation for steam, hydrogen

production with higher H_2O content has not yet been acquired. According to results discussed above, current and hydrogen production might be restricted by low steam content in fed-in gas. And it is supposed to have higher current and produce more hydrogen if sufficient steam is supplied.

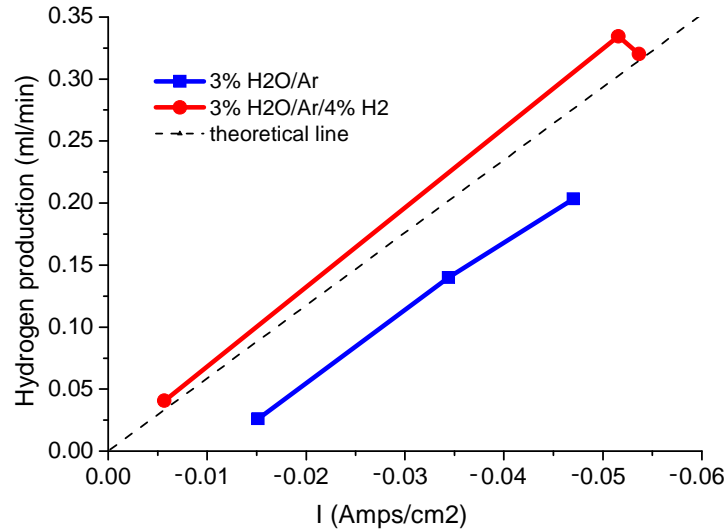**Figure 6.14. Hydrogen production versus current from a cell with LSCM/CGO cathode, 2 mm YSZ electrolyte and LSM anode running at 800°C in 3%H$_2$O/Ar and in 3%H$_2$O/Ar/4%H$_2$.**
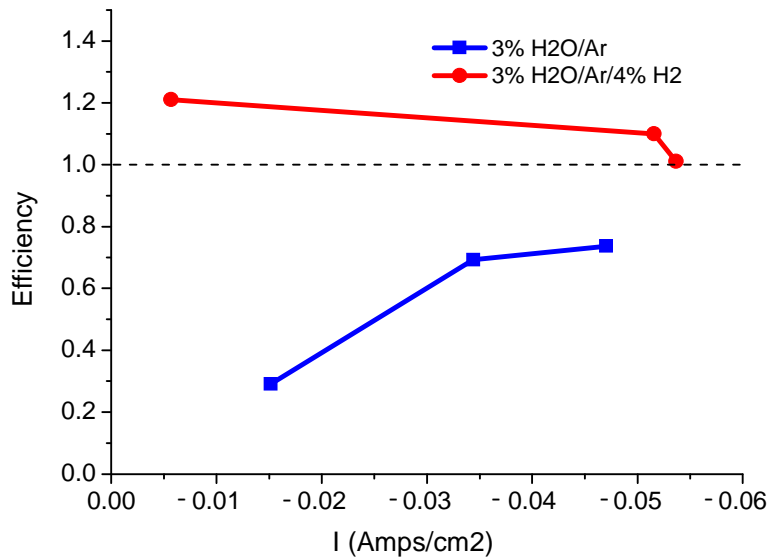

Figure 6.15. Current-to hydrogen efficiency versus current from a cell with LSCM/CGO cathode, 2 mm YSZ electrolyte and LSM anode running at 800°C in

3%H$_2$O/Ar and in 3%H$_2$O/Ar/4%H$_2$.

6.3 Hydrogen production from an SOEC with 50 micron thick YSZ electrolyte

Electrochemical measurement was done using an SOEC with the same electrodes as the cell described above but with thinner YSZ electrolyte (~50 μm thickness, see section 5.4). Figure 6.16 shows cell currents under different potential loads at 900°C and with 3%H$_2$O/Ar for cathode. This measurement was to sweep the potential between four separate potential set points in discrete potential steps: from -0.75 V to -1.5 V and -1.5 V to -0.75 V and then from -0.75 V to -1.5 V. Each step was 0.25V. The linear step (from -0.75V to -1.5V or from -1.5V to -0.75V) was repeated three times. The performance of the thin SOEC declines slightly after each cycle; however, the performance has been improved dramatically compared to the cell with 2mm thick YSZ electrolyte. Even in the last cycle, the current is about 140 mA at -1.5 V and is 126 mA at -1.25 V. By comparison, the current of the 2mm cell at 900 ^{o}C with 3% H$_2$O/Ar is 60 mA at -1.5 V and is 56 mA at -1.25 V. According to results shown above, the amount of hydrogen production is in accordance with current. Therefore, the thin cell is supposed to produce more hydrogen than the thick cell if sufficient steam is supplied.
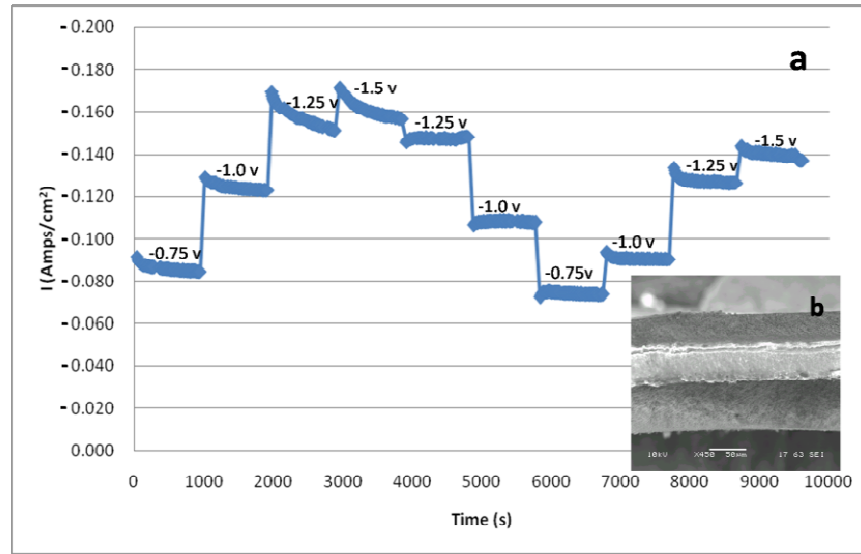
Figure 6.16. a. Current of SOEC with 50 μm thick YSZ electrolyte in potential step measurement at 900°C with 3% H$_2$O/Ar for cathode; b. SEM picture of the cross section of SOEC with 50 μm thick YSZ electrolyte.

6.4 Hydrogen production from cells with various catalysts in LSCM/CGO cathodes

In order to study influence of catalysts on SOEC performances, a series of cells with LSM anodes, 2mm YSZ electrolytes and LSCM/CGO cathodes with various catalysts have been made. Test conditions are as follows. Operating temperature is 900°C, operating pressure is atmosphere pressure, inlet gas of cathode (hydrogen electrode) is 3%H$_2$O/Ar or 3%H$_2$O/Ar/4%H$_2$, and anode (oxygen electrode) is open to air. AC impedance data and I-V curves are obtained (see chapter 4). Hydrogen production is measured by gas chromatography and efficiencies are calculated when constant potentials are applied.

6.4.1 3%H$_2$O/Ar

Figure 6.17 displays current-voltage curves from cells with various catalysts measured at 900°C with 3%H$_2$O/Ar (see section 4.3). performances are improved by

adding catalysts. At potentials more negative than -1.0 V, catalysts have a rating on improving cell performance: Pd > Fe > Rh > Ni > no catalyst.
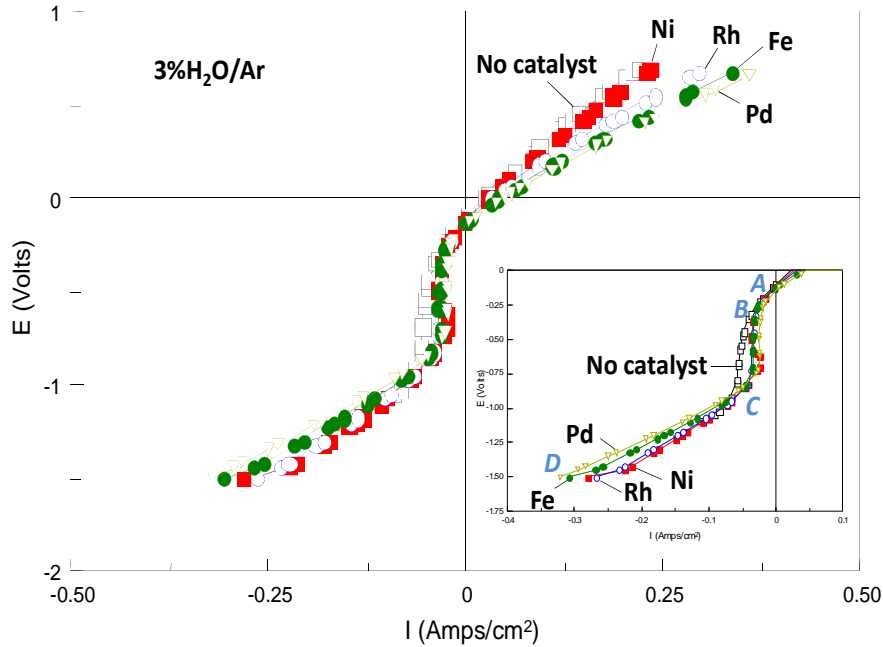

Figure 6.17. Polarization properties from cells having various catalysts in LSCM/CGO cathodes at 900°C with 3%H$_2$O/Ar.

Figure 6.18 shows cell current, hydrogen production and current-to-hydrogen efficiency at potentials of -1.0 V, -1.25 V and -1.5 V.

Generally speaking, cell current and hydrogen production at -1.0 V, -1.25 V and -1.5 V from cells with various catalysts could be rated as: Pd > Fe > Rh > Ni > no catalyst (see figure 6.18-a and figure 6.18-b). This is in accordance with result in I-V curves and indicates that hydrogen production from these cells depends on cell current.

Current-to-hydrogen efficiencies from cells with various catalysts are close to 100% at -1.0 V, -1.25 V and -1.5 V when cells are running at 900°C with 3%H$_2$O/Ar (see figure 6.18-c). Efficiency at -1.5 V from the cell with Pd is not shown in figure 6.18-c because the calculated efficiency is much higher than 100% (see figure 6.18-a and figure 6.18-b). The cell with Pd, followed by the cell with Fe, has the highest efficiency.
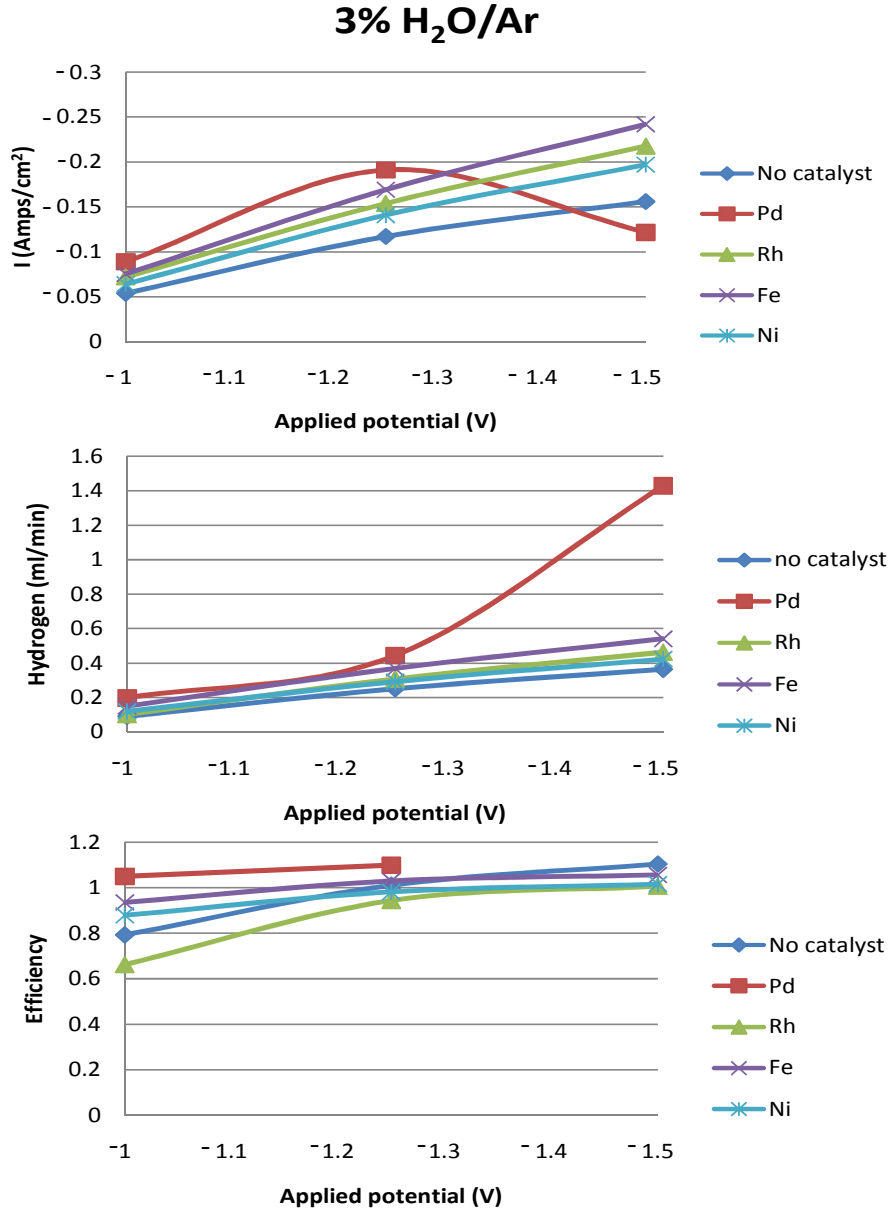
Figure 6.18. Current, hydrogen production and current-to-hydrogen efficiency at -1.0 V, -1.25 V and -1.5 V from cells with LSM anodes, 2 mm YSZ electrolytes and LSCM/CGO cathode with various catalysts running at 900°C with 3%H$_2$O/Ar.

In order to find out possible reasons for the strange low current at -1.5 V from the cell with Pd, the cell was measured again by applying continuous constant potentials (-1.0 V, -1.25 V and -1.5 V) in 3%H$_2$O/Ar. Results are shown in figure 6.19.

The black line is the result from original test, which shows a high current of 200

mA/cm^2 at -1.25 V but a highly decreased current of 120 mA/cm^2 after 1300 seconds when -1.25 V and -1.5 V are applied. It is strange to have a sudden decrease in current at 1300 seconds when the cell is still applied the same potential (-1.25 V) and has no improvement in current at a higher voltage (-1.5 V). The corresponding hydrogen production amount versus time is plotted in blue line in figure 6.19. It could be seen that at 1300 seconds, there is an increase in hydrogen production while current drops a lot. It is reasonable to assume high steam decomposition ratio decreases cell current because of steam starvation.

After a long time operation, the cell was again ran at -1.0 V, -1.25 V and -1.5 V continuously and the current-time curve is shown in red line. As is shown in figure 6.19, the repeated test has a poorer performance and has lower currents than the first test. The red line shows that current increases with potential in the repeated measurement, which is different from the result in the original test. The difference between two tests is that repeated measurement has reduced performance. This indicates that the decreased current at 1300 seconds in the first test could probably not come from change in cell materials but may be the high current/high steam decomposition ratio and insufficient steam supply.

There is another possibility that the strange low current at -1.5 V from the cell with Pd might relate to instrumental artifact.
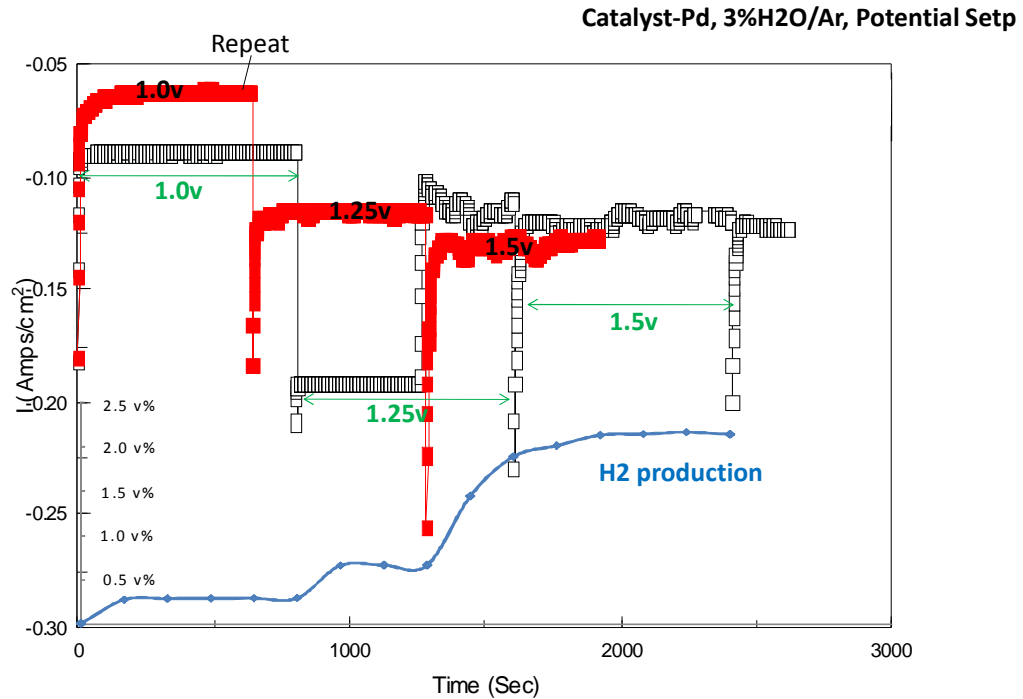
Figure 6.19. Current versus time while continuous constant potentials (-1.0 V, -1.25 V and -1.5 V) are applied. Black line: first test; red line: repeated test; blue line: hydrogen production versus time in the first test.

Figure 6.20 is hydrogen production with current density from cells with various catalysts running at 900°C with $3\%H_2O/Ar$. Neglecting the high hydrogen amount at -1.5 V from the cell with Pd, traces from various cells are linear. They are parallel and almost overlap with the theoretical line. This indicates a satisfying hydrogen production amount from these cells at 900°C with $3\%H_2O/Ar$.
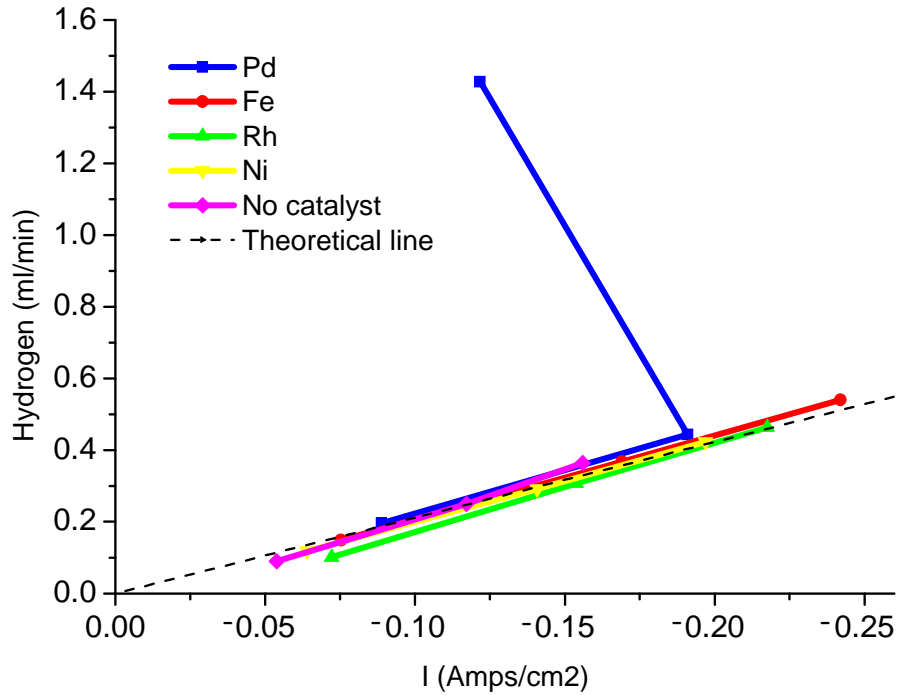
Figure 6.20. Hydrogen production with current density from SOECs with LSM anodes, 2 mm YSZ electrolytes and LSCM/CGO cathode with various catalysts running at 900°C with 3%H$_2$O/Ar.

6.4.2 3%H$_2$O/Ar/4%H$_2$

Cells with various catalysts were then tested at 900°C in 3%H$_2$O/Ar/4%H$_2$. Figure 6.21 shows polarization properties from cells having various catalysts in LSCM/CGO cathodes at 900°C with 3%H$_2$O/Ar/4%H$_2$. Performance has been improved bt adding catalysts. Cell with Pd and Fe has the best performances in electrolysis mode in 3%H$_2$O/Ar/4%H$_2$ (see section 4.2).
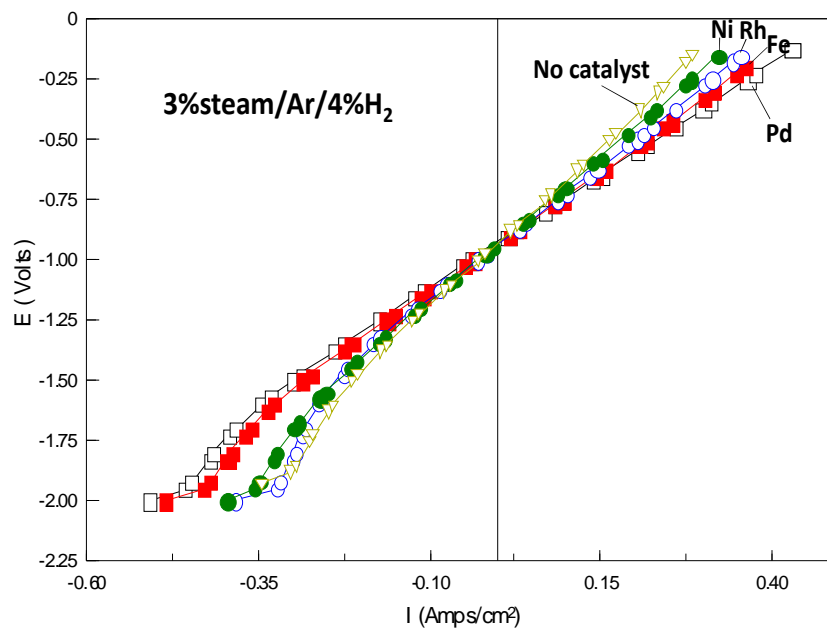
Figure 6.21. Polarization properties from cells having various catalysts in LSCM/CGO cathodes at 900°C with 3%H$_2$O/Ar/4%H$_2$.

Constant voltages were applied on these cells in 3%H$_2$O/Ar/4%H$_2$, while gas chromatograph was applied to detect hydrogen production at each potential. Cell current, hydrogen production and efficiency versus voltage are shown in figure 6.22. Current at potentials are in accordance with I-V curves in figure 6.21. Cells with Pd and Fe have the highest currents, followed by the cell with Ni. Hydrogen production from cells with various catalysts are in accordance with cell currents except the cell with Pd. The cell with Pd has a lower current-to-hydrogen efficiency which could not be explained. There seems to be no steam starvation occurring in these measurements. This might be due to higher gas flow rates for these tests (40 ~ 50 ml/min). And accordingly, the slope increase at around -1.5 V in I-V curves in figure 6.21 are not as much as the slope increase in figure 6.8. Current-to-hydrogen efficiencies from these cells are around 100%. Up to 86% steam was decomposed to hydrogen using cells with catalysts with no hydrogen supply when sufficient steam is supplied.
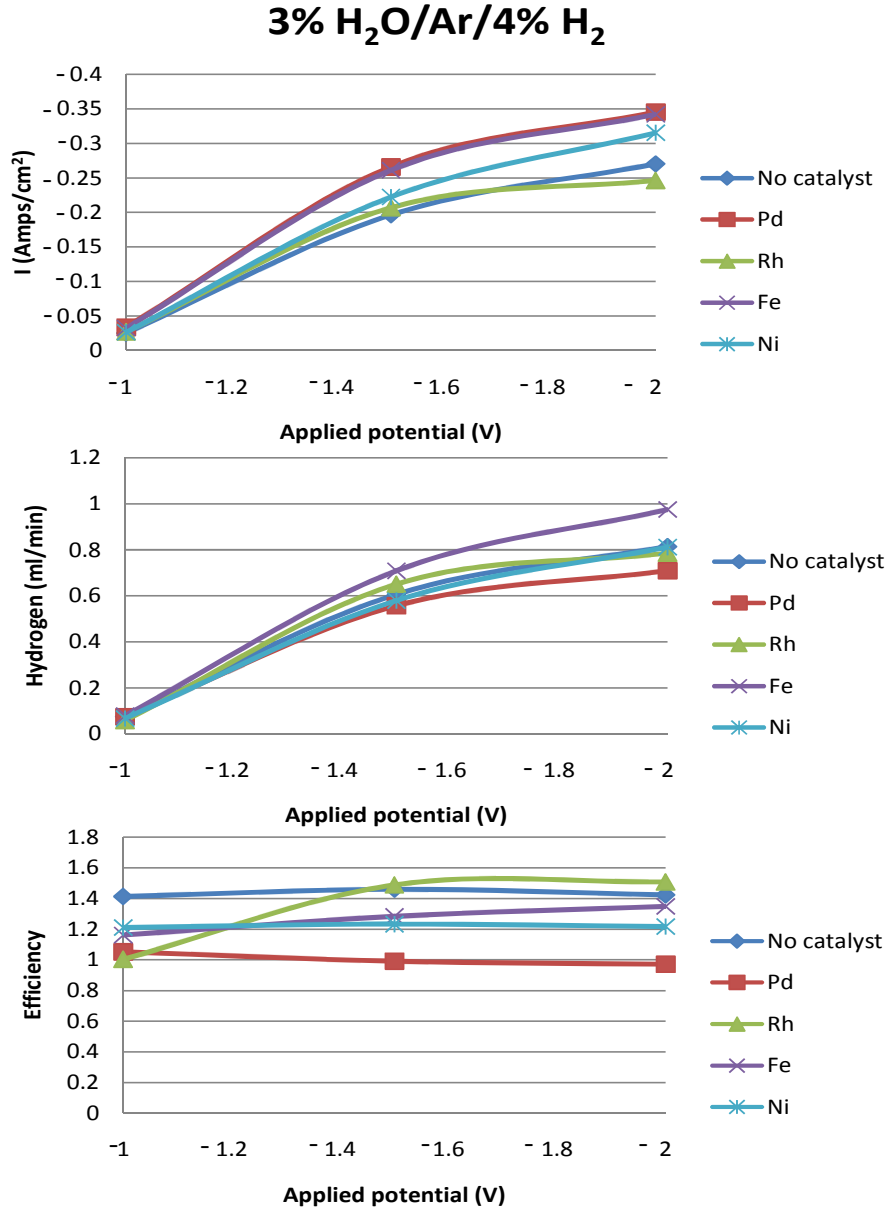
Figure 6.22. Current, hydrogen production and current-to-hydrogen efficiency at -1.0 V, -1.5 V and -2.0 V from cells with LSM anodes, 2 mm YSZ electrolytes and LSCM/CGO cathode with various catalysts running at 900°C with 3%H$_2$O/Ar/4%H$_2$O.

6.5 Conclusions

Herein we have demonstrated that hydrogen could be produced efficiently starting with a small amount of hydrogen (4% H$_2$) or with no content of hydrogen using SOECs with LSCM/CGO cathodes. Current-to-hydrogen efficiency from SOECs with LSCM/CGO cathodes could reach 80% at 850°C in 3%H$_2$O/Ar. Efficiencies are even

146

higher (close to 100%) in $3\%H_2O/Ar/4\%H_2O$ at 800~900°C. There seems to be steam starvation at high current when hydrogen production amount is approaching the theoretical value. It is supposed that high slope in I-V curves at high potentials may also relate to steam starvation. Hydrogen production is in good accordance with cell current when steam supply is sufficient. The conversion rates of steam to hydrogen was up to 86% with no hydrogen supply when sufficient steam is supplied.

Cell performance has been improved by adding catalysts. Cells with catalysts have smaller resistance and produce more hydrogen. The cell with Pd has a high hydrogen production amount at -1.5 V at 900°C in $3\%H_2O/Ar$ while has a highly reduced cell current in the meantime. This may stem from steam starvation which caused by high steam decomposition ratio.

Though more study on electrolysis processes in SOECs with LSCM cathodes, LSCM is a good candidate for cathode material of SOECs for high temperature hydrogen production especially starting with low/no content of hydrogen.

References

1. M. Ni, M. K. H. Leung, D. Y. C. Leung, *Int. J. Hydrogen Energy*, 2007, 32, 4648.

2. J. E. O'Brien, M. G. McKellar, C. M. Stoots, J. S. Herring, and G. L. Hawkes, *Int. J. Hydrogen Energy*, 2009, 34, 4216.

3. T. Sakai, S. Matsushita, H. Matsumoto, S. Okada, S. Hashimoto, and T. Ishihara, *Int. J. Hydrogen Energy*, 2009, 34, 56.

4. Roberto, F. S.; Janine, C. P.; Reinaldo, S. G.; Michele, O. S.; Jo¨elle, R. B. *J. Power Sources*, 2007, 164, 792.

5. J. Udagawa, P. Aguiar, N. P. Brandon, *J. Power Sources*, 2007, 166, 127.

6. S. Fujiwara, S. Kasai, H. Yamauchi, K. Yamada, S. Makino, K. Matsunaga, M. Yoshino, T. Kameda, T. Ogawa, S. Momma, and E. Hoashi, *Prog. Nucl. Energy*, 2008, 50, 422.

7. T. Kobayashi, K. Abe, Y. Ukyo, and H. Matsumoto, *Solid State Ionics*, 2001, 138, 243.

Chapter 7 SOEC performance with different compositions of the gas supplied to the steam/hydrogen electrode

7.1 Introduction

According to literature survey, it has been reported that solid oxide electrolysis cells (SOECs) perform better with more steam in cathode atmosphere[1]. And SOEC operation can be limited by the gas diffusion in the steam/hydrogen electrode, notably at moderate humidities[2].

It is discussed in last chapters that cell performance is suspected to be restricted by gas diffusion when running with 3% steam. At cathode side, steam diffuses to the three phase boundary and hydrogen produced diffuses out of the cathode. Increasing steam concentration is expected to facilitate steam diffusion process and therefore cathode reactions. As reactions at anode side are oxygen production and diffusion of oxygen from anode, increasing oxygen concentration at anode is not helpful for gas diffusion process.

If the performance is restricted by steam diffusion, to change steam concentration at cathode is expected to improve SOEC performance. In this chapter, to find out the effect of steam concentration, SOECs with LSCM/CGO (50% CGO by weight) cathodes (some were loaded with catalysts), YSZ electrolytes and LSM anodes were tested in atmospheres with/without hydrogen and with various steam contents.

3%, 10%, 20% and 50% steam were generated by flowing carrier gas (Ar/5%H_2 or Ar, with flowrates of 20~30 ml/min) through water at different temperatures. A cell with LSCM/CGO cathode, 2 mm YSZ electrolyte and LSM anode was tested with different compositions of the gas supplied to the steam/hydrogen electrode. Performances from this cell in different water contents and with/without hydrogen are discussed in this chapter.

Cells with various catalysts in cathodes (see chapter 4) were tested with 3% steam and 50% steam with and without presence of hydrogen. The performances with different steam contents are discussed in section 7.4.

According to the results in this chapter, humidity of the gas supplied to the cathode

has not much effect on the performance. And results in different conditions are discussed in the following.

7.2 Ar/H$_2$ with different humidities

Ar/H$_2$ with different steam contents (3% H$_2$O, 10% H$_2$O, 30% H$_2$O, 50% H$_2$O) were generated for cathode by passing Ar/5%H$_2$ though water at different temperatures (room temperature, 47°C, 69°C, 81°C). A cell with LSCM/CGO cathode, 2 mm thick YSZ electrolyte and LSM anode was tested at 900°C with different steam contents for cathode and with presence of hydrogen.

The polarization properties with presence of hydrogen and different water contents are displayed in figure 7.1. For all atmospheres, the current-voltage curves are close to but not absolutely linear, which is similar to the phenomena in cells described before (see section 3.3.2). For fuel cell mode, the cell has the best performance with 3% H$_2$O and the poorest performance with 50% H$_2$O. For electrolysis side, there is no big difference between current-voltage curves in different atmospheres. Current-voltage curve with 50% H$_2$O has slightly larger slope than with other three atmospheres. With 3% H$_2$O, 10% H$_2$O and 30% H$_2$O, slopes of I-V curves in electrolysis mode are quite similar to each other. The cell has a slightly better performance when running with 3% H$_2$O than with higher water contents. Current at the highest potential (OCV plus -1.0 V) decreases with steam content (0.3815 Amps with 3% H$_2$O, 0.3642 Amps with 10% H$_2$O, 0.3535 Amps for 30% H$_2$O, 0.3354 Amps for 50% H$_2$O). According to literature survey, it was reported that SOECs with Ni/YSZ cathodes perform better with more steam in cathode atmosphere within the humidity range of 30% steam ~ 70% steam and with presence of hydrogen[1]. And they found the SOEC operation can be limited by the gas diffusion in the steam/hydrogen electrode, notably at moderate humidities below 70 vol.% AH[2]. Uchida *et al*[3]. reported that an SEOC with Ni-dispersed SDC cathode has reduced overpotential with increasing p[H2O] and the IR-loss of this cell was found to increase with p[H2O]. The decrease of overpotential was suspected to be due to an increased transfer rate of water vapor to the reaction sites. And the increase

of E_{IR} was ascribed to a decrease in the n-type electronic conductivity in the mixed-conducting SDC.
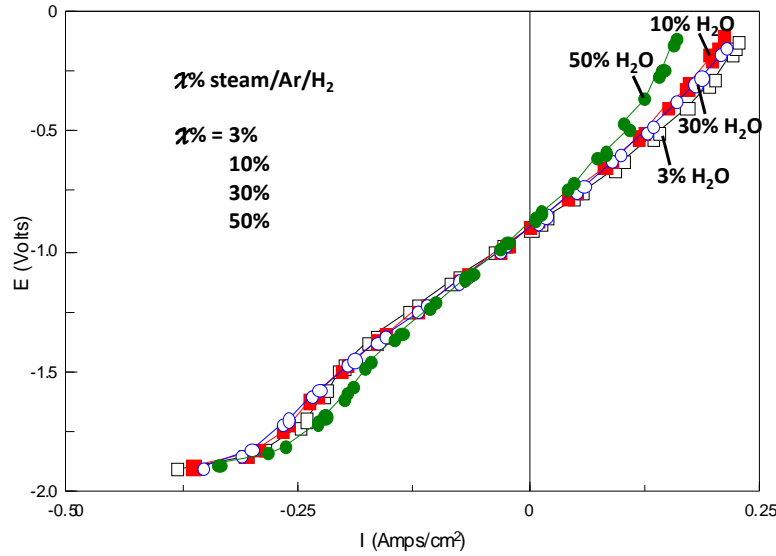

Figure 7.1. Current-voltage curves from an SOEC with LSCM/CGO cathode, 2mm thick YSZ electrolyte and LSM anode at 900°C with 3%, 10%, 30%, 50%steam/Ar/H$_2$ for cathode.

The steam/hydrogen ratio have influence on open circuit voltages of SOECs. Theoretically, the OCV decreases with increasing steam/hydrogen ratio[4]:

$$E = \frac{\Delta G}{2F} = \frac{\Delta G^o}{2F} - \frac{RT}{2F} \ln \frac{(P_{H_2O}/P^o)}{(P_{H_2}/P^o)(P_{O_2}/P^o)^{\frac{1}{2}}} = E^o + \frac{RT}{4F} \ln \frac{(P_{H_2}/P^o)^2 (P_{O_2}/P^o)}{(P_{H_2O}/P^o)^2}$$

Where E^o is the standard electrode potential, R is the gas constant, F is the Faraday constant, P_{O2} is the oxygen partial pressure in cathode atmosphere. P_{H2} and P_{H2O} are partial pressures of hydrogen and steam in cathode gas.

Figure 7.2 shows open circuit voltages at 900°C with presence of hydrogen and with 3% H$_2$O, 10% H$_2$O, 30% H$_2$O, 50% H$_2$O respectively. In general, OCV decreases with water content as expected except with 30% H$_2$O. The decrease of open circuit potential could stem from increased water content. And as cell performances with higher water contents were measured after those with lower water contents, the decrease of OCV could also relate to the slightly increased leakage as time passes by.
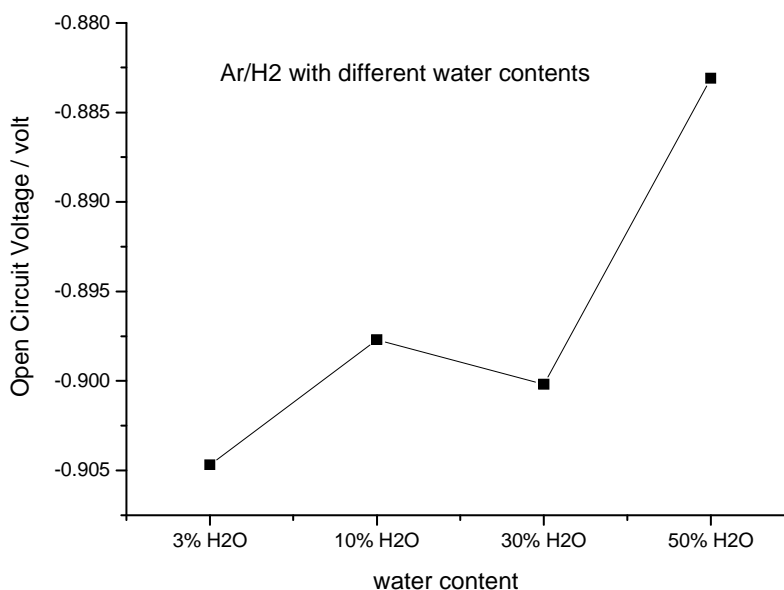
**Figure 7.2. Open circuit voltages from an SOEC with LSCM/CGO cathode, 2mm
thick YSZ electrolyte and LSM anode at 900^oC with 3%, 10%, 30%,
50%steam/Ar/H_2 for cathode.**

Figure 7.3 shows the dE/dI as a function of potential from the cell with 3%, 10%,
30%, 50%steam/Ar/H_2 at the cathode. The dE/dI values were derived from linear fit
of points in I-V curves in figure 7.1. In fuel cell mode, the dE/dI value decreases
when voltage is approaching open circuit voltage.

In electrolysis mode (when potential is more negative than -0.9 volt), dE/dI value
increases and then decreases as potential is increased from OCV to (OCV plus –1.0
V) . dE/dI has higher values with 50% H_2O than with other atmospheres. In each
atmosphere, dE/dI reaches the maximum value at potential of around -1.5 volt. The
summit dE/dI values (at around -1.5 volt) with 3 % H_2O and 50% H_2O are higher than
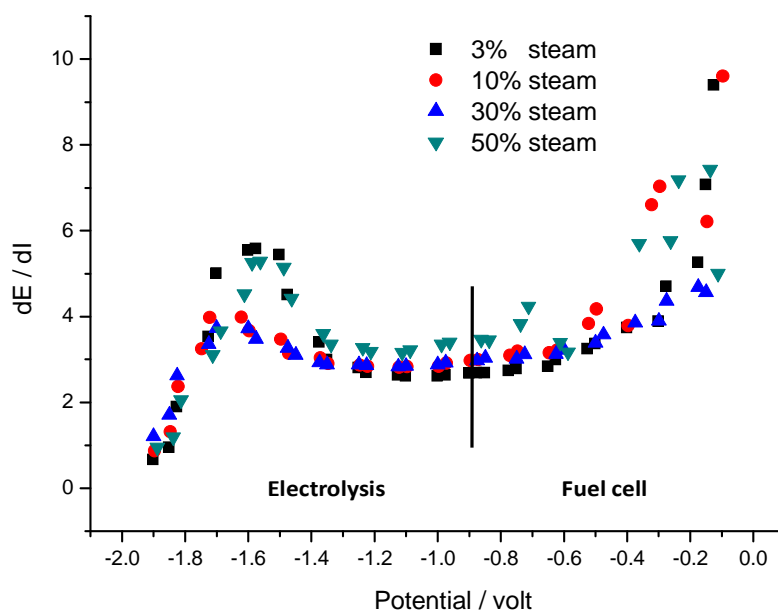those with 10% H_2O and 30% H_2O.

Figure 7.3. dE/dI at potentials from an SOEC with LSCM/CGO cathode, 2mm thick YSZ electrolyte and LSM anode at 900°C with 3%, 10%, 30%, 50%steam/Ar/H₂ for cathode.

Figure 7.4 shows the AC impedance data from an SOEC with LSCM/CGO cathode, 2 mm thick YSZ electrolyte and LSM anode at 900°C with 3%, 10%, 30%, 50%steam/Ar/H₂ for cathode. Generally, resistance of the cell slightly increases with increased water content in cathode atmosphere. Impedance spectra show arcs under all potentials except at -2.0 V. The cell has the largest resistance and the highest polarization resistances with 50% steam at each potential. It could be seen that Rs value increases with water content at open circuit, -1.0 V and -1.5 V. At -2.0 V, Rs values with different water contents does not differ that much as those at lower potentials. Series resistances and polarization resistances with different steam contents are discussed in the following section.
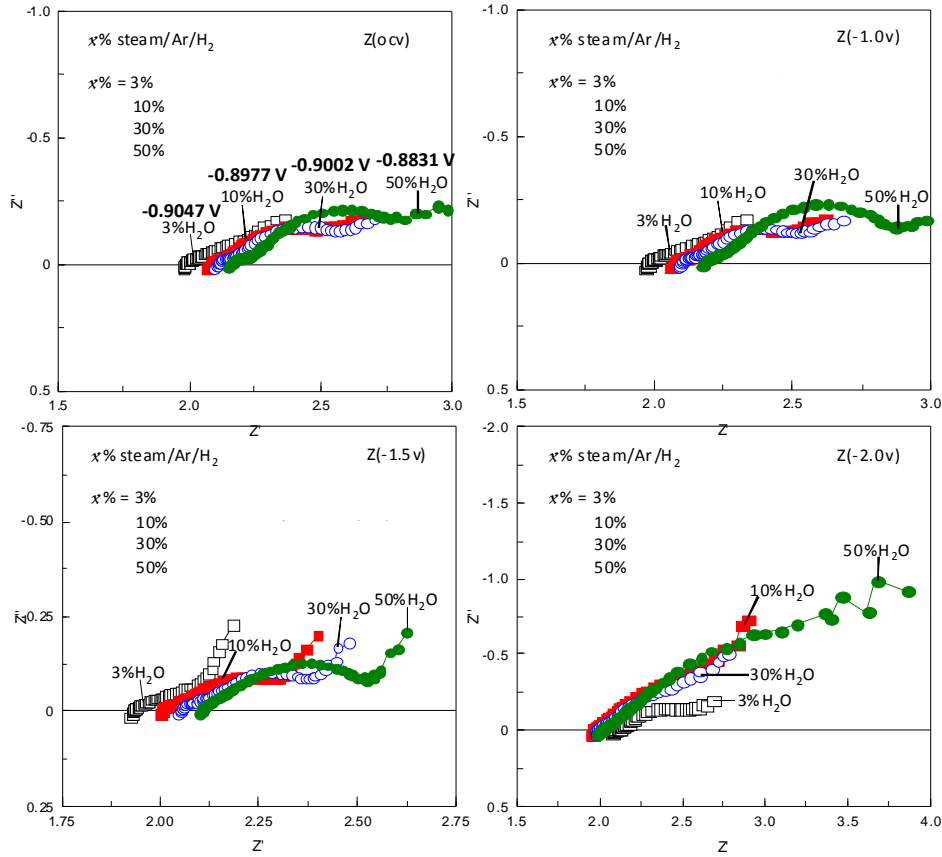
**Figure 7.4. AC impedance data from an SOEC with LSCM/CGO cathode, 2mm
thick YSZ electrolyte and LSM anode at 900°C with 3%, 10%, 30%,
50%steam/Ar/H_2 for cathode.**

Figure 7.5 displays series resistances at voltages from the cell running with 3%,
10%, 30%, 50%steam/Ar/H_2. Generally, series resistance of the cell decreases with
potential, which might relate to improved conductivity in the electrode structure or
improved electronic conductivity in YSZ electrolyte[1] under SOEC operation with
high potentials. There is an exception that when running with 3%steam, the cell has
higher series resistance at -2.0 V than at lower voltages. At each potential (except at
-2.0 V), Rs has higher values when the cell running with more steam content. At -2.0
V, the cell has smaller series resistances with higher steam contents than with
3%steam/Ar/H_2. The increase of Rs with steam content could relate to more resistive
CGO in more oxidizing cathode atmosphere as water content increases. There is also
the possibility that the increase of ohmic resistance with steam might also relate to the

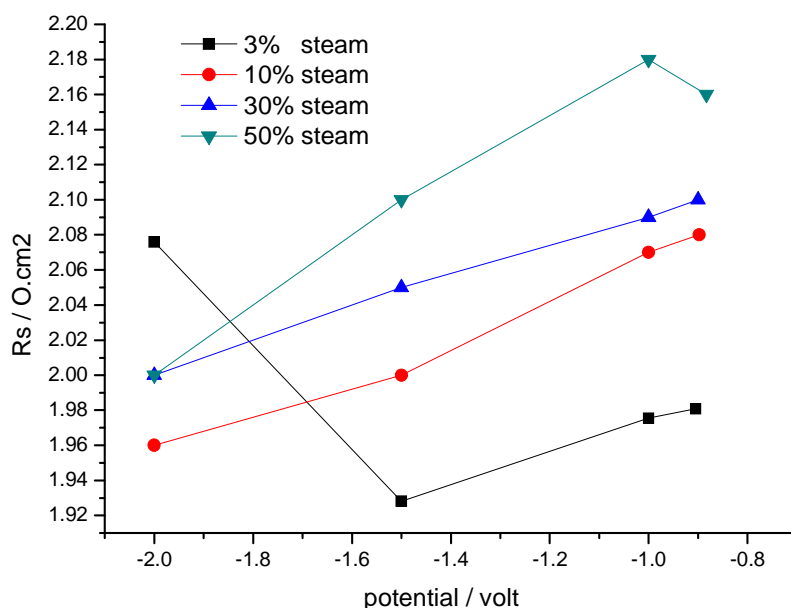153

performance decline as time passes by.

**Figure 7.5. Series resistances at voltages from an SOEC with LSCM/CGO
cathode, 2mm thick YSZ electrolyte and LSM anode at 900°C with 3%, 10%,
30%, 50%steam/Ar/H$_2$ for cathode.**

dE/dI values derived from I-V curves (see figure 7.1) could be considered as the
total resistances. dE/dI-Rs values can be roughly regarded as Rp values. As the I-V
curves have unreliable small slopes at -2.0 V, the dE/dI values for discussion are only
taken from data at OCV, -1.0 V and -1.5 V. Figure 7.6 displays dE/dI-Rs values at
potentials when the cell running with different steam contents. It could be seen that
polarization resistance generally increases with steam content. As measurements with
higher water contents were done after measurements with lower water contents, the
decline of performance with steam content might relate to depressed electrode
processes with more water and/or relate to longer operation time. There is a strange
high polarization resistance at -1.5 V when the cell running with 3% steam which is
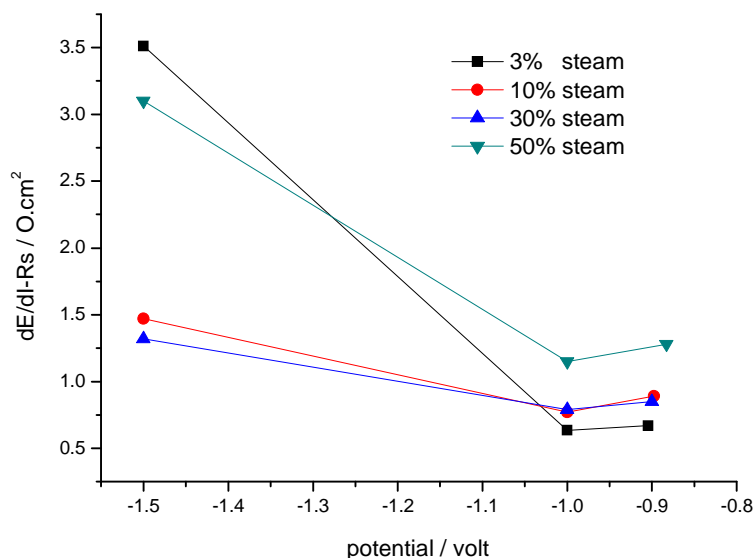the similar to the phenomena in Rs (see figure 7.5).

Figure 7.6. dE/dI-Rs values at potentials from an SOEC with LSCM/CGO cathode, 2mm thick YSZ electrolyte and LSM anode at 900°C with 3%, 10%, 30%, 50%steam/Ar/H₂ for cathode.

Figure 7.7 shows the Bode presentations from the cell at 900°C with 3%, 10%, 30%, 50%steam/Ar/H₂ for cathode. There are two rate limiting processes in all atmospheres. The high frequency process at around 3000 Hz might relate to transportation of oxygen ions/oxygen intermediates between LSCM and YSZ[5] and is very small in magnitude for all atmospheres. The dominating rate limiting process is the low frequency process. The summit frequencies of the low frequency arcs remain the same with different atmospheres, which suggests the cell might have the same low frequency limitation when running with different water contents. With characteristic frequency of 2 Hz, the low frequency process might stem from gas diffusion and/or surface adsorption/desorption limitations. It is shown that the magnitude of low frequency process is increased by increasing water content in cathode atmosphere. The low frequency process is small in magnitude when the cell is running with 3% steam and is much higher when the cell is running with 50% steam. Bode plots with 10%steam/Ar/H₂ and 30%steam/Ar/H₂ are quite similar to each other.

With more water content, the steam concentration increases and the hydrogen

concentration decreases. It is expected to have better steam diffusion with higher steam contents in cathode atmosphere. Therefore, if the low frequency process relates to steam diffusion, the increase of water content is expected to facilitate the low frequency process. However, it is shown that the process increases in magnitude with higher steam contents. Therefore, there is a chance that the low frequency process might have no relation with steam diffusion. Another possibility is that the steam concentrations at cathode were not as high as they were generated although a heating tape has been applied on the pathway.
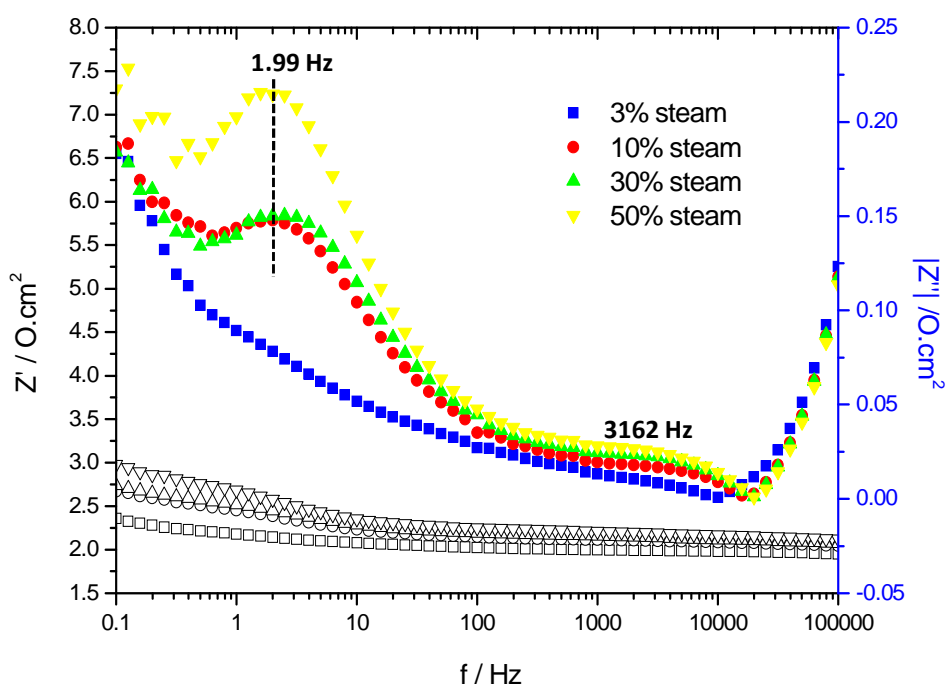

Figure 7.7. bode plots under open circuit from an SOEC with LSCM/CGO cathode, 2mm thick YSZ electrolyte and LSM anode at 900°C with 3%, 10%, 30%, 50%steam/Ar/H$_2$ for cathode.

Figure 7.8 shows bode plots under -1.0 V, -1.5 V and -2.0 V with different steam contents. The low frequency process at each potential increases with steam content. The cell has a more difficult low frequency process at -1.0 V than at -1.5 V in all atmospheres. At -2.0 V, bode plots with various steam content differ a lot with each other.
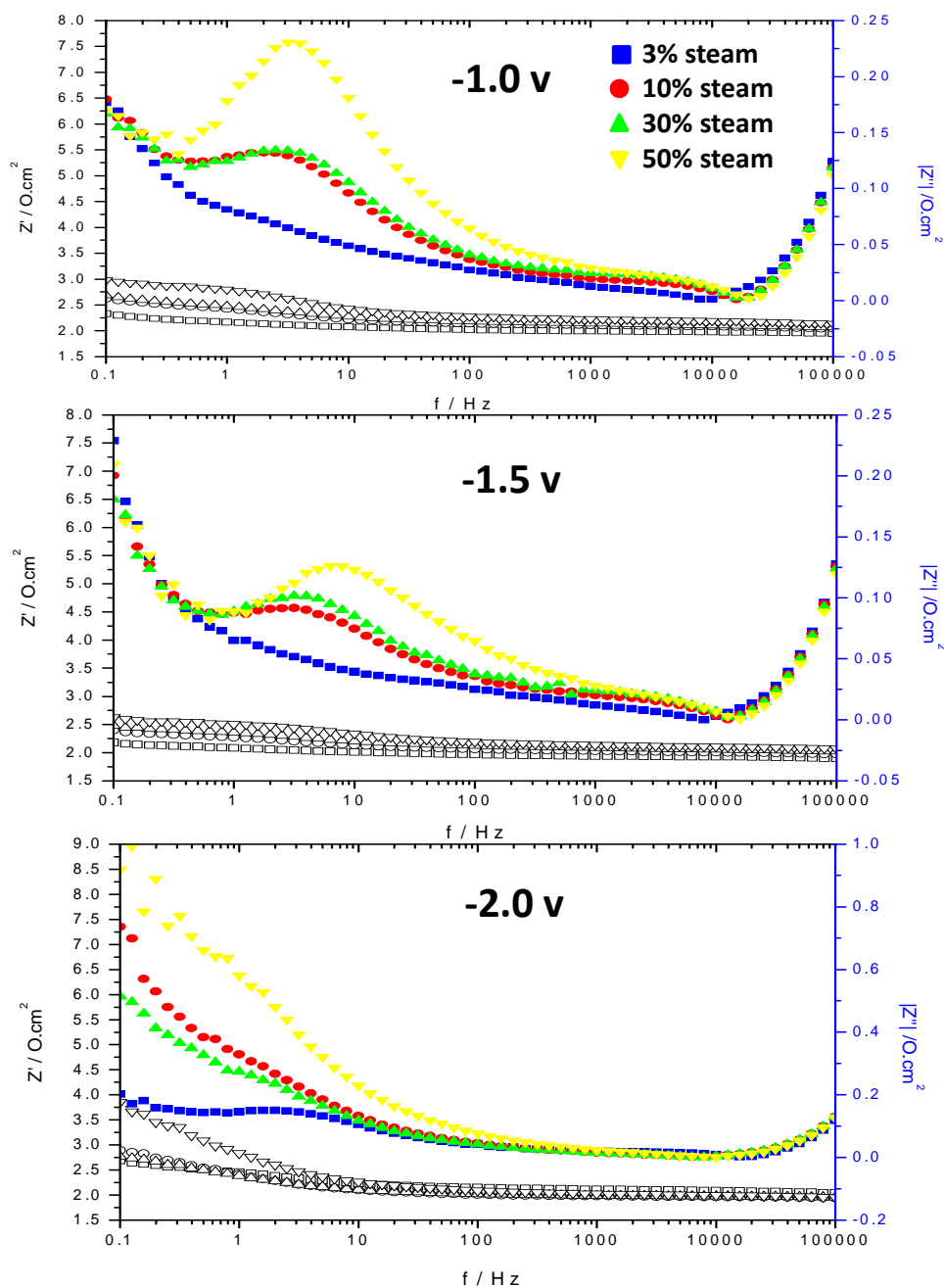
Figure 7.8. bode plots under open circuit from an SOEC with LSCM/CGO cathode, 2mm thick YSZ electrolyte and LSM anode at 900°C with 3%, 10%, 30%, 50%steam/Ar/H$_2$ for cathode.

7.3 Ar with different humidities

Ar with different steam contents (3% H$_2$O, 10% H$_2$O, 30% H$_2$O, 50% H$_2$O) were generated for cathode by passing Ar though water at different temperatures (room

temperature, 47°C, 69°C, 81°C). The cell with LSCM/CGO cathode, 2 mm thick YSZ electrolyte and LSM anode was tested at 900°C with different steam contents for cathode without presence of hydrogen.

Polarization performances without presence of hydrogen have steep slopes within potential range of -0.5~-0.9 V (see figure 7.9), which is the same phenomena to the results from cells described before (see section 3.3.3). Compared to the performances from atmospheres with hydrogen, the performances without hydrogen have smaller differences between different steam contents. In fuel cell mode, when running with no hydrogen, the cell has a smaller slope of I-V curve in lower water content than in higher water content. However, in electrolysis mode, the difference between performances from diverse steam contents is quite small when no hydrogen is present. The highest current at the maximum potentials (-1.10±0.01 V) for each atmosphere is: 96 mA for 3% H_2O, 92 mA for 10% H_2O, 90 mA for 30% H_2O, 89 mA for 50% H_2O. As the cell was measured with lower steam content before with higher steam content, the decline of performance with steam content might have some relationship to the longer operation time.
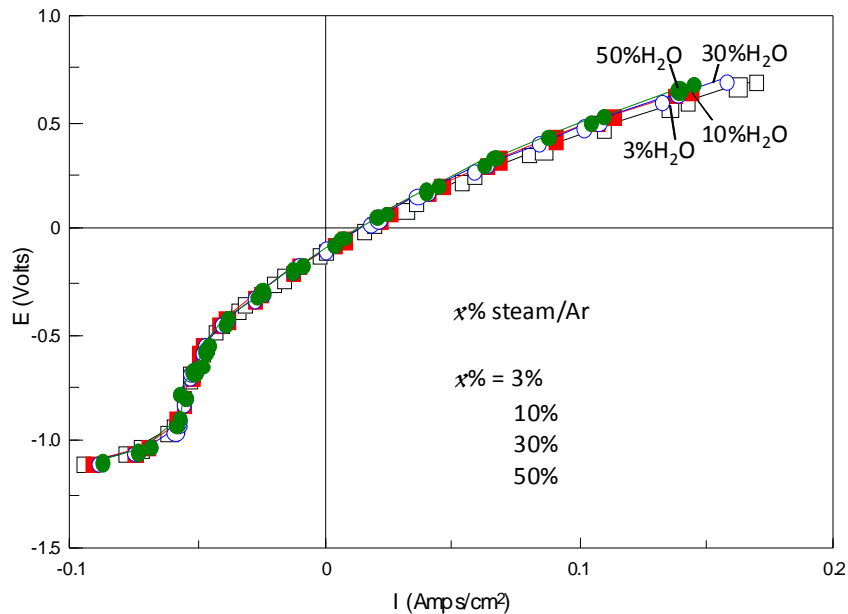

Figure 7.9. Current-voltage curves from an SOEC with LSCM/CGO cathode, 2mm thick YSZ electrolyte and LSM anode at 900°C with 3%, 10%, 30%,

50%steam/Ar for cathode.

Figure 7.10 shows open circuit voltages from different steam concentrations without presence of hydrogen. The open circuit voltage decreases with steam content as expected except when the cell is running with 30% steam. This phenomena is similar to that with presence of hydrogen (see figure 7.5), implying that that humidification was incomplete at 30%, probably similar to that at 10%.
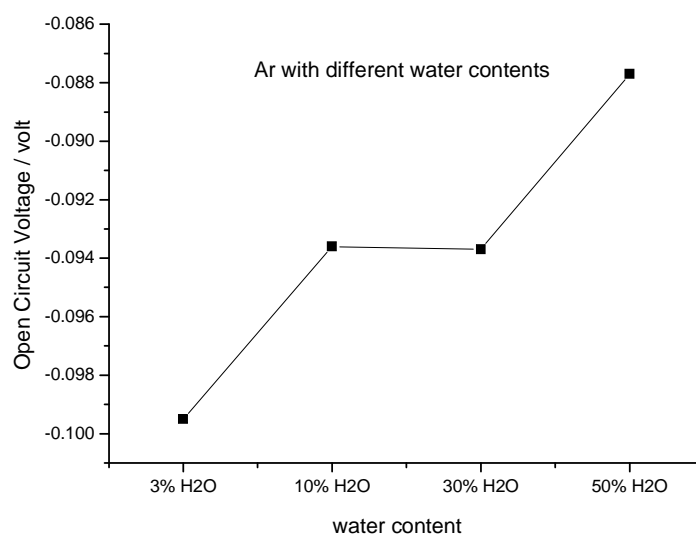

Figure 7.10. Open circuit voltages from an SOEC with LSCM/CGO cathode, 2mm thick YSZ electrolyte and LSM anode at 900°C with 3%, 10%, 30%, 50%steam/Ar for cathode.

Figure 7.11 shows the AC impedance data from the cell at 900°C with 3%, 10%, 30%, 50%steam/Ar for cathode. Under each potential, the cell has quite similar impedance data when running with different water contents. Total resistance for each atmosphere gets smaller as potential is increased.

Series resistances of the cell are 2.4 ~ 3.3 Ωcm^2, which is in reasonable agreement with the expected ohmic loss associated with a 2 mm YSZ electrolyte[6] at 900°C, 1.8 Ωcm^2. Figure 7.12 plotted the series resistances at open circuit, -1.0 V, -1.25 V and -1.5 V with different atmospheres. At each potential, Rs value gets slightly bigger when the cell is running with higher steam contents. Rs values with 10%, 30% and 50%

steam are close to each other but much higher than that with 3% steam.

Figure 7.13 is the polarization resistances at OCV, -1.0 V, -1.25 V and -1.5 V from
the cell at 900°C with 3%, 10%, 30% and 50% steam. The polarization resistances are
derived from impedance data in figure 7.11. They are Rp_1 values within the
measurement limit, neglecting the large diffusion curve for the lowest frequency
process. Rp_1 value decreased with potential for each atmosphere and varied between
3.0 and 8.0 $\Omega \cdot cm^2$. Polarization resistance with higher water content is a bit larger
than the value with lower water content. And the difference between different steam
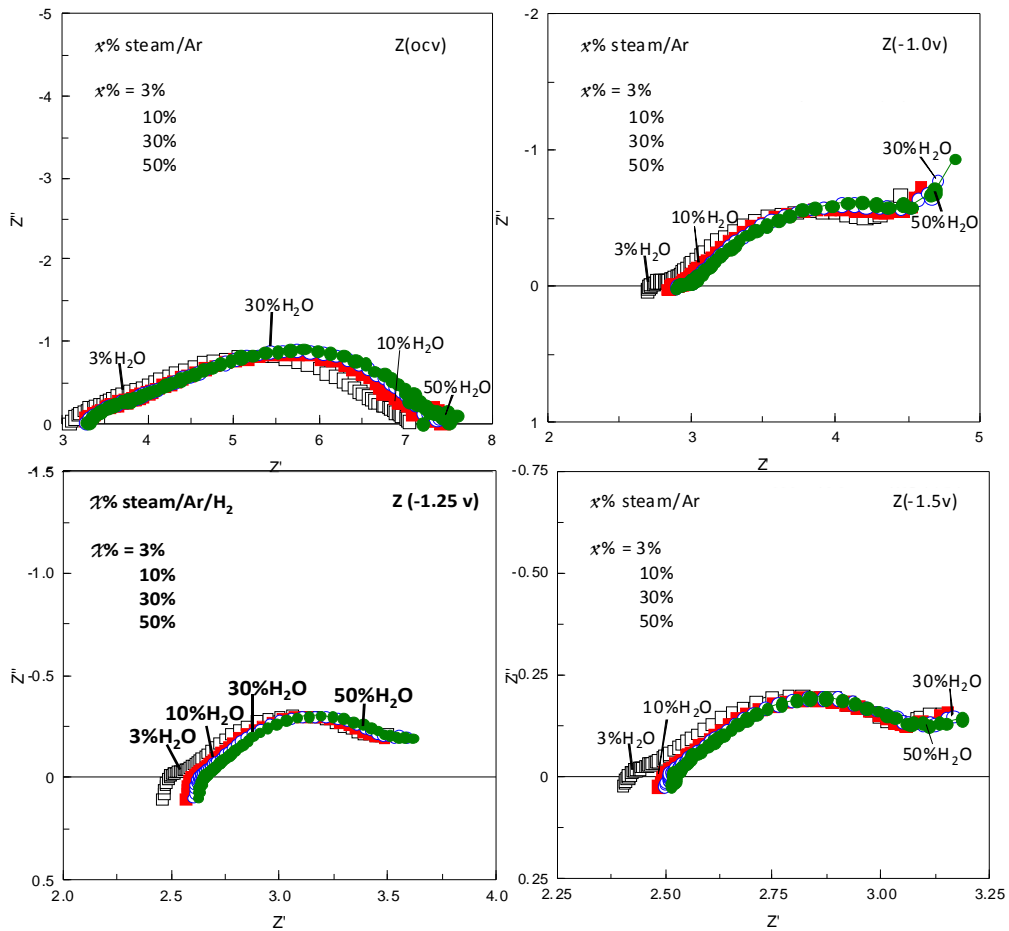contents decreased as potential is increased.

**Figure 7.11. AC impedance data from an SOEC with LSCM/CGO cathode, 2mm
thick YSZ electrolyte and LSM anode at 900°C with 3%, 10%, 30%,
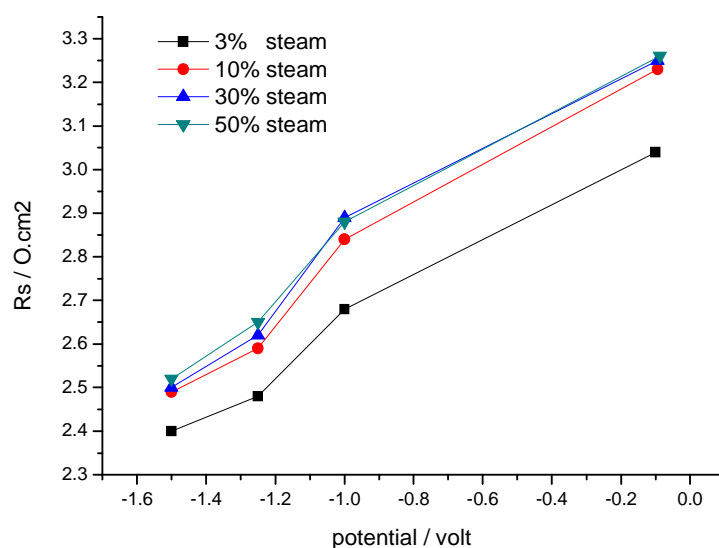50%steam/Ar for cathode.**

Figure 7.12. Series resistance from an SOEC with LSCM/CGO cathode, 2mm thick YSZ electrolyte and LSM anode at 900°C with 3%, 10%, 30%, 50%steam/Ar for cathode.
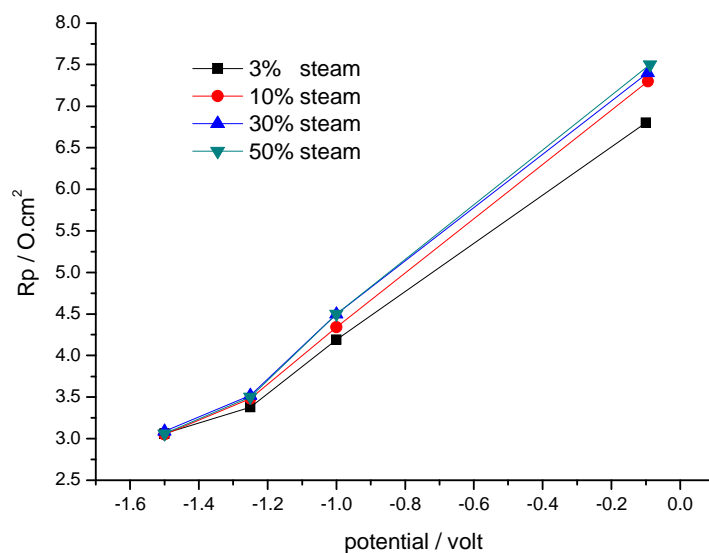

Figure 7.13. Polarization resistance from an SOEC with LSCM/CGO cathode, 2mm thick YSZ electrolyte and LSM anode at 900°C with 3%, 10%, 30%, 50%steam/Ar for cathode.

Figure 7.14 is the bode plots at OCV, -1.0 V, -1.25 V and -1.5 V from the cell running with 3% H_2O, 10% H_2O, 30% H_2O and 50% H_2O. There is only slight difference between bode presentations for different atmospheres. There are two limiting processes at different potentialsbut the dominating rate limiting processes at OCV and at potentials are different.

For all atmospheres, characteristic frequencies for both processes are lower at high voltages (-1.0 V, -1.25 V and -1.5 V) than at open circuit. The summit frequency of low frequency arc at OCV is 100 Hz, and varies from 1.25 Hz to 2.51 Hz at high potentials. The main limiting process at OCV (at 100 Hz) might relate to electrode activation while the main process at potentials (at 1~3 Hz) may steam from water electrolysis processes. With maximum frequencies of several thousands, the high frequency processes could relate to transportation of oxygen ions/oxygen intermediates.

Under open circuit, the cell has larger magnitude for both processes when running with higher water contents. The low frequency process under open circuit and -1.0 V are smaller in magnitude with 3% H_2O than with other atmospheres. However, at -1.5 V and -1.25 V, the cell has slightly larger magnitude for both processes when running with 3% H_2O.
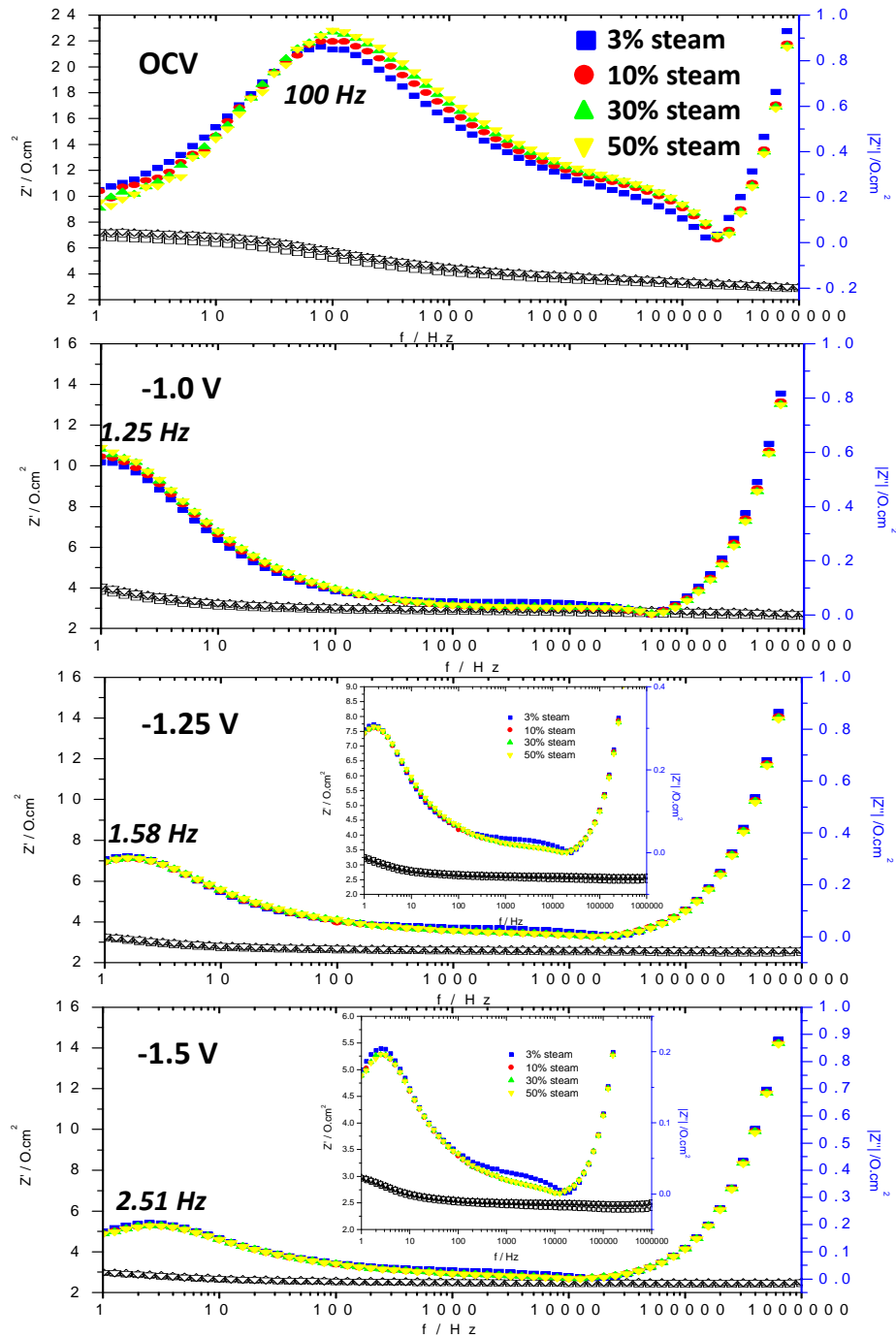
Figure 7.14. Bode presentations under different potentials from an SOEC with LSCM/CGO cathode, 2mm thick YSZ electrolyte and LSM anode at 900°C with 3%, 10%, 30%, 50%steam/Ar for cathode.

7.4 Cells with catalysts running with different compositions of gas supplied to cathode

7.4.1 Ar/H$_2$ with different humidities (with catalysts)

Performances form cells with various catalysts in LSCM/CGO cathodes running
with 3%H$_2$O/Ar/4%H$_2$ were discussed in section 4.2. In this section, performances
from these cells running with 50%H$_2$O/Ar/H$_2$ are discussed. 50%H$_2$O/Ar/H$_2$ were
generated by flowing Ar/5%H$_2$ through 81°C water.

Figure 7.15 shows polarization properties from cells with various catalysts running
with 50%H$_2$O/Ar/H$_2$ and 3%H$_2$O/Ar/H$_2$. With high steam content, catalysts have the
same ranking on improving cell performance compared to the ranking with
3%H$_2$O/Ar/4%H$_2$. The cell with Pd has the best performance in 50%H$_2$O/Ar/H$_2$. Ni
and Fe, which are much cheaper than Pd, also have good catalystic activity when the
cell is running with 50%H$_2$O/Ar/H$_2$. Performance from the cell with Ni was close to
the cell without catalyst when running with 3%H$_2$O/Ar/4%H$_2$, while it is close to the
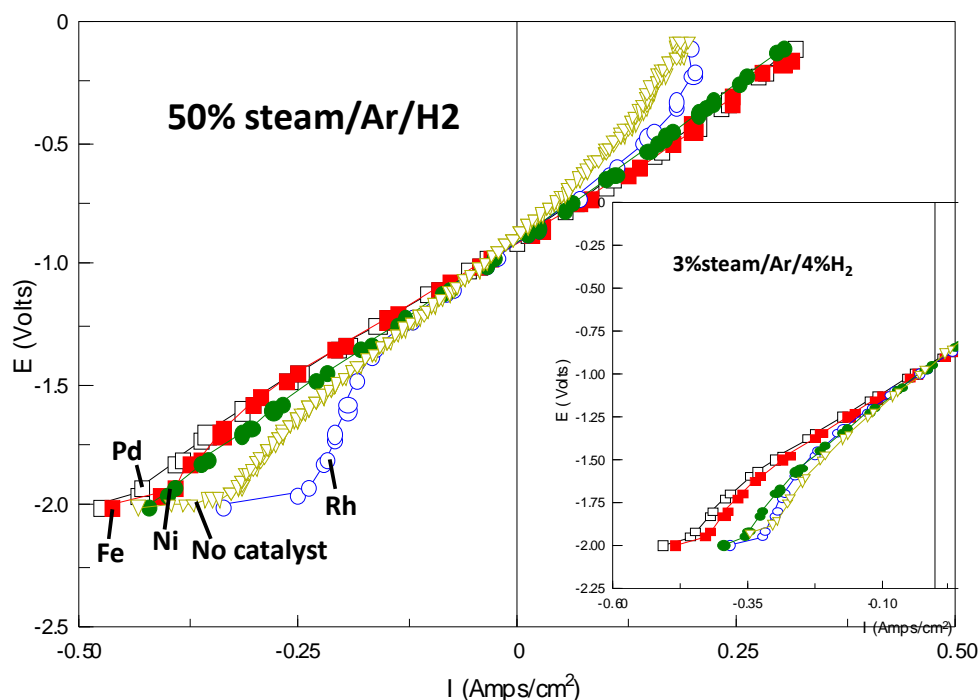performances from cells with Pd and Fe when running with 50%H$_2$O/Ar/H$_2$.

**Figure 7.15. Polarization properties from cells having various catalysts in
LSCM/CGO cathodes at 900°C with 50%H$_2$O/Ar/H$_2$ and 3%H$_2$O/Ar/4%H$_2$.**

Figure 7.16 are comparisons of polarization performances from cells with Pd, Fe

and Ni when running with $50\%H_2O/Ar/H_2$ and $3\%H_2O/Ar/4\%H_2$. Performances in different atmospheres only have slight differences for all the cells. It can be seen that slope of I-V curve from cells with Pd and Fe is higher in $50\%H_2O/Ar/H_2$ than in $3\%H_2O/Ar/4\%H_2$. However, the cell with Ni has slightly smaller slope when running with $50\%H_2O/Ar/H_2$. It is in agreement with the results shown in figure 7.15.
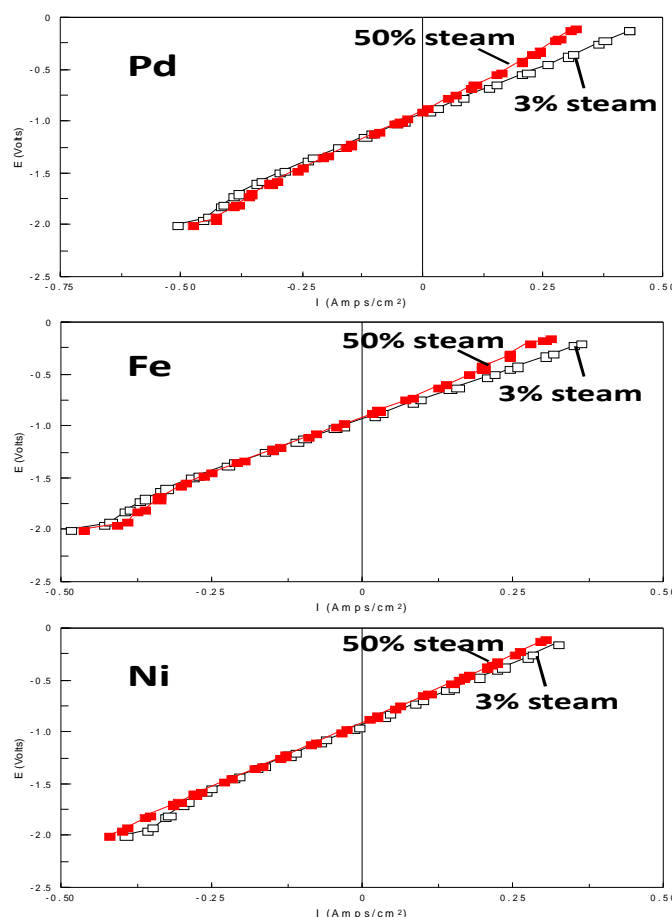

Figure 7.16. Comparisons of polarization performances from cells with Pd, Fe and Ni when running with $50\%H_2O/Ar/H_2$ and $3\%H_2O/Ar/4\%H_2$.

AC impedance data from the cell with Pd running with $50\%H_2O/Ar/H_2$ and $3\%H_2O/Ar/4\%H_2$ are displayed in figure 7.17. In general, resistance gets bigger when running with higher steam content.

Under OCV and -1.0 V, there are three processes in 50% steam while only two obvious arcs in 3% steam. The low frequency arcs (at OCV and -1.0 V) with 50% steam have no intercept with x axis. Polarization resistances with 50% steam are

165

larger than that with 3% steam.

Under higher potentials, the low frequency process shows lower characteristic frequencies and larger magnitude. This indicates the cell has more difficult low frequency process under -1.5 V and -2.0 V compared to that under open circuit. On the other hand, the low frequency process at -1.5 V and -2.0 V could be harder when the cell is running with higher steam content.
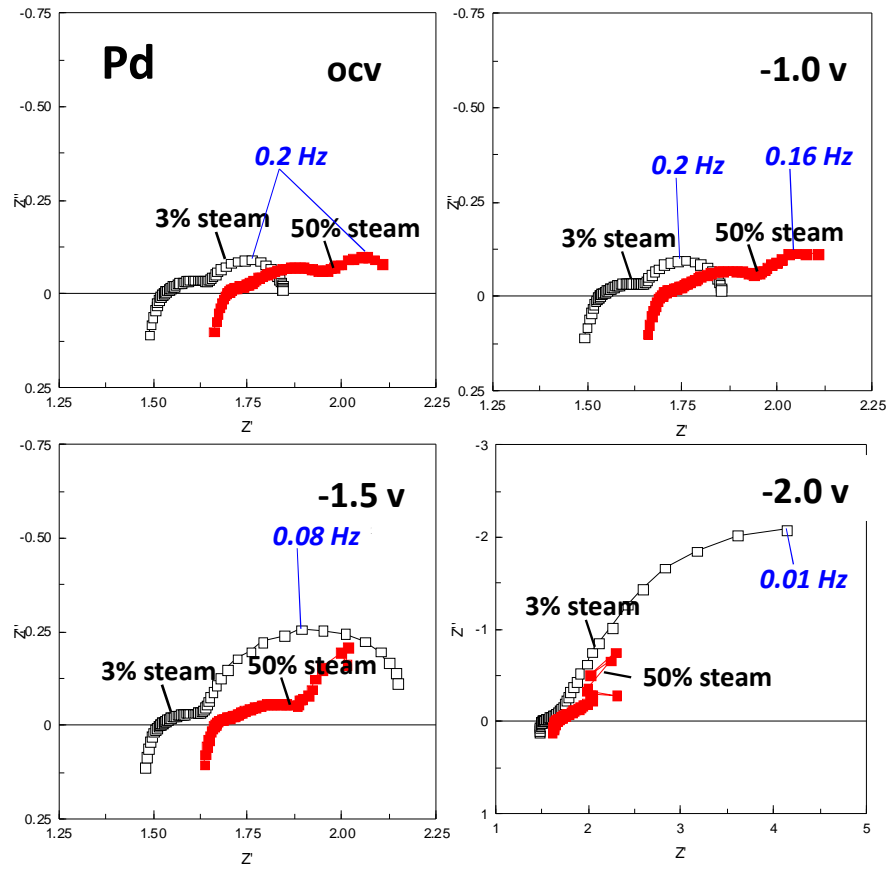

**Figure 7.17. AC impedance data from a cell with Pd in LSCM/CGO cathode at
900°C with 50%H$_2$O/Ar/H$_2$ and 3%H$_2$O/Ar/4%H$_2$.**

7.4.2 Ar with different humidities (with catalysts)

The differences in the I-V curves from cells with various catalysts at 900°C in 50%H$_2$O/Ar and 3%H$_2$O/Ar remain small (see figure 7.18). Running with 50% steam, cells have high slopes at potentials between -0.3 V and -0.85 V, which is

similar phenomena to that in 3% steam. The cell with Fe has slightly better performance than other cells in 50%H_2O/Ar. With a bit higher slopes of I-V curves, cells with Pd and Ni also performance well in 50%H_2O/Ar. By comparison, the cell with Pd has the smallest slope in I-V curve (when potentials > -0.85 V) in 3%H_2O/Ar. Between -0.3 V and -0.85 V, the cell with Pd has the highest slope of I-V curves for both atmospheres.
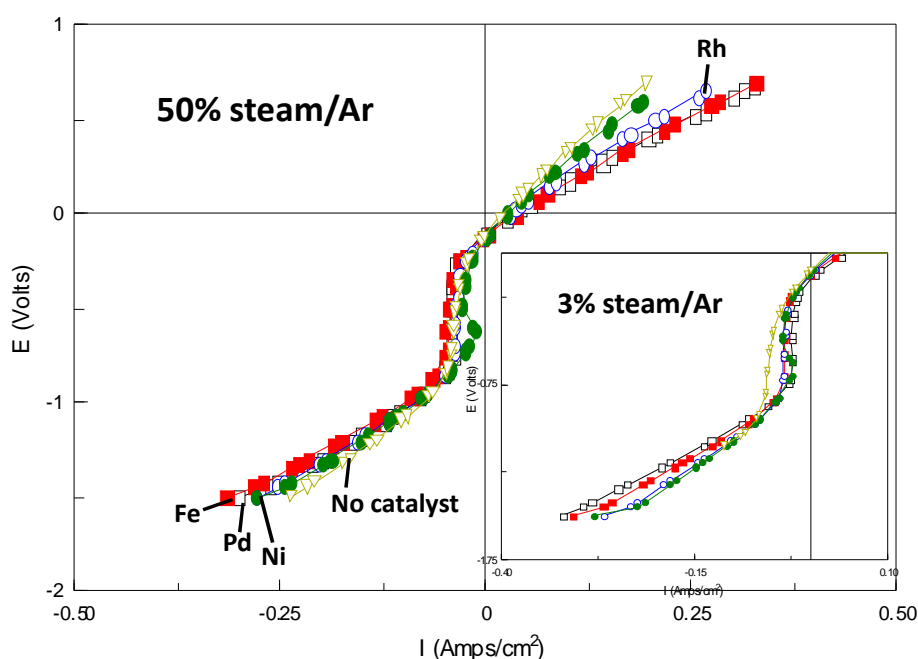

Figure 7.18. Polarization properties from cells having various catalysts in LSCM/CGO cathodes at 900°C with 50%H_2O/Ar and 3%H_2O/Ar.

Figure 7.19 and figure 7.20 are impedance responses from cells with Fe and Pd in atmospheres containing 3% steam and 50% steam in steam/Ar mixtures. It could be seen that total resistance and polarization resistance from the cell with Fe are reduced a bit when steam content is increased (Figure 7.19). Under open circuit, total resistance and polarization resistance from the Pd cell are smaller in 50% steam than in 3% steam (see figure 7.20). At high potentials (-1.0 V, -1.25 V and -1.5 V), polarization resistances in 50% steam from both cells remain similar to those in 3% steam.
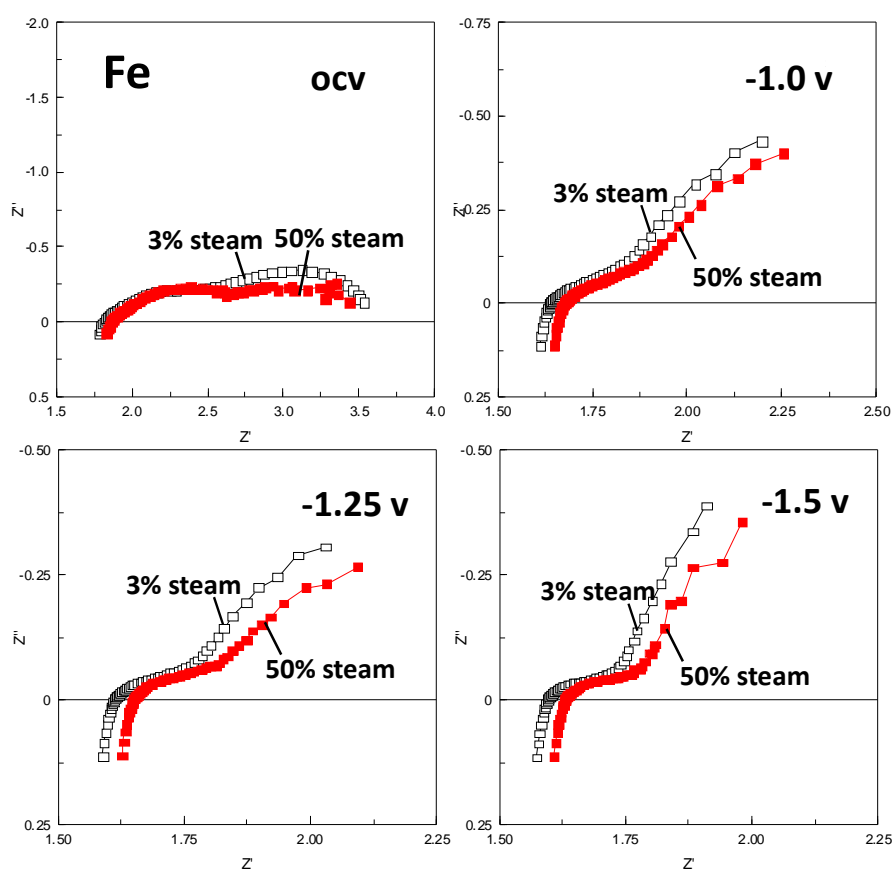
Figure 7.19. AC impedance data from a cell with Fe in LSCM/CGO cathode at 900°C with 50%H$_2$O/Ar and 3%H$_2$O/Ar.
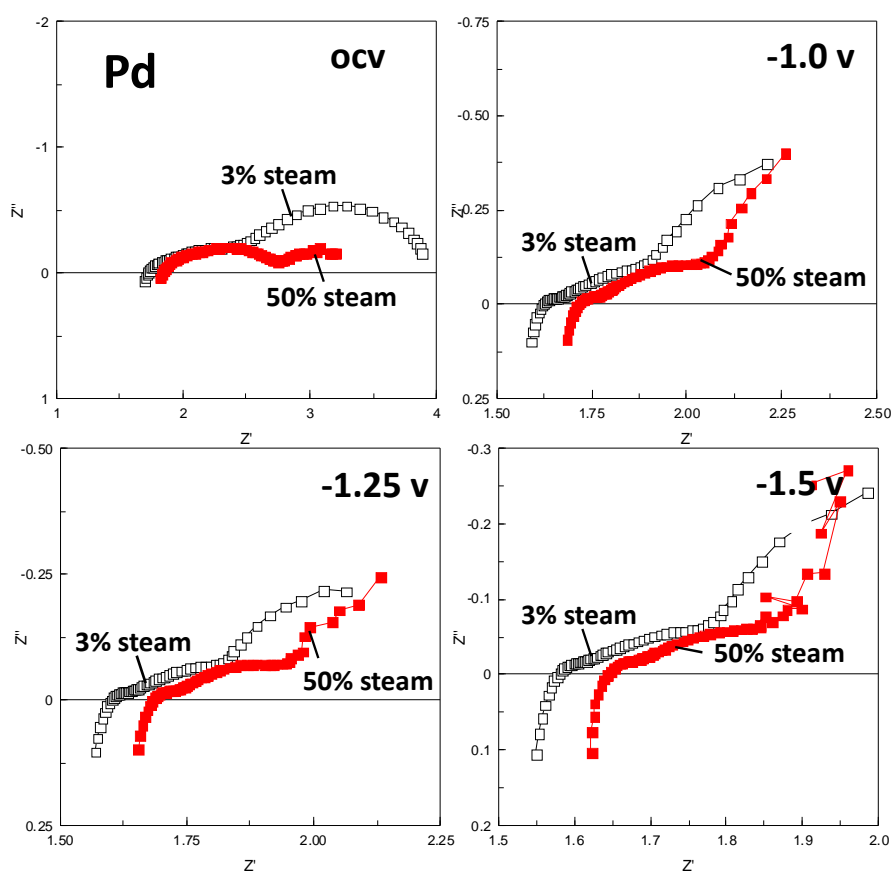
Figure 7.20. AC impedance data from a cell with Pd in LSCM/CGO cathode at 900°C with 50%H$_2$O/Ar and 3%H$_2$O/Ar.

7.5 Conclusions

It was expected to have better performance by increasing steam content in cathode atmosphere. But from the results in this chapter, different steam concentrations in cathode atmosphere do not benefit cell performances. Increasing water content did not facilitate the low frequency process (which could relate to gas diffusion process) in atmospheres with or without hydrogen. This indicates that the main rate limiting process might not be steam diffusion, as the polarization resistance was not reduced by increasing humidity. The possible limiting factor for cathode reactions might be desorption/adsorption of species rather than steam dissociation. The real steam concentration at cathode may be not as it was generated. The gas mixture might lose

some steam content in the gas pathway although a heating tape was applied to keep gas temperature. Another possible reason is that as measurements were taken in a sequence of 3% steam - 10% steam - 30% steam - 50% steam, longer operation time could cause decline in cell performance.

References

1. **J. Schefold, A. Brisse, and M. Zahid,** *J. Electrochem. Soc.***, 2009, 156, B897.**

2. **A. Brisse, J. Schefold, and M. Zahid,** *Int. J. Hydrogen Energy***, 2008, 33, 5375.**

3. **H. Uchida, N. Osada, and M. Watanabe,** *Electrochem. Solid-State Lett.***, 2004, 7, A500.**

4. **S. H. Jensen and M. Mogensen,** *Perspectives of High Temperature Electrolysis Using SOEC***, http://www.hi2h2.com/perspectives.htm, 2009.**

5. **M. J. Jorgensen and M. Mogenson,** *J. Electrochem. Soc.***, 2001, 148, A433.**

6. **F. T. Ciacchi, K. M. Crane, and S. P. S. Badwal,** *Solid State Ionics***, 1994, 73, 49.**

CONCLUSIONS

Traditional Ni/YSZ cathodes suffer from problems such as poor redox cycling and low tolerance to atmospheres without hydrogen or other reductant. LSCM $((La_{0.75}Sr_{0.25})_{0.95}Mn_{0.5}Cr_{0.5}O_3)$, exhibited many characteristics that make it a suitable cathode material for electrolysis, performed well as cathodes for HT-SOECs (high temperature solid oxide electrolysis cells) with low/no hydrogen supply. Adding metal catalysts to LSCM cathodes and improving cell microstructures were able to improve cell electrochemical performances. Hydrogen gas was produced with high efficiencies using SOECs with LSCM/CGO cathodes starting with low/no content of hydrogen.

Ni/YSZ cathodes were not practicable for non-reducing environments or intermittent hydrogen production despite of their good catalytic properties and current collection. By comparison, LSCM showed good stability and electrochemical performance when working as cathodes for SOECs in atmospheres of 3%steam/Ar/4%H_2 and 3%steam/Ar. Mixing pure LSCM with ionic conductors such as CGO $(Ce_{0.9}Gd_{0.1}O_{1.95})$ and YSZ $(Y_2O_3$-stabilized $ZrO_2)$ could further improve cell electrochemical performances due to the enlarged triple phase boundary (TPB). LSCM/CGO cell has a smaller polarization resistance (Rp) of around 1 $\Omega \cdot cm^2$ in 3%steam/Ar/4%H_2 at 920°C, compared to the Rp value of more than 10 $\Omega \cdot cm^2$ from the cell with Ni/YSZ cathode. With no hydrogen supply, the LSCM/CGO cell has fairly small Rp values when working under comparatively low potentials.
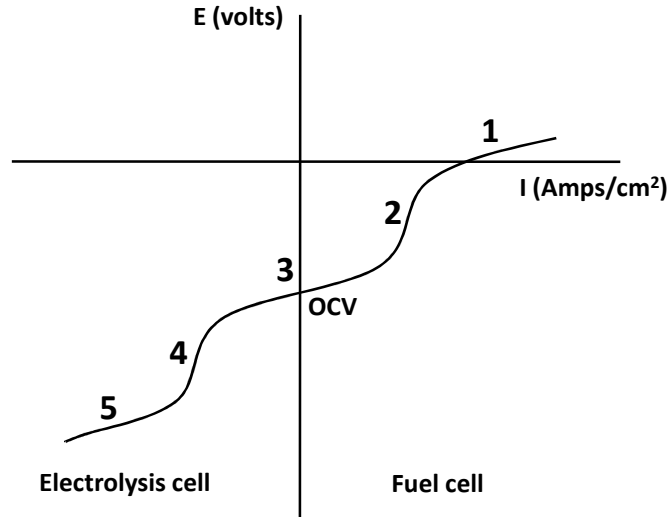
Electrochemical characteristics from SOECs with LSCM/CGO cathodes are schematised in the graph shown above. The I-V curve is composed of two parts: working as an electrolysis cell (when potential is more negative than OCV) and working as a fuel cell (when potential is less negative than OCV). The whole polarization curve could be divided into five segments. Processes 1, 3 and 5 refer to ohmic losses and electrochemical processes such as charge transfer. Processes 2 and 4 could be activation polarization and chemical change.

Adding metal catalysts to LSCM/CGO cathodes could facilitate cathode reactions. The addition of Pd, Fe, Rh and Ni have changed electrode processes and improved cell performances. The cell with Pd has the smallest polarization resistance in $3\%H_2O/Ar/4\%H_2$, followed by the cell with Fe. In $3\%H_2O/Ar$, cells with different catalysts and with no catalyst have various electrode processes. There are two obvious rate limiting processes for $3\%H_2O/Ar/4\%H_2$ and $3\%H_2O/Ar$. The low frequency process is the major process which might relate to gas diffusion and/or adsorption/desorption limitations.

Improving cell microstructures was another way tried to improve cell performances. By decreasing the thickness of YSZ electrolyte from 2 mm to 50 μ, the ohmic resistance of the cell has been dramatically reduced. Several techniques were used to

decrease electrolyte thickness such as cutting/polishing, tape casting, co-pressing and screen printing. The most practical way of making thin YSZ is tape casting. Some methods were tried such as tape casting/impregnation and addition of pore formers to get better electrode microstructures. But the impregnated electrodes were not stable enough at high temperatures.

Hydrogen production amounts from SOECs with LSCM/CGO cathodes were detected by gas chromatograph and current-to hydrogen efficiencies were worked out according to the law of conservation of charge. Herein we have demonstrated that hydrogen could be produced efficiently starting with a small amount of hydrogen (4% H_2) or with no content of hydrogen using SOECs with LSCM/CGO cathodes. Current-to-hydrogen efficiency LSCM/CGO cells was up to 80% at 850°C in 3%H_2O/Ar. Efficiencies in 3%H_2O/Ar/4%H_2O at 800~900°C were even higher (close to 100%).

It was supposed to be able to enhance gas diffusion and therefore to improve cell performance by increasing humidity of the gas supplied to the steam/hydrogen electrode. Measurements were taken with 3%, 10%, 20% and 50% steam supplied to the cathode however the electrochemical performance has not been improved by increasing humidity. The series resistance increased slightly under higher steam contents and less reducing conditions indicating that Rs changes were governed mainly by $p(O_2)$ linked to a decrease of n-type conduction probably due to Ce oxidation. There was a small increase in polarization resistance under higher humidity, although the polarization resistance did not change with reducing conditions. This possibly indicates that hydrogen evolution is the limiting process rather than steam reduction.